Catalysts for stereoselective transformations

Cooper, Christine

Award date:
2012

Awarding institution:
University of Bath

Catalysts for Stereoselective Transformations

Volume 1 of 2

Christine J. Cooper

A thesis submitted for the degree of Doctor of Philosophy

Department of Chemistry
University of Bath
January 2012

In memory of Brian George Cooper

1931-2009

Table of Contents

Chapter Six Experimental

Acknowledgements

Firstly, I would like to thank my supervisor, Dr Matthew Jones for providing me with the opportunity to work on this project. His enthusiasm, guidance and advice throughout my PhD has been invaluable. The EPSRC is also thanked for providing the funding for this project.

Dr John Lowe is thanked for assistance with NMR experiments, and Dr Anneke Lubben is thanked for her help with mass spectrometry. Drs Mary Mahon and Gabriele Kociok-Kohn, and Professor Paul Raithby are thanked for assistance with X-ray crystallography and powder X-ray diffraction. Drs Simon Brayshaw and Mark Russell must also receive thanks for their assistance with DFT calculations. Dr David Apperley of the EPSRC solid-state NMR service is thanked for his assistance with solid-state NMR. Dr Joanna Wolowska of the EPSRC EPR service is thanked for her assistance with EPR spectroscopy. Alan Carver and Russel Barlow are thanked for their assistance with elemental analysis and TGA, respectively. Carlo DiIulio is also thanked for assistance with GC-MS. All members of the Jones and Davidson research groups, past and present, are thanked for their friendship and advice, including my former MChem student Ben Sonnex. In addition, Chris Hawkins is thanked for being a fabulous office buddy, and a great friend.

Finally, my good friends Tom Paterson and Louise Phillips, and my family must be thanked for their constant support and belief in me. To my grampy, you inspired me so much, and you are and always will be sorely missed. To my granny, thank you for making me laugh, and for all the granny-burgers! To my granddad, your unwavering pride in me has helped me more than you know. To my sister, you are my best friend, and I couldn't have done this without you. Thank you. To my nieces, Emily and Taya, you two are the most beautiful, clever, funny and adorable people that I have ever encountered, and I can't wait

to see what the future holds. To my mum and dad, words cannot express the respect, appreciation and gratitude I have towards you. Thank you.

Papers Described in this Thesis

- Jones, M. D., Cooper, C. J., Mahon, M. F., Raithby, P. R., Apperly, D., Wolowska, J., Collison, D., "Cu(II) homogeneous and heterogeneous catalysts for the asymmetric Henry reaction", *Journal of Molecular Catalysis A: Chemical*, **2010,** 325, *1-2*, 8-14

- Cooper, C. J., Jones, M. D., Brayshaw, S. K., Sonnex, B., Russell, M. L., Mahon, M. F., Allan, D. R., "When is an imine not an imine? Unusual reactivity of a series of Cu(II) imine-pyridine complexes and their exploitation for the Henry reaction", *Dalton Transactions*, **2011**, 40, *14*, 3677-3682
    - ❖ This paper was amongst the top 10 most accessed articles in Dalton Transactions for March 2011.

Abstract

The area of asymmetric synthesis has been widely researched, as the need to synthesise a particular enantiomer of a compound has been shown to be vital for various applications, particularly within the pharmaceutical industry. This, coupled with the global move to perform chemistry in a greener, more efficient manner, has resulted in a flurry of research into the asymmetric catalysis of organic transformations, preferably using heterogeneous catalysts.

A library of diamine and diamine ligands have been prepared, many of which contain (*R*,*R*)-1,2-diaminocyclohexane. These ligands were complexed to Ir(I), Rh(I), Ru(II), Pt(II), Pd(II), Cu(II), Ti(IV) and Zr(IV). The precious metal complexes were used to catalyse the asymmetric hydrogenation of ketones, using either direct of transfer hydrogenation methods. Generally, good conversions were observed, along with moderate enantioselectivities. Some analogous heterogeneous catalysts were also prepared and screened for the hydrogenation of ketones. The use of direct hydrogenation methods yielded good conversions; unfortunately no enantioselectivity was observed.

Tetradentate copper(II) complexes of (*R*,*R*)-1,2-diaminocyclohexane based diimine ligands containing pyridine moieties were also prepared. When complexing one of these ligands to copper(II) triflate, in the presence of methanol or ethanol, the addition of the alcohol was observed across one of the imine bonds, forming a rare α-amino ether complex. This was studied with the use of mass spectrometry, single crystal X-ray diffraction and DFT calculations.

Copper(II) complexes of ligands containing phosphine moieties were also prepared. In one particular complex, the oxidation of the phosphine group gave rise to the reduction of copper(II) to copper(I), the kinetics of which were

followed using UV-vis spectroscopy. It was found that this redox process exhibited first-order kinetics.

The copper(II) complexes prepared were used to catalyse the asymmetric nitroaldol, aldol and allylic oxidation reactions. A suitable oxidant for the allylic oxidation reaction could not be found, and the copper(II) catalysed of the aldol reaction was unsuccessful. However, metal-free catalysis of the aldol reaction was successful, with homogeneous and heterogeneous systems, with good conversions and enantioselectivities observed. In addition, both the aldol addition and condensation reactions were observed on analysing the reaction using ^{1}H NMR spectroscopy. Usually, one of these reactions is favoured – it is rare to observe both reactions occurring in significant proportions. The copper(II) catalysis of the nitroaldol reaction was extremely successful. Excellent conversions and moderate enantioselectivities were observed in the homogeneous catalysis. Furthermore, the enantioselectivities were dramtically improved by reducing the reaction temperature and reducing the amount of base used, with no significant decrease in conversion observed. The heterogeneous catalysis of the nitroaldol reaction also yielded excellent conversions. However, further reaction of the nitroaldol product with nitromethane was observed, yielding a 1,3-dinitro alkane by-product. However, the selectivities for the desired nitroaldol product were moderate to excellent. Good enantioselectivities were observed, with the exception of the heterogeneous catalysis of the reaction between nitromethane and 4-nitrobenzaldehyde, where no enantioselectivity was observed.

The titanium(IV) and zirconium(IV) complexes were used to catalyse the stereoselective polymerisation of *rac*-lactide. Successful results were observed in the homogeneous catalysis under melt conditions.

Overall, a number of homogeneous and heterogeneous systems have been prepared, and used in the asymmetric catalysis of numerous organic transformations.

Introduction

1.1 The Importance of Chirality in Synthesis

In 1956, Thalidomide (pictured in fig. 1.1.1) was marketed as a sedative, and was commonly prescribed for morning sickness in pregnant women. However, the (*S*)-enantiomer was shown to have teratogenic activity, and caused serious birth defects in many of the resulting babies.[1]

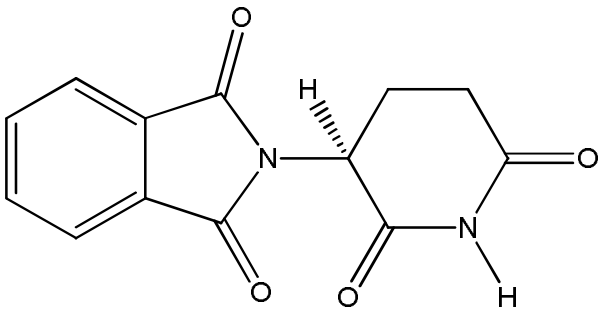

Fig. 1.1.1 (*S*)-Thalidomide

Similarly, the drug Benoxaprofen (pictured in fig. 1.1.2) was withdrawn from the market in 1982 upon reports of the drug causing serious liver toxicity. On further investigation, it was found that only the (*R*)-enantiomer binds to liver proteins, causing hepatotoxicity – the (*S*)-enantiomer has no effect.[2,3]

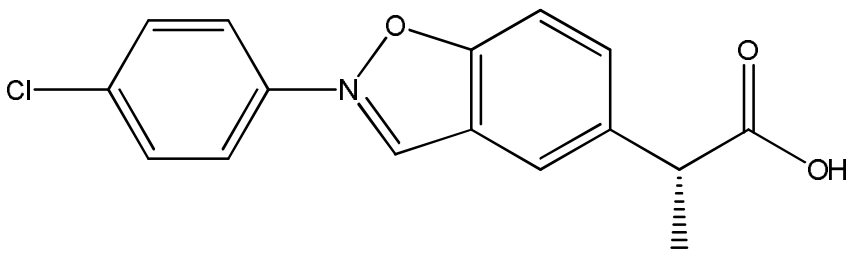

Fig. 1.1.2 (*R*)-Benoxaprofen

In 1988, the U.S. Food and Drugs administration began requiring information regarding the enantiomeric composition of any chiral substances in new drug applications.[4] By this time, the importance of chirality within molecules, particularly drugs, had become obvious.

In 2006, 80 % of small molecule drugs approved by the U.S. Food and Drugs Administration were chiral, and 75 % of those were single enantiomers.[5] Therefore, developing new methods of controlling chirality of molecules is of the utmost importance, and not just in the pharmaceutical industry. Enantioselectivity is also very important in the fragrance and flavourings industries. For example, (*R*)-limonene (displayed in fig. 1.1.3) is commonly used to provide citrus fragrances,[6] whereas the (S)-enantiomer has a pine odour.

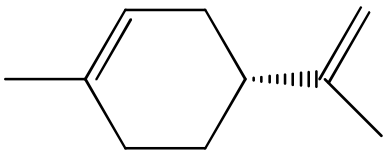

Fig. 1.1.3 (*R*)-Limonene

Therefore, given the increasing importance of obtaining a particular enantiomer of a molecule, the syntheses of these compounds must be designed to occur in a selective manner. This process is known as “asymmetric synthesis” or “asymmetric catalysis”, and both will be discussed at length in this introduction.

1.2 Asymmetric Synthesis

Asymmetric synthesis can be defined as "*organic synthesis that introduces one or more new and desired elements of chirality*".[7] Commonly, a chiral agent is introduced into the reaction to control the stereoselectivity of the subsequent product. The two most commonly used chiral agents are chiral auxiliaries and chiral catalysts.

A chiral auxiliary controls stereochemistry by becoming incorporated into the structure of the product. Often this part of the product then is removed either immediately during work-up or in a subsequent reaction step. Meyers et. al.[8] used a chiral auxiliary in the enantioselective syntheses of α-disubstituted carboxylic acids. The reaction scheme is given in fig. 1.2.1.

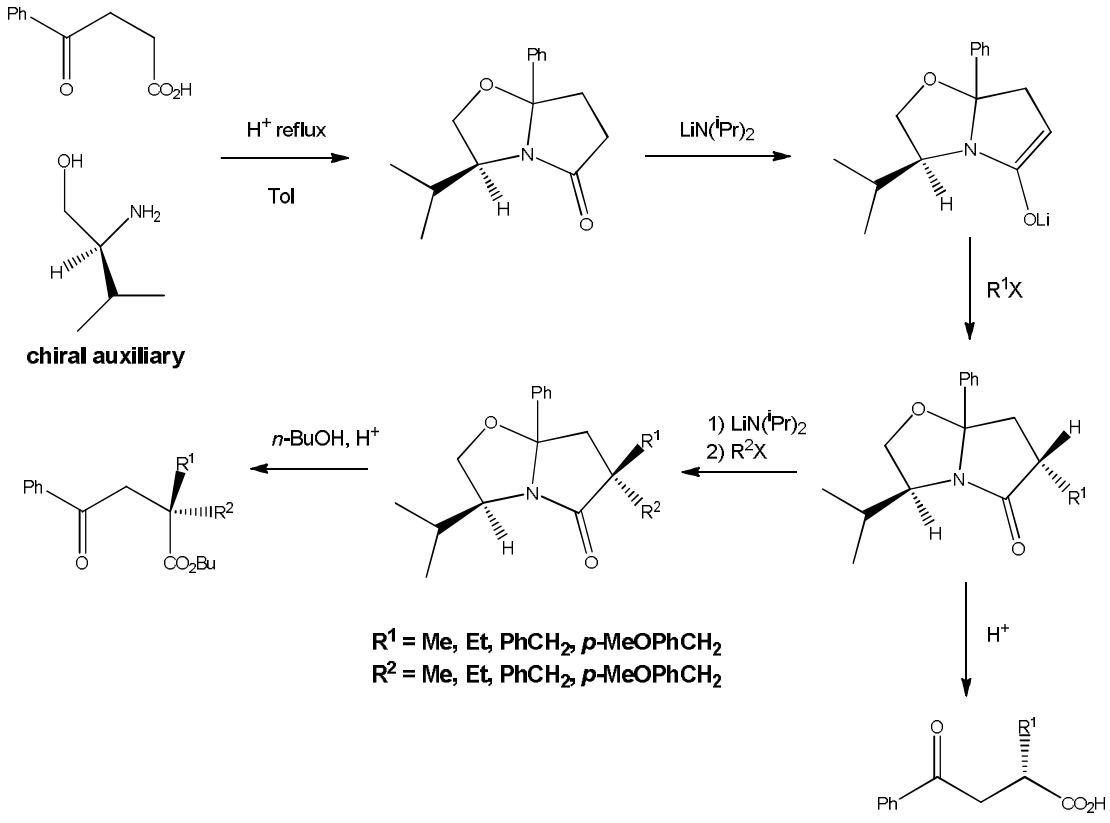

Fig. 1.2.1 Reaction scheme showing the chiral auxiliary enabled enantioselective preparation of α-disubstituted carboxylic acids, as described by Meyers[8]

A stoichiometric amount of the chiral auxiliary (*S*)-2-amino-3-methylbutan-1-ol was required, and extra reaction steps were necessary to add and cleave the auxiliary. Some of the results can be seen in table 1.2.1.

Table 1.2.1 A selection of the results from the enantioselective synthesis of α-disubstituted carboxylic acids. The positions of R^1 and R^2 within the product are shown in fig. 1.2.1

R^1	R^2	Yield* / %	Configuration
Me	$PhCH_2$	75	*S*
$PhCH_2$	Me	74	*R*
Me	Et	80	*S*
Et	Me	75	*R*
Me	*p*-$MeOPhCH_2$	85	*S*
p-$MeOPhCH_2$	Me	90	*R*

* Yield corresponds to the yield of pure diastereomer after chromatography.

The yields of diastereomeric product are consistently good, and the configuration at the new chiral centre appears to be well controlled by the alkyl halide. The authors reported minimal racemisation of the product during the auxiliary cleavage step, where acid hydrolysis is performed. However, if this step is performed following only the first addition of alkyl halide, significant racemisation of the enantiomeric product occurs (< 20 % ee). This behaviour has been observed in similar previous work by Meyers,[9] when an analogous chiral auxiliary was used to produce chiral α-monosubstituted carboxylic acids. This work is displayed in fig. 1.2.2.

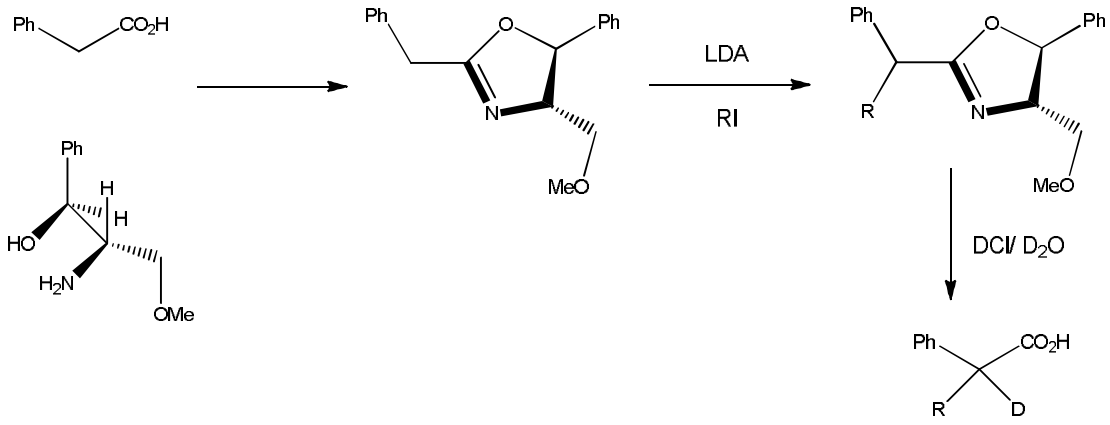

Fig. 1.2.2 Reaction scheme showing the chiral auxiliary enabled enantioselective preparation of α-monosubstituted carboxylic acids, as described by Meyers[9]

However, the racemisation is only observed where R = Ph, due to the greater acidity of the α-benzyl proton. This highlights common flaws in the usage of chiral auxiliaries. Firstly, when removing the chiral auxiliary, one must be very careful to avoid racemisation at the newly formed chiral centre. Keeping this in mind, it is apparent that the use of a chiral auxiliary can limit the substrates that can be used for the reaction, and can also dictate the way that a reaction is used, and if it is used at all. For example, in these related studies, when attempting to prepare the chiral α-monosubstituted carboxylic acids, this was successfully achieved provided that phenyl-substituted substrates were not used. If a phenyl-substituted substrate must be used, then the chiral α-disubstituted carboxylic acid must be prepared, in order to prevent racemisation of the product. If an α-disubstituted carboxylic acid is not appropriate in terms of its subsequent application, then enantiomeric separation of the racemic α-monosubstituted carboxylic acid is necessary, which can be difficult, costly and time-consuming. Therefore, the use of other agents (such as chiral catalysts) to direct chirality in organic transformations can often be favourable. On the other hand, the stereoselectivities seen when chiral auxiliaries are used can often be difficult to match with other chiral agents. In addition to this, diastereomeric products are easier to separate than enantiomeric ones. Issues may arise on separating the chiral auxiliary from the products following auxiliary cleavage, but can usually be overcome by various methods.

The latter two points are highlighted in research published by Oppolzer et. al.[10] The authors used camphor derivatives in the asymmetric hydrogenation of alkenes. The reaction scheme can be seen in fig. 1.2.3.

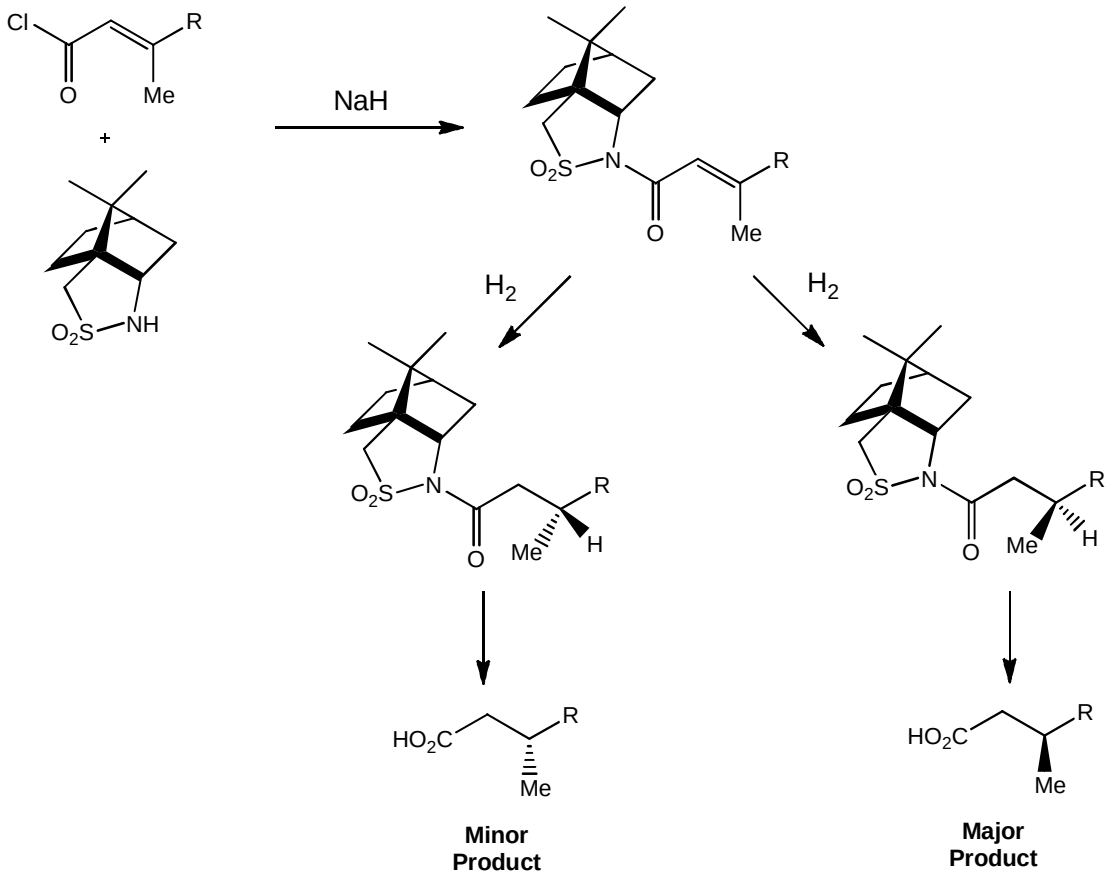

Fig. 1.2.3 Reaction scheme showing the chiral auxiliary enabled enantioselective hydrogenation of alkenes, as described by Oppolzer[10]

Stoichiometric amounts of the chiral auxiliary were required, as were very specific reaction conditions, which will be discussed shortly. The results are given in table 1.2.2.

Table 1.2.2 A selection of results from the enantioselective hydrogenation of alkenes. The position of R within the product is shown in fig. 1.2.3

R	Yield / %	Configuration
C_2H_5	99.5	*R*
nC_3H_7	98	*R*
iC_3H_7	95.5	*R*
nC_4H_9	95	*R*
nC_6H_{13}	96	*R*
nC_8H_{17}	96.2	*R*

* Yield corresponds to pure diastereomer by gas chromatography

The results show excellent stereoselectivities with a consistent configuration of (*R*) at the new chiral centre. As previously discussed, this remarkable degree of stereoselectivity is typical with chiral auxiliaries. The chiral auxiliary was then cleaved via a simple saponification reaction under mild conditions (8 eq. LiOH in 7:3 THF:water, for 18 h at room temperature). The authors reported this step to be high yielding (92-100 %) with no evidence of racemisation. Finally, the carboxylic acid products were separated from the chiral auxiliary easily by distillation. In this case, this addition and cleavage of the chiral auxiliary was simple, with no significant issues with respect to racemisation at the new chiral centre, and straightforward separation of the final enantiomers from the chiral auxiliary. In the case of the research by Meyers, the reaction was complicated by the use of a chiral auxiliary, which limited the substrates that could be used, and dictated the applicability of the approach. Finally, problems with racemisation were observed. This emphasises the importance of choosing the correct chiral agent to direct chirality during asymmetric synthesis, i.e. in the case of Oppolzer's work, a chiral auxiliary was perhaps the most suitable choice of chiral agent to achieve the outstanding results reported. In the case of Meyer's work, given the added complications of removing the chiral auxiliary in particular, perhaps chiral catalysis may have been more suitable. Also of notable mention is the specificity required in the use of chiral auxiliaries. In the case of Meyer's work, specific substrates were required for a successful asymmetric synthesis. In the case of Oppolzer's work, the specificity is required in the reaction conditions. Table 1.2.3 shows the results of varying the hydrogenation reaction conditions whilst keeping the substrate and chiral auxiliary constant (when R = $n$$C_3H_7$).

Table 1.2.3 Results of the enantioselective hydrogenation of the alkene shown in fig. 1.2.3 where R = *n*C_3H_7, with various reaction conditions

Conditions	Hydrogen Source	Solvent	Temp. / °C	Reaction Time / h	Yield / % (*R*)
$LiAlH_4$ (slurry) / $CoCl_2$	$LiAlH_4$	THF	78 →25	1	92
$LiAlH_4$ (soln) / $CoCl_2$	$LiAlH_4$	Et_2O	78 →25	3	16
$[Ir(cod)py(PCy)_3]^+ PF_6^-$	1 atm H_2	CH_2Cl_2	25	1	61
10 % Pd/C	30 psi H_2	EtOH	25	48	95
10 % Pd/C	95 psi H_2	EtOH	25	1.5	98
10 % Pt/C	90 psi H_2	EtOH	25	17	89

Much variation is seen in the yield of the major diastereomeric product, with even a reversal in configuration in one case (entry 2). For instance, in the case where $LiAlH_4$ is used as the hydrogenation source, the solvent used is the most likely cause of the difference in configuration and yield of the major diastereomer. Comparing the 10 % Pd/C and Pt/C at 95 and 90 psi H_2 respectively, there is a difference of almost 10 % yield, which is most likely due to the metal used. This suggests that chiral auxiliaries not only demand substrate specificity, but also very particular reaction conditions. To some extent this is seen in most asymmetric organic transformations, but is often particularly common with the use of chiral auxiliaries.

One of the most famous chiral auxiliaries is the Evans oxazolidinone,[11,12] shown in fig. 1.2.4. This chiral auxiliary was used for asymmetric synthesis in two of the most important reactions in organic synthesis: the α-alkylation of enolates and the aldol reaction, each of which will be discussed here. A paper by Evans in 1982 describes the use of the Evans oxazolidinone for the asymmetric α-alkylation of enolates.[11] The reaction scheme for this can be seen in fig. 1.2.4.

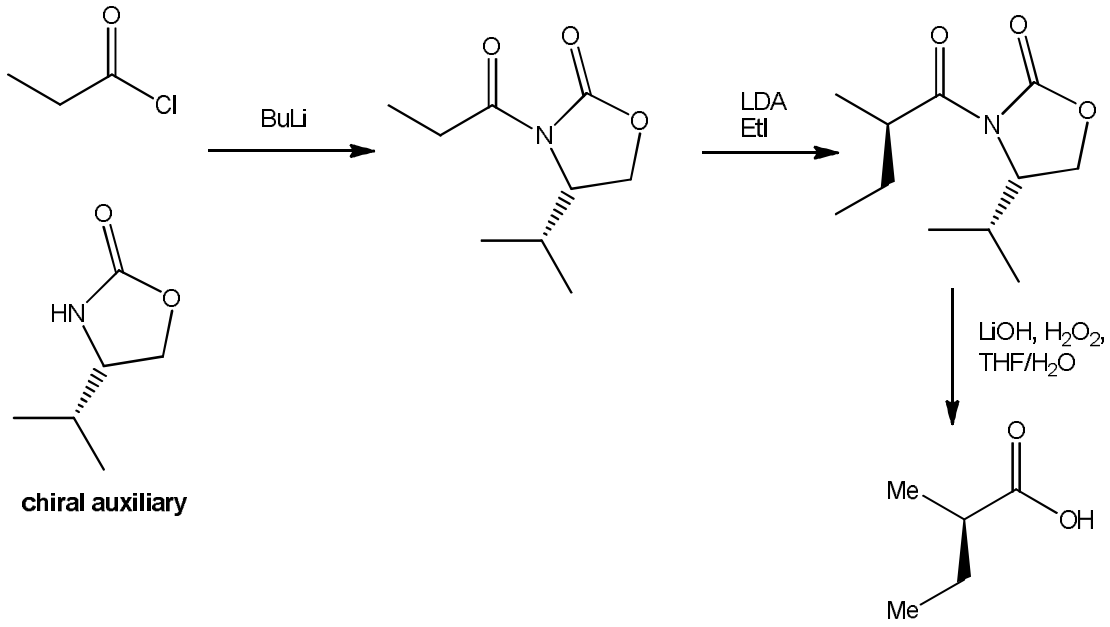

Fig. 1.2.4 The use of the Evans oxazolidinone chiral auxiliary in the enantioselective α-alkylation of enolates

This research was hugely successful for many reasons. Firstly, the stereoselectivities are very high. The results can be seen in table 1.2.4.

Table 1.2.4 A selection of results from the enantioselective α-alkylation of enolates. The positions of R^1 and R^2 within the product are shown in fig. 1.2.4

R^1	R^2	*Yield / %	Configuration
Me	$PhCH_2$	99	*R*
Me	CH_2=C(Me)CH_2	98	*R*
Me	CH_2=$CHCH_2$	98	*R*
Me	$PhCH_2OCH_2$	98	*R*
Me	EtO_2CH_2	95	*R*
Me	Et	94	*R*
Et	Me	89	*R*
nC_8H_{17}	Me	91	*R*

* Yield corresponds to % of major diastereomer as determined by gas chromatography.

In addition to this, the results were so predictable and reproducible that the reaction could be fine tuned by changing one of the R groups to force high

stereoselectivities, and in conjunction with the chiral auxiliary dictate the stereochemistry at the new chiral centre. The addition and cleavage of the chiral auxiliary is simple with no threat of racemisation or destruction to either product or auxiliary, which also means that the auxiliary can be recycled.

The Evans oxazolidinone can also be applied to the asymmetric aldol reaction.[12] The reaction scheme can be seen in fig. 1.2.5.

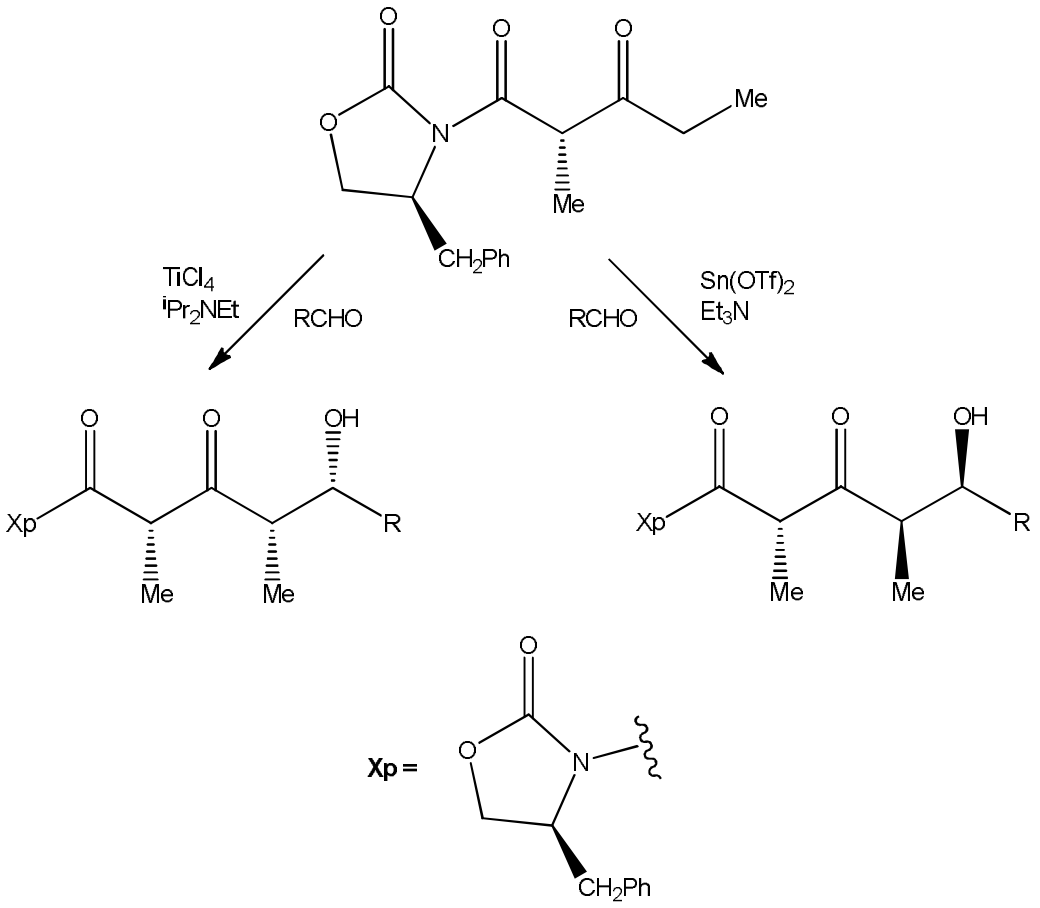

Fig. 1.2.5 The use of the Evans oxazolidinone chiral auxiliary in the asymmetric aldol reaction

The aldol reaction is one of the most important C-C bond forming reactions in organic synthesis, and so to achieve high stereoselectivities in this reaction with relative ease is of great significance, and this together with the previous success in the alkylation of enolates puts this chiral auxiliary as one of the most successful and versatile chiral auxiliaries ever reported. The results from the

asymmetric aldol reaction can be seen in table 1.2.5. The choice of reagent determines the configuration of the new chiral centres, and so the same chiral auxiliary can be used to obtain either diastereomer.

Table 1.2.5 A selection of the results of the enantioselective aldol reaction, as displayed in fig. 1.2.5

Reagent	R	*Yield / %	Configuration
$Sn(OTf)_2$.EtN	$CH(CH_3)_2$	95	*R* (Me), *S* (OH)
$TiCl_4$.$^iPr_2NEt$	$CH(CH_3)_2$	99	*S* (Me), *R* (OH)
$Sn(OTf)_2$.EtN	$C(CH_3)=CH_2$	95	*R* (Me), *S* (OH)
$TiCl_4$.$^iPr_2NEt$	$C(CH_3)=CH_2$	98	*S* (Me), *R* (OH)
$Sn(OTf)_2$.EtN	Et	79	*R* (Me), *S* (OH)
$TiCl_4$.$^iPr_2NEt$	Et	99	*S* (Me), *R* (OH)
$Sn(OTf)_2$.EtN	Ph	89	*R* (Me), *S* (OH)
$TiCl_4$.$^iPr_2NEt$	Ph	96	*S* (Me), *R* (OH)

* Yield corresponds to the % of major diastereomer when analysed by HPLC

There are many other examples of chiral auxiliaries and how they have been used to induce high levels of stereoselectivity in chiral products. For example Denmark used chiral amines as auxiliaries in the asymmetric S_N2 substitution of chiral carbamates.[13] Also Mukaiyama used a chiral oxazolidin-2-one auxiliary in the asymmetric aldol reaction.[14] However, given that a stoichiometric quantity of the chiral auxiliary is required and cleavage of the auxiliary can overcomplicate and even reduce stereoselectivity, chiral catalysis can often be a more suitable method of directing chirality during a reaction. In 2002, Paul Anastas and co-workers introduced the "12 principles of green chemistry".[15] This will be discussed in more detail later, in section 1.5, but generally states that waste should be prevented wherever possible. The use of chiral auxiliaries is very wasteful, as extra reaction steps are required to remove the chiral auxiliary. This uses extra chemicals and solvent, which could be avoided if chiral catalysts were used instead.

Chiral catalysts tend to allow a greater flexibility with the substrates that can be used, and as the threat of racemisation during a cleavage step is not present, in

some cases better stereoselectivities are observed. In addition to this, much smaller quantities of the catalyst can be used. Also, because the catalyst does not become incorporated into the structure of the product (the greatest degree of incorporation is in a transition state), a cleavage step is not required. This means that the catalyst is regenerated many times during the course of the reaction, and so the efficiency of these processes is much greater. Moreover, provided that the catalyst can be easily separated from the products, re-use of the catalyst is also very common. Chiral catalysts can be broadly divided into several categories, for example chiral bases, chiral lewis acids and chiral transition metal complexes.

There are many examples of chiral bases as catalysts; two types being cinchona alkaloids and amino acids. Amino acids as chiral catalysts are often used in the asymmetric aldol reaction, and will be examined alongside this reaction later.

Two commonly used cinchona alkaloids are quinine and quinidine, shown in fig. 1.2.6.

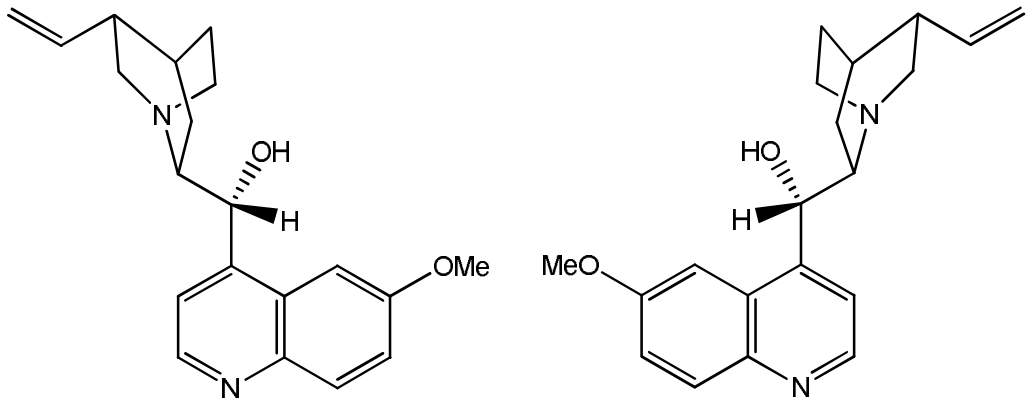

Fig. 1.2.6 Structures of quinine and quinidine, respectively

Wynberg used derivatives of these cinchona alkaloids to catalyse the asymmetric Michael reaction.[16] The reaction scheme is given in fig. 1.2.7.

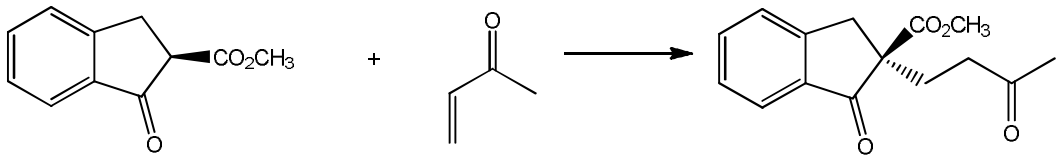

Fig. 1.2.7 The enantioselective Michael reaction, which is catalysed by cinchona alkaloids, as described by Wynberg[16]

At first glance, one could assume that chirality is not technically being introduced in this reaction, as the substrate and product both have a stereochemical configuration of (*R*) at the same chiral centre. We must look deeper into the mechanism of the reaction to understand where the chirality is induced. This is shown in fig. 1.2.8.

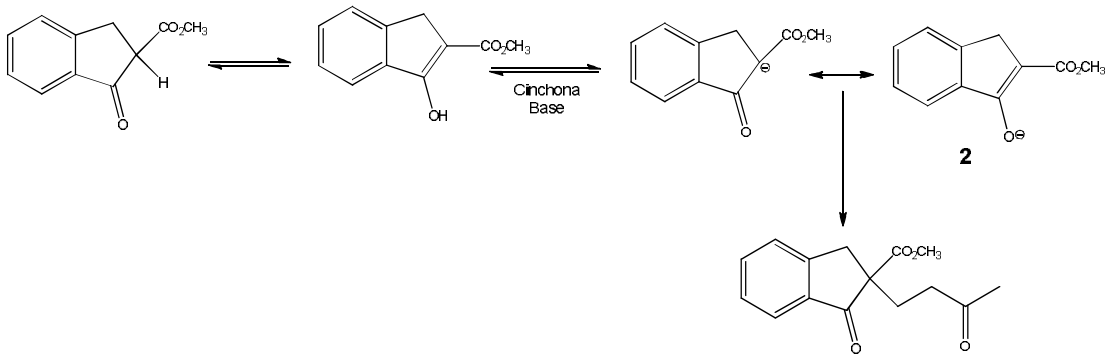

Fig. 1.2.8 Mechanism of the Michael reaction (previously shown in fig. 1.2.7)

The mechanism shows that the substrate is undergoing keto-enol tautomerism. When the substrate takes the form of the enol tautomer (**2**), there is no longer a chiral centre present. The planar nature of the now sp^2 hybridised carbon atoms of the C=C group allows for attack of a base (and subsequently the Michael addition) from either face, and leaves this potential chiral centre open to racemisation. The cinchona alkaloids used are chiral, and dictate which face the substrate is attacked from, thus dictating the chirality of the product. This is clearly an important factor with respect to enantioselectivity, with the reaction being highly substrate dependent. Take the substrates pictured in fig 1.2.9.

Fig. 1.2.9 Two of the substrates tested for the asymmetric Michael reaction (previously shown in fig. 1.2.7)

The cyclohexane ring will not be completely planar when in its enol form, which may influence which face the base attacks from. Also, there is so much steric bulk added to the substrate that this must certainly affect the stereochemistry of the product. The enantioselectivities are very low when these substrates are used (0-25 %), and a change is seen in the configuration at the chiral centre of the product (from *R* to *S*). When the substrate is more planar, much higher enantioselectivities (up to 76 %) are observed, with a uniform configuration of (*S*) at the product's chiral centre. This highlights how fickle chiral catalysis can be in terms of how applicable to different substrates a process can be. This is one of the more complex processes in preparing a good enantioselective catalyst for a reaction.

In addition to this, asymmetric catalysis can also be highly solvent dependent. Zhao[17] used cinchona alkaloids in the asymmetric catalysis of the chlorination of oxindoles, shown in fig. 1.2.10.

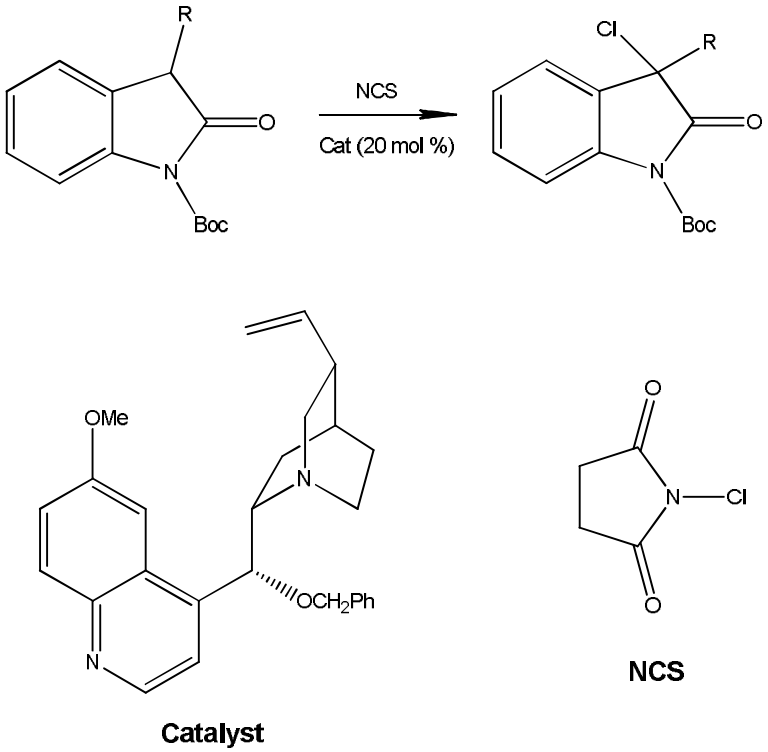

Fig. 1.2.10 Reaction scheme of the enantioselective chlorination of oxindoles, as described by Zhao[17]

The catalysis was performed in a variety of solvents, at room temperature for 2 h. The results can be seen in table 1.2.6, where R = Ph. The enantioselectivity was low in a non-polar solvent (toluene), but improved when more polar solvents were used, with a solvent of THF providing the highest enantioselectivity of 76 %.

Table 1.2.6 A selection of results from the chlorination of oxindoles (as previously shown in fig. 1.2.10), showing the effect of varying the reaction solvent

Solvent	Yield / %	ee / %
Toluene	99	37
Acetonitrile	99	58
Methanol	66	56
Acetone	99	72
THF	99	76
1,2-dichloroethane	82	70

Zhao also showed that lowering the reaction temperature made a great improvement to the enantioselectivities observed. This is a common observation, and is a widely used tool across asymmetric synthesis to improve enantioselectivities. It is based on the thermodynamic preferences of forming one enantiomer over another, due to the presence of a diastereomeric intermediate. Fig. 1.2.11 shows a typical example of the difference in reaction profiles (and activation energies) between two enantiomers. By lowering the reaction temperature, the activation energy of only one enantiomer is accessible, which increases enantioselectivity. The change in Gibbs free energy is also shown.

$$\Delta G = \Delta H - T\Delta S$$

where G corresponds to Gibbs free energy, H corresponds to enthalpy, T corresponds to temperature and S corresponds to entropy.

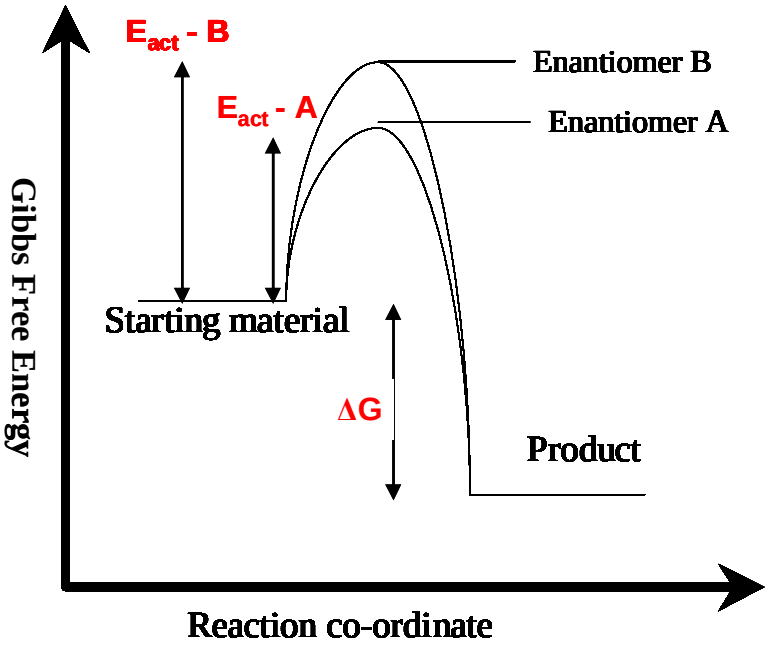

Fig. 1.2.11 Reaction profiles showing the difference in activation energies between two enantiomers

Lewis acids can also be used to induce enantioselectivity.[18-20] Often they bind to the substrate with a very particular geometry, which in turn manipulates the substrate into such a specific geometry that sterically, only one enantiomer can form. To a certain extent, this can be seen in all aspects of asymmetric synthesis.

In 1991, Hawkins[18] published research into the use of chiral lewis acids in the asymmetric Diels-Alder reaction. The preparation of the chiral lewis acid and the reaction scheme for this can be seen in fig 1.2.12.

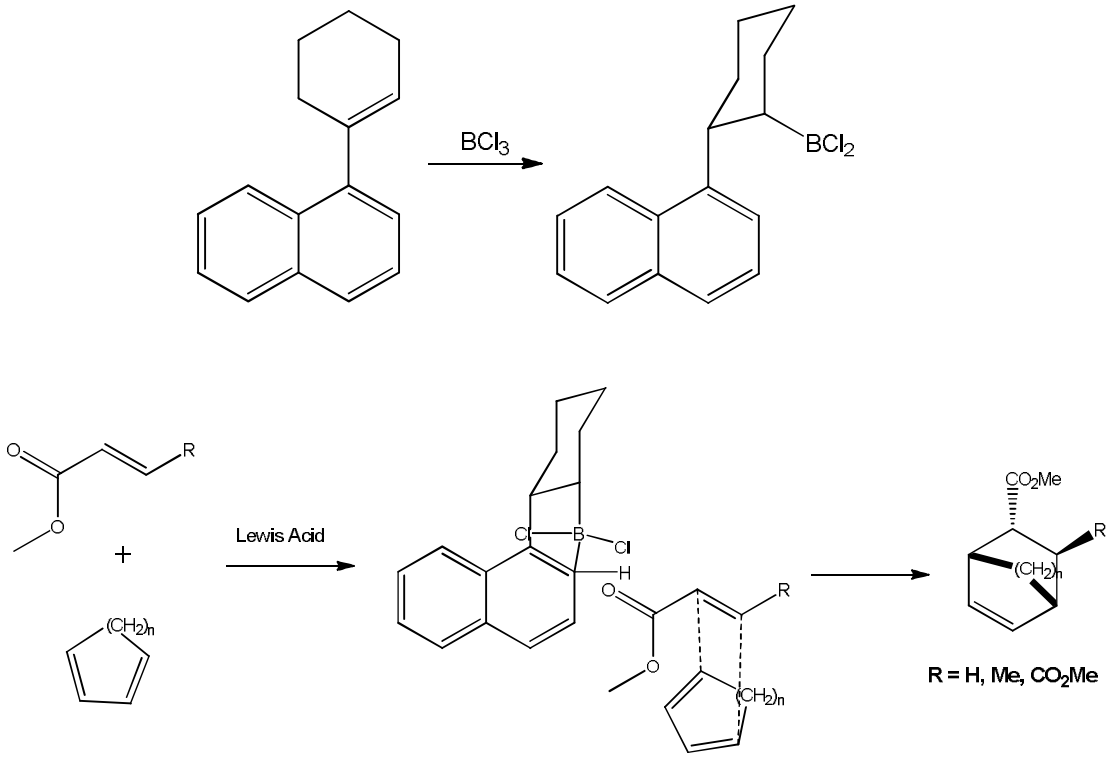

Fig. 1.2.12 Reaction schemes showing the formation of a lewis acid, and the use of this lewis acid in the asymmetric Diels-Alder reaction

He showed the addition of the lewis acid BCl_3 across a double bond, producing a cyclohexane ring with the BCl_2 group in the equatorial position. Fig 1.2.12 shows the resulting structure of the intermediate formed when the dienophile binds to the lewis acid group, still in the equatorial position. Conformational analysis suggested that this position is highly favoured, due to electrostatic interactions and dipole-induced-dipole interactions between the bound dienophile and the now adjacent naphthalene ring. Thus, the dienophile is held in position when the second substrate comes in to react, which can now only react at one face of the dienophile, yielding the product in high enantioselectivity (86-97 % ee).

Yamamoto[19] used an aluminium based lewis acid catalyst in the asymmetric ene reaction of aldehydes and alkenes, displayed in fig. 1.2.13.

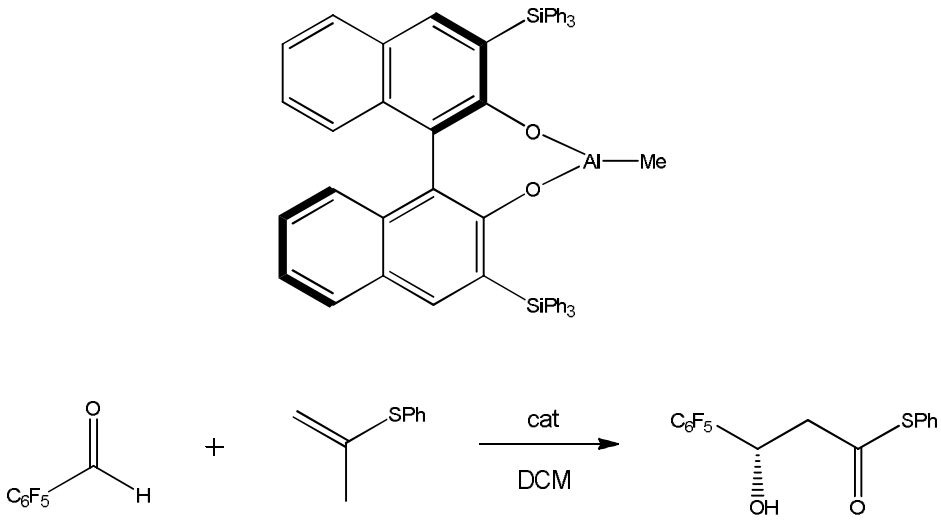

1.2.13 The aluminium-based lewis acid catalyst is displayed, and the reaction scheme for its use in the asymmetric ene reaction of an aldehyde and an alkene

Enantiomeric excesses of 88 % were observed under various conditions (-20 or -78 °C, and with or without molecular sieves, 4 Å). More variation (30-92 % ee) was observed with the substrates, which as previously discussed is not an uncommon phenomenon. Yamamoto has also published similar work using chiral (acyloxy)borane complexes in the catalysis of asymmetric Diels-Alder reactions.[20] The (*R*,*R*) diastereomer of the chiral agent used and the reaction scheme corresponding to this research can be seen in fig. 1.2.14.

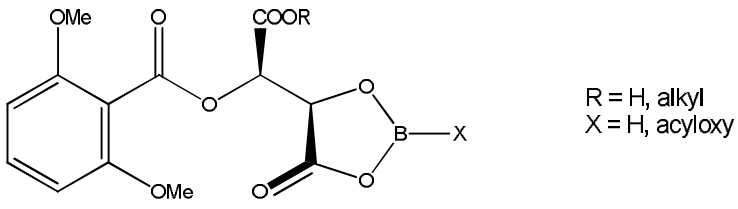

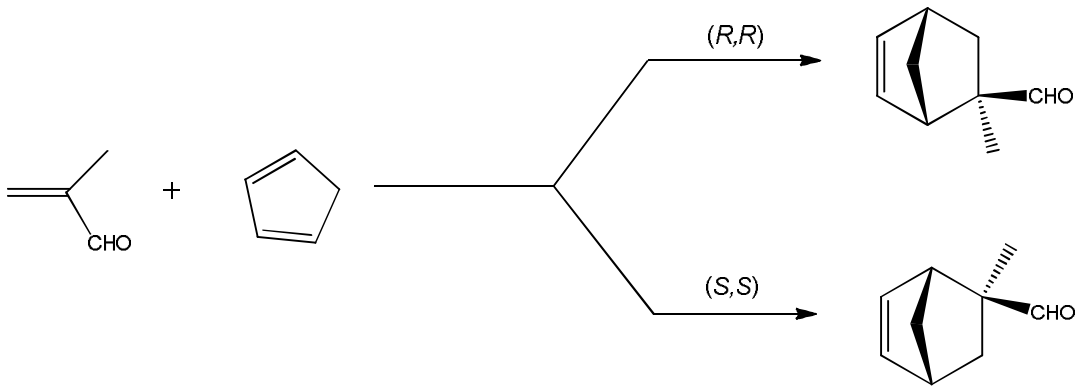

Fig. 1.2.14 The chiral (acyloxy) borane catalyst is shown, and the reaction scheme for the use of the diasteromers of this catalyst in the asymmetric Diels-Alder reaction

High yields and enantioselectivities are observed (85 % yield, 95 % ee). Interestingly, with the nature of this catalyst, either enantiomer can be prepared by simply using the appropriate enantiomer of tartaric acid during catalyst preparation (Sigma Aldrich supplies both enantiomers at low cost; the L and D versions cost 12 and 62 pence per gram respectively). Considering this, one can then choose which version of the catalyst to use according to which enantiomer of product is required. This is extremely useful, and something that is relatively rare. More often than not, one enantiomer of chiral catalyst or auxiliary is either much more expensive or difficult to prepare, and so possessing the ability to obtain either enantiomer by simply changing the enantiomer of tartaric acid is extremely advantageous.

Another method of catalysing asymmetric synthesis is through the use of chiral transition metal complexes. This will now be discussed extensively.

1.3 Homogeneous Catalysis

One huge advantage in homogeneous catalysis is the ability to make slight modifications to the catalyst in order to “fine-tune” it to its substrate and reaction conditions. Thiel et. al. showed that by varying the steric and electronic properties of ligand donor sites, conversions and enantioselectivities could be greatly improved, which is an advantage over heterogeneous catalysts, where this

is often more difficult to achieve.[21] Other advantages of homogeneous catalysis include higher selectivities (in general), and deeper insights into catalytic mechanisms, given the relative ease of characterising and analysing ligands, catalysts, and even following the reaction *in situ*. This section will encompass the discussion of numerous asymmetric reactions which are commonplace in organic synthesis. Specifically, the transition metal complexes that have been used to catalyse these reactions will be discussed.

1.3.1 Asymmetric Hydrogenation Reaction

In 1968, Knowles[22] reported his research in catalysing the asymmetric hydrogenation of alkenes, which led to the first commercial application of an asymmetric catalytic reaction.[23] The catalysts were rhodium complexes of tertiary phosphines, which were similar to that reported by Wilkinson in 1966.[24] Knowles reported optical purities of up to 15 %, and reported yields of 100 moles of product using only 1 mole of catalyst. They also reported that stereospecificity with a range of substrates could be achieved by modifying the ligand, introducing the concept of "fine-tuning" the catalysis of a particular substrate by simply tweaking the catalyst. Asymmetric synthesis with the use of chiral catalysts (rather than other chiral agents previously discussed) was a reasonably new area of chemistry at this time, and so these results marked significant progress within organic chemistry. Hence, it is no surprise that a flurry of research in asymmetric hydrogenation reactions was observed using phosphine-containing ligands shortly after this.

Of particular note is the research completed by Noyori, and specifically his work with the phosphine-containing ligand BINAP (shown in fig. 1.3.1), which was first introduced in 1980.[25]

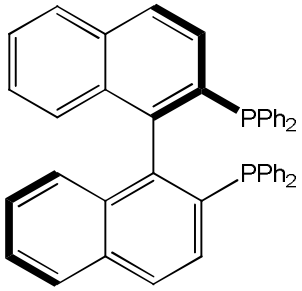

Fig. 1.3.1 (*R*)-BINAP

Initially, the rhodium complexes of both enantiomers of BINAP were prepared and used to catalyse the hydrogenation of the C=C bond of α-(acylamino) acrylic acids. High conversions (93-99 %) and optical purities (79-100 %) were observed in the hydrogenation of various α-(acylamino) acrylic acids, and crucially, the configuration of the product could be controlled by using the appropriate enantiomer of BINAP, each of which were easily obtained.[25] Ruthenium(II) complexes of BINAP were also prepared[26], and used to catalyse the hydrogenation of α,β-unsaturated carboxylic acids.[27] Conversions up to 100 % were seen for a variety of substrates, with enantiomeric excesses ranging from 83 to 97 %. Again, the product configuration could be controlled by using the appropriate enantiomer of ligand. In 1988 Noyori also showed that catalytic hydrogenation using ruthenium(II) complexes of BINAP could be used to chirally resolve racemic mixtures of allylic alcohols.[28] Later work by Noyori demonstrated the asymmetric hydrogenation of ketones using ruthenium(II) complexes of BINAP.[29] High conversions (93-97 %) and enantiomeric excesses (91-99 %) of various substrates were used, with the product configurations being dictated by the enantiomer of BINAP used. The range of substrates and classes of compounds that have been catalysed by complexes of the BINAP ligand and its variations are vast, with excellent conversions and enantioselectivities associated with it. In 2001, Noyori was awarded the Nobel Prize for Chemistry, along with Knowles (who has previously been discussed) and Sharpless (who will be discussed later).[30-32]

There are also examples of successful asymmetric hydrogenation reactions that do not involve phosphine-containing ligands. Such ligands can often by easier to work with and more open to reuse and recycling, given the readiness of

phosphine groups to oxidise. On the other hand, hydrogenation complexes are often based on precious group metals, which are also often air-sensitive and expensive. Such is the case with the iridium catalysts prepared by Fuentes.[33] Chiral diamine ligands were used in conjunction with $[IrCp^*Cl_2]_2$ and $[Ir(cod)Cl]_2$ to produce their catalysts – an example of which is given in fig. 1.3.2.

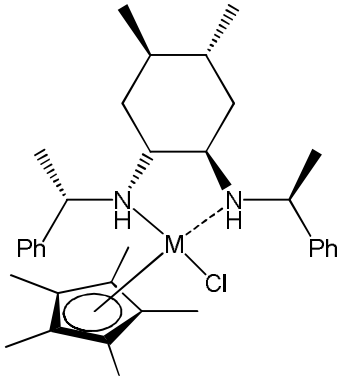

Fig. 1.3.2 Catalyst prepared by Fuentes[33] for asymmetric hydrogenation reactions

These catalysts were then used in the asymmetric transfer hydrogenation of ketones. The reaction scheme can be seen in fig. 1.3.3. Interestingly attempts to prepare an iridium cyclooctadiene complex were unsuccessful and yielded iridium black.

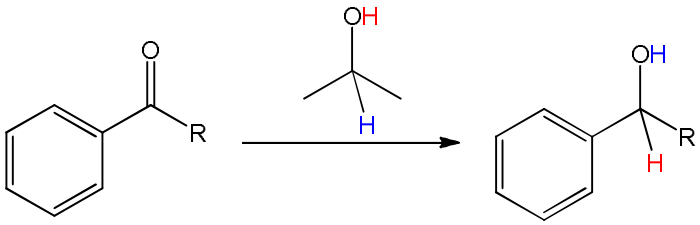

Fig. 1.3.3 Reaction scheme showing the transfer hydrogenation of ketones

Transfer hydrogenation usually involves the generation of a hydrogen source from an organic molecule in the presence of a base, rather than from hydrogen gas (direct hydrogenation). It is sometimes more appropriate to use this method,[34,35] as some substrates may be incompatible with hydrogen gas, especially given its inflammable nature.[36] Also, on a small scale, this is sometimes the preferred method as specialist equipment for higher pressures that would be required for direct hydrogenation may not be available or suitable.[35]

Some results for this reaction can be seen in table 1.3.1. The first feature to notice is that good conversions and enantioselectivities can be achieved using these chiral diamine catalysts, and so successful asymmetric hydrogenation reactions can be achieved without the use of phosphine-containing ligands. Also, of noteworthy mention is the difference on conversions and enantioselectivities observed on changing the achiral ligand {Cp* and 1,5-cyclooctadiene (cod)}. Much higher conversions and enantiomeric excesses are seen when the achiral ligand is cod. Different achiral ligands will exert different electronic effects upon the metal centre, which then binds the substrate (and in this case the hydrogen source) for catalysis. It is therefore of no surprise that with more or less electron density at the metal centre, depending on the surrounding ligands, that conversion is affected. Enantioselectivity would also be affected, as it is very much dependent on thermodynamics as previously discussed, and which enantiomer is thermodynamically favoured to form, which in turn would be heavily influenced by electronic differences around the metal centre.

Table 1.3.1 A selection of the results of the hydrogenation of ketones, as described by Fuentes et al.[33] The position of R in the product is shown in fig. 1.3.3

R	Iridium Complex	Conversion / %	ee / %
^{i}Pr	$[IrCp^*Cl_2]_2$	19	17
^{i}Pr	$[Ir(cod)Cl]_2$	61	53
Cy	$[IrCp^*Cl_2]_2$	17	26
Cy	$[Ir(cod)Cl]_2$	80	58
^{t}Bu	$[IrCp^*Cl_2]_2$	18	26
^{t}Bu	$[Ir(cod)Cl]_2$	100	60

1.3.2 Asymmetric Hydrosilylation Reaction

The asymmetric hydrosilylation reaction is similar to the hydrogenation reaction. An example of a hydrosilylation reaction is shown in fig. 1.3.4. Typical catalysts for this reaction are similar to those which catalyse the hydrogenation reaction. For example, precious metal complexes (rhodium, ruthenium, iridium, platinum

and palladium), with ligands often based around chiral phosphines and chiral diamines.

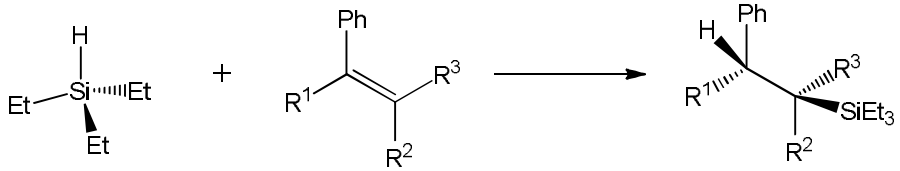

Fig. 1.3.4 Reaction scheme showing the hydrosilylation of alkenes

For example, Nishiyama reported up to 98 % conversions and 90 % enantioselectivities using a rhodium bis(oxazolinyl)bipyridine complex.[37] Ito also used a rhodium complex to catalyse the asymmetric hydrosilylation of keto esters.[38] The ligand used in this interesting complex can be seen in fig. 1.3.5.

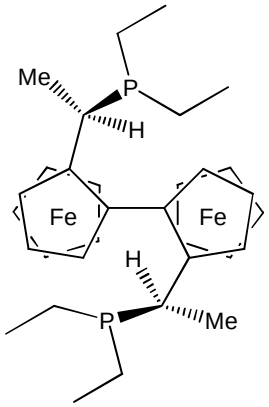

Fig. 1.3.5 Ligand used by Ito, in the subsequent preparation of rhodium complexes[38]

Ito's rhodium complex was generated in situ, and then used to catalyse the hydrosilylation of various keto esters. This was subsequently followed by the solvolysis of the product to yield the chiral alcohols. This process can be seen in fig. 1.3.6.

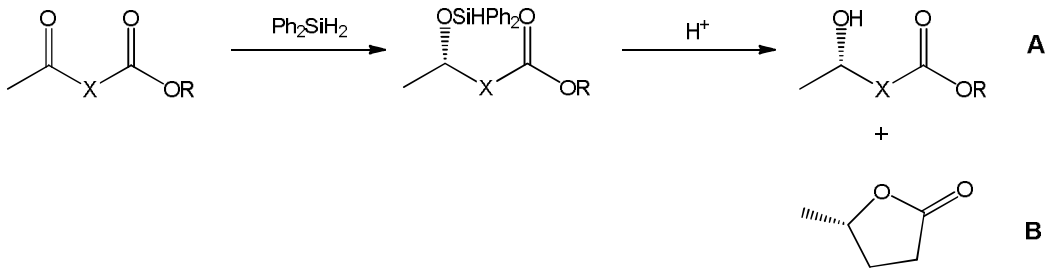

Fig. 1.3.6 Reaction scheme showing the hydrosilylation of keto esters, yielding the two products A and B

Moderate yields and good enantioselectivities were observed, which can be observed in table 1.3.2. At first glance, these results indicate that the catalysis has been quite successful. However, this reaction is not selective, in that a mixture of two products (A and B) are formed, and the resulting yields of the major product are not high enough to be able to say that this reaction is very or highly selective. In addition to this two enantiomers of each product are present, although where X is $C(CH_3)_2$ or $(CH_2)_2$, the enantiomeric excess is high enough to argue that this is acceptable in terms of product selectivity. Typically, to improve enantioselectivity and minimise the formation of the minor product, the temperature would be decreased. This is based on the difference in activation energies between two enantiomers or two products, and exploiting this fact to only provide enough energy to overcome one activation barrier (of the favourable reaction), but not both. However, in this case, the temperature is already quite low (-30 °C), and so there is little scope in optimising the temperature. Having said this, these results provide a good base for fine tuning the ligand and resulting catalyst, upon which improvements in the selectivity and enantioselectivity may be observed.

Table 1.3.2 A selection of the results of the hydrosilylation of keto esters, as previously displayed in fig. 1.3.6

X	R	Major Product, A or B	Yield / %	ee / %
CH_2	Et	A	43	32 (*S*)
$C(CH_3)_2$	Et	A	69	93 (*S*)
$(CH_2)_2$	Me	B	74	88 (*S*)
$(CH_2)_3$	Me	A	74	69*

* configuration unconfirmed

Hayashi has published research which also used ferrocenyl-phosphine type ligands.[39] The rhodium complexes of these ligands were also generated in situ and used to catalyse the asymmetric hydrosilylation of ketones. In this work, the conversions and enantioselectivities reported were much higher in comparison to that reported by Ito.[38] The ligand used and subsequent results can be seen in fig. 1.3.7 and table 1.3.3, respectively.

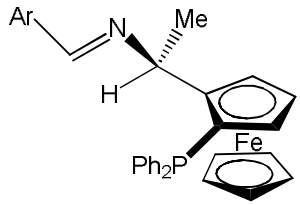

Fig. 1.3.7 Ligand used by Hayashi et. al. in the subsequent preparation of rhodium complexes[39]

Table 1.3.3 A selection of results of the hydrosilylation of ketones

Ar (Ligand)	Ketone	Yield / %	ee / %
Ph	PhCOEt	98	86 (*S*)
Ph	PhCOMe	98	87 (*S*)
(*m*-CF_3)Ph	*p*-ClC_6H_4COMe	98	81 (*S*)
(*m*-CF_3)Ph	PhCOMe	98	90 (*S*)
(*p*-CF_3)Ph	PhCOMe	98	89 (*S*)
C_6F_5	PhCOMe	97	89 (*S*)

Recently, less traditional metals have been used to catalyse asymmetric hydrosilylations. This is due to cost and scarcity of certain metals. Zhang used copper(II) in conjunction with their phosphine containing ligands in the hydrosilylation of ketones, with good results.[40] High conversions of up to 95 % and enantiomeric excesses of up to 96 % were recorded for a variety of ketones. Given the expense and air sensitivity of precious group metals, to find complexes that produce equally good catalytic results that are cheaper and easier to prepare and handle is a significant challenge of the 21st century and these results are very promising. On a similar topic, Inagaki has reported iron(II) and cobalt(II) complexes that catalyse the asymmetric hydrosilylation of ketones.[41] Their trinitrogen-chelating ligand can be seen in fig. 1.3.8, and selected catalytic results in table 1.3.4.

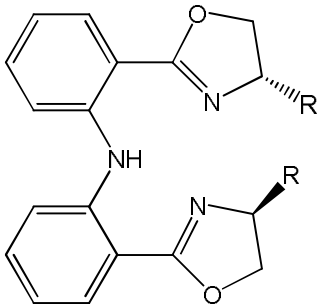

Fig. 1.3.8 Ligand used by Inagaki in the subsequent preparation of iron and cobalt complexes[41]

Table 1.3.4 A selection of results of the hydrosilylation of ketones, using iron(II) or cobalt(II) complexes which were generated *in situ*

R (Ligand)	Metal Precursor	Yield / %	ee / %
^{i}Pr	$Fe(OAc)_2$	99	61
^{t}Bu	$Fe(OAc)_2$	90	68
$CHPh_2$	$Fe(OAc)_2$	99	73
Ph	$Fe(OAc)_2$	92	20
^{i}Pr	$Co(OAc)_2$	99	70
^{t}Bu	$Co(OAc)_2$	99	69
$CHPh_2$	$Co(OAc)_2$	99	54
Ph	$Co(OAc)_2$	99	94

1.3.3 Asymmetric Aldol Reaction

The C-C bond forming asymmetric aldol reaction is arguably one of the most important reactions in organic chemistry. Up until 1989, this incredibly important reaction was controlled using stoichiometric amount of chiral auxiliaries,[42] which for reasons previously discussed is not ideal. In 1989, Mukaiyama presented research detailing a *catalysed* asymmetric aldol reaction,[43] and this, together with Mukaiyama's subsequent research in this area, changed the way the aldol reaction was approached and utilised. Some of Mukaiyama's work will now be discussed.

In 1991, Mukaiyama showed that a chiral diamine tin(II) complex could be generated *in situ* and used to generate chiral α-unsubstituted β-hydroxy thioesters.[42] The diamine can be seen in fig. 1.3.9.

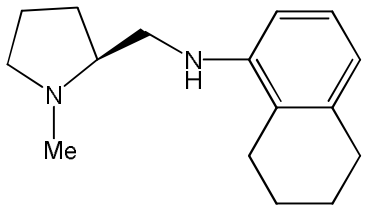

Fig. 1.3.9 Ligand used by Mukaiyama et. al. in the subsequent preparation of tin(II) complexes[42]

Results using this tin complex can be seen in table 1.3.5. Good yields (up to 81 %) and high enantiomeric excesses (up to 93 %) were observed for a range of substrates. However, this particular piece of research demanded specific reaction conditions in order to achieve these results. Firstly, there is a need to add trimethylsilyl triflate into the reaction to regenerate the catalyst. However, in doing this the enantioselectivity is lowered, as the trimethylsilyl triflate enables a competing achiral aldol reaction to occur. In order to minimise this, a very specific slow addition rate of the substrates to the catalyst was used. Moreover, the variation of solvent has a substantial effect on the catalytic results. Having said this, this work provided a strong basis for future research into the asymmetric aldol reaction.

Table 1.3.6 A selection of the results of the aldol reaction catalysed by Mukaiyama,[42] using the tin(II) complex of the ligand shown in fig. 1.3.9

Aldehyde	Yield / %	ee / %
$CH_3(CH_2)_6CHO$*	79	93
$CH_3(CH_2)_3CHO$	79	91
o-$C_6H_{11}CHO$	81	92
$^{i}PrCHO$	48	90

* Dichloromethane was used as a solvent. Otherwise, propionitrile was the reaction solvent

Since then, numerous transition metal complexes have been employed to catalyse the asymmetric aldol reaction. For example, Ito has published a considerable amount of research in the catalysis of the aldol reaction by precious metal complexes, namely gold,[44] silver[45] and rhodium.[46] Group 4 transition metal complexes of BINOL have also been used in the asymmetric aldol reaction[47,48], BINOL chiral ligand that is commonly utilised in asymmetric synthesis. Other transition metals that have been used in catalysing the aldol reaction include zinc,[49] nickel[50] and commonly, copper,[51-55] which will now be discussed in more detail.

The vast contribution to asymmetric synthesis by David Evans has previously been described. Among many reactions, the asymmetric aldol reaction has been heavily researched by Evans, and in particular, how it can be catalysed by copper(II) complexes.[53] In 1999, Evans used the chiral copper(II) complex shown in fig. 1.3.10 to catalyse the asymmetric aldol addition of enolsilanes to pyruvate esters, as shown in fig. 1.3.11.

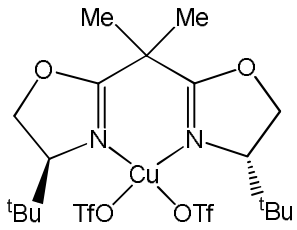

Fig. 1.3.10 Copper(II) complex, which Evans used to catalyse the aldol reaction given in fig. 1.3.11

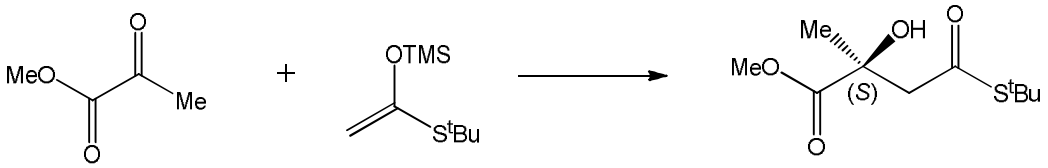

Fig. 1.3.11 Aldol addition of enolsilanes to pyruvate esters, as described by Evans[53]

Evans varied the reaction conditions in a number of ways, including slight modifications to the ligand, changing the counterion of the complex, different substrates, solvents, catalyst loadings, temperatures and reaction times. High

conversions (up to 100 %) and enantiomeric excesses (up to 99 %) were observed upon optimisation of the reaction conditions. On varying the conditions, the results observed were as expected. Decreasing the reaction temperature increased enantioselectivity, for reasons previously discussed. This then had a knock-on effect on the solvent variation. THF was found to be the most effective solvent, at a temperature of -78 °C, giving a yield of 95 % and enantiomeric excess of 99 %. This was closely followed by dichloromethane, giving a yield of 93 % and an enantiomeric excess of 98 %. However, when other solvents such as acetonitrile, nitromethane and dioxane were employed, higher temperatures were required due to their melting points, and so significantly lower enantioselectivities were observed. When designing an asymmetric synthesis, where both temperature and solvent can be so crucial to the outcome of the reaction, the factor of melting points of solvents is clearly an important consideration in terms of future optimisation of the reaction. Evans also found that the solvent used affected the catalyst loading that could be used. For example, in THF, the lowest loading that could be successfully employed was 1 mol %, requiring a reaction time of only 1 hour for nearly full conversion. However, on changing the solvent to dichloromethane, the lowest loading to be used successfully was 2 mol %, double that of THF. Also, the reaction time required for nearly full conversion was 14 hours, and so it is obvious that solvent choice in a reaction can be very important, perhaps the most important factor after substrate and ligand choices. Also, noteworthy in the choice of substrate and ligand, Evans found that variation of the substrate had a massive effect on the enantioselectivities observed, seeing enantiomeric excesses range from 2 to 95 %. This is common in asymmetric catalysis, as previously discussed. However, Evans showed that by modifying the ligand to suit the substrates used, very high enantiomeric excesses could be achieved.

Langner published work on copper(II) catalysed aldol reactions in 2005, and found very similar finding to that of Evans.[55] An example of this reaction and the ligand used by this group can be seen in fig. 1.3.12.

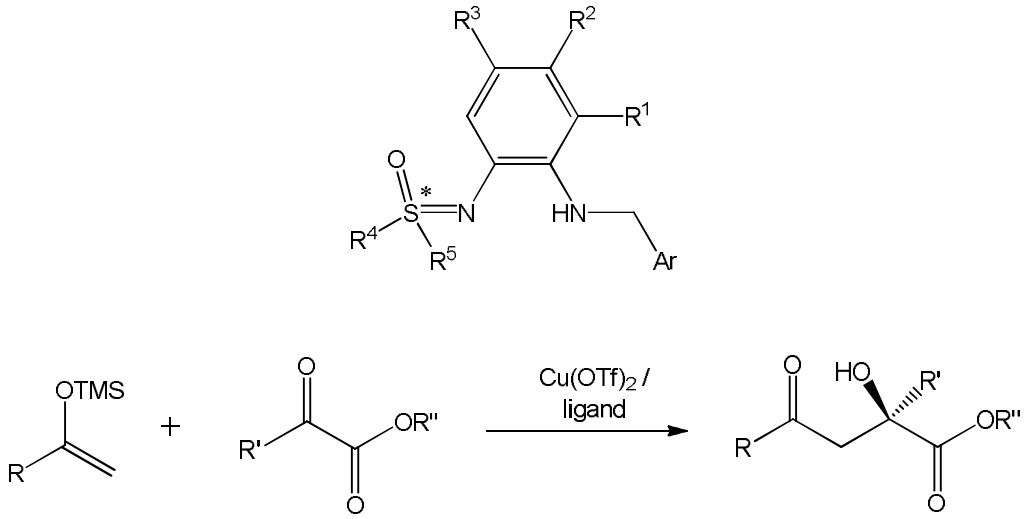

Fig. 1.3.12 The ligand used in the preparation of the copper(II) complex is shown, along with the aldol reaction that the copper(II) complex catalysed

The group varied substrate, ligand, temperature, solvent and loading. Again, they found that an increase in temperature saw a drop in enantioselectivity, and they also observed that the most effective reaction solvent was THF, closely followed by dichloromethane. The conversions and enantiomeric excesses observed were high (86 % conversion, 93 % enantiomeric excess), although not as high as those seen by Evans – this is probably more to do with the catalysts (and in particular the ligands) themselves. Langner also showed that in varying the substrates used, the ligands (containing many sites where simple modifications could be made) could be tailored to suit the substrates. Furthermore, he also found that successful substrate-ligand combinations were very predictable, and so any future trial and improvement methods of finding a suitable ligand to suit a substrate could be massively reduced, if not removed entirely. This is a very useful tool to have in asymmetric catalysis, and can be attributed to a more thorough understanding of the reaction mechanism.

Another common area of work within the asymmetric aldol reaction is that of "metal-free" catalysis. Much of this work has involved the amino acid proline, and its deriviatives, and has been investigated by many research groups.[56-60] Although it can be useful not to use potentially expensive and sometimes toxic metals, research has highlighted some fundamental problems with these proline catalysed reactions. Often, long reaction times are required with large amounts

of proline needed for catalysis (in comparison with similar transition metal catalysts). In addition to this, large excesses of the substrate were often necessary, which in the cases of expensive and difficult to prepare ketones, is completely impractical. Also, on varying the substrates, in some cases results can be quite poor, and proline, shown in fig. 1.3.13. does not have many positions where modifications could be made improve catalytic results.

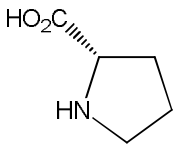

Fig. 1.3.13 (*S*)-Proline

Therefore, it is clear that although this metal-free catalysis shows much promise for future catalysis, there are sizeable problems that must be addressed first, which in turn has spawned a great deal of research. Gong used amide derivatives of proline to catalyse the aldol reaction; the catalyst and reaction can be seen in fig. 1.3.14.[61]

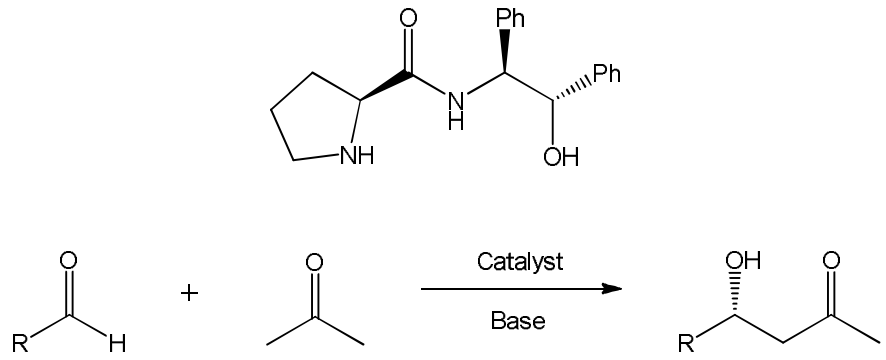

Fig. 1.3.14 A derivative of proline is shown, which was used to catalyse the aldol reaction also pictured here

A variety of substrates were tested, with a range of conversions (12-93 %) and enantiomeric excesses (81-99 %) being observed. These results are very promising, in that by modifying proline to a prolinamide derivative the range of substrates that can be reacted successfully has dramatically improved. However, large amounts of the catalyst (20 mol%) are still required, with long reaction times (24-48 hours). Zhao saw promise in this work, and proposed that these

issues could be addressed by introducing another prolinamide group into the catalyst, thus doubling the catalytic sites available per catalyst molecule.[62] The catalyst is displayed in fig. 1.3.15.

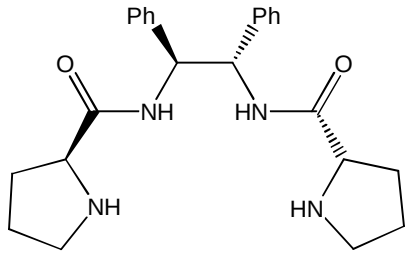

Fig. 1.3.15 A derivative of proline is pictured, which was used to catalyse the asymmetric aldol reaction described by Zhao[62]

In testing a similar range of substrates as Gong, the conversions observed show a marked improvement (52-88 %), and enantiomeric excesses are still high (82-98 %). Also, the reaction time has been halved (12-24 hours), which is preferable. Comparing these results to that of transition metal catalysts, it can be seen that conversions and enantioselectivities can be matched in the absence of a metal centre. Thus, reducing the overall expense of the reaction, and in some cases simplifying the process by not having to remove all traces of metal from the product, which is important in industries such as pharmaceuticals. However, the amounts of catalyst required are still much greater in metal-free catalysis.

1.3.4 Asymmetric Nitroaldol Reaction

An adapted version of the aldol reaction is the nitroaldol, or Henry reaction. It is named after Louis Henry, who first reported this in 1895. An example of the nitroaldol reaction can be seen in fig. 1.3.16.

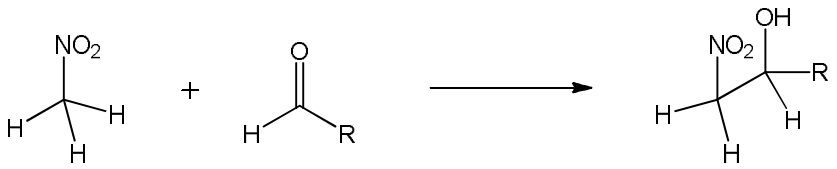

Fig. 1.3.16 An example of the nitroaldol reaction

The niroaldol reaction is a carbon-carbon bond forming reaction, producing a β-hydroxy nitro product. This can be reacted further to yield various functional groups, including β-aminoalcohols and α-hydroxy carboxylic acids.[63,64] Often a base is required, in order to deprotonate the nitroalkane (which is an essential part of the reaction mechanism). However, there are examples catalysing this reaction in the absence of a base.[64-67] In these cases, commonly the counterion or ligand contains basic moieties, which take on the role of the absent base. A variety of transition metals have been used to catalyse the nitroaldol reaction, which include zinc,[68] cobalt,[69] chromium,[70] rhodium[71] and lanthanides.[72] The most commonly used transition metal complex used is copper, and in particular copper(II), some examples of which will be discussed shortly.

Kowalczyk used a chromium complex with Jacobsen-type ligands[73] to catalyse the asymmetric nitroaldol reaction.[74] Firstly, they kept their substrates constant, and varied the substituents of the ligand, in order to determine which catalyst performed best in terms of enantioselectivity. The resulting catalyst can be seen in fig. 1.3.17. There was much variation in conversion and enantioselectivity, as expected; we have seen previously that the catalyst often has to be fine tuned to suit the substrates.

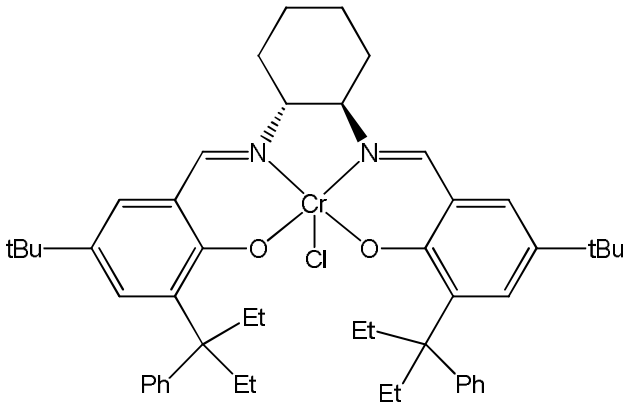

Fig. 1.3.17 Jacobsen-type complex, used by Kowalczyk to catalyse the asymmetric nitroaldol reaction[74]

The catalyst was then tested with a multitude of aldehyde substrates (the nitroalkane was nitromethane, and was kept constant). Some of these results can be seen in table 1.3.7.

Table 1.3.7 A selection of the results of the nitroaldol reaction catalysed by Kowalczyk[74]. The reaction was previously shown in fig. 1.3.16

R	Yield / %	ee / %
Ph	77	93
p-Ph-C_6H_4	82	94
p-Cl-C_6H_4	76	85
m-Cl-C_6H_4	74	84
2-naphthyl	92	91
1-naphthyl	51	70
2-furyl	56	86
PhCH=CH	25	80
cyclohexyl	38	90

The catalyst was originally chosen on the strength of the high enantioselectivities observed (93 %), which also gave a good yield (62 %). The results demonstrate that the enantioselectivities are still very high, however, there is much variation in the yield, with one yield being as low as 25 %. This highlights a common feature of asymmetric catalysis, in that often there is a trade-off to be made between conversion and enantioselectivity. In asymmetric catalysis, enantioselectivity is commonly favoured, however when chiral auxiliaries are used, enantioselectivity is less of an issue, due to the greater ease of separating diastereomers post-reaction, as previously discussed.

As previously mentioned, copper(II) complexes are heavily used to catalyse the asymmetric nitroaldol reaction. Christensen used copper(II) bisoxazoline complexes in the nitroaldol reaction of α-keto esters and nitromethane;[75] the ligand is shown in fig. 1.3.18.

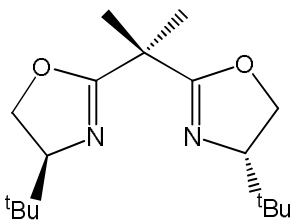

Fig. 1.3.18 Bisoxazoline ligand, subsequently used to prepare copper(II) complexes

When varying the substrate, good conversions (up to 99 %) and enantiomeric excesses (up to 94 %) were observed. The interesting features of their research are in varying other factors within the reaction. The group varied the base used, the results of which can be seen in table 1.3.8.

Table 1.3.8 A selection of results which show the effect of varying the base on the nitroaldol reaction

Base	Yield / %	ee / %
Et_3N	95	92
N-Me-morpholine	65	83
$PhNMe_2$	14	9
Bn_3N	10	14
$Et(^iPr)_2N$	31	69
pyridine	6	13
K_2CO_3	95	27

The results show a range of yields (6-95 %) and enantiomeric excesses (9-92 %), which demonstrate that the choice of base can be a very important factor in finding suitable reaction conditions. This set of results corresponds to one catalyst and set of substrates specifically. The role of the base in the nitroaldol reaction is to deprotonate the nitroalkane, which then binds to the metal centre along with the aldehyde substrate, and subsequently the nitroaldol reaction occurs.[75,76] However, just as modification of catalysts to suit substrates is commonly observed, so could changing the base to suit activation of a particular substrate for reaction. In addition to this, the catalyst used is important, as some bases may bond strongly to the metal centre, and hence the rate of substrate activation may change dramatically. Therefore in this case, triethylamine is clearly the best base to use, providing the highest yields and enantioselectivity, but it may be that on varying substrate and catalyst in the future, this is no longer the case.

The catalysis so far has described the nitroaldol reaction of various substrates with nitromethane, and unfunctionalised nitroalkane. The nitroaldol reaction of functionalised nitroalkanes can also be successfully catalysed. Blay used a

copper(II) dinitrogen-chelating complex to catalyse the nitroaldol reaction with bromonitromethane.[77] The ligand and reaction scheme is shown in fig. 1.3.19.

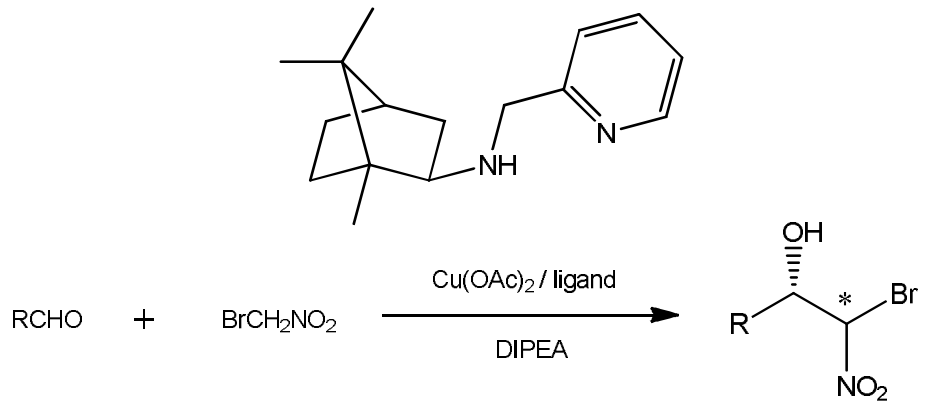

Fig. 1.3.19 The ligand is shown which is subsequently used to generate a copper(II) complex *in situ*, which catalyses the nitroaldol reaction, also pictured here

A variety of aldehydes were reacted with bromonitromethane, with excellent yields observed in all cases (72-99 %). A wide range of diasteroselectivities (8-74 %) were observed, although most diasteroselectivities were high. In addition, excellent enantioselectivities were observed (81-98 %). This research is significant because through using functionalised nitroalkanes, the synthesis of polyfunctionalised molecules is more accessible. This is of particular importance within the synthesis of natural products.

Bandini used tetrachelating amine and imine ligands in conjunction with copper(II) acetate to catalyse the nitroaldol reaction.[78] The corresponding ligands are shown in fig. 1.3.20.

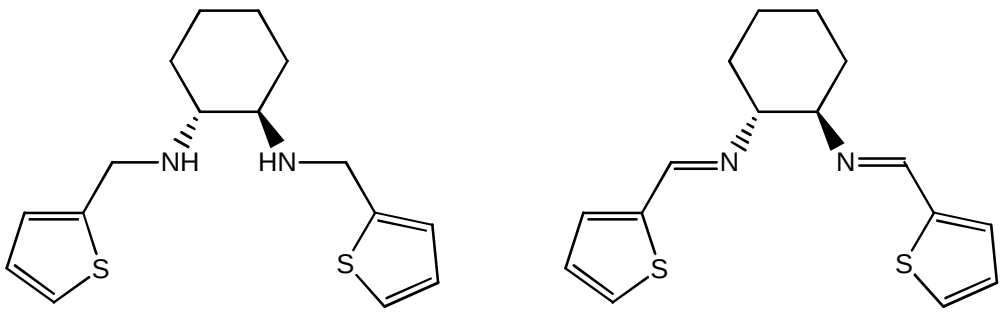

Fig. 1.3.20 Bandini's chiral thiophene ligands

A variety of aldehydes were reacted with nitromethane, with excellent conversions and enantioselectivities. Interestingly, the authors showed that by either using the amine ligand (DAT) or the imine ligand (DIT), the stereochemical configuration of the product could be dictated, with the DAT forming (*S*) and DIT the (*R*) enantiomer.

Constable compared monometallic and bimetallic copper(II) complexes in the asymmetric catalysis of the nitroaldol reaction of nitromethane and 4-nitrobenzaldehyde.[79] The catalysts used by the authors are shown in fig. 1.3.21. A selection of results can be seen in table 1.3.9.

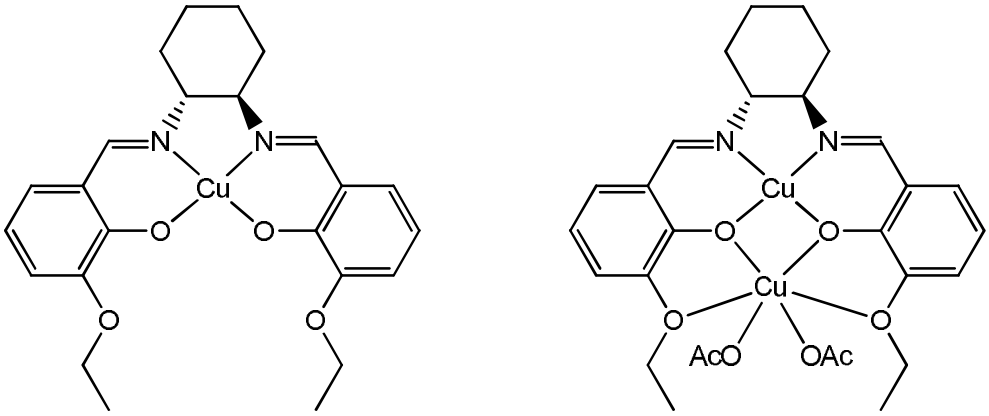

Fig. 1.3.21 The monometallic and bimetallic copper(II) complexes used by Constable in the catalysis of the asymmetric nitroaldol reaction[79]

Table 1.3.9 A selection of results of the nitroaldol reaction comparing the catalysts shown in fig. 1.3.21

Catalyst	Solvent	Yield / %	ee / %
Monometallic	Ethanol	86	23
Bimetallic	Ethanol	94	39
Monometallic	THF	81	25
Bimetallic	THF	92	39
Monometallic	Toluene	41	48
Bimetallic	Toluene	61	77

The results show a significant increase in enantioselectivity with the bimetallic catalyst. In the bimetallic catalyst, there will be less room sterically around the metal centres for catalysis to occur, which could force the substrates into specific positions, which in turn could increase enantioselectivity. This highlights the importance of effective catalyst design in asymmetric catalysis.

1.3.5 Asymmetric Epoxidation Reaction

The epoxidation reaction represents one of the most useful and effective methods of introducing a carbon-oxygen bond into a molecule. An example of this reaction can be seen in fig. 1.3.22.

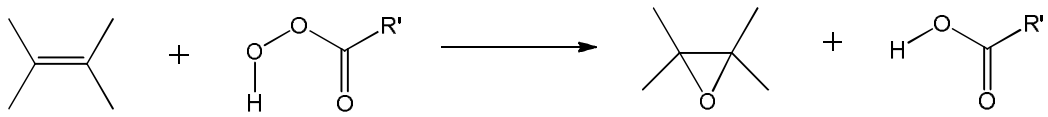

Fig. 1.2.22 A typical epoxidation reaction

In 1990, Eric Jacobsen published his research detailing the catalysis of the asymmetric epoxidation reaction.[80] He showed that the manganese(III) complex of his ligand, shown in fig. 1.3.23, could be used to catalyse epoxidations.

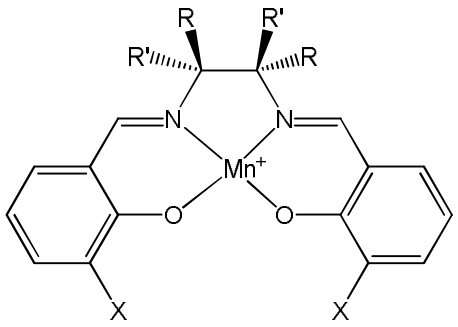

Fig. 1.2.23 Jacobsen's manganese(III) complex, for the catalysis of epoxidation reactions

A range of conversions (36-93 %) and enantiomeric excesses (20-93 %) were observed when the complex was used to catalyse the epoxidation of a wide variety of alkenes. The research showed a great deal of promise for the

improvement of these initial results in a number of ways. Firstly, the ligands were simple to prepare, and contained many sites for varying substituents within the ligand, and so there is tremendous scope for fine tuning the catalyst. Also, the chiral centres within the ligand were very close in proximity to the metal centre, and so Jacobsen hypothesised that this would provide "better stereochemical communication in the epoxidation step".[80] Finally, due to the geometry of the ligand, it was clear to Jacobsen that by providing steric bulk in the appropriate regions of the ligand, the direction of the entry of the substrate and subsequent binding could be dictated, thus providing greater stereoselectivities. A short time after this initial work was published, Jacobsen confirmed his hypotheses.[73] In this research, Jacobsen had modified the ligand by "locking" the ligand in place across the diimine bridge, by introducing a cyclohexane moiety, as shown in fig. 1.3.24.

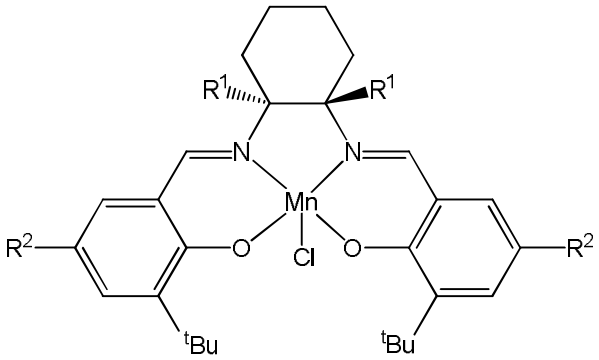

Fig. 1.3.24 The manganese(III) complex of Jacobsen's diaminocyclohexane-based ligand

Since the movement and rotation within the ligand was so much more restricted, Jacobsen was able to introduce sterically bulky groups in certain positions, so as to direct the entrance of the alkene substrate from a particular face. This can be seen in fig. 1.3.25.[73]

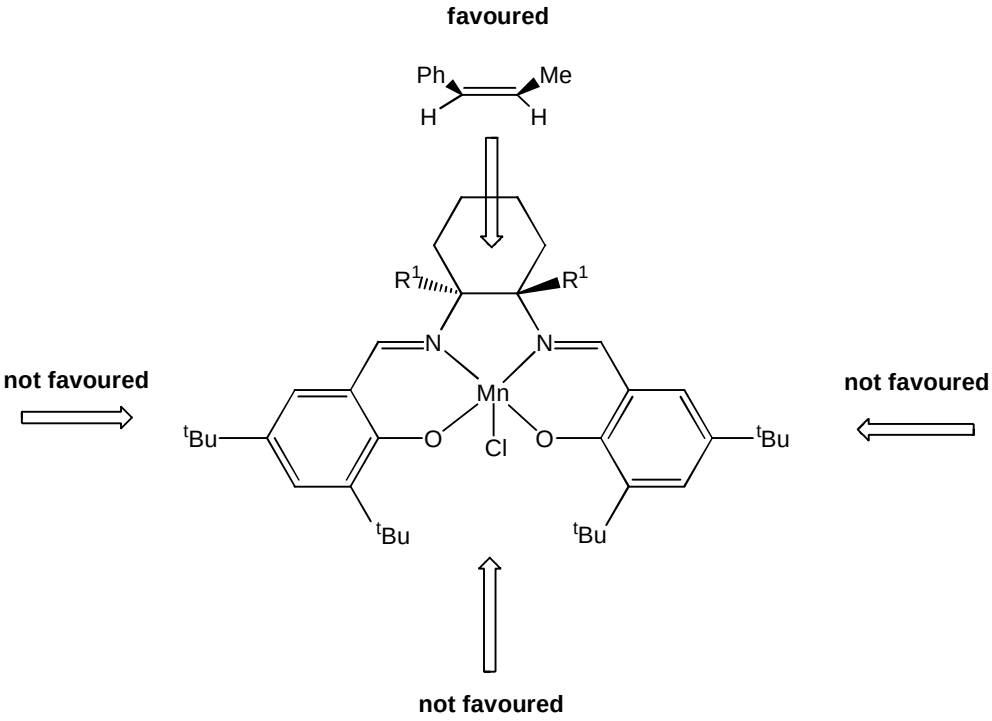

Fig. 1.3.25 Showing the possible directions of substrate approach towards the metal centre

As a result of this, the catalytic results were markedly greater, with conversions now ranging from 63 to 96 % and excellent enantiomeric excesses of up to 98 %. The results can be seen in table 1.3.10. The improvement in results highlights the importance of fully understanding a reaction mechanism, as once this has been grasped, the mechanism can then be manipulated to suit the substrates, catalysts and reaction conditions.

Table 1.3.10 A selection of results of the asymmetric epoxidation reaction, catalysed by the complex shown in fig. 1.3.24

Alkene	Yield / %	ee / %
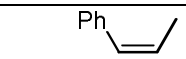	84	92
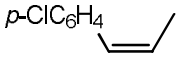	67	92
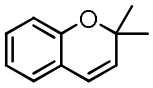	72	98
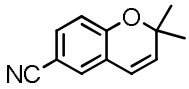	96	97
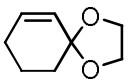	63	94
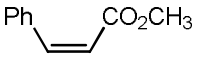	65	89

Over the past 20 years, Jacobsen has built on this success, mainly for asymmetric epoxidations, but it has also been shown that due to the versatility of his ligands, many different transition metal complexes can be formed, and so many reactions can be catalysed. Jacobsen more recently showed that as well as exerting diastereoselectivity and enantioselectivity on a reaction, regiocontrol could also be exerted on an already chiral substrate.[81] The catalyst and reaction scheme for this can be seen in fig. 1.3.26.[81,82]

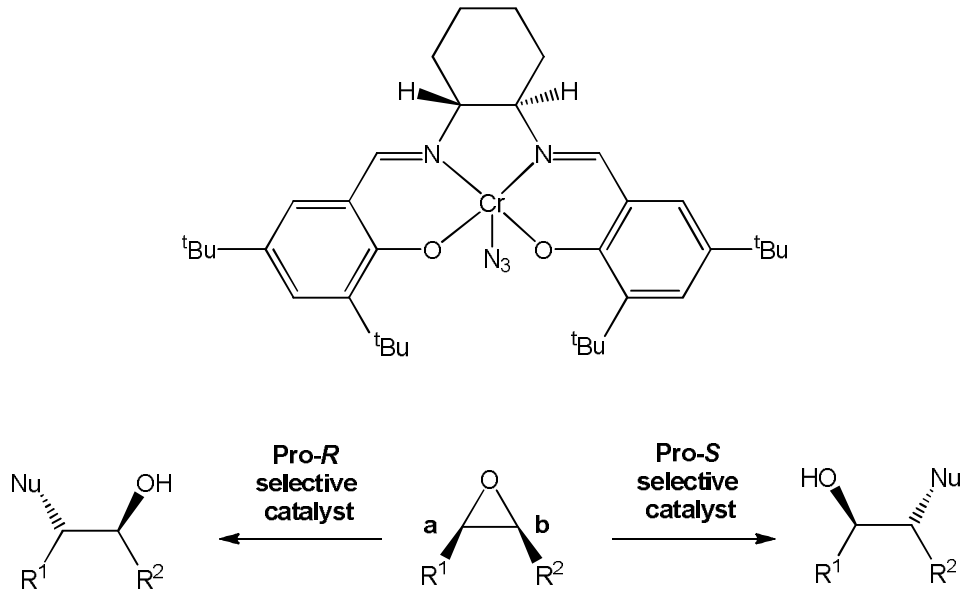

Fig. 1.3.26 Showing the chromium(III) catalyst based on Jacobsen's ligand, and the use of either diastereomer of Jacobsen's ligand in the asymmetric ring-opening of an epoxide, through attack at either site a or b.

The results can be seen in table 1.3.11. The use of the achiral catalyst acts as a control, and is set as a marker to compare the performance of the chiral catalysts against for their performance in exerting regiocontrol. The results clearly show that the chirality within the catalysts can be used in conjunction with the chirality in the substrates to promote nucleophilic attack at a particular C-O bond. In terms of the range of substrates available, the results indicate that both *cis* and *trans* epoxides can be successfully ring-opened, although to be able to say this with more certainty, further testing of many more epoxides would be required.

Table 1.3.11 A selection of the results of the ring-opening of epoxides, as shown in fig. 1.3.26

Epoxide	Catalyst	Regioselectivity*
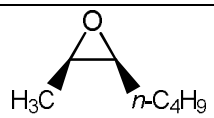	Achiral	1:1
	R,R	2:1
	S,S	1:4
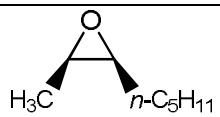	Achiral	1:1
	R,R	2:1
	S,S	1:4
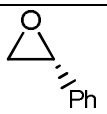	Achiral	4:1
	R,R	1:7
	S,S	18:1
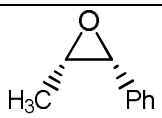	Achiral	3:1
	R,R	1:4
	S,S	45:1
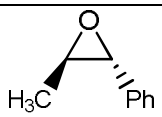	Achiral	1:9
	R,R	1:1
	S,S	1:84

* Regioselectivity is expressed as a ratio of (attack at site a):(attack at site b)

Many research groups have since used Jacobsen's ligand, or deviations of it in asymmetric catalysis. For example, Gilheany has used a variation of Jacobsen's ligand in the preparation of a chromium(V) catalyst for asymmetric epoxidations, seeing conversions of 40-60 % and high enantiomeric excesses of up to 92 %.[83] Similarly, Katsuki has also used a derivative of Jacobsen's ligand to prepare a

manganese catalyst for asymmetric epoxidations, although somewhat less successfully than other groups (conversions of 12-37 % and enantiomeric excess of 20-50 %).[84]

Sharpless has also published a considerable amount of research into catalysing asymmetric epoxidation reactions, using titanium tartrate catalysts. At first, stoichiometric quantities of catalyst were required, which is not ideal. However, Sharpless reported an interesting method to reduce the amount of catalyst needed, which was to perform the reactions in the presence of molecular sieves.[85] In using less catalyst, the reaction is cheaper to perform and more efficient. Also, the group found that using less catalyst improved the selectivity of the epoxidations, with lower quantities of side-products observed. Sharpless investigated the reasons into this behaviour with molecular sieves, and concluded that its role was to remove water from the reaction, which otherwise poisons the catalyst. This is an important consideration in catalysis, as not only can it hinder the reaction, it can also render the catalyst useless. One may then ask the question: why not perform the reaction in dry, air free conditions? Sharpless also addressed this, and found that the problem lay in the unavoidable side reactions that occur. Such reactions include oxidation of the alkene to an aldehyde, and the catalyst encouraging the decomposition of the oxidant, a hydroperoxide. The molecular sieves absorb the water generated, thus saving the catalyst from poisoning, and hence allowing the reaction to work with better conversions, enantioselectivities and at a faster rate.

1.3.6 Asymmetric Michael Reaction

Much work has been carried out with respect to the asymmetric Michael reaction, however much if this has involved the use of chiral auxiliaries, rather than catalysts. The transition metals that are commonly used to catalyse this reaction are cobalt,[86,87] copper,[88,89] and nickel.[87]

Botteghi used nickel(II) and cobalt(II) complexes to catalyse the asymmetric Michael reaction.[87] The nickel(II) complexes catalysed the addition of nitromethane to chalcone (ligand shown in fig. 1.3.27), and the cobalt(II) complexes catalysed the addition of methyl-1-oxo-2-indanecarboxylate to methyl vinyl ketone (ligand shown in fig. 1.3.28).

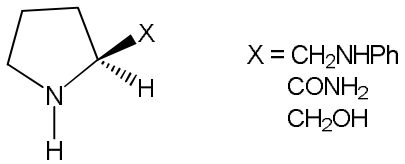

Fig. 1.3.27 Ligand which is subsequently used to prepare nickel(II) complexes for use in the asymmetric Michael reaction

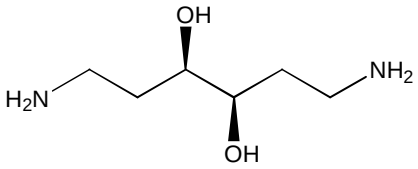

Fig. 1.3.28 Ligand which is subsequently used to prepare cobalt(II) complexes for use in the asymmetric Michael reaction

In the case of the nickel(II) catalysis, there was a considerable amount of variation seen in yield (0-84 %) and enantioselectivity (5-61 %). In the case of the cobalt(II) catalysis, the yields were much improved (46-95 %), but enantioselectivity had dropped dramatically (1-38 %). However, there is scope here for future work and potential improvements to be made. For example, lowering the temperature may increase the enantioselectivity considerably without detrimentally affecting the conversion too much. Also, the catalyst could be modified to improve the results. Also, we have seen previously that varying the substrate can have huge effects on the catalytic results – perhaps

there are a specific group of substrates that would suit these catalysts more than the substrates used in this piece of research.

Shi has reported the use of copper(I) catalysts in the asymmetric Michael addition of diethylzinc to α,β-unsaturated ketones. The ligand used and the reaction catalysed can be seen in fig. 1.3.29.

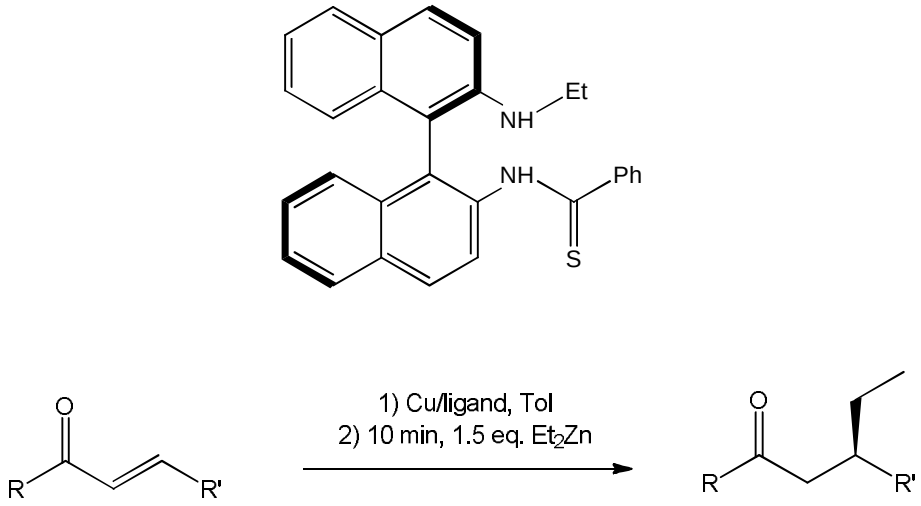

Fig. 1.3.29 Shows the ligand used to generate copper(I) complexes *in situ*, to catalyse the Michael reaction also shown here

The results can be seen in table 1.3.12. The yields and enantioselectivities can be described as moderate. This group tried varying the reaction conditions in multiple ways, including changing temperature, substrate and catalyst variation, copper salt variation, and changing the reaction time. The only change in conditions that had a notable effect on the catalytic results was to shorten the reaction time (from 48 h to 12 h). Although the resulting yield was excellent (98 %), the enantioselectivity was very poor (6 %). Again, this shows us that there is often a trade-off between conversion and enantioselectivity. In this case, in order to obtain an enantioselectivity that is acceptable, a lower conversion may have to be accepted.

Table 1.3.12 A selection of the results of the asymmetric Michael reaction, as previously shown in fig. 1.3.29

R	R'	Yield / %	ee / %
Ph	Ph	47	51
1-$C_{10}H_7$	Ph	28	73
Ph	*p*-BrC_6H_4	36	64
p-BrC_6H_4	Ph	25	51

1.3.7 Asymmetric Diels-Alder Reaction

In 1983, Danishefsky published the first example of a transition metal complex used as a catalyst for the *asymmetric* Diels Alder reaction.[90] Prior to this, the asymmetric Diels Alder reaction was enabled by the use of chiral auxiliaries. Danishefsky reported the use of a chiral europium catalyst, and used it in conjunction with chiral auxiliaries based on menthol. The idea of this was to test what effect, if any, a chiral catalyst would have on the reaction, and if a significant effect was observed, one could decide on a direction in which to take future research. Significant diastereoselectivities were seen, which could not be attributed to the chiral auxiliary alone, and the group concluded that chiral catalyst-chiral auxiliary intereactions were occurring. Not only is this an interesting method to impart diastereoselectivity into the Diels Alder reaction, it also showed that chiral transition metal catalysts could be used to impart enantioselectivity into a Diels Alder reaction.

Jacobsen's extensive research into the asymmetric epoxidation reaction has already been discussed. It was commented on that given the versatility of his ligand, it could be used in other asymmetric reactions, and the asymmetric Diels Alder reaction is one of these.[91] The catalyst used and reaction catalysed can be seen in fig. 1.3.30.

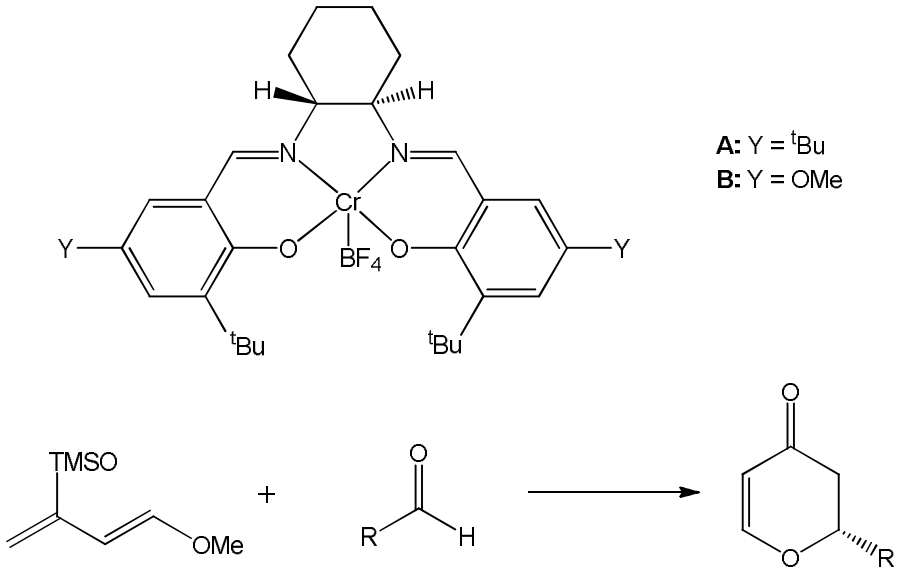

Fig. 1.3.30 Shows Jacobsen's chromium(III) complex, and the Diels-Alder reaction that this complex catalyses

The group used molecular sieves during the reaction, they reported that without this, low conversions and enantioselectivities were observed. This behaviour has been previously discussed with respect to asymmetric epoxidations – it was concluded that competing side reactions were producing water which was poisoning the catalyst. Some of the results can be seen in table 1.3.13.

Table 1.3.13 A selection of results from the catalysis of the Diels-Alder reaction previously shown in fig. 1.3.30

Catalyst	R	Yield / %	ee / %
A	Ph	85	87
B	Ph	98	65
A	C_6H_{11}	71	93
B	C_6H_{11}	76	85
A	*n*-C_5H_{11}	86	83
B	*n*-C_5H_{11}	85	62

Good yields and enantiomeric excesses are observed. There is a slight pattern in comparing catalysts A and B (shown in fig. 1.3.30), in that catalyst A tends to favour enantioselectivity, and catalyst B conversion. However, the results are so good and the differences in results between catalysts small, that this is only a

minor point. On the whole, these results demonstrate the point that was made earlier that Jacobsen's ligand can be successfully employed in various reactions. Moreover, many other research groups have taken this into consideration when completing their own research into the asymmetric Diels Alder reaction, and used variations of Jacobsen's ligand.[92-94]

Other transition metals that have commonly been used to catalyse the asymmetric Diels Alder reaction are titanium,[95-97] copper,[98-100] rhodium,[101] zinc[102] and cobalt.[103] Yu used a titanium complex to catalyst the asymmetric Diels Alder reaction – the corresponding ligand is shown in fig. 1.3.31. The reaction scheme was shown previously in fig. 1.3.30.

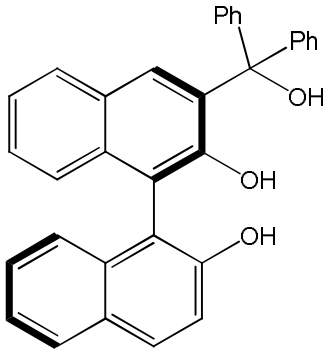

Fig. 1.3.31 Ligand used in the subsequent preparation of titanium complexes for the catalysis of the asymmetric Diels-Alder reaction

The results can be seen in table 1.3.14. Excellent yields and enantioselectivities were observed for a wide range of aldehyde substrates, which without modifying the catalyst somehow, is a rare occurrence. Having said this, if the diene was varied with the aldehyde remaining constant, perhaps this would not be the case, and some catalyst modification would be required to achieve results analogous to those displayed in table 1.3.13. The authors stated that other catalysts were screened in addition, but the results observed were poor in comparison.

Table 1.3.14 A selection of results of the Diels-Alder reaction previously shown in fig. 1.3.30, catalysed by the titanium complex of the ligand shown in fig. 1.3.31

Catalyst	Yield / %	ee / %
Benzaldehyde	98	94
4-nitrobenzaldehyde	91	99
3-nitrobenzaldehyde	86	96
2-nitrobenzaldehyde	94	92
4-chlorobenzaldehyde	99	93
3-chlorobenzaldehyde	99	95
2-chlorobenzaldehyde	82	87
4-methylbenzaldehyde	89	93
3-methylbenzaldehyde	98	90
2-naphthbenzaldehyde	99	93
4-cyanobenzaldehyde	92	99
4-bromobenzaldehyde	98	92
4-trifluoromethylbenzaldehyde	98	88
2-furaldehyde	98	86
Propionaldehyde	86	90
Butyraldehyde	91	99
Isobutyraldehyde	75	92
Valeraldehyde	94	92
Heptaldehyde	92	97
Crotonaldehyde	86	91

Jorgensen has published research into the asymmetric nitroaldol, aldol and Michael reactions, but also into the Diels Alder reaction.[98] Previously, he has used his chiral bisoxazoline copper(II) complexes to catalyse these reactions, which he has also used in the Diels Alder reaction. This ligand can be seen in fig. 1.3.32. Moderate yields were observed (42-83 %), and moderate to excellent enantioselectivities accompanied these (55-95 %). This, along with Jacobsen's work, demonstrates that some ligands are so versatile they can catalyse many different reactions with success. One could look at this from the point of view that the resulting catalysts from these types of ligands are very useful and extremely efficient.

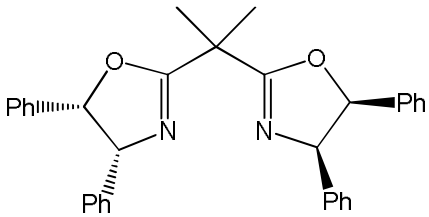

Fig. 1.3.32 Bisoxazoline ligand, that was subsequently used to generate a copper(II) complex for the catalysis of the Diels-Alder reaction

1.4 Heterogeneous Catalysis

A heterogeneous catalyst can be defined as "a catalyst which exists in a different phase from the reactant molecules".[104] Because of this, heterogeneous catalysts tend to be much easier to separate from the products post-reaction. In situations where the catalyst is expensive or toxic, heterogeneous catalysis may be preferable for this reason. Moreover, heterogeneous catalysts tend to be more amenable to recycling, as their stability means that degradation during catalysis is reduced. In addition, the ease of separation of the catalyst from the products means that this process is less likely to result in the catalyst becoming poisoned or destroyed. This is particularly notable with air-sensitive catalysts,[105] such as iridium and rhodium catalysts, or catalysts containing phosphine ligands.

Heterogeneous catalysts are often preferred in industry as they are highly suited to continuous flow processes,[106] which can be more efficient as generally, reaction conditions such as heat transfer and rates of mixing can be controlled more easily, which increases efficiency. However, there is an argument that reduced activities and selectivities are seen with heterogeneous catalysts in comparison with their homogeneous counterparts. This argument will now be discussed.

As previously stated, a heterogeneous catalyst exists in a different phase to the reactants, and so reductions in catalytic activity can be seen, which is often

attributed to reduced rates of diffusion between the substrates, catalyst and products.[107] However, the material upon which the catalyst is attached (the support) often has a high surface area, especially extended inorganic materials such as silica. This will be discussed later in more detail, but the support may affect the catalytic site in some way, either by changing it (and thus creating a less active catalytic site) or by impeding it in terms of accessibility by the substrates. Of course, the support can also have a positive effect on the catalytic site, which will also be discussed later in more detail.

Also with heterogeneous catalysis, a drop in selectivity, particularly enantioselectivity is often seen.[108] Occasionally, there are cases where the correct choice of support can actually enhance enantioselectivity,[107] though these cases are rare. This is most commonly seen when using inorganic materials as supports, particularly silica, so this will be used as an example to explain the drop in selectivity. The silica surface is covered in hydroxyl groups known as silanols. Fig. 1.4.1 shows the type of surface groups that one may encounter.

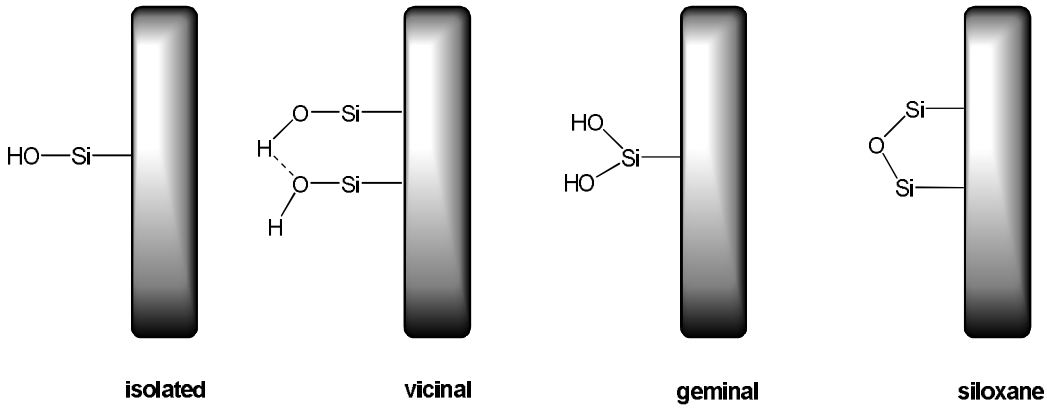

Fig. 1.4.1 Various types of surface groups present on a silica surface

The silanols are very reactive, and readily become involved in reactions. However, these groups are not chiral, so whenever they contribute to a reaction, they do so achirally, thus a drop in enantioselectivity is observed, for example in an acid catalysed process.[109] Often, the silanol groups are reacted with trialkoxy silanes in order to remove the reactive hydroxyl functionality. This process is called "capping", and will be discussed later in more detail. Similarly, when

using polymers as supports, one must ensure that the polymer is reasonably inert, so as not to interfere with the reaction.

An advantage of homogeneous catalysts over their heterogeneous counterparts is that in terms of analysis, homogeneously catalysed reactions can be followed in much more depth in terms of intermediates, and also what is occurring at the catalyst at these points during the reaction. This means that the mechanism of the reaction can be understood more fully, and so the reaction can be optimised in response to this, as previously discussed. This can mean that more assumptions need to be made regarding mechanisms of heterogeneously catalysed reactions. However, analytical techniques for solid-state materials are growing and improving all the time, which will be discussed later in more detail. Also, where the support used is silica-based, silsesquioxanes can be used to model the effect of a catalyst being tethered to a support, whilst still being soluble and therefore suitable to be analysed using solution state techniques. This will be discussed later in more detail.

There are a variety of different supports that can be used in preparing a heterogeneous catalyst. Unsurprisingly, different supports will suit different reactions. For example, during the epoxidation reaction an oxidant is required, and sometimes these oxidants can be unavoidably strong. So a polymer support may not be as suitable as a silica support, as the oxidant may cause the polymer to decompose, destroying the catalyst.[110,111] Some of the supports that are commonly used in heterogeneous catalysis will be discussed here, along with methods of preparing these catalysts.

1.4.1 Preparation of Heterogeneous Catalysts

There are numerous factors to consider when designing and preparing heterogeneous catalysts, and perhaps the most sensible place to start is by looking at the reaction being catalysed. Firstly, what substrates and reagents are being used? Some reactions use harsh reagents such as peroxides in epoxidations, which may attack and break down some supports, as previously mentioned. Also,

what solvents are suitable for the reaction? When polymers are used as supports, the amount that the polymer swells when immersed in a solvent can have a huge effect on the catalytic activity and selectivity, and different solvents will encourage swelling to different extents. Also, solvents can be used to increase selectivity in heterogeneous catalysts, which will be discussed in more detail shortly. Then, when the most appropriate support has been chosen, which is the best way to attach the catalyst to the support? Also, how does one ensure that on attaching the catalyst to the support, the catalyst will subsequently have enough space to effectively catalyse a reaction, and not be hindered or inhibited by the support? These questions will now be discussed in more detail.

Catalysts can be anchored to supports either with a covalent or ionic interaction. Sometimes, it can be difficult to ascertain which of these is occurring predominantly – it is often assumed that covalent bonding is the most prevalent as energetically speaking, it is the most favourable. The most common form of ionic bonding that occurs in tethering catalysts to supports is hydrogen bonding. Although this is a strong interaction, "leaching" of the catalyst into the solution is often observed. Irreversible covalent bonding can significantly reduce leaching. It usually involves a covalent bond being formed between the ligand and the support. The metal then binds to the ligand, presumably in the same manner as it would in its homogeneous equivalent. Hence, the catalytic activity of a heterogeneous catalyst that is formed using covalent bonding is more likely to be closer to that of its homogeneous counterpart. The disadvantage of this is that the ligand then has to have an extra functional group incorporated into it (a "tether group") for subsequent attachment to a support.[112] In introducing this extra functionality, the ligand synthesis may become much more complicated, difficult and lengthy, and the catalyst itself is now different from its homogeneous version, which may make a difference to the catalytic results.

When attaching the ligand to the support, one factor to consider is the distance between the catalyst and the support. There is a general belief that if catalysts do not have enough space around them, they may not be able to adopt the necessary conformations required during catalysis, which could have a detrimental effect on activity and selectivity.[113] This also applies to tethering a catalyst inside a

pore in porous supports. To overcome this, "spacers" can be inserted between the catalyst and support, in order to add extra distance between the two, which can result in remarkable differences in catalytic performance. Lee prepared the mesoporous silica-supported version of a cinchona alkaloid ligand with various lengths of spacer incorporated, and tested these in the asymmetric dihydroxylation of alkenes.[114] The catalyst can be seen in fig. 1.4.2.

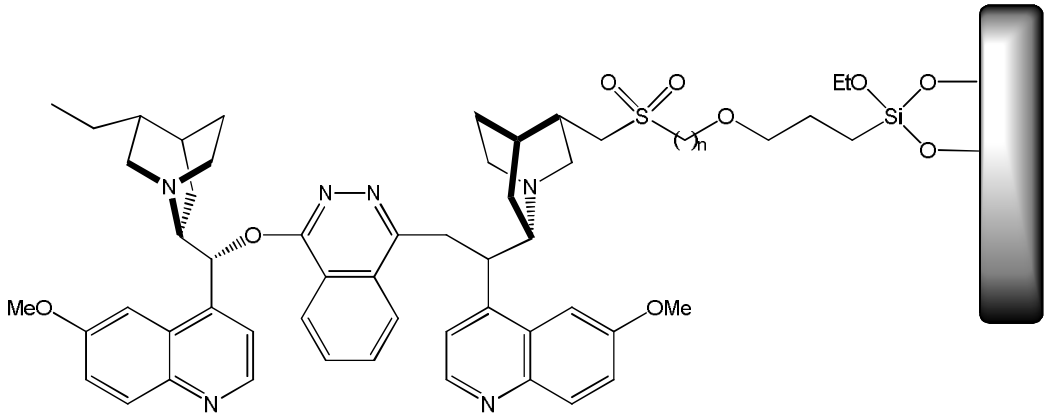

Fig. 1.4.2 Silica supported cinchona alkaloid, for subsequent catalytic use in the asymmetric dihydroxylation of alkenes

The results can be seen in table 1.4.1. The results show that by increasing the length of the spacer, not only does enantioselectivity increase for every substrate tested, it increases to the point where it is almost comparable to the homogeneous version of the catalyst. This is supportive of the thinking that the support can be detrimental to enantioselectivity, as previously discussed, and that the more distance that can be put between the catalyst and the support, the better the enantioselectivity will be. This also suggests that the catalytic mechanism does not change dramatically between unsupported and supported catalysts provided that there is no direct interference in the reaction from the support. Other research groups have also varied spacer length and compared the catalysts to their homogeneous counterparts, and find similar effects.[115,116]

Table 1.4.1 A selection of results from the catalysed dihydroxylation of alkenes, using the catalyst shown in fig. 1.4.2, and comparing this to an analogous homogeneous catalyst

Alkene	ee / %		
	Homogeneous	**n = 2**	**n = 6**
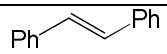	99	99	99
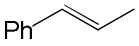	97	95	98
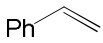	97	87	96
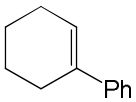	97	82	94
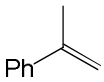	93	75	90
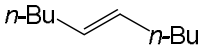	93	75	87
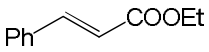	95	98	98

As previously mentioned, in the case of using polymers as supports, solvent choice can be important as it affects the swelling of the polymer, which will be discussed in more detail later. Solvent choice can also be important to improve enantioselectivities. Itsuno prepared polymer supported chiral *N*-sulfonylamino acids, and used them to catalyse the asymmetric Diels Alder reaction.[117] The reaction scheme and the catalyst in question can be seen in fig. 1.4.3.

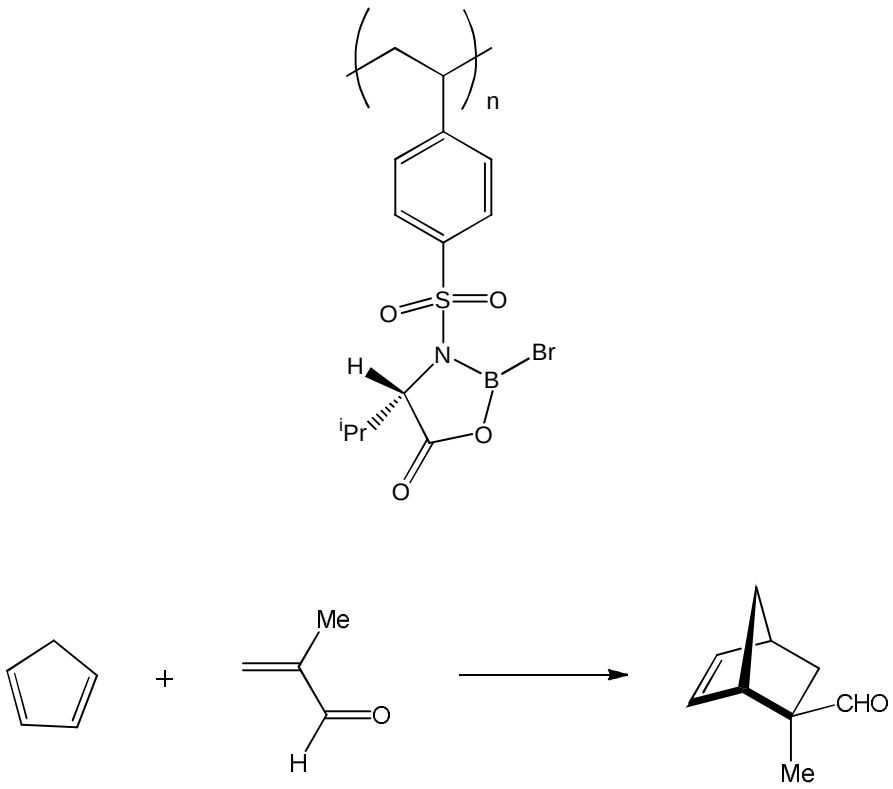

Fig. 1.4.3 Shows a polymer-supported catalyst, and the Diels-Alder reaction that it catalyses

Of the results presented, the only set of results that were truly comparable showed that with the reaction normally run in dichloromethane, the addition of THF improved the enantioselectivity from 44 to 52 %; a substantial increase. This behaviour was in accordance by some research published by Helmchen[118] The authors proposed that there was association between catalytic sites that was sterically hindering a reactive face of the catalyst, and causing a decrease in enantioselectivity. This can be seen in fig. 1.4.4. The THF molecule disrupts the interaction between catalytic sites, and thus enantioselectivity is improved.

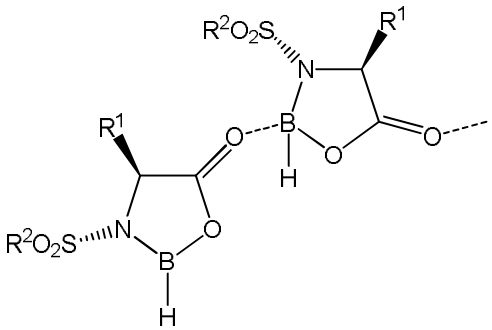

Fig. 1.4.4 Interaction between two catalytic sites can be observed

1.4.2 Polymers as Supports

Using a polymer as a support can be very useful for numerous reasons. Firstly, the nature of organic polymers means that modification of the support is simpler than with an inorganic material. Fan reported the use of polyether dendrimers as a support for a ruthenium(II) BINAP catalyst, to catalyse the asymmetric hydrogenation of alkenes.[119] The catalyst and reaction scheme can be seen in fig. 1.4.5.

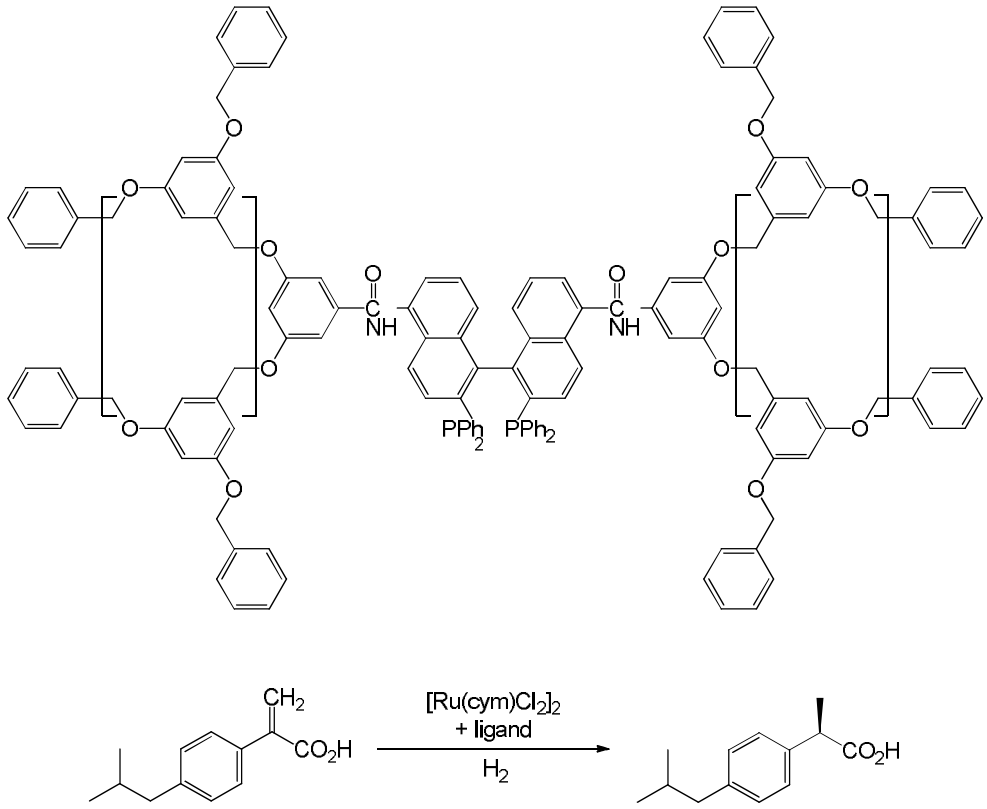

Fig. 1.4.5 Dendrimer-supported BINAP ligand – its ruthenium(II) complex is used in the asymmetric hydrogenation of alkenes

The results can be seen in table 1.4.2. The results show that the dendrimer-supported catalysts are more active and more selective than the homogeneous catalyst. This shows that if the right support is used, supporting a catalyst can actually enhance catalytic results. Interestingly, the results also show that on supporting the catalyst, the configuration of the product switches from (*S*) to (*R*). This behaviour is a fairly common occurrence in heterogeneous catalysis.

Further testing showed that recycling the catalyst three times gave no drop in activity or enantioselectivity.

Table 1.4.2 A selection of results of the asymmetric hydrogenation shown in fig. 1.4.5

Ligand	Conversion / %	ee / %	Configuration
Homogeneous, (S)-BINAP	10	90	*S*
Dendritic, n = 0	10	92	*R*
Dendritic, n = 1	13	93	*R*
Dendritic, n = 2	34	92	*R*

When using polymers in preparing heterogeneous catalysts, either soluble or insoluble polymers may be used. When soluble polymers are used as supports, the resulting catalyst is not strictly heterogeneous, but has the advantage of heterogeneous systems in the catalyst-separation process post-reaction, in that recovering the catalyst (and subsequently re-using it) is often very simple. Such separation techniques include solvent or heat precipitation, membrane filtration or size exclusion chromatography.[23] Also, the catalytic activities of soluble-polymer-supported catalysts are often closer to that of true heterogeneous catalysts, as diffusion through polymeric material, even when soluble, is much slower than in typical homogeneous systems. Therefore using soluble polymers as supports can be thought of as being between the two extremes.

The first example of using a soluble polymer supported catalyst was provided by Bayer in 1975.[120] Bayer showed that the catalysts could be recycled effectively. However, the complete lack of enantioselectivity and moderate conversions meant that this work did not attract much interest, and so this area of supported catalysis was left relatively untouched for the following 20 years.[23] In 1996, Janda published research into the use of soluble polymers as supports for catalysts.[121] A polyethylene glycol derivative was used as a support in the

catalysis of the asymmetric dihydroxylation of alkenes. The results can be seen in table 1.4.3.

Table 1.4.3 A selection of results from the asymmetric dihydroxylation of alkenes

Alkene	Catalyst	Yield / %	ee / %
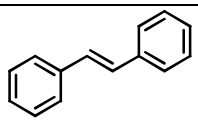	Homogeneous	89	88
	Supported	89	88
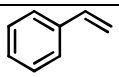	Homogeneous	80	60
	Supported	80	60
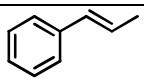	Homogeneous	80	84
	Supported	80	85
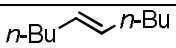	Homogeneous	62	42
	Supported	65	43

Excellent yields and enantioselectivities were achieved by this group for a range of substrates, and more importantly, the results from the supported catalysts matched that of the homogeneous. This, in conjunction with the ease of recovering the catalyst post-reaction, and the ability to re-use the catalyst up to five times without any loss in activity or selectivity, sparked a great deal of interest in this area.

When using polymers as supports, the degree of cross-linking can contribute greatly to catalytic performance. This can be seen in the research published by Bayston in 1998.[122] The authors tested a homogeneous catalyst, polystyrene-supported catalyst and polyethyleneglycol-linked polystyrene supported catalyst for the asymmetric transfer hydrogenation of acetophenone. The results can be seen in table 1.4.4.

Table 1.4.4 A selection of results from the catalysed transfer hydrogenation of acetophenone

Catalyst	Conversion / %	ee / %
Homogeneous	93	94
PS supported	88	91
PEG-PS supported	9	55

The conversions and enantioselectivities are highest in the case of the homogeneous catalyst, which is often the case for reasons previously discussed. Interestingly, the polymer with cross-linking had very poor conversions, and much lower enantioselectivities than the polystyrene supported with no cross linking. This suggests that cross linking can have a very detrimental effect on catalysis. This is likely to be due to the catalytic sites being less accessible to the substrates. Other research groups have also reached similar conclusions with respect to this.[123] With cross-linked polymers, the reaction solvent is usually carefully selected so as to promote maximum swelling of the polymer. This then allows easier diffusion between the substrates, catalytic sites and products. However, in this case, on varying the reaction solvent, the cross-linked polymer only swelled to a maximum of 1.5 times its initial volume; sterically this is insufficient, which is reflected in the poor results. Other research groups have also highlighted the importance of polymer swelling when using it as a catalyst support.[124,125] Reaction temperature can also be important to encourage sufficient swelling; however, this is more difficult to adjust, as increasing temperature can have a detrimental effect on enantioselectivity. When recycling the supported catalysts, both showed no change in catalytic performance on subsequent reuse. Often with cross-linked polymers, particularly cross-linked polystyrene, as a support they have low mechanical stability, which means that with stirring over time the support often breaks down, degrading the catalyst and reducing its lifetime.[23] The mechanical stabilities and tendencies to break down will vary between polymers, so this can be affected by initial choice of polymer.

There are examples where the use of cross-linked polymers as supports can have a positive effect of catalytic performance. Locatelli used polyurea derivatives to support rhodium diamine catalysts for the asymmetric hydrogenation of

ketones.[126] He compared cross-linked and non-linked polymer supported catalysts, and found that that the cross-linked polymers yielded the best catalytic performance, with a conversion of 100 % and an enantiomeric excess of 60 %, which was double that of the non-linked polymer supports. The authors reported that enantioselectivity increased with greater cross-linking up to a point, and any more cross linking would impede the accessibility of the catalytic sites too much, and catalytic performance would decrease. In the case of this research, the authors were using a "molecular imprinting" technique in an attempt to produce highly selective heterogeneous catalysts.

Molecular imprinting as a concept came from nature's ability to produce organic compounds with very high selectivity. Often, this is achieved with enzymes, where the specificity comes from the famous "lock-and-key" mechanism, whereby the 3D structure of the enzyme matches exactly the geometry of the substrate. If a polymer support can be forced to take on a specific structure, to accommodate a particular substrate (in this case a ketone), perhaps a very specific catalyst can be prepared. In nature, intermolecular bonds such as hydrogen bonding holds the structure in place – in this case, cross-linking keeps the polymer backbone (and hence catalyst position) in place. This explains why the enantioselectivities were so much higher with higher levels of cross-linking, and hence more catalyst stability. Other research groups have also used the molecular imprinting technique to achieve higher enantioselectivities, and been successful.[127]

1.4.3 Mesoporous Inorganic Supports

The term "inorganic support" encompasses a vast array of materials. Commonly though, in heterogeneous catalysis this refers to an extended inorganic oxide, such as silica, alumina, or zirconia. Silica as a catalytic support will now be discussed in more detail.

Silica is also known as silicon dioxide (SiO_2), which has an extended structure. It has the advantage of having a very large surface area (typically 500 $m^2\ g^{-1}$),

which means that a small amount of heterogeneous catalyst could contain a large quantity of catalytic sites. This in turn increases catalytic activity (per amount of heterogeneous catalyst). The high surface area arises from the high porosity within the structure. Microporous silica has pore diameters of less than 2 nm – these tend to fall into the category of zeolites, which will be discussed shortly. Mesoporous silica typically has pore diameters of 2-50 nm, and can have regular pore geometries, such as MCM-41.[128] Raja[129] used MCM-41 as a support for a diphoshine ferrocenyl palladium complex for the asymmetric hydrogenation of ethyl nicotinate. He also prepared a silsesquioxane-supported version of this catalyst for comparitative purposes. This technique will be discussed in more detail shortly, but is used to produce a *soluble* model of a supported catalyst that simulates binding to a silica support. The authors found that while the homogeneous silsesquioxane-supported catalyst showed no enantioselectivity, the MCM-41 supported catalyst showed a 17 % enantioselectivity with a 50 % conversion. These results were markedly better than any other catalytic results achieved by other groups with respect to this reaction,[130] and highlight the positive effect that a support can have on a reaction.

The type of silica used often depends on the requirements of the reaction, for instance the size of the substrate could dictate the pore size of the silica support, and to achieve high selectivities during catalysis, more a more regular, well-defined structure may be required, which will be discussed shortly.

As previously discussed, a drop in selectivity is often observed when using silica as a support. These groups can contribute to catalytic reactions but do so achirally, thus reducing enantioselectivity. Often, following the attachment of the catalyst to the support, any remaining silanol groups are "capped".[23,131,132] This means that they are reacted with a reagent such as trimethylchlorosilane[133] in order to render these groups relatively inert.

As well as their high surface areas, silica materials have another advantage in that they have high mechanical and thermal stability. This robustness means that catalyst degradation through stirring for long periods of time is reduced, the catalyst can withstand harsher reaction conditions if necessary, and also the

resulting catalysts are highly suited to continuous flow processes, given that they are non-compressable materials.[23,134]

Jacobsen's massive success within asymmetric catalysis has been previously discussed with respect to homogeneous catalysis, but he has also achieved great success within asymmetric heterogeneous catalysis. In 1999, he published research detailing a silica-supported cobalt salen complex, and its use in catalysing the asymmetric kinetic resolution of epoxides.[134] The catalyst and reaction scheme can be seen in fig. 1.4.6.

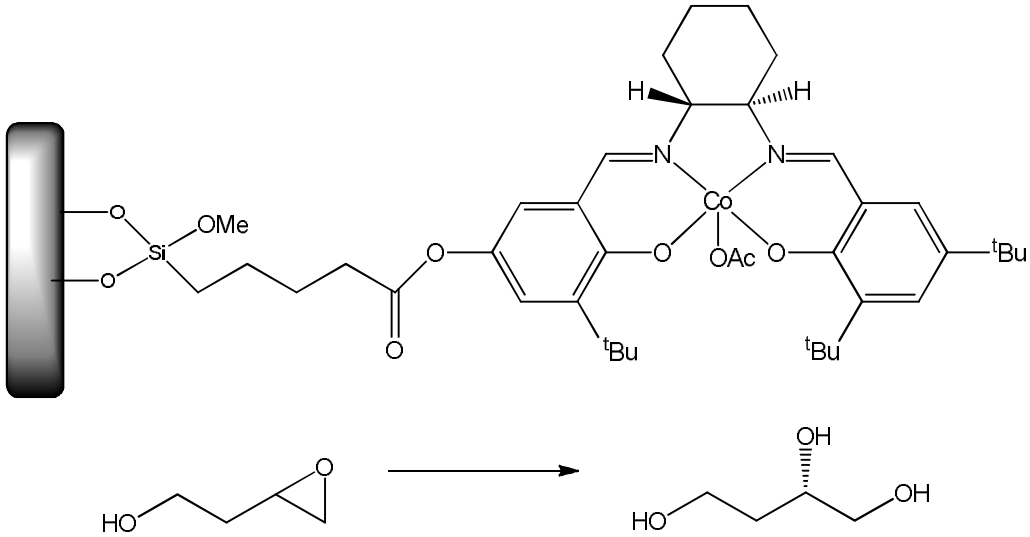

Fig. 1.4.6 Showing the silica-supported cobalt(III) Jacobsen's catalyst, and its use in the ring-opening of epoxides, also shown here

The catalysis was performed in a continuous flow reactor. Moderate conversions (39 %) and high enantioselectivities (94 %) were observed. Furthermore, on recycling the catalyst, there was no drop in conversion or enantioselectivity. The authors stated that this showed significant promise for future work in using silica-supported versions of Jacobsen-type catalysts in continuous flow processes.

In 1996, Pugin reported the use of silica-supported diphosphine ligands in conjunction with rhodium to catalyse the asymmetric hydrogenation of methyl-acetamidecinnamate.[135] Pugin varied the catalyst loading, and examined the effect that this had on the catalytic results. Whilst enantioselectivity did not vary significantly, Pugin found that increasing the loading, and hence increasing the

concentration of catalytic sites was extremely detrimental to the activity of the catalyst. The results can be seen in table 1.4.5.

Table 1.4.5 A selection of results of the asymmetric hydrogenation of methyl-acetamidecinnamate by a silica-supported rhodium catalyst

Loading / mmol g^{-1}	Rate / min^{-1}
0.016	12.5
0.058	6.7
0.092	4.7
0.110	3.9
0.190	1.4
0.200	1.2

Pugin proposed that the formation of dimers is favoured with bis-ligands, and that with the increase in loading, the distance between catalytic sites is reduced, and so dimers would be even more likely to form. The dimers are inactive, which explains the dramatic decrease in catalytic activity. Hence, this research highlights the importance of catalyst loading, and how through careful adjustment of this, the heterogeneous catalyst can be optimised.

Motorina compared amorphous silica and molecular sieves as supports for cinchona alkaloids, to subsequently catalyse the asymmetric dihydroxylation of alkenes.[136] The ligand and reaction scheme can be seen in fig. 1.4.7.

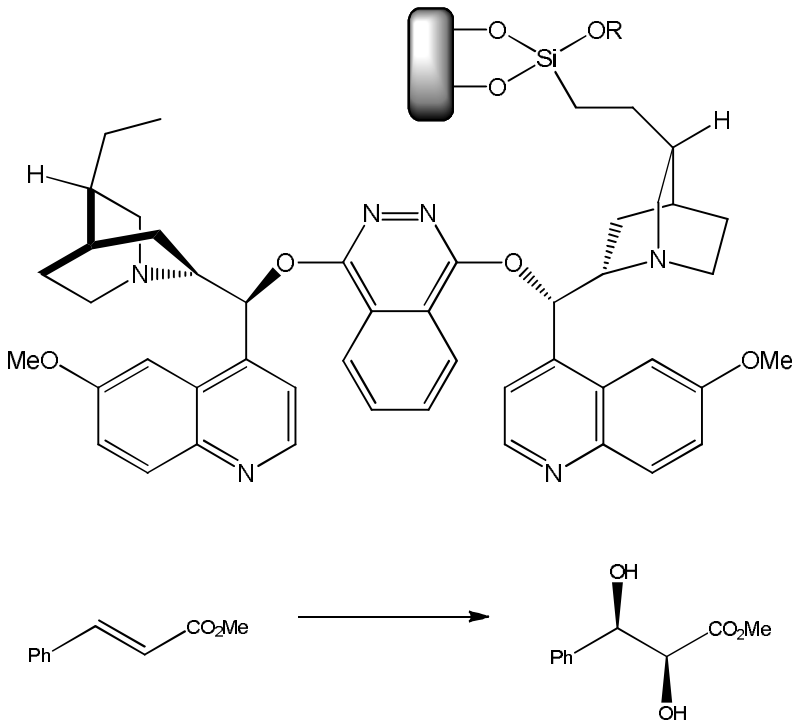

Fig. 1.4.7 Showing the silica-supported cinchona alkaloid derivative, and the reaction scheme of the dihydroxylation of alkenes that it catalyses

Some of the results can be seen in table 1.4.6. The results show that conversion and enantioselectivity are both significantly higher when molecular sieves are used as a support rather than amorphous silica. When tested with other substrates, the same pattern was observed. The authors theorised that the reason for this was the extremely ordered "microenvironment" that is present in the pores of molecular sieves, imparts an extra selectivity upon the reaction, as the surrounding of the catalytic sites are of a very specific and well defined geometry, and crucially, exactly the same for each catalytic site. The reason for the higher conversions is due to a greater surface area; the molecular sieves had a surface area of 761 m^2 g^{-1} compared to a surface area of 436 m^2 g^{-1} in the amorphous silica. These results suggest that in porous supports, this characteristic can be utilised to effectively modify the heterogeneous catalyst to optimise catalytic performance.

Table 1.4.6 A selection of results of the asymmetric dihydroxylation of the alkene shown in fig. 1.4.7

Catalyst	Conversion / %	ee / %
Homogeneous	44	97
Amorphous Supported	46	94
Molecular Sieve Supported	54	98

1.4.4 Silsesquioxanes as Model Compounds

Silsesquioxanes are soluble models of a silica material with a cubic-cage structure.[137] They are often used as a soluble (and hence can be analysed by solution techniques) way of studying the effects of binding a ligand to a silica support, and are said to bridge the gap between homogeneous and heterogeneous catalysis. Previously, the various types of silanol group were represented pictorially (fig. 1.4.1). The three types of silanol group can also be represented in silsesquioxanes, and are shown in fig. 1.4.8.[138]

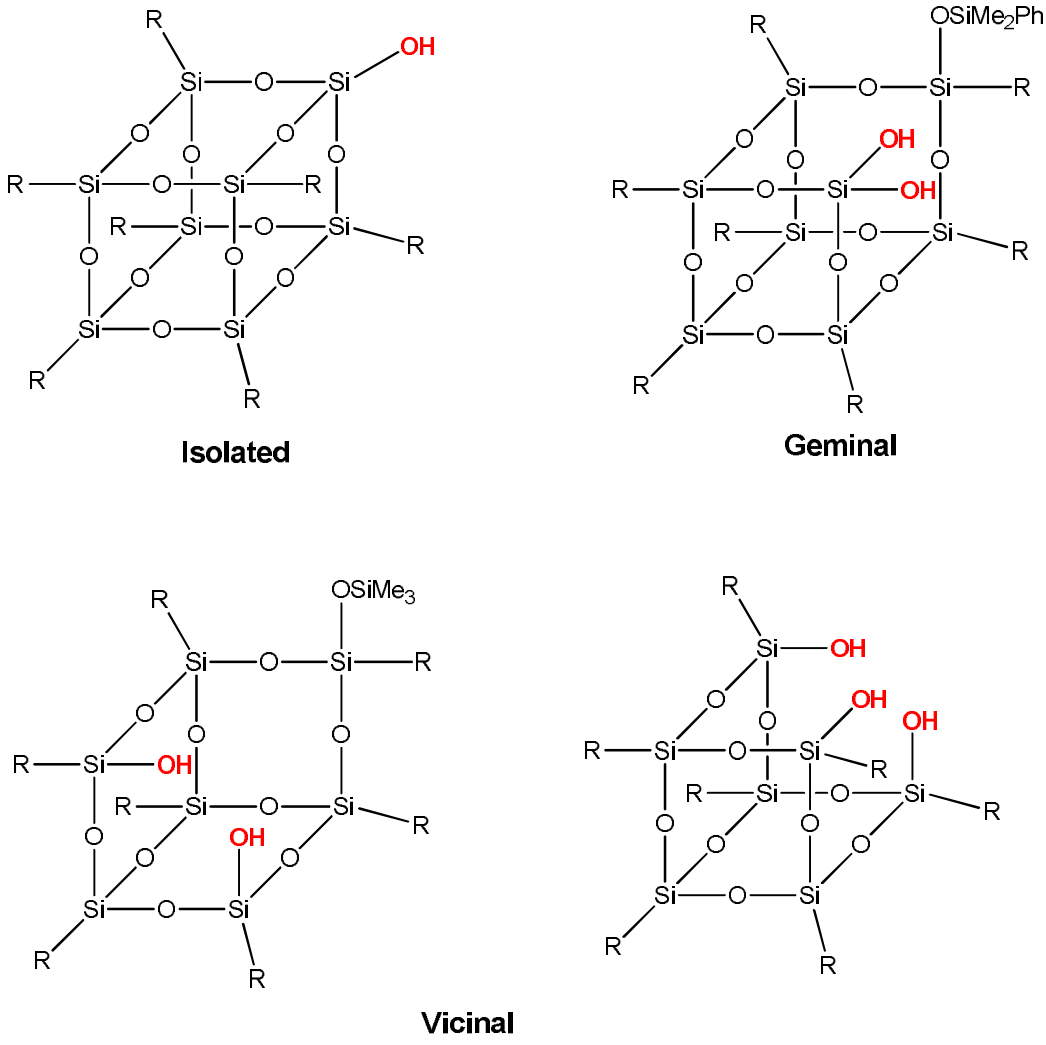

Fig. 1.4.8 Various types of silanol groups within silsesquioxanes

The first example of using silsesquioxanes for this purpose came from Feher in 1986,[139] incorporating a zirconium complex into one of the corners of the cubic silsesquioxanes. Feher demonstrated the relative ease of the synthesis and characterisation of this compound, and since then, many research groups have followed suit.

Fraile had previously carried out research into the titanium heterogeneous catalysis of alkene epoxidation.[140] The authors mentioned the importance of the titanium species being highly dispersed on the silica support, and wanted to know whether the titanium species was monopodal, bipodal or tripodal when supported. This is shown pictorially in fig. 1.4.9.

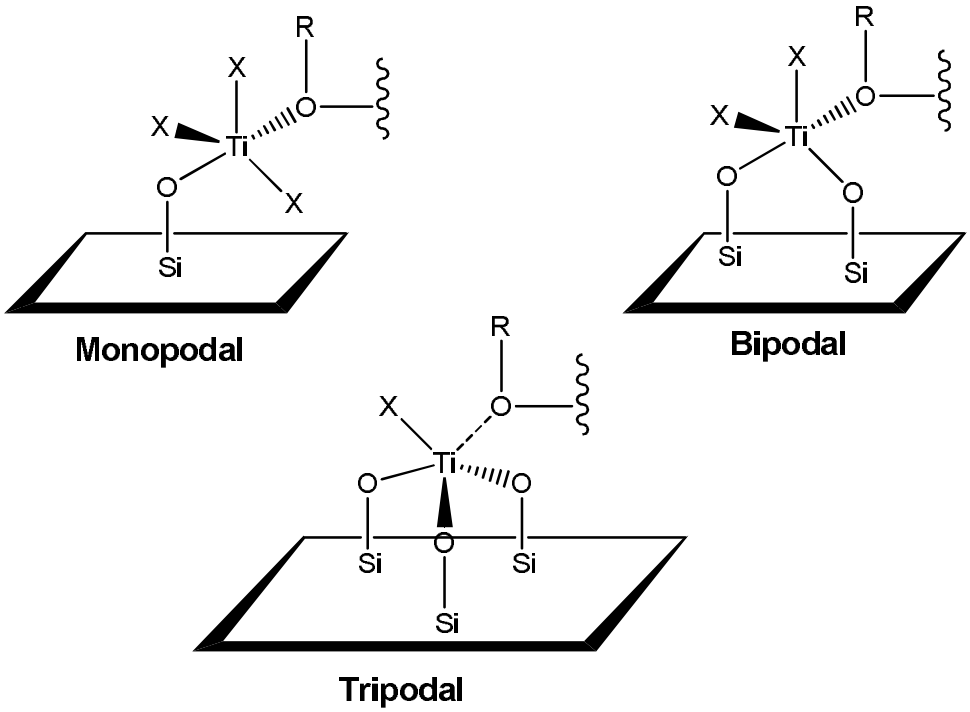

Fig. 1.4.9 Binding modes of titanium to a silica support

Three silsesquioxane complexes were prepared to simulate these binding modes, and characterised by elemental analysis, NMR spectroscopy, IR spectroscopy and UV-vis spectroscopy. By comparing the characterisation of the silsesquioxane compounds to that of the silica-supported catalysts, this sheds light onto the nature of the heterogeneous system. Direct comparisons allowed the three binding modes on the silica surface to be assigned to the peaks observed from various spectroscopic analyses. Hence, the authors were able to identify which binding mode was the least common (monopodal), and which modes would give rise to the best selectivities in the epoxidation reactions being catalysed. It was shown that pentacoordinated titanium species gave rise to much better selectivities than octahedral. Therefore, in the preparation of future catalysts for this reaction this can be taken into account. Previous work by Das used silsesquioxanes for a very similar purpose, to identify the binding bode of a vanadium species on a silica surface, which was successfully achieved.[141]

The use of silsesquioxanes can be useful in terms of helping with spectroscopic assignments with silica-supported species. This can provide insight into reaction mechanisms that without being able to simulate the supported catalyst in solution phase would be challenging. However, one must be careful with making

comparisons between silsesquioxanes and heterogeneous catalysts, as due to their solubility, sometimes silsesquioxanes can undergo chemistry that heterogeneous catalysts cannot. For example, solvents have been known to take part in reactions, which will be much more prevalent in silsesquioxanes than silica supported materials. Also, the formation of dimeric species is much more likely to happen in silsesquioxanes than in the rigid extended material of silica, which can have an enormous effect on catalytic performance.

1.5 Bimetallic Catalysis

In 1998, Paul Anastas developed the twelve principles of green chemistry, which have since shaped the direction that chemistry is moving in.[15] These principles are as follows.

1. Prevent waste
2. Be atom efficient
3. Avoid production of toxic or harmful by-products
4. Products should be designed efficiently
5. Avoid the use of solvents where possible
6. Reduce energy requirements and environmental impact of any process
7. Use renewable feedstocks
8. Avoid unnecessary protection chemistry whenever possible
9. Catalytic reagents are superior to stoichiometric reagents
10. The final products are not harmful to the environment
11. Develop real-time analytical methods to allow the detection of hazardous materials
12. All materials should minimise the risk of explosion or harm to health and the environment

They stated that waste should be minimised wherever possible, including the use of solvents and chiral auxiliaries, and hence chiral catalysis should be encouraged. They emphasized the importance of atom economy, which suggests that ideally, the quantity of starting material should equal the amount of product in a reaction. The also highlighted the importance of efficiency in a reaction, and particularly energy efficiency, for example, if milder reaction conditions can be used they should be, and synthetic processes should be made to be as efficient as possible. And finally, the generation of hazardous substances should be minimised wherever possible.

These principles can be satisfied with the use of bimetallic catalysts. Bimetallic catalysts contain two metal centres, and when used to catalyse tandem processes - two reactions occurring sequentially in one-pot. By removing separation and purification steps in between the two reactions, the process is made more efficient in terms of atom economy and is environmentally friendly, in using less solvent and purification materials.[142] This area of catalysis has remained relatively unexplored, leaving much scope for development of new bimetallic catalysts. Some of the bimetallic catalysis reported will be discussed here.

Chung used silica-supported palladium and cobalt nanoparticles to catalyse the allylic alkylation reaction, followed by the Pauson-Khand reaction.[143] The overall reaction can be seen in fig. 1.5.1.

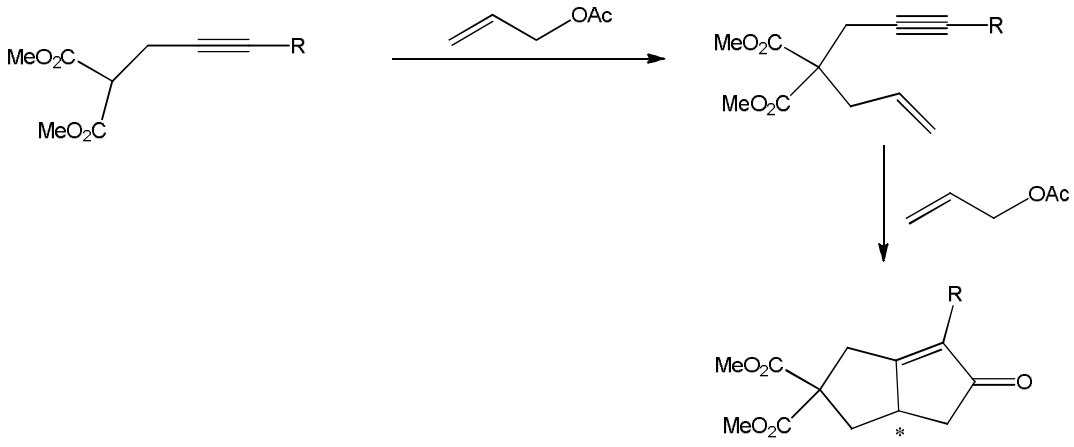

Fig. 1.5.1 Reaction scheme of the sequential allylic alkylation and Pauson-Khand reaction, enabled by palladium and cobalt nanoparticles

The group optimised the reaction conditions for the first reaction (the allylic alkylation) by varying solvent, base and reaction time. The most successful set of conditions yielded an 89 % yield. It is useful to optimise one reaction before concentrating on the bimetallic process, as when the second reaction comes into play it may be more difficult to adjust reaction conditions to achieve the best results. The authors tested the catalyst for a range of substrates; some of the results can be seen in table 1.5.1.

Table 1.5.1 A selection of results of the sequential allylic alkylation followed by the Pauson-Khand reaction, as shown in fig. 1.5.1

R	Yield / %
CH_3	88
Bu	82
TIPS	84

Reaction conditions: THF, NaH, 0.54 mmol substrates, 0.1 g catalyst, 130 °C, 10 atm CO, 18 h.

The results show high yields. Although the results may not be improved much further, as much optimisation has already been carried out with respect to the reactions, they show promise for future work in this field, in that bimetallic catalysts for completely different reactions can be synthesised and produce successful results. Having said this, when assessing the recyclability of this catalyst, large amounts of palladium leaching was observed, which reduces the applicability of these systems. This must be improved upon if this catalyst is to compete with other catalysts with longer lifetimes that catalyses these two reactions separately.

Leaching was also observed in the bimetallic catalysis carried out by Choudary.[144] The authors prepared a silica-supported palladium-thiol and osmium-cinchona alkaloid catalyst, for the catalysis of a Heck reaction followed by the asymmetric dihydroxylation of alkenes. The catalyst can be seen in fig. 1.5.2.

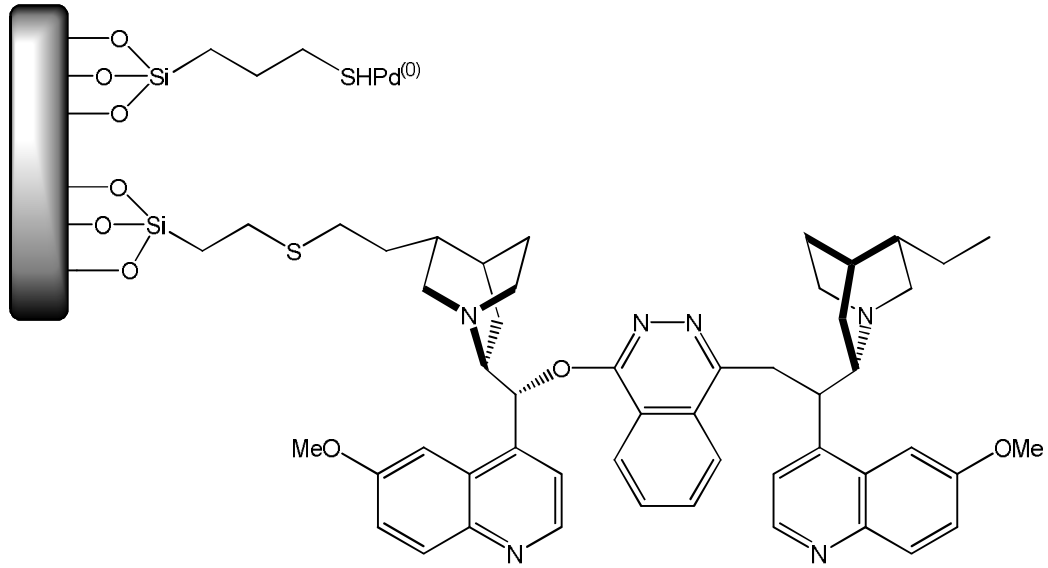

Fig. 1.5.2 Silica-supported catalyst for the sequential Heck reaction followed by the asymmetric dihydroxylation of alkenes

The results can be seen in table 1.5.2. Excellent yields and enantioselectivities were obtained. The catalyst was also tested for the individual reactions; there were no changes in the results. This suggests that there is no interaction between palladium and osmium. This can be very important, as an interaction between metals can often have a detrimental effect on catalytic performance. Unfortunately, on recycling the catalyst, significant reductions in activity and enantioselectivity were observed for the dihydroxylation reaction, which was caused by leaching of the osmium. Having said this, osmium leaching is commonly observed in monometallic catalysts in the dihydroxylation of alkenes, and the catalysts in those cases and this case could be regenerated by adding more OsO_4. However, given the expense and toxicity of osmium, this is not ideal.

Table 1.5.2 A selection of results for the sequential Heck reaction followed by the asymmetric dihydroxylation of alkenes, catalysed by the catalyst shown in fig. 1.5.2

Aryl Iodide	Alkene	Yield / %	ee / %
PhI	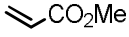	99	92
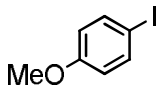	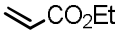	96	99
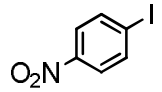	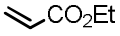	95	98
PhI	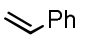	92	99

Thiot used a polyionic gel to support rhodium and palladium, to catalyse the hydrosilation reaction followed by the Hiyama cross-coupling reaction.[145] Good results were observed with yields of up to 99 %, and again, he found that the metals catalysed the reaction without interacting with each other, which as previously discussed is a very important factor in bimetallic catalysis. However, there were limitations to this reaction, in that the N-heterocyclic iodide for the Hiyama cross-coupling reaction had to be added in separately, after the hydrosilylation had occurred, in order to avoid poisoning the rhodium catalyst. Although this still retains the advantages of a one pot process, in that less solvent is used and a separation step is removed between the two reactions, it would still be much more convenient and efficient to be able to add in all of the reagents and substrate at the beginning of the process. Also, on recycling the catalyst, testing showed that the catalyst could be reused once successfully, but beyond this, significant reductions in product yield were observed, by approximately 10 % with each recycle, presumably due to leaching issues.

1.6 Concluding remarks

This chapter has encompassed an in depth discussion regarding asymmetric synthetic methods. Asymmetric catalysis has clear advantages over other synthetic methods, not least because the resulting synthesis of the chiral target molecule is often simpler and more efficient. In addition, simpler, less wasteful syntheses are essential to develop, given that chemistry must now be performed using "greener attitudes", as previously discussed.

A number of organic transformations have been discussed, with a view of using asymmetric catalysis to achieve stereoselectivity. In particular, Jacobsen's ligand has been successfully employed in a multitude of complexes, to subsequently catalyse various different organic transformations, highlighting how versatile this ligand type is. For this reason, the ligands that have been designed and prepared, and will be discussed in this thesis, bear close resemblance to Jacobsen's ligand. In addition, the chelating amine groups will bind to a wide variety of metals, increasing the scope of the complexes prepared for catalysis. Also, these ligands are relatively simple to modify, thus the introduction of specific functional groups, be it hydroxyl groups to bind hard metals such as titanium(IV), or electron withdrawing or donating groups to influence catalysis, can be more readily achieved.

The main aim of this research is to prepare a range of homogeneous complexes using a multitude of transition metals, and to use these complexes as catalysts in a variety of asymmetric organic transformations. Following this, decisions can be made with respect to a number of factors. Firstly, it is important to investigate in depth the structural qualities of these complexes as ideally, a catalyst must be stable, so that it does not break down during catalysis and it has the potential to be recycled. Furthermore, it is important to fully understand the structure and behaviour of the catalyst as this may provide insight into the manner in which the catalysis proceeds, which can then be used to optimise the asymmetric catalytic reaction to its full potential. Secondly, on examining all of the catalytic data gathered, the reactions that show the most potential can be developed further in

future research, catalysts modified and conditions optimised, to produce outstanding novel catalysts.

Also, heterogeneous analogues of a selection of these complexes will be prepared and used as catalysts for the same organic transformations. The aim of this is to identify potential in these heterogeneous complexes that, on further investigation and modification in future research, could be used as successful catalysts. Where the most success is observed, the incorporation of two metals in one heterogeneous catalyst may be investigated to produce a bimetallic catalyst, the advantages of which have previously been discussed.

1.7 References

(1) Yamada, T.; Okada, T.; Sakaguchi, K.; Ohfune, Y.; Ueki, H.; Soloshonok, V. A. *Org. Lett.* **2006**, *8*, 5625.

(2) Mohri, K.; Okada, K.; Benet, L. Z. *Pharm. Res.* **2005**, *22*, 79.

(3) Dong, J. Q.; Liu, J. H.; Smith, P. C. *Biochem. Pharmacol.* **2005**, *70*, 937.

(4) De Camp, W. H. *Chirality* **1989**, *1*, 2.

(5) Thayer, A. M. *Chemical and Engineering News* **2007**, *85*, 11

(6) Lopez, J. A. S.; Li, Q.; Thompson, I. P. *Crit. Rev. Biotechnol.* **2010**, *30*, 63.

(7) Dr A D McNaught, A. W. *IUPAC Compendium of Chemical Terminology* 2nd Revised edition ed.; Wiley-Blackwell, 1997.

(8) Meyers, A. I.; Harre, M.; Garland, R. *J. Am. Chem. Soc.* **1984**, *106*, 1146.

(9) Meyers, A. I.; Knaus, G.; Kamata, K.; Ford, M. E. *J. Am. Chem. Soc.* **1976**, *98*, 567.

(10) Oppolzer, W.; Mills, R. J.; Reglier, M. *Tetrahedron Lett.* **1986**, *27*, 183.

(11) Evans, D. A.; Ennis, M. D.; Mathre, D. J. *J. Am. Chem. Soc.* **1982**, *104*, 1737.

(12) Evans, D. A.; Clark, J. S.; Metternich, R.; Novack, V. J.; Sheppard, G. S. *J. Am. Chem. Soc.* **1990**, *112*, 866.

(13) Denmark, S. E.; Marble, L. K. *J. Org. Chem.* **1990**, *55*, 1984.

(14) Ogawa, Y.; Kuroda, K.; Mukaiyama, T. *Bull. Chem. Soc. Jpn.* **2005**, *78*, 1309.

(15) Anastas, P. T.; Kirchhoff, M. M. *Accounts of Chemical Research* **2002**, *35*, 686.

(16) Hermann, K.; Wynberg, H. *The Journal of Organic Chemistry* **1979**, *44*, 2238.

(17) Zhao, M. X.; Zhang, Z. W.; Chen, M. X.; Tang, W. H.; Shi, M. *Eur. J. Org. Chem.* **2011**, 3001.

(18) Hawkins, J. M.; Loren, S. *J. Am. Chem. Soc.* **1991**, *113*, 7794.

(19) Maruoka, K.; Hoshino, Y.; Shirasaka, T.; Yamamoto, H. *Tetrahedron Lett.* **1988**, *29*, 3967.

(20) Furuta, K.; Shimizu, S.; Miwa, Y.; Yamamoto, H. *J. Org. Chem.* **1989**, *54*, 1481.

(21) Sun, Y.; Ahmed, M.; Jackstell, R.; Beller, M.; Thiel, W. R. *Organometallics* **2004**, *23*, 5260.

(22) Knowles, W. S.; Sabacky, M. J. *Chem. Commun.* **1968**, 1445.

(23) Fan, Q. H.; Li, Y. M.; Chan, A. S. C. *Chem. Rev.* **2002**, *102*, 3385.

(24) Osborn, J. A.; Jardine, F. H.; Young, J. F.; Wilkinso.G *Journal of the Chemical Society a -Inorganic Physical Theoretical* **1966**, 1711.

(25) Miyashita, A.; Yasuda, A.; Takaya, H.; Toriumi, K.; Ito, T.; Souchi, T.; Noyori, R. *J. Am. Chem. Soc.* **1980**, *102*, 7932.

(26) Ohta, T.; Takaya, H.; Noyori, R. *Inorg. Chem.* **1988**, *27*, 566.

(27) Ohta, T.; Takaya, H.; Kitamura, M.; Nagai, K.; Noyori, R. *J. Org. Chem.* **1987**, *52*, 3174.

(28) Kitamura, M.; Kasahara, I.; Manabe, K.; Noyori, R.; Takaya, H. *J. Org. Chem.* **1988**, *53*, 708.

(29) Kitamura, M.; Tokunaga, M.; Ohkuma, T.; Noyori, R. *Tetrahedron Lett.* **1991**, *32*, 4163.

(30) Knowles, W. S. *Angew. Chem.-Int. Edit.* **2002**, *41*, 1999.

(31) Sharpless, K. B. *Angew. Chem.-Int. Edit.* **2002**, *41*, 2024.

(32) Noyori, R. *Angew. Chem.-Int. Edit.* **2002**, *41*, 2008.

(33) Fuentes, J. A.; France, M. B.; Slawin, A. M. Z.; Clarke, M. L. *New J. Chem.* **2009**, *33*, 466.

(34) Ikariya, T.; Blacker, A. J. *Accounts of Chemical Research* **2007**, *40*, 1300.

(35) Noyori, R.; Hashiguchi, S. *Accounts of Chemical Research* **1997**, *30*, 97.
(36) Gladiali, S.; Alberico, E. *Chem. Soc. Rev.* **2006**, *35*, 226.
(37) Nishiyama, H.; Yamaguchi, S.; Park, S. B.; Itoh, K. *Tetrahedron: Asymmetry* **1993**, *4*, 143.
(38) Sawamura, M.; Kuwano, R.; Shirai, J.; Ito, Y. *Synlett* **1995**, 347.
(39) Hayashi, T.; Hayashi, C.; Uozumi, Y. *Tetrahedron: Asymmetry* **1995**, *6*, 2503.
(40) Zhang, X. C.; Wu, F. F.; Li, S. J.; Zhou, J. N.; Wu, J.; Li, N.; Fang, W. J.; Lam, K. H.; Chan, A. S. C. *Adv. Synth. Catal.* **2011**, *353*, 1457.
(41) Inagaki, T.; Phong, L. T.; Furuta, A.; Ito, J.; Nishiyama, H. *Chem.-Eur. J.* **2010**, *16*, 3090.
(42) Kobayashi, S.; Furuya, M.; Ohtsubo, A.; Mukaiyama, T. *Tetrahedron: Asymmetry* **1991**, *2*, 635.
(43) Kobayashi, S.; Mukaiyama, T. *Chem. Lett.* **1989**, 297.
(44) Ito, Y.; Sawamura, M.; Hayashi, T. *J. Am. Chem. Soc.* **1986**, *108*, 6405.
(45) Hayashi, T.; Uozumi, Y.; Yamazaki, A.; Sawamura, M.; Hamashima, H.; Ito, Y. *Tetrahedron Lett.* **1991**, *32*, 2799.
(46) Inoue, H.; Kikuchi, M.; Ito, J.; Nishiyama, H. *Tetrahedron* **2008**, *64*, 493.
(47) Mahrwald, R.; Ziemer, B. *Tetrahedron Lett.* **2002**, *43*, 4459.
(48) Yao, W. G.; Wang, J. B. *Org. Lett.* **2003**, *5*, 1527.
(49) Trost, B. M.; Silcoff, E. R.; Ito, H. *Org. Lett.* **2001**, *3*, 2497.
(50) Mouri, S.; Chen, Z. H.; Matsunaga, S.; Shibasaki, M. *Chem. Commun.* **2009**, 5138.
(51) Gathergood, N.; Juhl, K.; Poulsen, T. B.; Thordrup, K.; Jorgensen, K. A. *Org. Biomol. Chem.* **2004**, *2*, 1077.
(52) Xu, Z. H.; Daka, P.; Budik, I.; Wang, H.; Bai, F. Q.; Zhang, H. X. *Eur. J. Org. Chem.* **2009**, 4581.
(53) Evans, D. A.; Burgey, C. S.; Kozlowski, M. C.; Tregay, S. W. *J. Am. Chem. Soc.* **1999**, *121*, 686.
(54) Mandoli, A.; Arnold, L. A.; de Vries, A. H. M.; Salvadori, P.; Feringa, B. L. *Tetrahedron: Asymmetry* **2001**, *12*, 1929.
(55) Langner, M.; Remy, P.; Bolm, C. *Chem.-Eur. J.* **2005**, *11*, 6254.
(56) List, B.; Lerner, R. A.; Barbas, C. F. *J. Am. Chem. Soc.* **2000**, *122*, 2395.

(57) Seebach, D.; Beck, A. K.; Badine, D. M.; Limbach, M.; Eschenmoser, A.; Treasurywala, A. M.; Hobi, R.; Prikoszovich, W.; Linder, B. *Helv. Chim. Acta* **2007**, *90*, 425.

(58) Enders, D.; Grondal, C. *Angew. Chem.-Int. Edit.* **2005**, *44*, 1210.

(59) Tokuda, O.; Kano, T.; Gao, W. G.; Ikemoto, T.; Maruoka, K. *Org. Lett.* **2005**, *7*, 5103.

(60) Bogevig, A.; Kumaragurubaran, N.; Jorgensen, K. A. *Chem. Commun.* **2002**, 620.

(61) Tang, Z.; Jiang, F.; Yu, L. T.; Cui, X.; Gong, L. Z.; Mi, A. Q.; Jiang, Y. Z.; Wu, Y. D. *J. Am. Chem. Soc.* **2003**, *125*, 5262.

(62) Samanta, S.; Liu, J. Y.; Dodda, R.; Zhao, C. G. *Org. Lett.* **2005**, *7*, 5321.

(63) Palomo, C.; Oiarbide, M.; Laso, A. *Eur. J. Org. Chem.* **2007**, 2561.

(64) Arai, T.; Watanabe, M.; Yanagisawa, A. *Org. Lett.* **2007**, *9*, 3595.

(65) Evans, D. A.; Seidel, D.; Rueping, M.; Lam, H. W.; Shaw, J. T.; Downey, C. W. *J. Am. Chem. Soc.* **2003**, *125*, 12692.

(66) Zhang, G. Q.; Yashima, E.; Woggon, W. D. *Adv. Synth. Catal.* **2009**, *351*, 1255.

(67) Oila, M. J.; Tois, J. E.; Koskinen, A. M. P. *Lett. Org. Chem.* **2008**, *5*, 11.

(68) Trost, B. M.; Yeh, V. S. C.; Ito, H.; Bremeyer, N. *Org. Lett.* **2002**, *4*, 2621.

(69) Kogami, Y.; Nakajima, T.; Ikeno, T.; Yamada, T. *Synthesis* **2004**, 1947.

(70) Kowalczyk, R.; Sidorowicz, L.; Skarzewski, J. *Tetrahedron: Asymmetry* **2007**, *18*, 2581.

(71) Kiyooka, S.; Tsutsui, T.; Maeda, H.; Kaneko, Y.; Isobe, K. *Tetrahedron Lett.* **1995**, *36*, 6531.

(72) Arai, T.; Yamada, Y. M. A.; Yamamoto, N.; Sasai, H.; Shibasaki, M. *Chem.-Eur. J.* **1996**, *2*, 1368.

(73) Jacobsen, E. N.; Zhang, W.; Muci, A. R.; Ecker, J. R.; Deng, L. *J. Am. Chem. Soc.* **1991**, *113*, 7063.

(74) Kowalczyk, R.; Kwiatkowski, P.; Skarzewski, J.; Jurczak, J. *J. Org. Chem.* **2009**, *74*, 753.

(75) Christensen, C.; Juhl, K.; Hazell, R. G.; Jorgensen, K. A. *J. Org. Chem.* **2002**, *67*, 4875.

(76) Ginotra, S. K.; Singh, V. K. *Org. Biomol. Chem.* **2007**, *5*, 3932.

(77) Blay, G., Hernandez-Olmos, V., Pedro, J. R. *Chem. Commun.* **2008**, 4840.

(78) Bandini, M.; Piccinelli, F.; Tommasi, S.; Umani-Ronchi, A.; Ventrici, C. *Chem. Commun.* **2007**, 616.

(79) Constable, E. C., Zhang, G. Q., Housecroft, C. E., Neuberger, M., Schaffner, S., Woggon, W. D. *New J. Chem.* **2009**, *33*, 1064.

(80) Zhang, W.; Loebach, J. L.; Wilson, S. R.; Jacobsen, E. N. *J. Am. Chem. Soc.* **1990**, *112*, 2801.

(81) Brandes, B. D.; Jacobsen, E. N. *Synlett* **2001**, 1013.

(82) Jacobsen, E. N. *Accounts of Chemical Research* **2000**, *33*, 421.

(83) Daly, A. M.; Renehan, M. F.; Gilheany, D. G. *Org. Lett.* **2001**, *3*, 663.

(84) Irie, R.; Noda, K.; Ito, Y.; Matsumoto, N.; Katsuki, T. *Tetrahedron Lett.* **1990**, *31*, 7345.

(85) Gao, Y.; Hanson, R. M.; Klunder, J. M.; Ko, S. Y.; Masamune, H.; Sharpless, K. B. *J. Am. Chem. Soc.* **1987**, *109*, 5765.

(86) Brunner, H.; Kraus, J. *Journal of Molecular Catalysis* **1989**, *49*, 133.

(87) Botteghi, C.; Paganelli, S.; Schionato, A.; Boga, C.; Fava, A. *Journal of Molecular Catalysis* **1991**, *66*, 7.

(88) Desimoni, G.; Quadrelli, P.; Righetti, P. P. *Tetrahedron* **1990**, *46*, 2927.

(89) Shi, M.; Duan, W. L.; Rong, G. B. *Chirality* **2004**, *16*, 642.

(90) Bednarski, M.; Danishefsky, S. *J. Am. Chem. Soc.* **1983**, *105*, 6968.

(91) Schaus, S. E.; Branalt, J.; Jacobsen, E. N. *J. Org. Chem.* **1998**, *63*, 403.

(92) Wender, P. A.; Hilinski, M. K.; Soldermann, N.; Mooberry, S. L. *Org. Lett.* **2006**, *8*, 1507.

(93) Lucas, B. S.; Luther, L. M.; Burke, S. D. *J. Org. Chem.* **2005**, *70*, 3757.

(94) Paterson, I.; Luckhurst, C. A. *Tetrahedron Lett.* **2003**, *44*, 3749.

(95) Fan, Q.; Lin, L. L.; Liu, J.; Huang, Y. Z.; Feng, X. M.; Zhang, G. L. *Org. Lett.* **2004**, *6*, 2185.

(96) Leveque, L.; Le Blanc, M.; Pastor, R. *Tetrahedron Lett.* **2000**, *41*, 5043.

(97) Yang, X. B.; Feng, J.; Zhang, J.; Wang, N.; Wang, L.; Liu, J. L.; Yu, X. Q. *Org. Lett.* **2008**, *10*, 1299.

(98) Landa, A.; Richter, B.; Johansen, R. L.; Minkkila, A.; Jorgensen, K. A. *J. Org. Chem.* **2007**, *72*, 240.

(99) Dalko, P. I.; Moisan, L.; Cossy, J. *Angew. Chem.-Int. Edit.* **2002**, *41*, 625.

(100) Bolm, C.; Verrucci, M.; Simic, O.; Hackenberger, C. P. R. *Adv. Synth. Catal.* **2005**, *347*, 1696.

(101) Wang, Y.; Wolf, J.; Zavalij, P.; Doyle, M. R. *Angew. Chem.-Int. Edit.* **2008**, *47*, 1439.

(102) Du, H. F.; Long, J.; Hu, J. Y.; Li, X.; Ding, K. L. *Org. Lett.* **2002**, *4*, 4349.

(103) Kezuka, S.; Mita, T.; Ohtsuki, N.; Ikeno, T.; Yamada, T. *Chem. Lett.* **2000**, 824.

(104) Brown, L., Bursten, Langford, Sagatys, Duffy *Chemistry*; Pearson, 2007.

(105) De, B. B.; Lohray, B. B.; Sivaram, S.; Dhal, P. K. *Tetrahedron: Asymmetry* **1995**, *6*, 2105.

(106) Baleizao, C.; Gigante, B.; Garcia, H.; Corma, A. *J. Catal.* **2003**, *215*, 199.

(107) Xiang, S.; Zhang, Y. L.; Xin, Q.; Li, C. *Chem. Commun.* **2002**, 2696.

(108) Kureshy, R. I.; Ahmad, I.; Khan, N. H.; Abdi, S. H. R.; Pathak, K.; Jasra, R. V. *Tetrahedron: Asymmetry* **2005**, *16*, 3562.

(109) Baleizao, C.; Gigante, B.; Sabater, M. J.; Garcia, H.; Corma, A. *Appl. Catal. A-Gen.* **2002**, *228*, 279.

(110) Song, C. E.; Roh, E. J.; Yu, B. M.; Chi, D. Y.; Kim, S. C.; Lee, K. J. *Chem. Commun.* **2000**, 615.

(111) Angelino, M. D.; Laibinis, P. E. *Macromolecules* **1998**, *31*, 7581.

(112) Kleij, A. W. *European Journal of Inorganic Chemistry* **2009**, 193.

(113) Peerlings, H. W. I.; Meijer, E. W. *Chem.-Eur. J.* **1997**, *3*, 1563.

(114) Lee, H. M.; Kim, S. W.; Hyeon, T.; Kim, B. M. *Tetrahedron: Asymmetry* **2001**, *12*, 1537.

(115) Minutolo, F.; Pini, D.; Petri, A.; Salvadori, P. *Tetrahedron: Asymmetry* **1996**, *7*, 2293.

(116) Alvarez, R.; Hourdin, M. A.; Cave, C.; d'Angelo, J.; Chaminade, P. *Tetrahedron Lett.* **1999**, *40*, 7091.

(117) Kamahori, K.; Tada, S.; Ito, K.; Itsuno, S. *Tetrahedron: Asymmetry* **1995**, *6*, 2547.

(118) Sartor, D.; Saffrich, J.; Helmchen, G.; Richards, C. J.; Lambert, H. *Tetrahedron: Asymmetry* **1991**, *2*, 639.

(119) Fan, Q. H.; Chen, Y. M.; Chen, X. M.; Jiang, D. Z.; Xi, F.; Chan, A. S. C. *Chem. Commun.* **2000**, 789.

(120) Bayer, E.; Schurig, V. *Angew. Chem.-Int. Edit. Engl.* **1975**, *14*, 493.

(121) Han, H. S.; Janda, K. D. *J. Am. Chem. Soc.* **1996**, *118*, 7632.

(122) Bayston, D. J.; Travers, C. B.; Polywka, M. E. C. *Tetrahedron: Asymmetry* **1998**, *9*, 2015.

(123) terHalle, R.; Schulz, E.; Lemaire, M. *Synlett* **1997**, 1257.

(124) Halm, C.; Kurth, M. J. *Angew. Chem.-Int. Edit.* **1998**, *37*, 510.

(125) Dangel, B. D.; Polt, R. *Org. Lett.* **2000**, *2*, 3003.

(126) Locatelli, F.; Gamez, P.; Lemaire, M. *J. Mol. Catal. A-Chem.* **1998**, *135*, 89.

(127) Polborn, K.; Severin, K. *Chem. Commun.* **1999**, 2481.

(128) Beck, J. S., Vartuli, J. C., Roth, W. J., Leonowicz, M. E., Kresge, C. T., Schmitt, K. D., Chu, C. T. W., Olson, D. H., Sheppard, E. W., McCullen, S. B., Higgins, J. B., Schlenker, J. L. *J. Am. Chem. Soc.* **1992**, *114*, 10834.

(129) Raynor, S. A.; Thomas, J. M.; Raja, R.; Johnson, B. F. G.; Bell, R. G.; Mantle, M. D. *Chem. Commun.* **2000**, 1925.

(130) Blaser, H. U., Honig, H., Studer, M., Wedemeyer-Exl, C. *Journal of Molecular Catalysis A: Chemical* **1999**, *139*, 253.

(131) Lee, J. M., Kim, J., Shin, Y., Yeom, C. E., Lee, J. E., Hyeon, T., Kim, B. M. *Tetrahedron: Asymmetry* **2010**, *21*, 285.

(132) Pathak, K., Bhatt, A. P., Abdi, S. H. R., Kureshy, R. I., Khan, N. H., Ahmad, I., Jasra, R. V. *Tetrahedron: Asymmetry* **2006**, *17*, 1506.

(133) Cazes, J. *Encyclopedia of Chromatography*; 3rd ed.; CRC Press, 2009.

(134) Annis, D. A., Jacobsen, E. N. *J. Am. Chem. Soc.* **1999**, *121*, 4147.

(135) Pugin, B. *Journal of Molecular Catalysis A: Chemical* **1996**, *107*, 273.

(136) Motorina, I., Crudden, C. M. *Org. Lett.* **2001**, *3*, 2325.

(137) Caplan, N. A., Hancock, F. E., Page, P. C. B., Hutchings, G. J. *Angew. Chem.-Int. Edit.* **2004**, *43*, 1685.

(138) Xiang, S., Zhang, Y. L., Xin, Q., Li, C. *Chem. Commun.* **2002**, 2696.

(139) Feher, F. J.; Newman, D. A.; Walzer, J. F. *J. Am. Chem. Soc.* **1989**, *111*, 1741.

(140) Quadrelli, E. A.; Basset, J. M. *Coord. Chem. Rev.* **2010**, *254*, 707.

(141) Feher, F. J. *J. Am. Chem. Soc.* **1986**, *108*, 3850.

(142) Fraile, J. M.; Garcia, J. I.; Mayoral, J. A.; Vispe, E. *J. Catal.* **2005**, *233*, 90.

(143) Das, N.; Eckert, H.; Hu, H. C.; Wachs, I. E.; Walzer, J. F.; Feher, F. J. *J. Phys. Chem.* **1993**, *97*, 8240.

(144) Felpin, F. X.; Fouquet, E. *ChemSusChem* **2008**, *1*, 718.

(145) Park, K. H.; Son, S. U.; Chung, Y. K. *Org. Lett.* **2002**, *4*, 4361.

(146) Choudary, B. M.; Chowdari, N. S.; Jyothi, K.; Kumar, N. S.; Kantam, M. L. *Chem. Commun.* **2002**, 586.

(147) Thiot, C.; Schmutz, M.; Wagner, A.; Mioskowski, C. *Chem.-Eur. J.* **2007**, *13*, 8971.

Preparation of (*R,R*)-1,2-diaminocyclohexane Ligands

2.1 Introduction

Jacobsen's extensive work within asymmetric catalysis has been documented in chapter one.[1-8] It was demonstrated that his ligand-type, that is now known as the "Jacobsen ligand", is very versatile, in that the ligand forms complexes with many transition metals, and hence a vast array of reactions can be catalysed both homogeneously and heterogeneously. This ligand, based on (*R,R*)-1,2-diaminocyclohexane, can be seen in fig. 2.1.1.

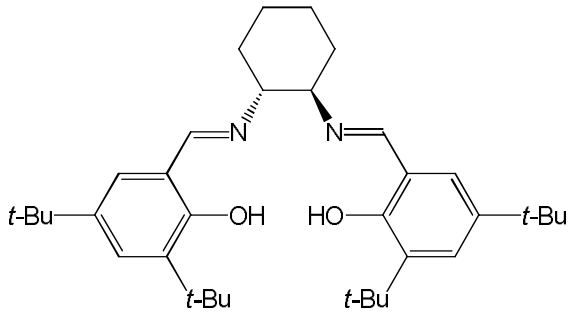

Fig. 2.1.1 Jacobsen's ligand, based on (*R,R*)-1,2-diaminocyclohexane

The purpose of the research described herein was to generate a library of chiral ligands that could then be complexed with a variety of transition metals. One aim of this research is to use the complexes prepared here as catalysts in a variety of asymmetric organic transformations. Following the extensive catalytic screening of these complexes, assessments can be made regarding which reactions display promise, and should be developed further. In addition, one can gauge which reactions are suitable to be performed in one pot in tandem, and therefore further research into the preparation of the appropriate bimetallic catalysts can begin. However, at this early stage of the research, it is unknown which reactions will possess the most scope for further development. This ligand is easily to modify, thus certain functional groups can be introduced to suit certain reactions. For example, a hydroxy group can be introduced in order to bind hard metals, which are more suitable for catalysing the asymmetric epoxidation reaction. In addition to this, the amine or imine functionalities bind

with ease to many metals, increasing the number of complexes that can be prepared with this ligand library, thus increasing the number of organic transformations that can be catalysed.

2.2 Chiral Resolution of 1,2-diaminocyclohexane

In 1994, Jacobsen reported using his (*R,R*)-1,2-diaminocyclohexane in the backbone to prepare ligands and catalysts for the asymmetric epoxidation reaction.[5] Part of this research detailed the chiral resolution of a mixture of *cis* and *trans* isomers of 1,2-diaminocyclohexane, which yielded the tartaric acid salt of the diastereomer, **1**. This was taken from procedures reported by Gasbol.[9] The experimental details of this process can be found in chapter 6. The reaction scheme can be seen in fig. 2.2.1.

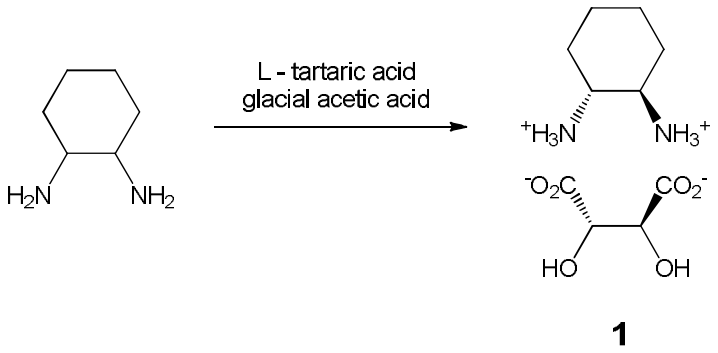

Fig. 2.2.1 Reaction scheme of the chiral resolution of 1,2-diaminocyclohexane

Compound **1** could be reacted with derivatives of benzaldehyde in the presence of potassium carbonate to produce the desired ligand, where an organic:aqueous solvent separation would be required post reaction to remove any inorganic salts. However, this procedure would not be suitable for certain ligands. For example, if this procedure is performed with ligands containing alcohol moieties, the yield is greatly reduced due to a significant portion of the ligand being taken into the aqueous phase. If the ligand contains a phosphine group, the aqueous phase may encourage oxidation of these groups, and so this procedure is unsuitable. Hence,

compound **1** is reacted further to remove the tartaric acid group, as shown in fig. 2.2.2, and purified via sublimation.

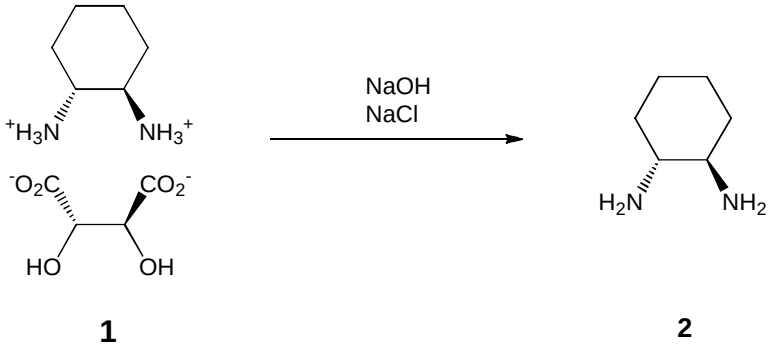

Fig. 2.2.2 Reaction scheme of the preparation of (*R*,*R*)-1,2-diaminocyclohexane

The product, compound **2**, was analysed by multinuclear NMR spectroscopy and mass spectrometry, as was compound **1**. However, the physical appearance and behaviour of compounds **1** and **2** are very different, which can be used in conjunction with analytical characterisation. For instance, compound **1** is a highly crystalline and a relatively stable material; compound **2** is much less crystalline in appearance and at room temperature, is extremely hydroscopic. For this reason, compound **2** is stored at -20 °C. From this point, compound **2** can be reacted with various aldehydes to produce the library of ligands that will now be discussed.

2.3 Reaction of (*R*,*R*)-1,2-diaminocyclohexane with Derivatives of Benzaldehyde

Compound **2** was reacted with various derivatives of benzaldehyde, as shown in fig. 2.3.1.

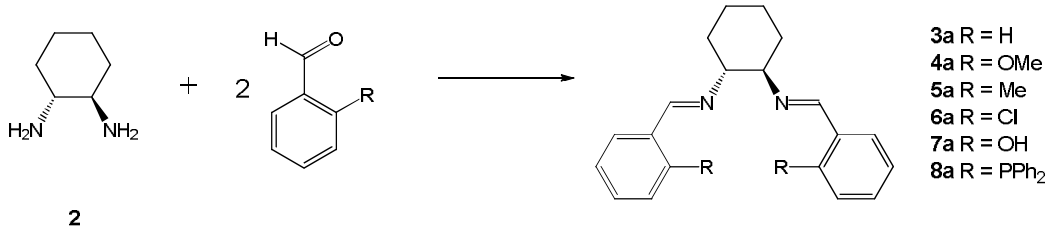

Fig. 2.3.1 Reaction scheme of the reaction of derivatives of benzaldehyde with (*R,R*)-1,2-diaminocyclohexane

The ligands were characterised by multinuclear NMR spectroscopy and mass spectrometry. Compound **3a** was also characterised by single crystal X-ray diffraction. The structure can be seen in fig. 2.3.2, and a selection of bond lengths and angles are provided in table 2.3.1.

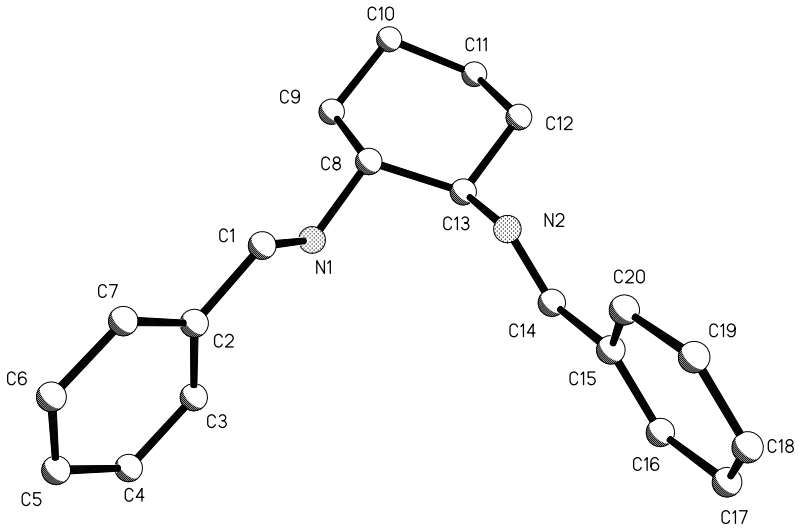

Fig. 2.3.2 Solid-state structure of ligand 3a, all hydrogen atoms have been removed for clarity

Table 2.3.1 A selection of bond lengths and angles for ligand 3a

Bond Length / Å		**Bond Angle / °**	
N(1)-C(8)	1.465 (2)	C(8)-N(1)-C(1)	117.92 (15)
N(1)-C(1)	1.264 (2)	N(1)-C(1)-C(2)	122.93 (16)
N(2)-C(13)	1.471 (2)	C(13)-N(2)-C(14)	117.60 (14)
N(2)-C(14)	1.261 (2)	N(2)-C(14)-C(15)	122.45 (15)

The data shows that the structure belongs to the orthorhombic $P2_12_12_1$ space group. The bonds N(1)-C(1) and N(2)-C(14) are shorter than the bonds N(1)-C(8) and N(2)-C(13), which is expected as N(1)-C(1) and N(2)-C(14) are sp^2 hybridised. The double bonds are shorter due to the π-bonding that occurs due to the overlapping of the p-orbitals.

The bond angles of C(8)-N(1)-C(1) and C(13)-N(2)-C(14) are slightly below the expected values of 120 °, which can be explained by the repulsion between the lone pair of the nitrogen atom and the N(1)-C(1) {or N(2)-C(14)} double bond. The bond angles of N(1)-C(1)-C(2) and N(2)-C(14)-C(15) are slightly above the expected values of 120 °, which is explained by the repulsion between the electron dense N(1)-C(1) or N(2)-C(14) double bond and the electron dense aromatic ring. The bond lengths and angles discussed here are in agreement with literature values of similar ligands.[10-12]

Ligands containing imine groups may be unsuitable for certain catalytic processes. For example in catalysing the asymmetric hydrogenation reaction, there is a chance that these imine groups may be reduced, thus altering the catalyst and potentially the catalytic results. Hence, for these applications these ligands were reduced prior to complex preparation, producing the amine-containing ligand systems. The reaction scheme can be seen in fig. 2.3.3.

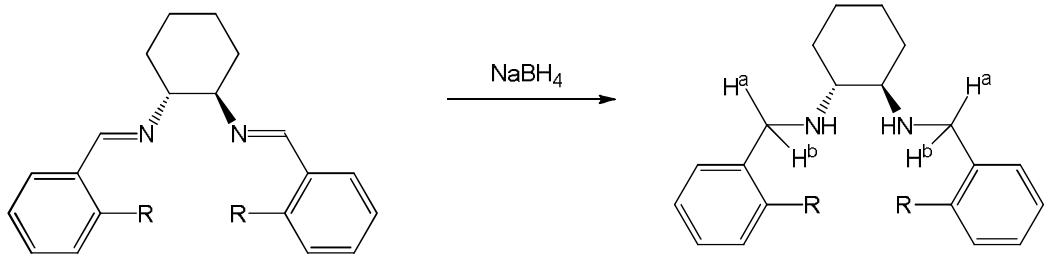

3a R = H
4a R = OMe
5a R = Me
6a R = Cl
7a R = OH
8a R = PPh_2

3b R = H
4b R = OMe
5b R = Me
6b R = Cl
7b R = OH
8b R = PPh_2

Fig. 2.3.3 Reaction scheme of the reduction of the imine ligands 3a-8a to the corresponding amines 3b-8b

The ligands were characterised by multinuclear NMR spectroscopy and mass spectrometry. All characterisation indicated that the reaction had been successful, as did comparing the physical aspects of the ligands; the amine ligands were very oily in comparison with their imine counterparts. Fig. 2.3.4 shows the NMR spectra for ligands **3a** and **3b**. Comparing the spectra, one can clearly see the disappearance of the imine peak at 8.21 ppm on reduction from **3a** to **3b**. In addition, the appearance of a doublet of doublets can be seen at 3.61 and 3.80 ppm, with each doublet having identical J coupling constants of 13 Hz. This is due to the geminal protons of the C**H**$_2$NH group within the ligand being diastereotopic, as shown in fig. 2.3.3. The nearby chiral centre and restricted rotation means these protons are chemically non-equivalent, giving rise to the splitting pattern observed. These features of the NMR spectrum of **3b**, which are also seen in ligands **(4-8)b**, suggest that the reductions have been successful.

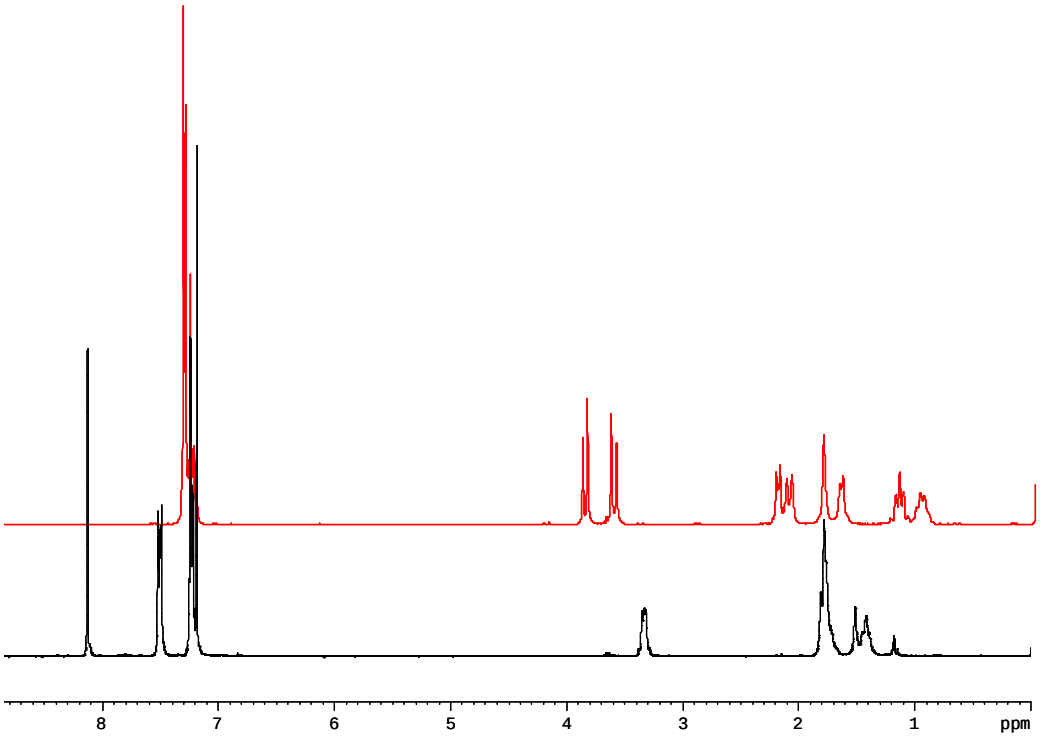

Fig. 2.3.4 ^{1}H NMR spectra of the imine ligand 3a (black), and its reduced amine version 3b (red)

2.4 Reaction of (*R,R*)-1,2-diaminocyclohexane with Aromatic Aldehydes Containing Heteroatoms

The ligands described in section 2.3 contain two sites for chelation to the metal centre. The ligands described in this section contain four potential chelation points. This may mean that the resulting metal complex is more rigid, and so sterically there is less freedom around the metal centre during catalysis. This in turn may provide greater enantioselectivity during the catalytic process.

Pyridine-type aldehydes can be used in conjunction with compound **2** to form a library of ligands with four chelation sites. The reaction scheme can be seen in fig 2.4.1.

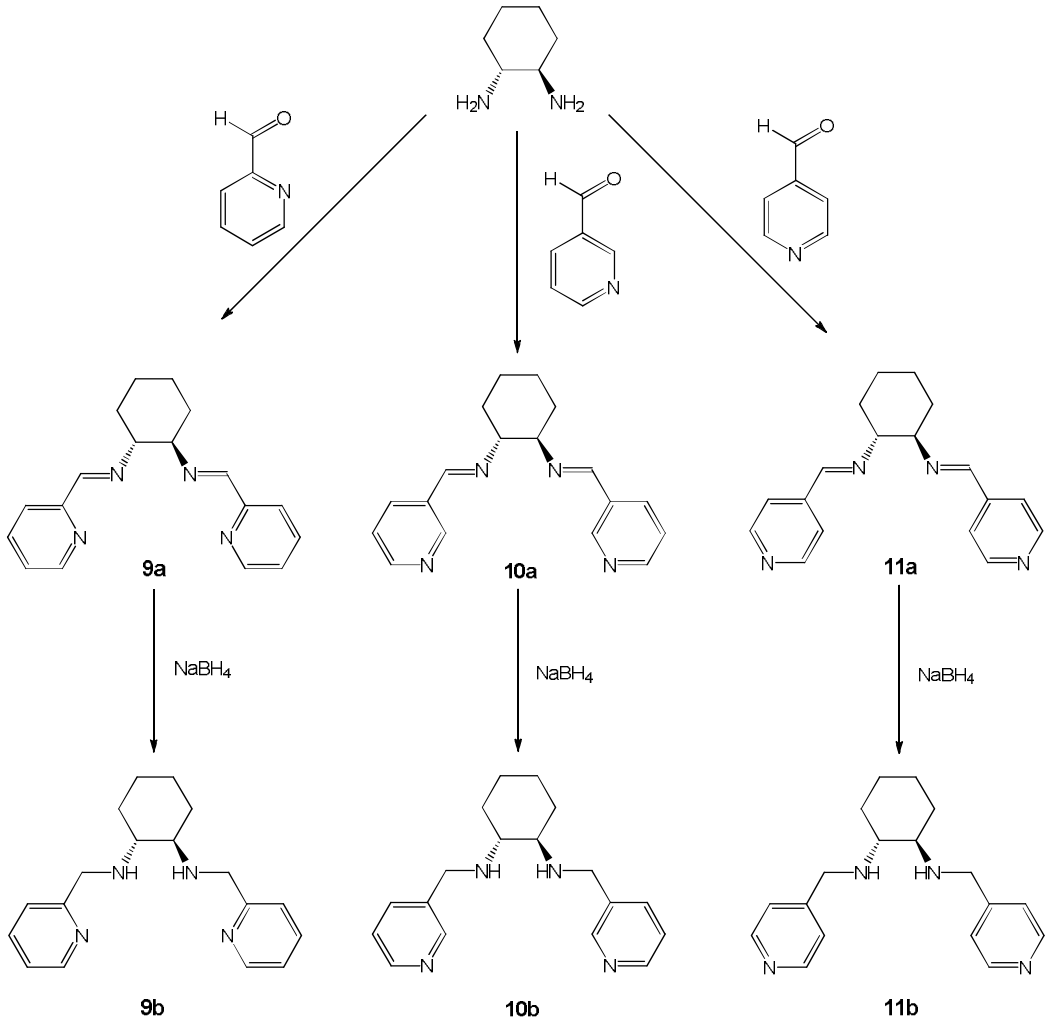

Fig. 2.4.1 Reaction schemes of the reaction of (*R,R*)-1,2-diaminocyclohexane with various aldehyde derivatives of pyridine, and the reduction of these compounds

The ligands were analysed by multinuclear NMR spectroscopy and mass spectrometry. By varying the position of the heteroatom within the aromatic ring, the geometry of the subsequent complexes will be significantly affected. This in turn could have a notable effect upon catalytic performance. The ease of complex formation may also be affected. For instance with ligands **9a/9b**, transition metal complexes may be readily formed in comparison to ligand **11a/11b**, where the position of the heteroatom in the aromatic ring could provide too much steric strain to form a tetra-chelating complex.

Further steric bulk was added in the ligands shown in fig. 2.4.2. In adding steric bulk, the direction that the substrate enters from and the binding position of the substrate during catalysis could be affected, and so enantioselectivity may be improved further.

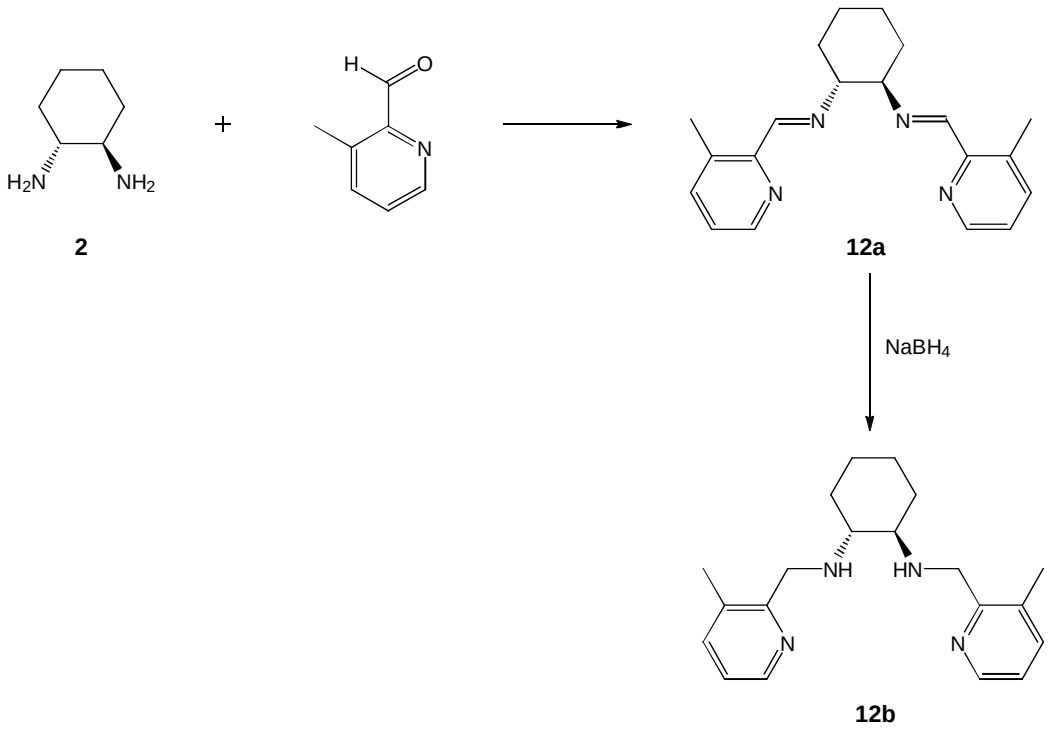

Fig. 2.4.2 Reaction scheme of (*R,R*)-1,2-diaminocyclohexane and 3-methylpyridine-2-carboxaldehyde, and the reduction of the resulting compound

Finally, the heteroatom itself was varied, as shown in fig 2.4.3. This could be important for a number of reasons. One is that the electron densities on the metal centre of the resulting complexes may vary with the change in heteroatom. This

in turn could affect catalytic behaviour. Also, varying the heteroatom could affect the stability of the complex. This can be explained by considering ligands and metals in terms of "hardness". In general terms, this describes the bonding between the ligand and metal. "Hard" lewis acids and bases exhibit bonding that is more ionic in character, and "soft" acids and bases show bonding that is more covalent in character. The bonding is between the ligand and metal, and so to produce the most stable complexes, hard metals should complex to hard ligands and soft metals to soft ligands, in order to allow a match between the preferred bonding characters of the two. Examples of hard metals include Ti^{4+}, Al^{3+}, Cr^{2+}, Cr^{3+}; softer metals include Pd^{2+}, Pt^{2+}, Cu^{+}. In terms of hard ligands, $R_2O > R_2S > R_3N > R_3P$.[13] In the context of the research reported here, if these ligands were bound to Ti(IV), it is predicted that the phenoxide-containing ligands would produce the most stable complexes, whereas if the ligands were bound to Rh(I), perhaps the phosphine- or pyridine-containing ligands would be more suitable.

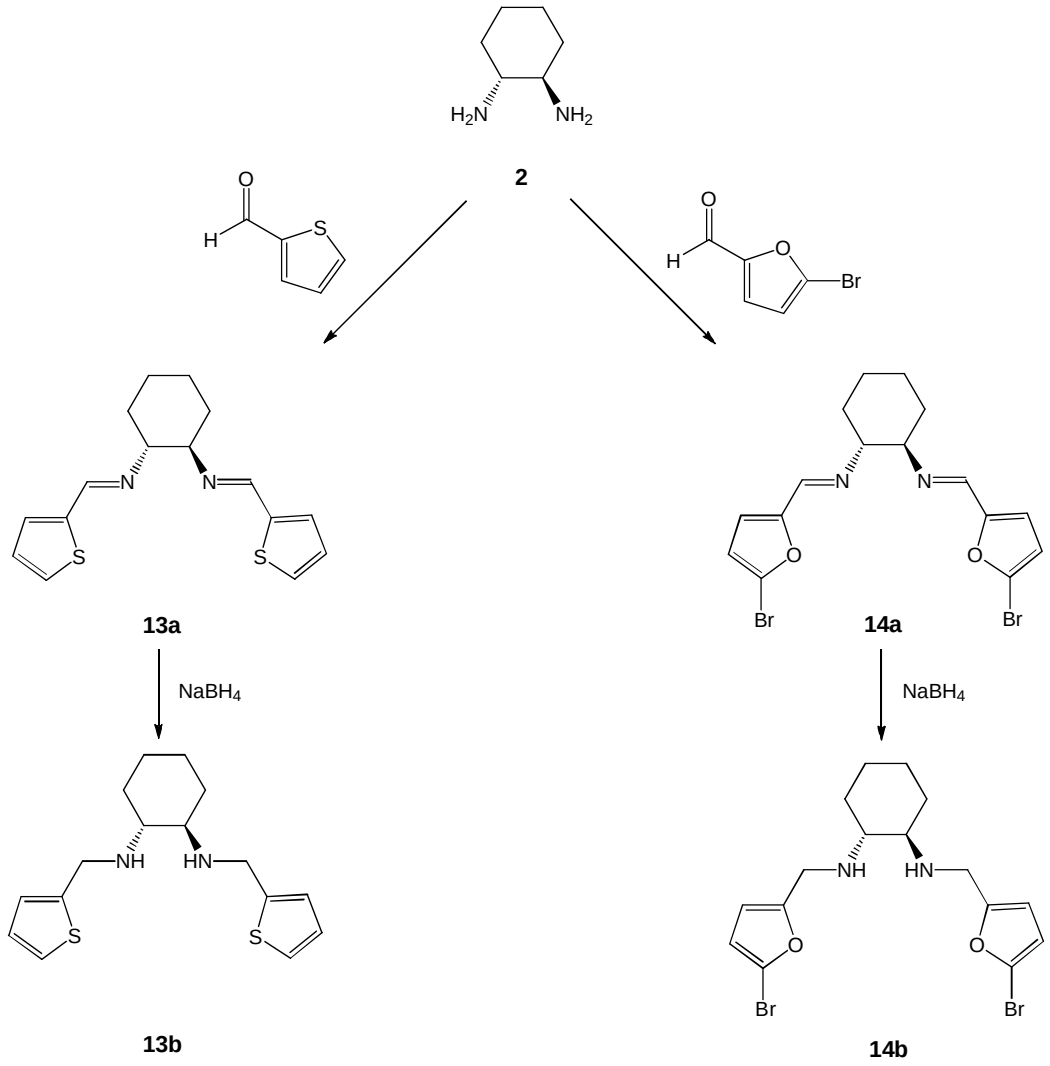

Fig. 2.4.3 Reaction schemes of the preparation of imine and amine thiophene- and furanyl-based ligands containing (*R,R*)-1,2-diaminocyclohexane

In the preparation of ligands **13a/13b** and **14a/14b**, the aldehyde precursors were chosen firstly on their similarity to the pyridine-type precursor previously described, and secondly on which precursors were commercially readily available. Ligands **14a** and **14b** have a halogen functionality attached to the aromatic ring, which could have significant effects on any future catalysis performed with the complexes of these ligands. Therefore when discussing the catalysis, it must be remembered that the complexes based on these type of ligands are not strictly like for like.

Ligand **13a** was analysed using single crystal X-ray diffraction. The crystal structure and a selection of bond lengths and angles can be seen in fig. 2.4.4 and table 2.4.1 respectively.

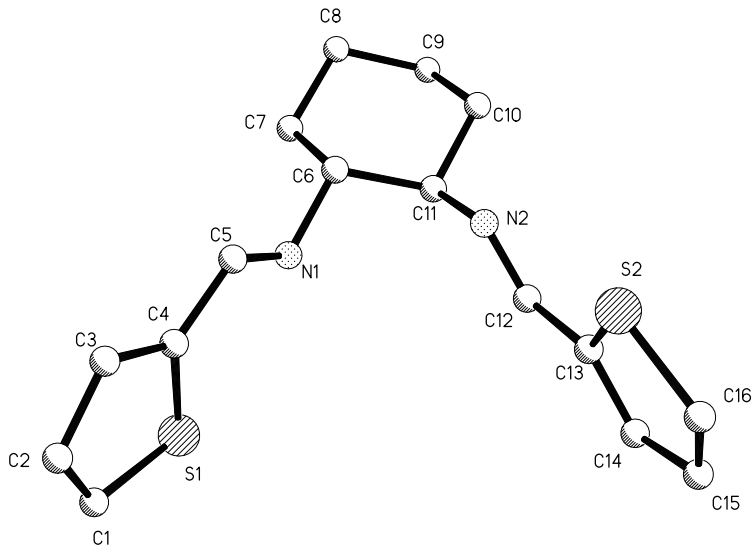

Fig. 2.4.4 Solid-state structure of imine ligand 13a, all hydrogen atoms have been removed for clarity

Table 2.4.1 A selection of bond lengths and angles for ligand 13a

Bond Length / Å		**Bond Angle / °**	
N(1)-C(6)	1.4632 (16)	C(6)-N(1)-C(5)	117.06 (12)
N(1)-C(5)	1.2636 (18)	N(1)-C(5)-C(4)	122.40 (12)
N(2)-C(11)	1.4638 (16)	C(11)-N(2)-C(12)	116.47 (11)
N(2)-C(12)	1.2655 (18)	N(2)-C(12)-C(13)	124.49 (13)

The bond lengths and angles discussed here are in agreement with literature values of similar ligands.[10-12] The data shows that the structure belongs to the monoclinic $P2_1$ space group. The bonds N(1)-C(5) and N(2)-C(12) are shorter than the bonds N(1)-C(6) and N(2)-C(11), which is expected as N(1)-C(5) and N(2)-C(12) are double bonds. The double bonds are shorter due to the π-bonding that occurs due to overlapping of the p-orbitals.

The bond angles of C(6)-N(1)-C(5) and C(11)-N(2)-C(12) are slightly below the expected values of 120 °, which can be explained by the repulsion between the

lone pair of the nitrogen atom and the N(1)-C(5) or N(2)-C(12) double bond. The bond angles of N(1)-C(5)-C(4) and N(2)-C(14)-C(15) are slightly above the expected values of 120 °, which is explained by the repulsion between the electron dense N(1)-C(5) or N(2)-C(12) double bond and the electron dense aromatic ring.

2.5 Preparation of Ligands Containing Naphthalene Groups

There have been vast amounts of research into the use of BINAP and related ligands in asymmetric catalysis, particularly in hydrogenation reactions.[14-19] Although BINAP in particular has not been used in this research, binaphthalene-type ligands have. These ligands can be seen in fig. 2.5.1.

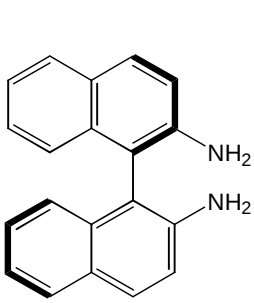

15

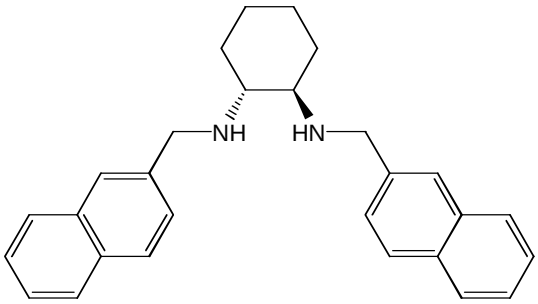

16

Fig. 2.5.1 Binaphthalene-type ligands 15 and 16. 15 was purchased and 16 was prepared as in fig. 2.3.1

Binaphthalene-type ligands have a very particular 3-D structure, and any degree of freedom that is present in terms of rotation about bonds will be greatly reduced when bound to a metal centre. Thus, potentially a very rigid complex will be formed, which as previously discussed in section 2.4, may improve enantioselectivity.

2.6 Use of 2-(aminomethyl)-1-ethyl-pyrrolidine for Ligand Preparation

So far, the ligands described have encompassed (*R*,*R*)-1,2-diaminocyclohexane as the chiral cyclic diamine from which the imine and amine ligands are formed. As previously discussed in chapter one, Jacobsen found that the use of a cyclic diamine restricts rotation within the ligand, which not only produces a more rigid complex, but more importantly, dictates the direction from which the substrate enters from during catalysis.[2] For this reason, cyclic diamines are used in the research reported here.[20] 2-(aminomethyl)-1-ethyl-pyrrolidine provides an alternative cyclic diamine to 1,2-diaminocyclohexane. The reaction scheme for preparing these ligands is given in fig. 2.6.1.

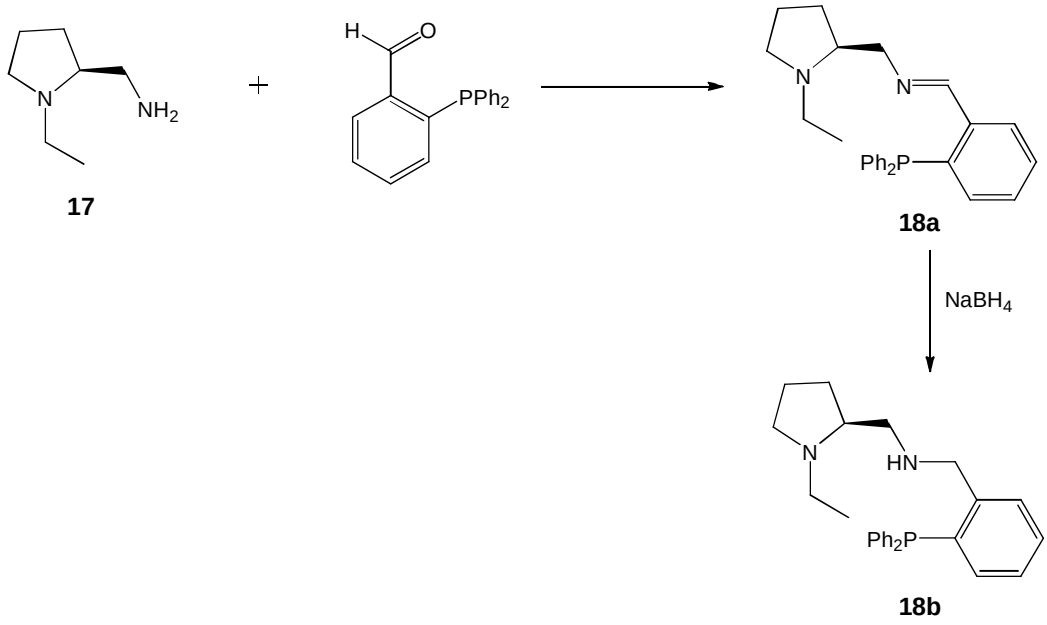

Fig. 2.6.1 Reaction scheme showing the preparation of ligands based on (*S*)-2-(aminomethyl)-1-ethyl-pyrrolidine

2.7 Preparation of Unsymmetrical Ligands

The ligands described so far have been suitable for monometallic complexes and are symmetrical. The ligands described in this section are unsymmetrical and potentially designed to produce bimetallic complexes. The preparation of these ligands can be seen in fig. 2.7.1.

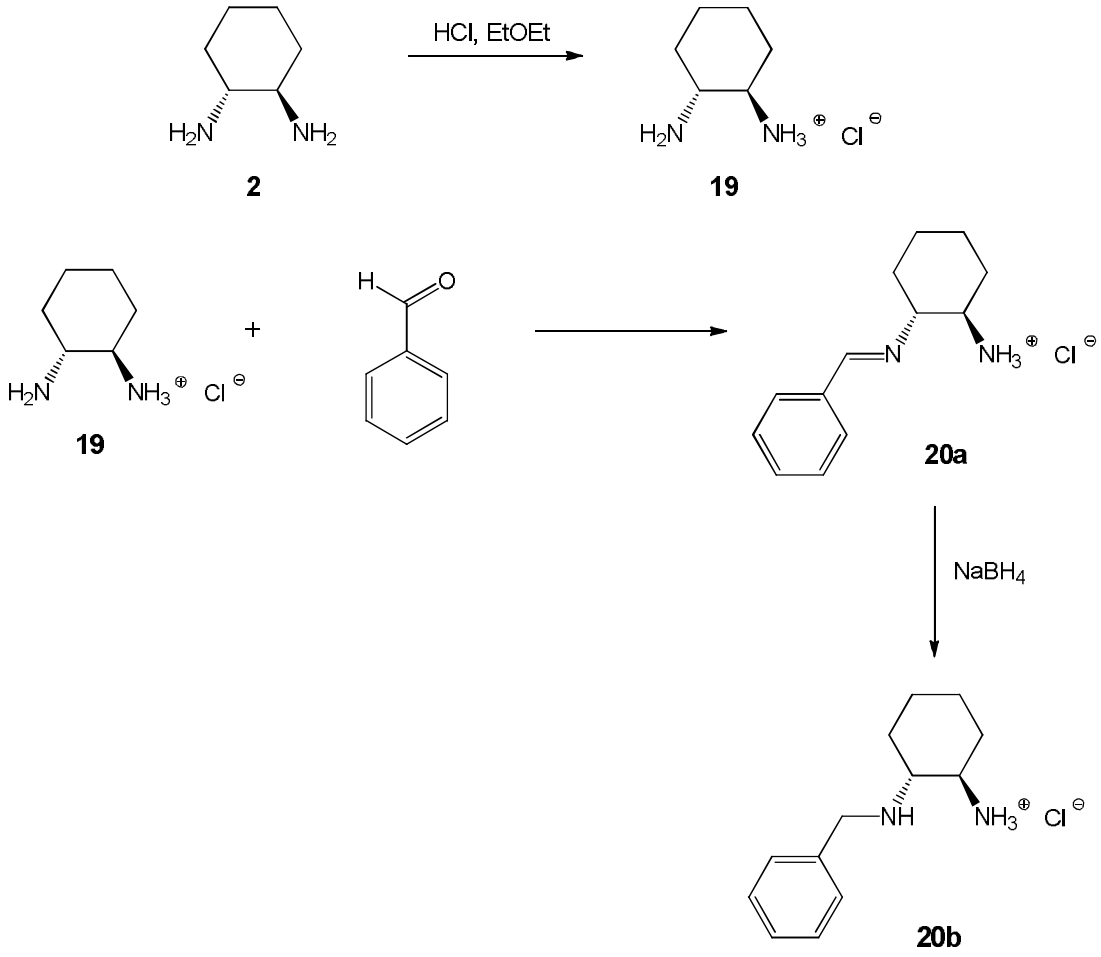

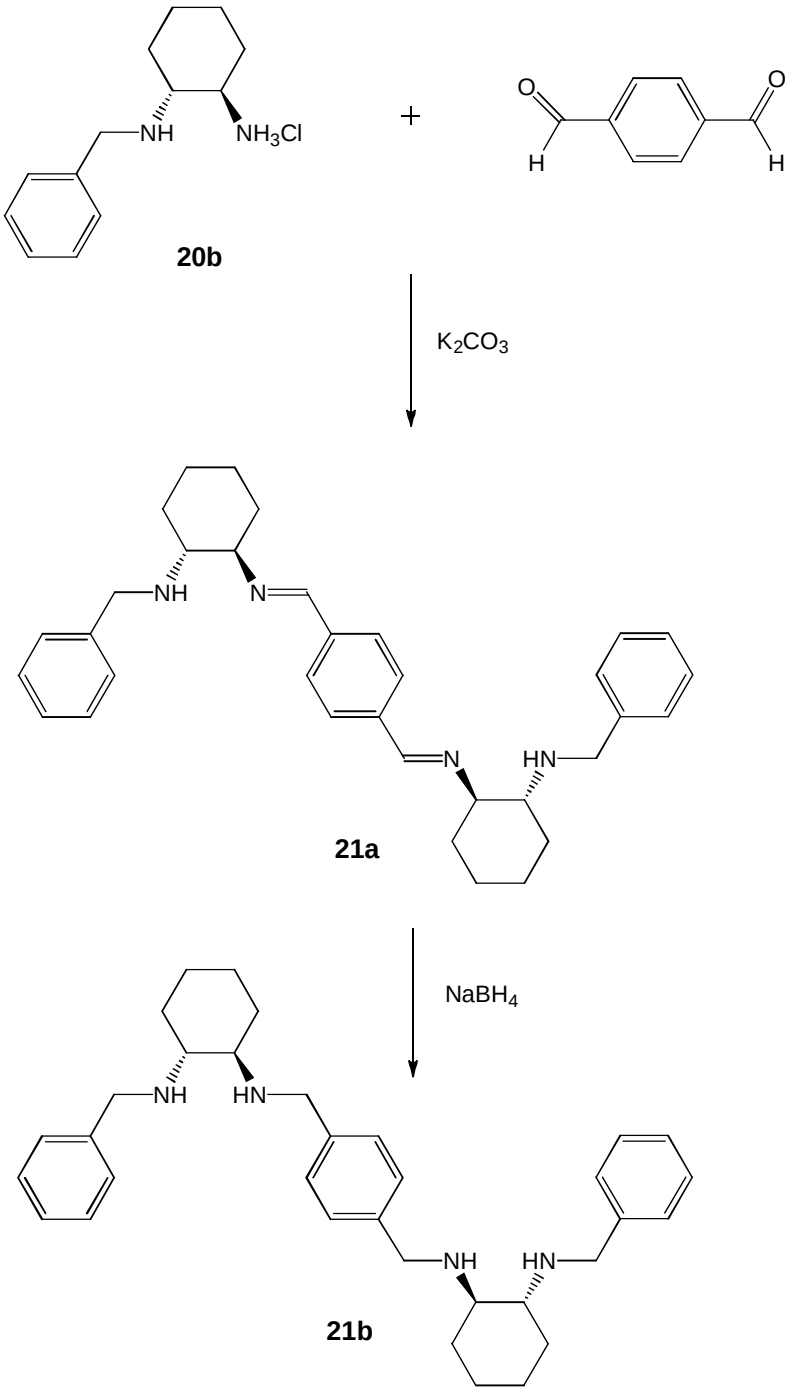

Fig. 2.7.1 Reaction scheme showing the preparation of a non-symmetrical ligand based on (*R*,*R*)-1,2-diaminocyclohexane

In the research reported here, the two metals will be the same, as the nature of the ligand means that if two different metals are used, there is no way of controlling where the metals bind, and in which particular combination. For example, if copper(II) and rhodium(I) were added to ligand **21b**, a solely bimetallic copper(II) complex, a solely bimetallic rhodium(I) complex or a mixture of copper(II) and

rhodium(I) bimetallic complex could form. Alternatively, combinations of monometallic and bimetallic complexes could be observed. Nevertheless, it will be interesting to see if bimetallic complexes do form, and from this, how the catalytic properties are affected, and allow any synergetic effects to be investigated. As previously discussed in chapter one, significant amounts of leaching were observed from both homogeneous and heterogeneous bimetallic catalysts, although in the cases discussed the two metals were different. It would be interesting to observe if leaching was seen in the bimetallic catalysts reported in this work.

2.8 Incorporation of phenoxide groups

As previously discussed in section 2.4, the presence of certain heteroatoms can encourage (or discourage) complex formation with certain metals. This is due to the "hardness" of the ligand and metal, for instance, where titanium (IV) is used (a hard metal), the ligand must bind through a hard atom, such as oxygen. Therefore a collection of ligands have been prepared which contain phenoxide groups, and are described here.

Fig. 2.8.1 shows a collection of ligands that are based on (*R*,*R*)-1,2-diaminocyclohexane. Jacobsen has used this cyclic diamine in preparing his ligands, and as has already been discussed, excellent catalytic results were observed.

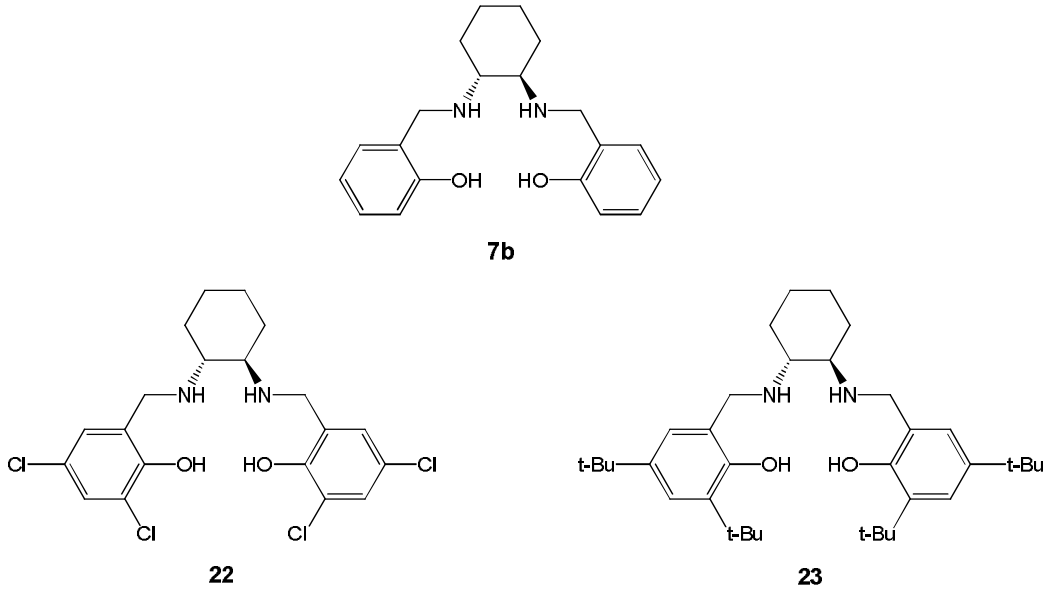

Fig. 2.8.1 Amine ligands containing phenoxide moieties

2.9 Concluding remarks

A library of ligands has been prepared. These ligands differ in terms of the functional groups that are present, hence expanding the range of transition metal complexes that can be prepared herein. In addition, the number of sites for chelation has been varied, that subsequently will produce complexes of varying rigidity, which in turn may affect catalytic properties. The amines and aldehydes used have been varied to produce a variation of classes of salen and salan ligands, rather than just varying substituents within one class of ligand. Also, ligands have been prepared specifically designed for the preparation of bimetallic complexes. Table 2.9.1 shows which of the ligands reported in this chapter are novel.

Table 2.9.1 Of the ligands described in this chapter, the ligands given in this table are novel

Ligand	
5a	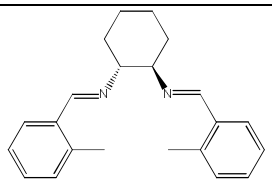
5b	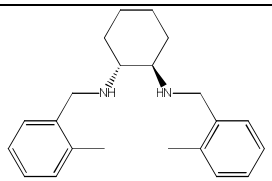
6a	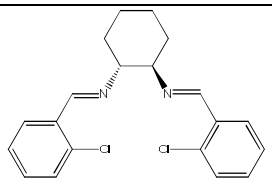
6b	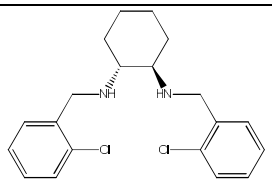
12a	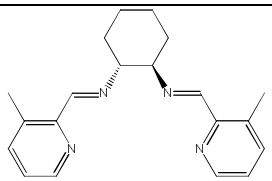
12b	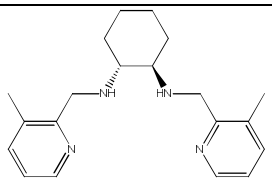
14b	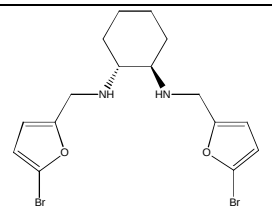
16	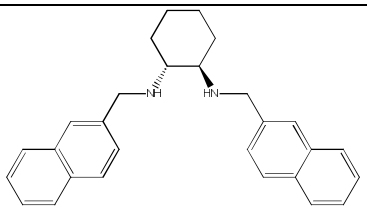

18a	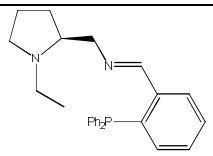
18b	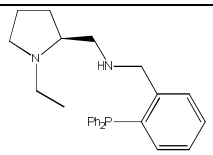

2.10 References

(1) Zhang, W.; Loebach, J. L.; Wilson, S. R.; Jacobsen, E. N. *J. Am. Chem. Soc.* **1990**, *112*, 2801.

(2) Jacobsen, E. N.; Zhang, W.; Muci, A. R.; Ecker, J. R.; Deng, L. *J. Am. Chem. Soc.* **1991**, *113*, 7063.

(3) Jacobsen, E. N. *Accounts of Chemical Research* **2000**, *33*, 421.

(4) Schaus, S. E.; Branalt, J.; Jacobsen, E. N. *J. Org. Chem.* **1998**, *63*, 403.

(5) Larrow, J. F.; Jacobsen, E. N.; Gao, Y.; Hong, Y. P.; Nie, X. Y.; Zepp, C. M. *J. Org. Chem.* **1994**, *59*, 1939.

(6) Brandes, B. D.; Jacobsen, E. N. *Synlett* **2001**, 1013.

(7) Brandes, B. D.; Jacobsen, E. N. *J. Org. Chem.* **1994**, *59*, 4378.

(8) Annis, D. A., Jacobsen, E. N. *J. Am. Chem. Soc.* **1999**, *121*, 4147.

(9) Gasbol, F., Steenbol, P., Sorensen, B. S. *Acta. Chem. Scand.* **1972**, *26*, 3605.

(10) Lalehzari, A.; Desper, J.; Levy, C. J. *Inorg. Chem.* **2008**, *47*, 1120.

(11) Khalaji, A. D.; Akerdi, S. J.; Grivani, G.; Stoeckli-Evans, H.; Das, D. *Russ. J. Coord. Chem.* **2011**, *37*, 578.

(12) Tang, B. B.; Sun, X. P.; Liu, G. L.; Li, H. *J. Mol. Struct.* **2010**, *984*, 111.

(13) Shriver, D. F., Atkins, P. W. *Inorganic Chemistry*; 3rd ed.; Oxford University Press, 1999.

(14) Miyashita, A.; Yasuda, A.; Takaya, H.; Toriumi, K.; Ito, T.; Souchi, T.; Noyori, R. *J. Am. Chem. Soc.* **1980**, *102*, 7932.

(15) Ohta, T.; Takaya, H.; Kitamura, M.; Nagai, K.; Noyori, R. *J. Org. Chem.* **1987**, *52*, 3174.

(16) Ohta, T.; Takaya, H.; Noyori, R. *Inorg. Chem.* **1988**, *27*, 566.

(17) Kitamura, M.; Kasahara, I.; Manabe, K.; Noyori, R.; Takaya, H. *J. Org. Chem.* **1988**, *53*, 708.

(18) Kitamura, M.; Tokunaga, M.; Ohkuma, T.; Noyori, R. *Tetrahedron Lett.* **1991**, *32*, 4163.

(19) Fan, Q. H.; Chen, Y. M.; Chen, X. M.; Jiang, D. Z.; Xi, F.; Chan, A. S. C. *Chem. Commun.* **2000**, 789.

(20) Jones, M. D.; Raja, R.; Thomas, J. M.; Johnson, B. F. G.; Lewis, D. W.; Rouzaud, J.; Harris, K. D. M. *Angew. Chem.-Int. Edit.* **2003**, *42*, 4326.

Preparation of Transition Metal Complexes of the Ligands Prepared in Chapter Two

3.1 Introduction

The ligands synthesised were described in chapter two. Chapter one detailed a variety of catalytic asymmetric reactions of current interest. It highlighted the fact that different metals are suited to catalyse different reactions, and also that ligand modification is required to improve on the catalytic results subsequently observed. Hence, the ligands discussed in chapter two have been designed with specific functionalities to encourage complexing with certain metals, for example, phenoxide moieties are found in the ligands that will be complexed to titanium(IV) and zirconium(IV). Also, the cyclic amine within the ligand has been varied, along with other substituents, in anticipation of the need to modify and fine-tune the ligand for a particular catalytic purpose.

This chapter sees the discussion of the homogeneous complexes of these ligands, their characterisation, and any surprising behaviour that these complexes may exhibit.

3.2 Precious Group Metal Complexes

3.2.1 Iridium(I) Complexes

A selection of the ligands described in chapter two were used to prepare iridium(I) complexes. Initial attempts at this saw the use of $[Ir(cod)Cl]_2$ in conjunction with Ag(I) triflate, as shown in fig. 3.2.1.

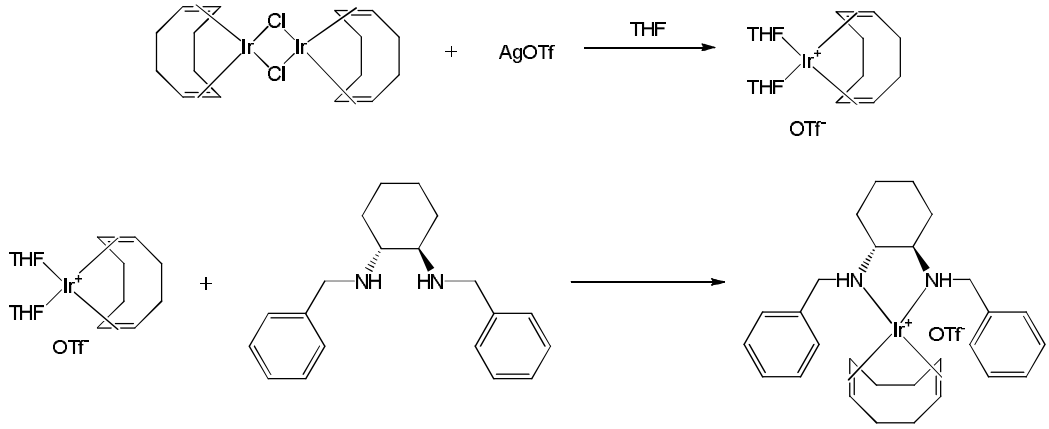

Fig. 3.2.1 Reaction scheme of the preparation of iridium(I) complexes

The resulting complexes were analysed by NMR spectroscopy and mass spectrometry. During NMR analysis, a black precipitate was observed, which was thought to be "*iridium black*". This phenomenon has also been observed by other research groups.[1] This prompted further investigation into these complexes. Initially it was thought was that an impurity in the ligand could be present such as water (a by-product in our ligand preparation) at a low level that destabilises the complex. This was the reason for introducing ligand **15** which is commercially available, but still as a diamine with restricted rotation has similar steric and electronic properties to the Jacobsen-type ligands. Another feature for investigation was the effect of the counterion on the stability of the complex, which saw the introduction of BF_4^-.

Ligand **15** was purchased from Strem Chemicals. [Ir(**15**)(cod)](OTf) was subsequently prepared and characterised under an inert atmosphere, and once again iridium black was observed. This suggests that the formation of iridium

black in this case is not caused by small levels of impurities that may be present in our ligand preparation but due to the instability of the complexes.

Single crystal X-ray diffraction was performed on the [Ir(**15**)(cod)]OTf complex. The crystal structure can be seen in fig. 3.2.2, and a selection of bond lengths and angles are given in table 3.2.1.

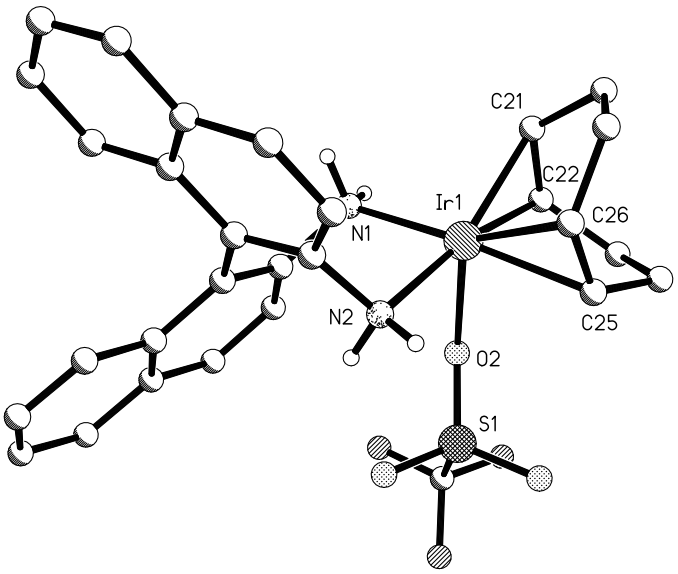

Fig. 3.2.2 Solid-state structure of [Ir(15)(cod)]OTf. All hydrogen atoms and a molecule of triflic acid have been removed for clarity

Table 3.2.1 A selection of bond lengths and angles for [Ir(15)(cod)]OTf

Length / Å		**Angle / °**	
Ir(1)-N(1)	2.132(4)	N(1)-Ir(1)-N(2)	86.69(16)
Ir(1)-N(2)	2.141(4)	N(1)-Ir(1)-C(21)	91.6(2)
Ir(1)-C(21)	2.231(6)	N(1)-Ir(1)-C(22)	93.23(18)
Ir(1)-C(22)	2.189(5)	N(2)-Ir(1)-C(25)	96.7(2)
Ir(1)-C(25)	2.198(5)	N(2)-Ir(1)-C(26)	90.1(2)
Ir(1)-C(26)	2.197(5)	C(21)-Ir(1)-C(22)	36.3(2)
Ir(1)-O(2)	2.259(4)	C(22)-Ir(1)-C(25)	81.4(2)
		N(1)-Ir(1)-O(2)	84.10(14)
		C(22)-Ir(1)-O(2)	78.85(18)

The data showed that the structure belongs to the orthorhombic $P22_12_1$ space group. The absolute structure parameter is -0.007(7), which indicates that the complex is enantiomerically pure. The bond lengths and angles are in agreement with literature values for similar complexes.[2-4] It must be noted that there are relatively few examples of Ir(I) cod diamine complexes compared to Rh(I) on the Cambridge Crystallographic Database (CCD). The scarcity of such complexes is presumably due to the ease of decomposition of these complexes to iridium black.

The C(21)-Ir(1)-C(22) bond angle is small, which is expected. The remaining bond angles provided have iridium as their central atom, and are all fairly close to 90 °. This suggests that the complex takes a pseudo square-based pyramidal form with the coordinated triflate. The slight deviations in bond angles away from 90 ° are likely to result from steric constraints, given the fact that the two ligands (the chiral amine and cod) are bulky. The widest bond angles are those that separate the two ligands, i.e. N(1)-Ir(1)-C(21), N(1)-Ir(1)-C(22), N(2)-Ir(1)-C(25) and N(2)-Ir(1)-C(26). This also supports the theory that the bond angles are distorted due to steric hindrance between the chiral ligand and the cod.

The data also showed a molecule of triflic acid within the unit cell, which is not indicated in fig. 3.2.2. The triflic acid could be produced by trace levels of water or oxygen present in the reaction. However, even under stringent Schlenk and glove box techniques the formation of iridium black was unavoidable. The acidity of the triflic acid present could be encouraging the decomposition of the complex. Some iridium complexes were prepared using BF_4^- as a counterion rather than OTf^-. On preparing and characterising these complexes, no iridium black was observed. This suggests that the triflate counterion is likely to be facilitating the decomposition of the afore-mentioned complexes. Following this, any future iridium(I) complexes were prepared using $AgBF_4$. These complexes were also analysed by NMR spectroscopy and mass spectrometry. A typical NMR spectrum of a iridium(I) complex, and the comparison with the free ligand can be seen in fig. 3.2.3.

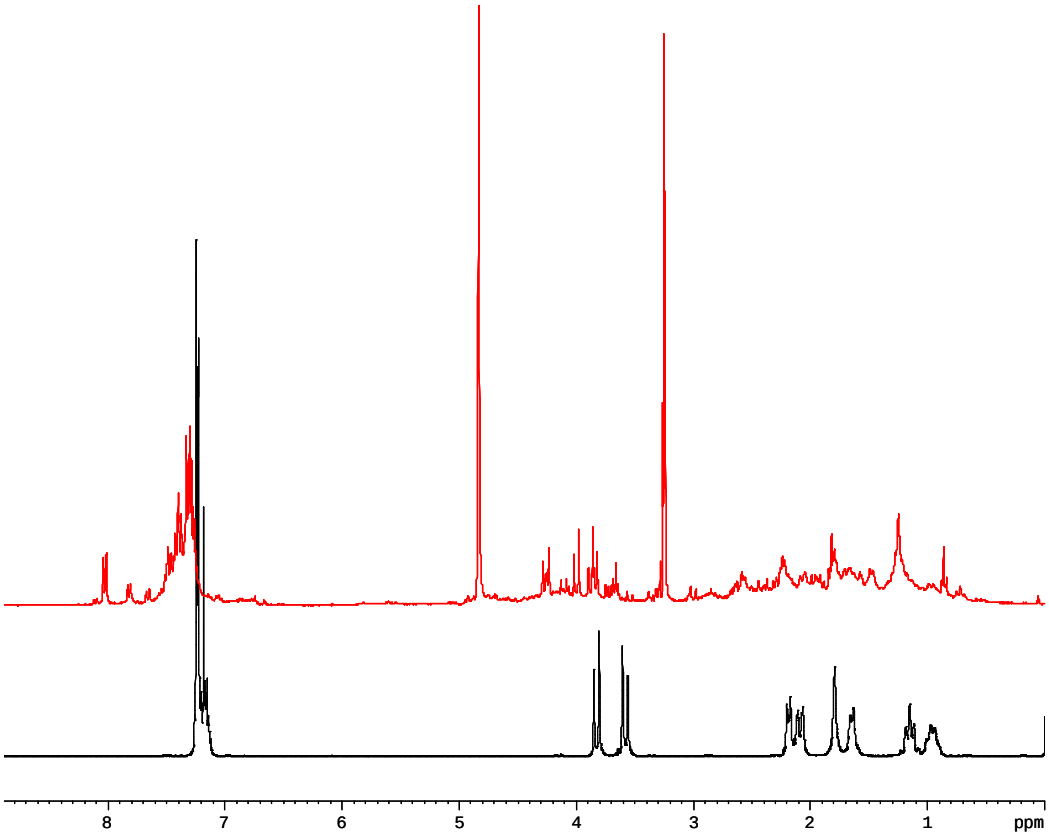

Fig. 3.2.3 ^{1}H NMR spectra of ligand 3b (black), and its iridium complex [Ir(3b)(cod)]BF_4 (red)

The aliphatic region (0-4 ppm) of the complex is very broad, which is not uncommon for such complexes. There are more resonances in this region than would be seen for the free ligand. However, there are extra resonances due to the aliphatic protons of the cyclooctadiene ligand. In the spectrum of the free ligand, a well defined double doublet can be seen at 3.71 ppm. In the spectrum of the complex, this doublet of doublets can be observed, but is overlapped to some extent by other peaks in this region, likely to be due to the alkene protons of the cyclooctadiene ligand. Furthermore, once the ligand is coordinated it becomes "locked" in configuration. Now all the protons which were equivalent in the free ligand are no longer equivalent in the complexes – this is an example of the diastereotopic effect. In the aromatic region, the major resonances have broadened substantially on complexing to the iridium centre, which again is not uncommon for such complexes.

3.2.2 Rhodium(I) Complexes

A selection of the ligands described in chapter two were used to prepare rhodium(I) complexes. The reaction scheme for this can be seen in fig. 3.2.4.

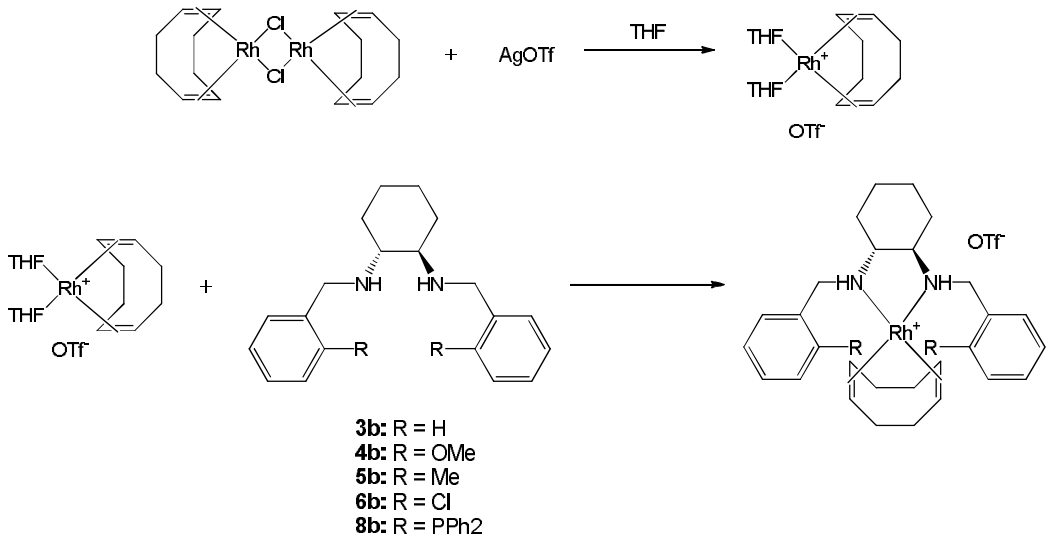

Fig. 3.2.4 Reaction scheme of the preparation of rhodium(I) complexes

The resulting complexes were analysed by multinuclear NMR spectroscopy and mass spectrometry. A typical NMR spectrum of a rhodium(I) complex, and the comparison with the free ligand can be seen in fig. 3.2.5.

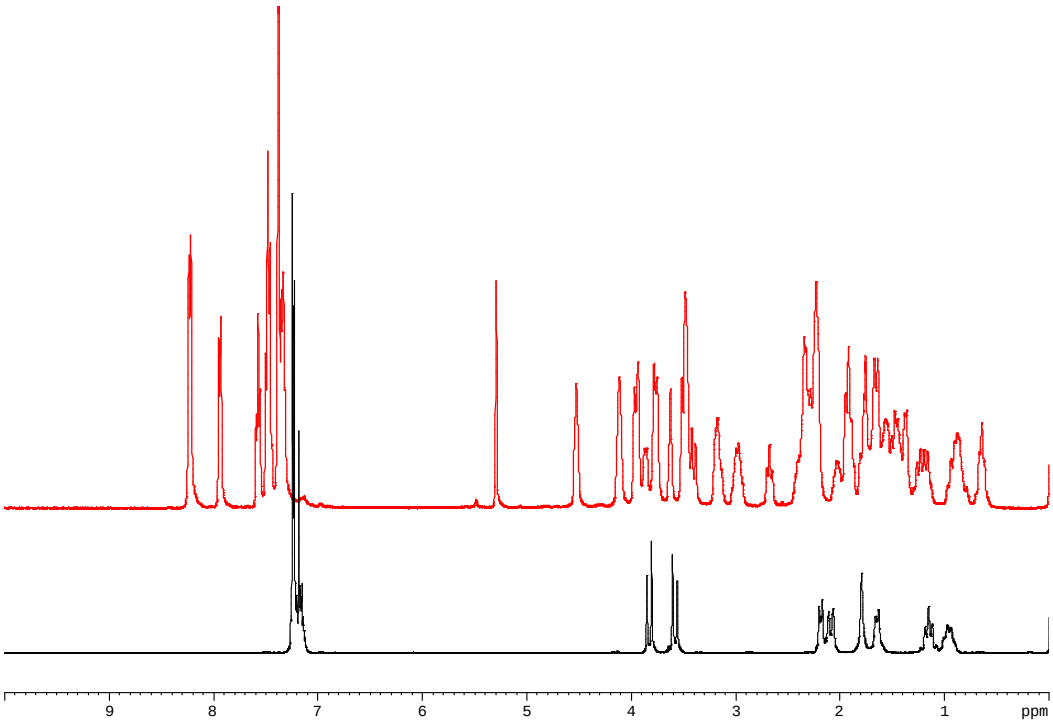

Fig. 3.2.5 ^{1}H NMR spectra of ligand 3b (black), and its rhodium complex [Rh(3b)(cod)]BF_4 (red)

On examining the aliphatic region (0-4 ppm), the resonances corresponding to the ligand in the complex can be seen clearly. The extra resonances in the spectrum of the complex are due to the cyclooctadiene ligand. In the spectrum of the free ligand, a well defined doublet of doublets can be seen at 3.71 ppm. In the spectrum of the complex, this doublet of doublets is not observed. The protons of this doublet of doublets are bonded to the adjacent carbon to the chelating nitrogen atoms. When bound to the metal, the amine and adjacent carbon (and hence its protons) are held in one position. Therefore, these protons are now all in a different chemical environment, and are therefore chemically inequivalent, so will give rise to separate resonances. This explains the absence of the doublet of doublets and the appearance of a significantly more complex NMR spectrum. In addition to this, extra resonances will be observed in this region due to the CH/CH_2's of the cyclooctadiene ligand. It is not uncommon for complexes of this type to yield complicated NMR spectra, for example those prepared by Johnson, Raja and Jones.[5] In these examples all protons are now inequivalent due to the fact that the ligand is "locked" upon coordination, hindering rotation around C-C/N bonds which causes certain environments, which are equivalent in the ligand, to be non-equivalent once complexed.

[Rh(**3b**)(cod)]BF_4 was analysed by single crystal X-ray diffraction. The crystal structure can be seen in fig. 3.2.6 and a selection of bond lengths and angles are given in table 3.2.2.

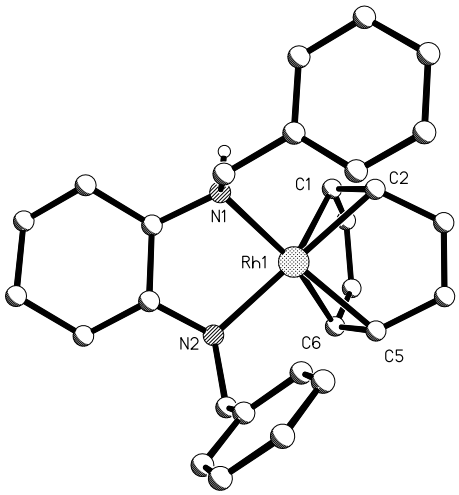

Fig. 3.2.6 Solid-state structure of [Rh(3b)(cod)]BF_4. All hydrogen atoms {except those bound to N(1) and N(2)} and the BF_4^- counterion have been removed for clarity

Table 3.2.2 A selection of bond lengths and angles for [Rh(3b)(cod)]BF_4

Length / Å		**Angle / °**	
Rh(1)-N(1)	2.133(3)	N(1)-Rh(1)-N(2)	81.50(9)
Rh(1)-N(2)	2.147(2)	N(1)-Rh(1)-C(1)	93.63(12)
Rh(1)-C(1)	2.230(3)	N(1)-Rh(1)-C(2)	96.36(11)
Rh(1)-C(2)	2.154(3)	N(2)-Rh(1)-C(5)	99.00(14)
Rh(1)-C(5)	2.137(4)	N(2)-Rh(1)-C(6)	90.72(13)
Rh(1)-C(6)	2.139(3)	C(1)-Rh(1)-C(2)	37.81(12)
		C(2)-Rh(1)-C(5)	81.26(13)

The data showed that the structure belongs to the orthorhombic $P2_12_12_1$ space group. The absolute structure parameter is -0.04(3), which indicates that the complex is enantiomerically pure. The bond lengths and angles are in agreement with literature values of similar complexes.[2-7]

When comparing this complex with the [Ir(**15**)(cod)]OTf complex, as both metals are in the same group and similar ligands are employed, their geometric behaviour should be similar. From the crystal data, it was concluded that

[Ir(**15**)(cod)]OTf preferred a pseudo square-based pyramidal geometry. Given that in this case, the counterion is not bound to the metal it is assumed that [Rh(**3b**)(cod)]BF_4 will prefer a square planar geometry, which is in agreement with many Rh(I) species.[5] In general, the bond angles support this, with the angles being close to 90 °, and any deviation is minor. As has been previously discussed, the use of the ring system of 1,2-diaminocyclohexane dramatically decreases the flexibility in the ligand. This explains why the bond angle N(1)-Rh(1)-N(2) is lower than the expected 90 ° (approximately 81 °). The bond angles N(1)-Rh(1)-C(2) and N(2)-Rh(1)-C(5) are higher than expected, due to steric hindrance between the two bulky ligands, thus the angles are increased to minimise this, causing distortion of the bond angles within the rest of the complex.

[Rh(**6b**)(cod)]BF_4 was also analysed by single crystal X-ray diffraction. The crystal structure can be seen in fig. 3.2.7, and a selection of bond lengths and angles are given in table 3.2.3, these are in agreement with [Rh(**3b**)(cod)]BF_4. This is the first example of a solid state structure involving ligand **6b** with any metal.

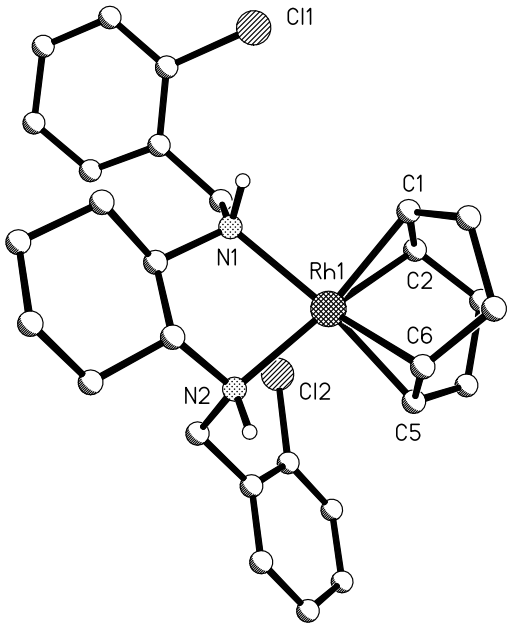

Fig. 3.2.7 Solid-state structure of [Rh(6b)(cod)]BF_4. All hydrogen atoms and the BF_4^- counterion have been removed for clarity

Table 3.2.3 A selection of bond lengths and angles for [Rh(6b)(cod)]BF_4

Length / Å		Angle / °	
Rh(1)-N(1)	2.137(8)	N(1)-Rh(1)-N(2)	80.4(3)
Rh(1)-N(2)	2.152(8)	N(1)-Rh(1)-C(5)	93.3(4)
Rh(1)-C(1)	2.144(11)	N(1)-Rh(1)-C(6)	97.9(4)
Rh(1)-C(2)	2.144(9)	N(2)-Rh(1)-C(1)	93.7(4)
Rh(1)-C(5)	2.116(12)	N(2)-Rh(1)-C(2)	97.1(3)
Rh(1)-C(6)	2.155(11)	C(1)-Rh(1)-C(2)	37.3(4)
		C(2)-Rh(1)-C(5)	82.2(4)

The data showed that the structure belongs to the monoclinic *C*2 space group. The absolute structure parameter is -0.02(8), which indicates that the complex is enantiomerically pure. The bond lengths and angles are in agreement with literature values of similar complexes.[2-7]

Comparing this complex with the [Rh(**3b**)(cod)]BF_4 complex, they both prefer a square planar geometry, as is commonplace for d^8 complexes. The bond angles support this, with the angles being close to 90 °, and any deviation is either due to steric repulsion between the two ligands, or dependent on the lack of rotation within the chiral ligand, as previously discussed with regards to the [Rh(**3b**)(cod)]BF_4 complex. Importantly, elemental analysis is also in agreement with the proposed structures, indicating pure complexes are formed, ready for catalytic screening.

3.2.3 Ruthenium(II) Complexes

A selection of the ligands described in chapter two were utilised to prepare ruthenium(II) complexes. The reaction scheme for this can be seen in fig. 3.2.8.

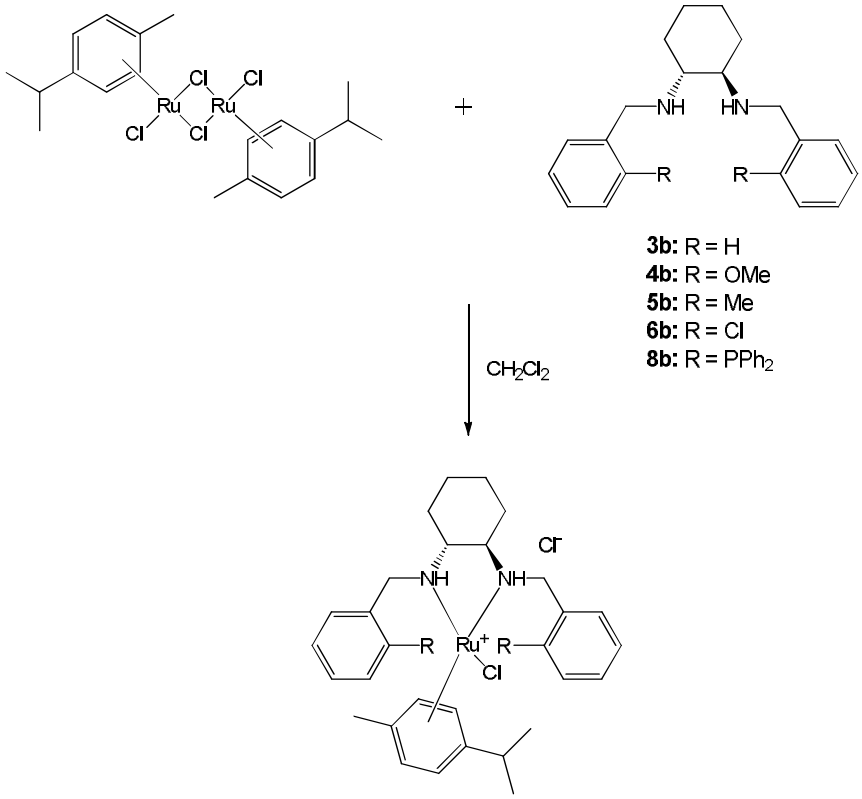

Fig. 3.2.8 Reaction scheme of the preparation of ruthenium(II) complexes

The resulting complexes were analysed by NMR spectroscopy and mass spectrometry. A typical NMR spectrum of a ruthenium(II) complex, and the comparison with the free ligand can be seen in fig. 3.2.9.

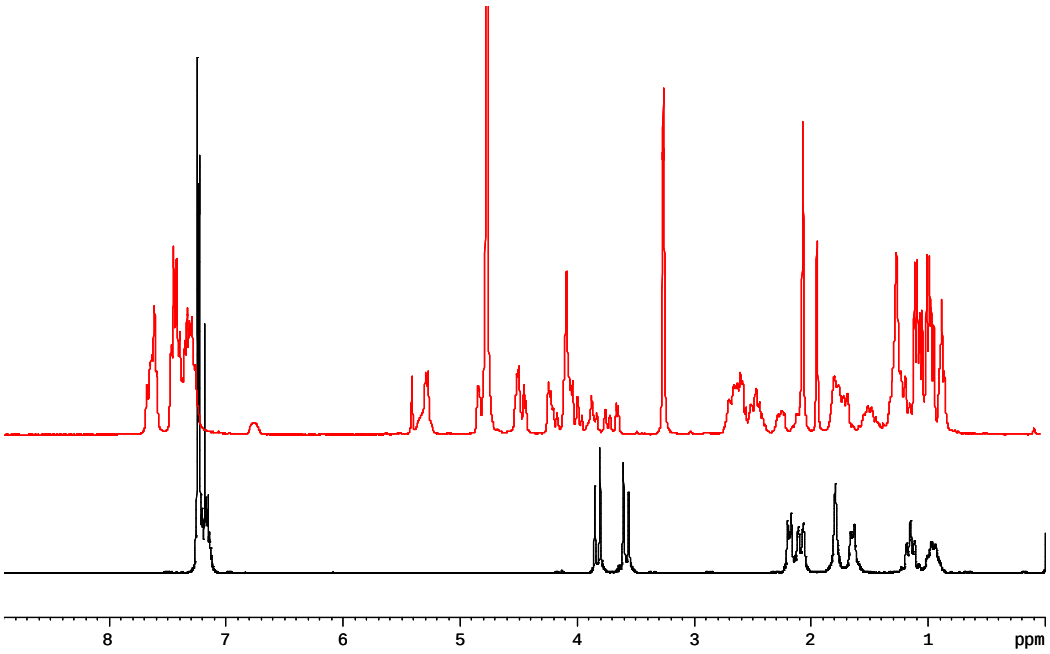

Fig. 3.2.9 ^{1}H NMR spectra of the ligand 3b (black), and its ruthenium(II) complex Ru(3b)(*p*-cym)Cl_2 (red)

On examining the aliphatic region (0-4 ppm), the resonances corresponding to the ligand in the complex can be seen clearly. The extra resonances in the spectrum of the complex are due to the *p*-cymene ligand, (for example, at approximately 4.5 and 5.4 ppm). In the spectrum of the free ligand, a well defined doublet of doublets can be seen at 3.71 ppm. In the spectrum of the complex, this doublet of doublets is not observed. The protons of this doublet of doublets are bonded to the adjacent carbon to the chelating nitrogen atoms. When bound to the metal, the amine and adjacent carbon (and hence its protons) are completely held in one position. Therefore, these protons are now all in a different environment, and will therefore give rise to separate resonances. This explains the absence of the doublet of doublets and the appearance of more peaks in this region of the spectrum. In comparing the aromatic regions of the two spectra, there are more peaks, which is to be expected with the presence of the *p*-cymene ligand.

3.2.4 Platinum(II) and Palladium(II) Complexes

Ligands **3b** and **9a** were used to prepare platinum(II) and palladium(II) complexes. The reaction scheme for this can be seen in fig. 3.2.10.

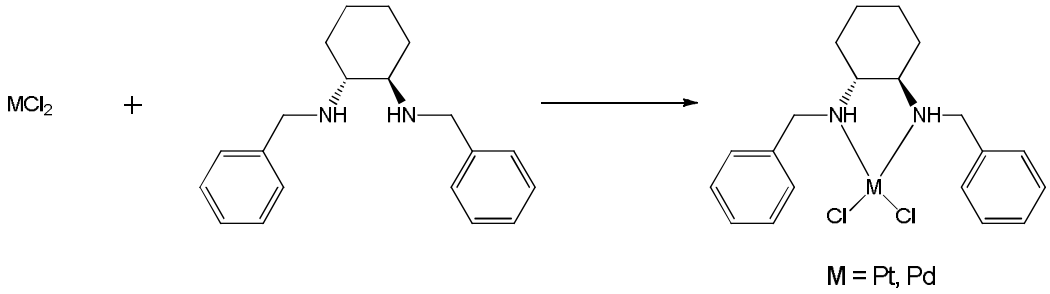

Fig. 3.2.10 Reaction scheme of the preparation of platinum(II) and palladium(II) complexes

The resulting complexes were analysed by NMR spectroscopy and mass spectrometry. The NMR spectrum of Pd(**3b**)Cl_2 is shown in fig. 3.2.11 along with the free ligand, for comparison.

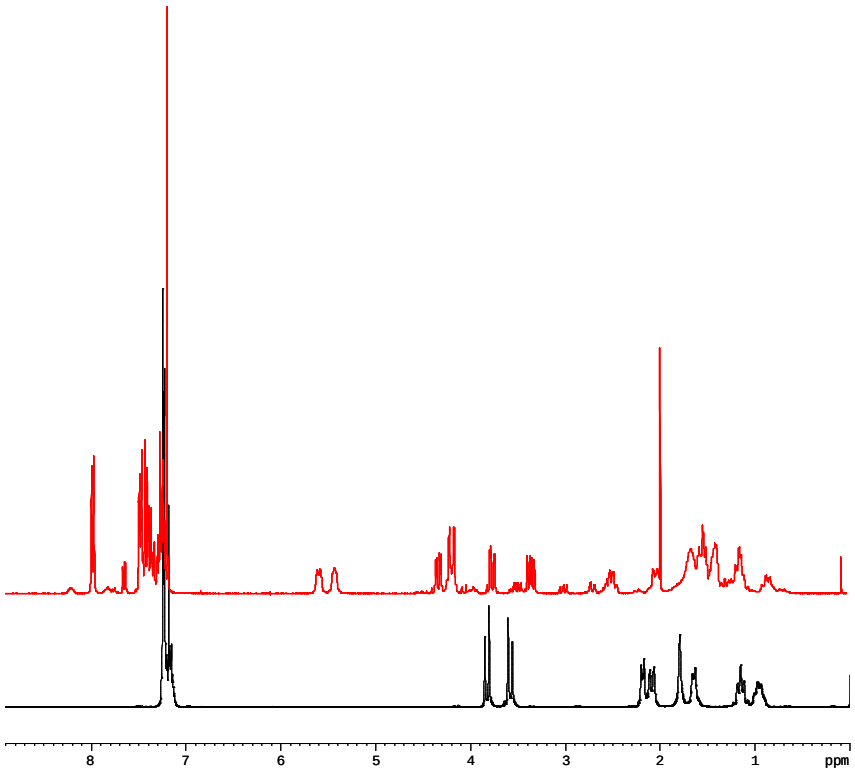

Fig. 3.2.11 ^{1}H NMR spectra of the ligand 3b (black), and its palladium(II) complex Pd(3b)Cl_2 (red)

In comparing the two spectra, with close examination they are relatively similar; this is to be expected given that the only protons in the complex are provided by the ligand. The main difference between spectra is in the aliphatic region. As previously discussed, when the ligand binds to the metal, the majority of the rotation about bonds and movement within the ligand is removed, fixing the atoms of the ligand in one position. Because of this, the number of protons in "equivalent" environments is reduced, and so more resonances are observed due to this. The resonances in the aliphatic region (0-3 ppm) are due to the protons of the cyclohexane ring, which will be fixed in one position on complexing of the ligand to the metal. This explains the increase of the number of resonances in this region, in comparison to the free ligand. A similar observation was observed for Pt(**3b**)Cl_2.

3.3 Copper(II) Complexes

3.3.1 Copper(II) Complexes of Bichelating Ligands

A selection of the ligands described in chapter two were used to prepare copper(II) complexes. The reaction schemes for this are shown in figs. 3.3.1, 3.3.2 and 3.3.3.

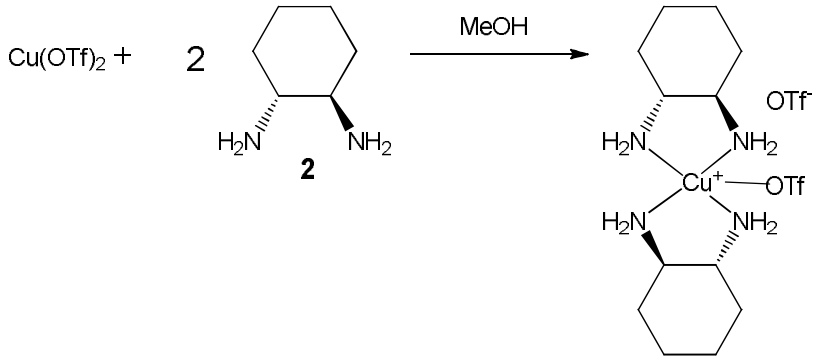

Fig. 3.3.1 Reaction scheme of the preparation of $Cu(2)_2(OTf)_2$

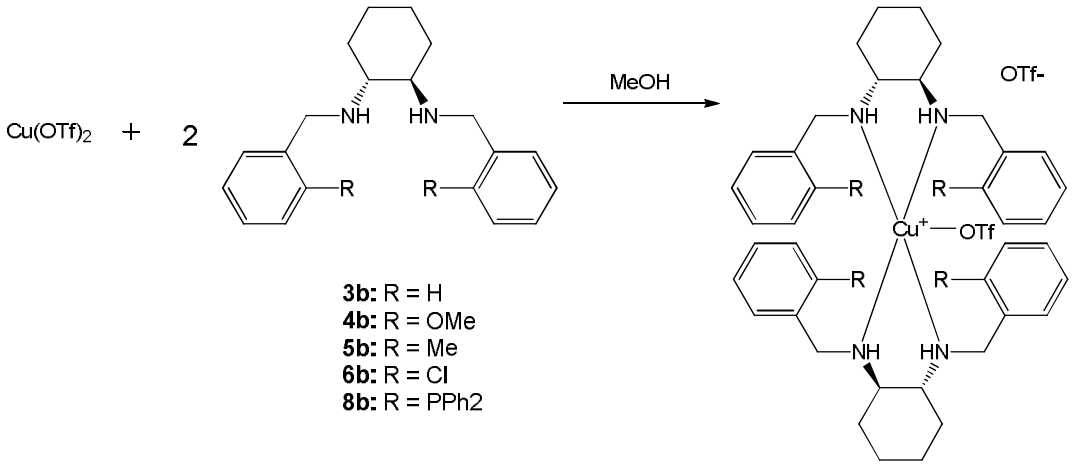

Fig. 3.3.2 Reaction scheme of the preparation of copper(II) complexes containing bichelating ligands

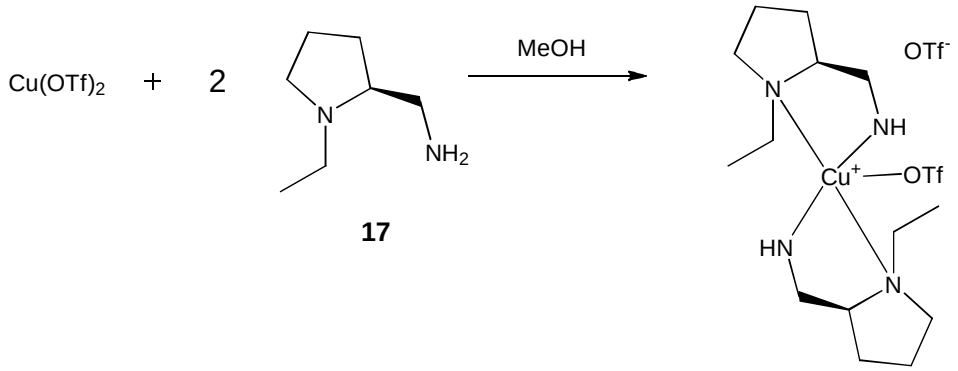

Fig. 3.3.3 Reaction scheme of the preparation of $Cu(17)_2(OTf)_2$

The complexes were characterised by mass spectrometry, elemental analysis and EPR spectroscopy. Many of the complexes were also characterised by single crystal X-ray diffraction.

$Cu(\mathbf{17})_2(OTf)_2$ and $Cu(\mathbf{3b})_2(OTf)_2$ were analysed by EPR spectroscopy. EPR is a common technique to study systems with unpaired electrons. Their axial g and A values can be seen in table 3.3.1.

Table 3.3.1 EPR spectroscopy data for complexes $Cu(17)_2(OTf)_2$ and $Cu(3b)_2(OTf)_2$. Powder, frozen and solution spectra were recorded

Complex	Spectrum Type	g⊥	g‖	A⊥ / $\times 10^{-4}$ cm^{-1}	A‖ / $\times 10^{-4}$ cm^{-1}
$Cu(\mathbf{17})_2(OTf)_2$	Powder	2.05	2.20	-	-
	Frozen	2.05	2.20	52.6	187.6
	Solution	g_{iso} = 2.09		A_{iso} = 77.3	
$Cu(\mathbf{3b})_2(OTf)_2$	Powder	2.05	2.20	17.2	148.9
	Frozen	2.05	2.20	23.9	180.8
	Solution	g_{iso} = 2.10		A_{iso} = 76.0	

- A values not obtainable, as there was no hyperfine structure detected

These values are in agreement with literature values for similar complexes.[8-11] In both complexes there was evidence of multiple copper(II) sites present in solution, which could be due to the triflate counterion or solvent molecules. For $Cu(\mathbf{3b})_2(OTf)_2$, there was also evidence to support dimer formation in solution. The crystal structure of this complex showed indicated it to be monomeric in the solid-state. Due to these complexes having a d^9 electronic configuration NMR was obviously not applicable.

$Cu(\mathbf{17})_2(OTf)_2$ was analysed by single crystal X-ray diffraction. The crystal structure is shown in fig. 3.3.4, and a selection of bond lengths and angles are given in table 3.3.2.

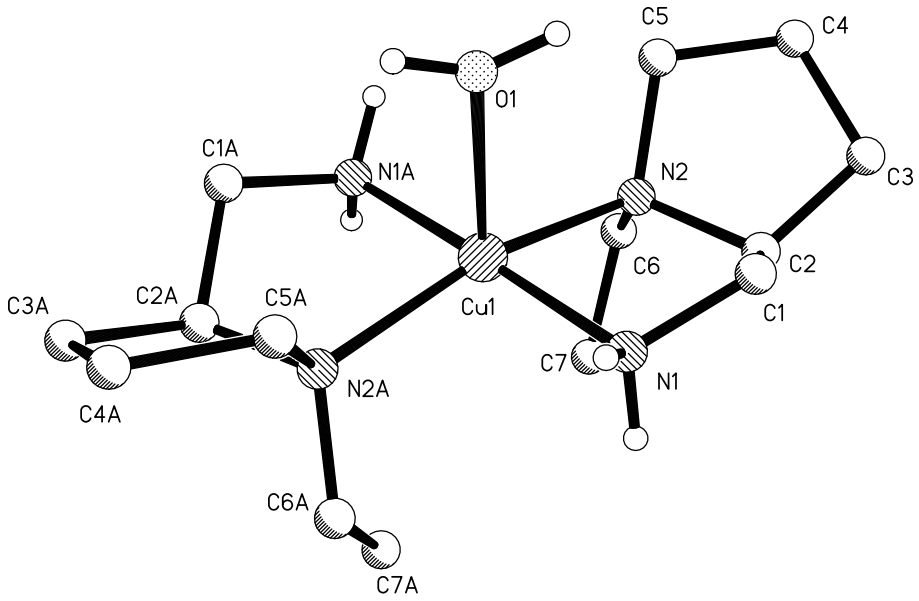

Fig. 3.3.4 Solid-state structure of $Cu(17)_2(OTf)_2$. All hydrogen atoms (except those involved in hydrogen bonding interactions) have been removed for clarity

Table 3.3.2 A selection of bond lengths and angles for $Cu(17)_2(OTf)_2$

Length / Å		**Angle / °**	
Cu(1)-N(1A)	1.985(4)	N(1A)-Cu(1)-N(2A)	84.25(15)
Cu(1)-N(2A)	2.108(4)	N(1)-Cu(1)-N(2)	95.38(14)
Cu(1)-O(1)	2.3076(4)	N(1A)-Cu(1)-O(1)	91.32(12)
		N(1A)-Cu(1)-N(1)	177.4(2)
		N(2A)-Cu(1)-N(2)	163.9(2)

The data shows that the structure belongs to the tetragonal $P4_12_12$ space group. The absolute structure parameter is -0.01(3), suggesting that the complex is enantiomerically pure. The bond lengths and angles are in agreement with literature values of similar complexes.[12-13]

$Cu(\mathbf{2})_2(OTf)_2$ was characterised by single crystal X-ray diffraction. The crystal structure is shown in fig. 3.3.5, and a selection of bond lengths and angles given in table 3.3.3.

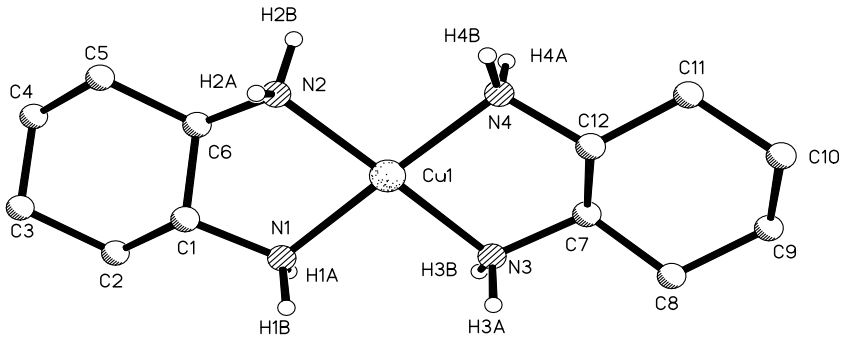

Fig. 3.3.5 Solid-state structure of $Cu(2)_2(OTf)_2$. Hydrogen atoms not involved in hydrogen bonding have been removed for clarity

Table 3.3.3 A selection of bond lengths and angles for $Cu(2)_2(OTf)_2$

Length / Å		**Angle / °**	
Cu(1)-N(1)	2.0109(18)	N(1)-Cu(1)-N(2)	84.13(8)
Cu(1)-N(2)	2.0143(19)	N(3)-Cu(1)-N(4)	84.51(8)
Cu(1)-N(3)	2.0145(19)	N(2)-Cu(1)-N(4)	94.08(7)
Cu(1)-N(4)	2.0220(19)	N(1)-Cu(1)-N(3)	97.29(7)
		N(2)-Cu(1)-N(3)	178.55(8)
		N(1)-Cu(1)-N(4)	177.44(9)

The data shows that the structure belongs to the triclinic *P*1 space group. The absolute structure parameter is -0.006(5), suggesting that the complex is enantiomerically pure. The bond lengths and angles are in agreement with literature values of similar complexes.[12-13]

The bond angles for N(1)-Cu(1)-N(3) and N(2)-Cu(1)-N(4) are slightly larger than the expected 90 °, although this can be explained by increased repulsion between the two ligands due to steric hindrance. Overall, the complex has adopted a square planar geometry, which is indicated by the bond angles, and matches the behaviour of the other copper complexes discussed here, with weakly coordinating triflate counterions.

$Cu(\mathbf{3b})_2(OTf)_2$ was characterised by single crystal X-ray diffraction. The crystal structure is shown in fig. 3.3.6, and a selection of bond lengths and angles given in table 3.3.4.

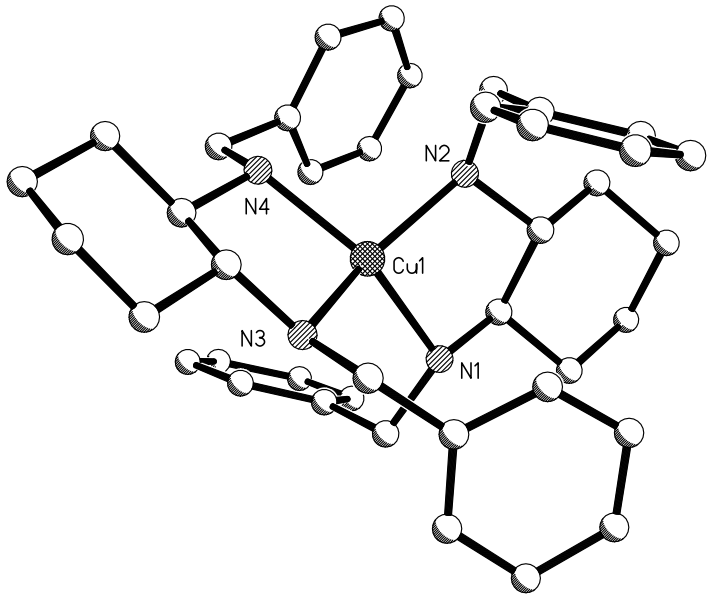

Fig. 3.3.6 Solid-state structure of $Cu(3b)_2(OTf)_2$. All hydrogen atoms and triflate counterions have been removed for clarity

Table 3.3.4 A selection of bond lengths and angles for $Cu(3b)_2(OTf)_2$

Length / Å		**Angle / °**	
Cu(1)-N(1)	2.057(4)	N(1)-Cu(1)-N(2)	85.24(16)
Cu(1)-N(2)	2.045(4)	N(3)-Cu(1)-N(4)	86.72(16)
Cu(1)-N(3)	2.046(3)	N(1)-Cu(1)-N(3)	100.94(16)
Cu(1)-N(4)	2.028(4)	N(2)-Cu(1)-N(4)	100.34(16)

The data showed that the structure belongs to the monoclinic $P2_1$ space group. The absolute structure parameter is -0.009(9), suggesting that the complex is enantiomerically pure. The bond lengths and angles are in agreement with literature values of similar complexes.[12-13] The complex is in a highly distorted square planar geometry, as indicated by the deviation in bond angles from 90 °. Noteworthy, is that this structure shows a significant degree of twinning. Twinning is observed when two crystals share some of the same crystal lattice points in a symmetrical fashion.

Cu(**4b**)$_2$(OTf)$_2$ was characterised by single crystal X-ray diffraction. The crystal structure is shown in fig. 3.3.7, and a selection of bond lengths and angles given in table 3.3.5.

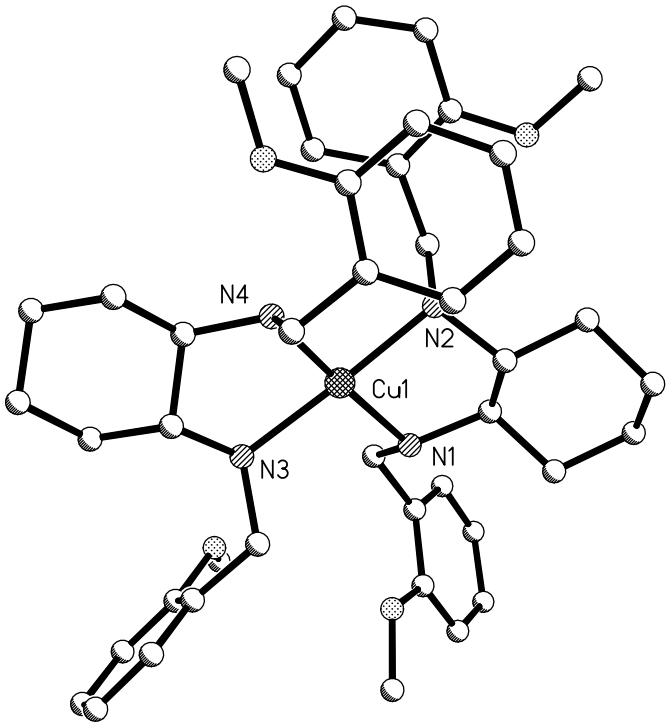

Fig. 3.3.7 Solid-state structure of Cu(4b)$_2$(OTf)$_2$. All hydrogen atoms and triflate counterions have been removed for clarity

Table 3.3.5 A selection of bond lengths and angles for Cu(4b)$_2$(OTf)$_2$

Length / Å		**Angle / °**	
Cu(1)-N(1)	2.047(5)	N(1)-Cu(1)-N(2)	83.5(2)
Cu(1)-N(2)	2.033(5)	N(3)-Cu(1)-N(4)	85.1(2)
Cu(1)-N(3)	2.054(5)	N(1)-Cu(1)-N(3)	97.0(2)
Cu(1)-N(4)	2.030(5)	N(2)-Cu(1)-N(4)	94.6(2)

The data showed that the structure belongs to the monoclinic $P2_1$ space group. The absolute structure parameter is -0.010(19), which indicates that the complex is enantiomerically pure. The bond lengths and angles are in agreement with literature values of similar complexes.[12-13]

There are significant differences in the coordination geometries of Cu(**3b**)$_2$(OTf)$_2$ and Cu(**4b**)$_2$(OTf)$_2$. These differences manifest themselves by analysis of the Cu-NH-CH$_2$-C$_{Ar}$ torsion angles, which for Cu(**3b**)$_2$(OTf)$_2$ are in the range 47.6 – 65.7 ° and for Cu(**4b**)$_2$(OTf)$_2$ 85.9 – 169.3 °. There is also a significant difference between the angle of the planes formed from N(1)-Cu(1)-N(2) and N(3)-Cu(1)-N(4) which are close to parallel (i.e. 180 °) for Cu(**2**)$_2$(OTf)$_2$ and Cu(**4b**)$_2$(OTf)$_2$, however for Cu(**3b**)$_2$(OTf)$_2$ the analogous angle is 139 °. On inspection of the solid-state structure of Cu(**4b**)$_2$(OTf)$_2$ there are intramolecular H-bonding interactions between the amine hydrogen atoms on N(1) and N(3) and the adjacent methoxy moiety {N(1)-H(1A) 0.93 Å, H(1A)-O(1) 2.32 Å, N(1)-H(1A)-O(1) 2.973(7) Å 127.1 °, and N(3)-H(3) 0.93 Å, H(3)-O(3) 2.33 Å N(3)-H(3)-O(3) 2.981(7) Å, 126.8°}. There are obviously no such interactions in the case of Cu(**3b**)$_2$(OTf)$_2$ and it could potentially be the reason for the observed deviation in the geometry of the copper centres.

Cu(**5b**)$_2$(OTf)$_2$ was characterised by single crystal X-ray diffraction. The crystal structure is shown in fig. 3.3.8, and a selection of bond lengths and angles are given in table 3.3.6.

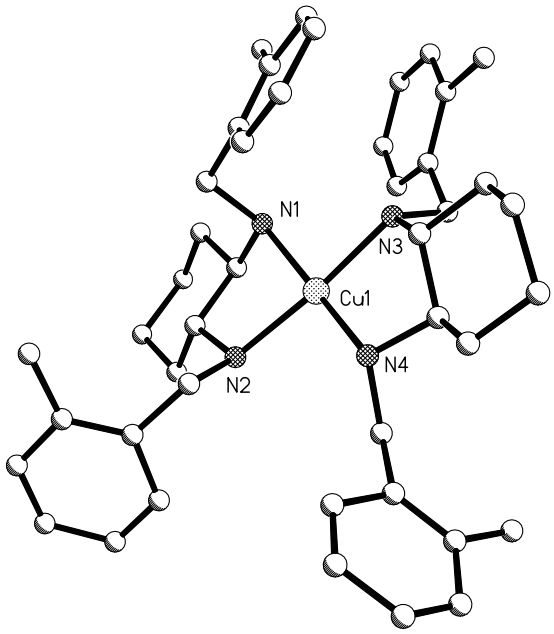

Fig. 3.3.8 Solid-state structure of Cu(5b)$_2$(OTf)$_2$. All hydrogen atoms and triflate counterions have been removed for clarity

Table 3.3.6 A selection of bond lengths and angles for $Cu(5b)_2(OTf)_2$

Length / Å		Angle / °	
Cu(1)-N(1)	2.032(5)	N(1)-Cu(1)-N(2)	82.5(2)
Cu(1)-N(2)	2.064(5)	N(3)-Cu(1)-N(4)	84.5(2)
Cu(1)-N(3)	2.062(5)	N(1)-Cu(1)-N(3)	93.38(2)
Cu(1)-N(4)	2.045(5)	N(2)-Cu(1)-N(4)	99.18(2)

The data showed that the structure belongs to the monoclinic $P2_1$ space group. The absolute structure parameter is -0.027(19), which indicates that the complex is enantiomerically pure. The bond lengths and angles are in agreement with literature values of similar complexes.[12-13]

The bond angles show no significant differences from those previously been observed in the other complexes with these diamine ligands.[12-13] The complex adopts a square planar geometry with weakly coordinating triflate anions, which has been observed in the previous complexes.

3.3.2 Copper(II) Complexes of Tetrachelating Ligands

As previously discussed, a series of tetrachelating ligands were prepared in an attempt to prepare a library of more rigid complexes. These ligands were complexed to copper(II), as previously described. The resulting complexes were analysed by mass spectrometry, elemental analysis, and in some cases, IR spectroscopy and EPR spectroscopy together with single crystal X-ray diffraction.

When the ligand **9a** was complexed to copper(II) triflate in methanol, the complex shown in fig. 3.3.9 was expected to be formed.

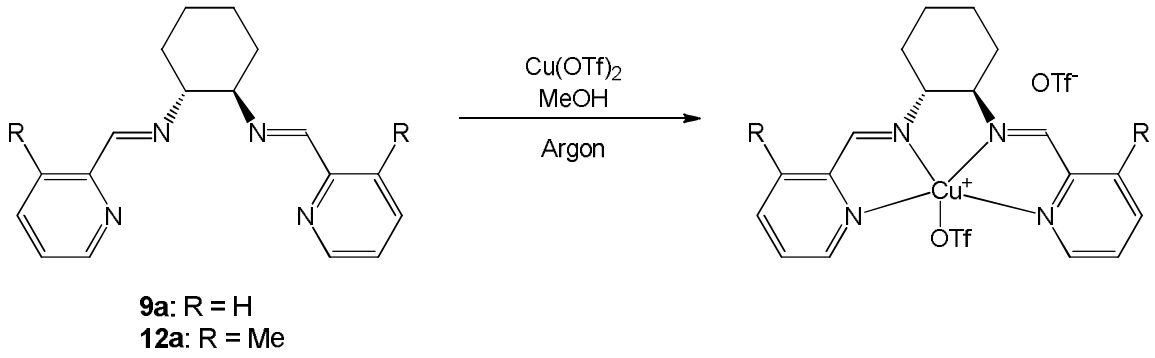

Fig. 3.3.9 Predicted reaction scheme of the preparation of copper(II) complexes of some tetrachelating ligands

Instead, the complexes shown in fig. 3.3.10 were formed.

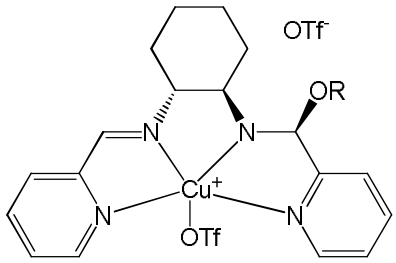

Fig. 3.3.10 α-amino ether complexes, formed during the preparation of the copper(II) complexes described in fig. 3.3.9

The methanol has added across one of the imine bonds to form an α-amino ether. This functional group is very reactive, and can act as a precursor to many other useful organic functionalities. Only a handful of research groups have previously characterised such groups.[14-17] Such species are believed to be short lived intermediates in the formation of imines.[18] Very recently, and for the first time, Fujita was able to crystallographically characterise a transient hemiaminal trapped in a porous Zn(II) network.[18] However, pertinent to this study are the very limited crystallographically characterised examples of such ligated species. Notable examples include those of Pregosin (Pt),[14] Hoskins (Cu),[15] Rybak-Akimova (Cu)[16] and Mitra (Ni)[17] where the coordination of the metal ion is believed to stabilise the highly reactive α-amino ether.

The crystallography of the complexes reported here will be discussed shortly. The first question that was asked upon discovering this phenomenon was if this were specific to methanol, or would the same behaviour be exhibited in the presence of other alcohols. Also, an interesting feature was that the alcohol added across only one of the imine bonds. Furthermore, was this behaviour specific for this ligand, or would the same behaviour be observed on ligand modification. These questions were subsequently investigated, and will be discussed herein.

The Cu(**9a**)$(OTf)_2$ complex was prepared in methanol, ethanol and isopropanol. Characterisation by mass spectrometry was performed on the resulting complexes, the results of which can be seen in figs. 3.3.11 and 3.3.12.

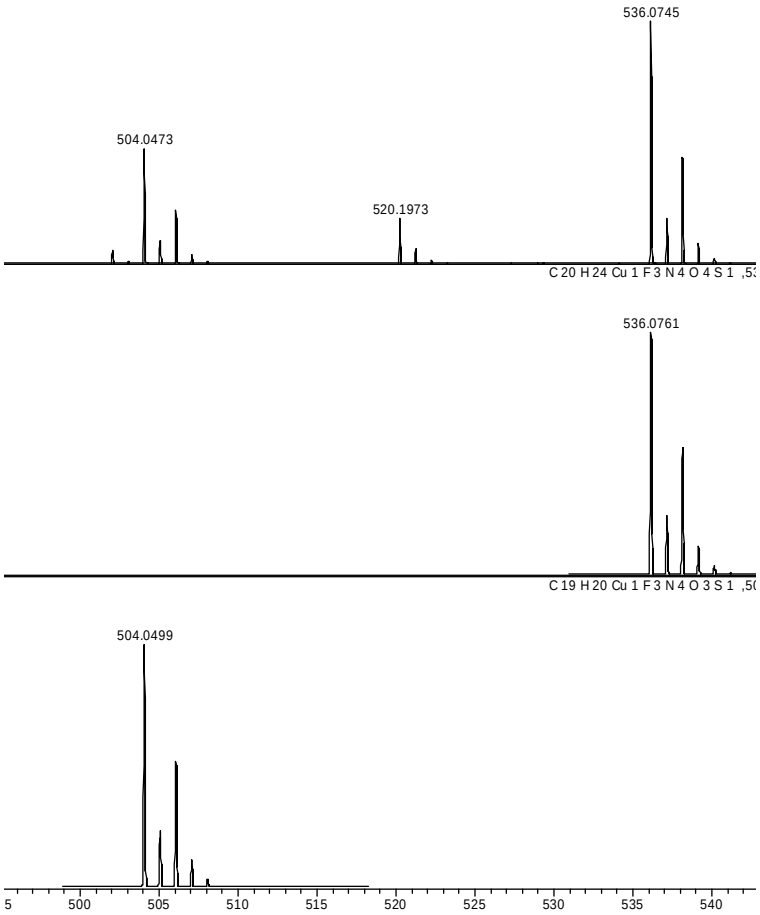

Fig. 3.3.11 Mass spectra of the Cu(9a)$(OTf)_2$ complex prepared in methanol, comparing the actual spectrum (top), the predicted spectrum of the α-amino ether complex (middle), and the predicted spectrum of the complex with no α-amino ether formation (bottom)

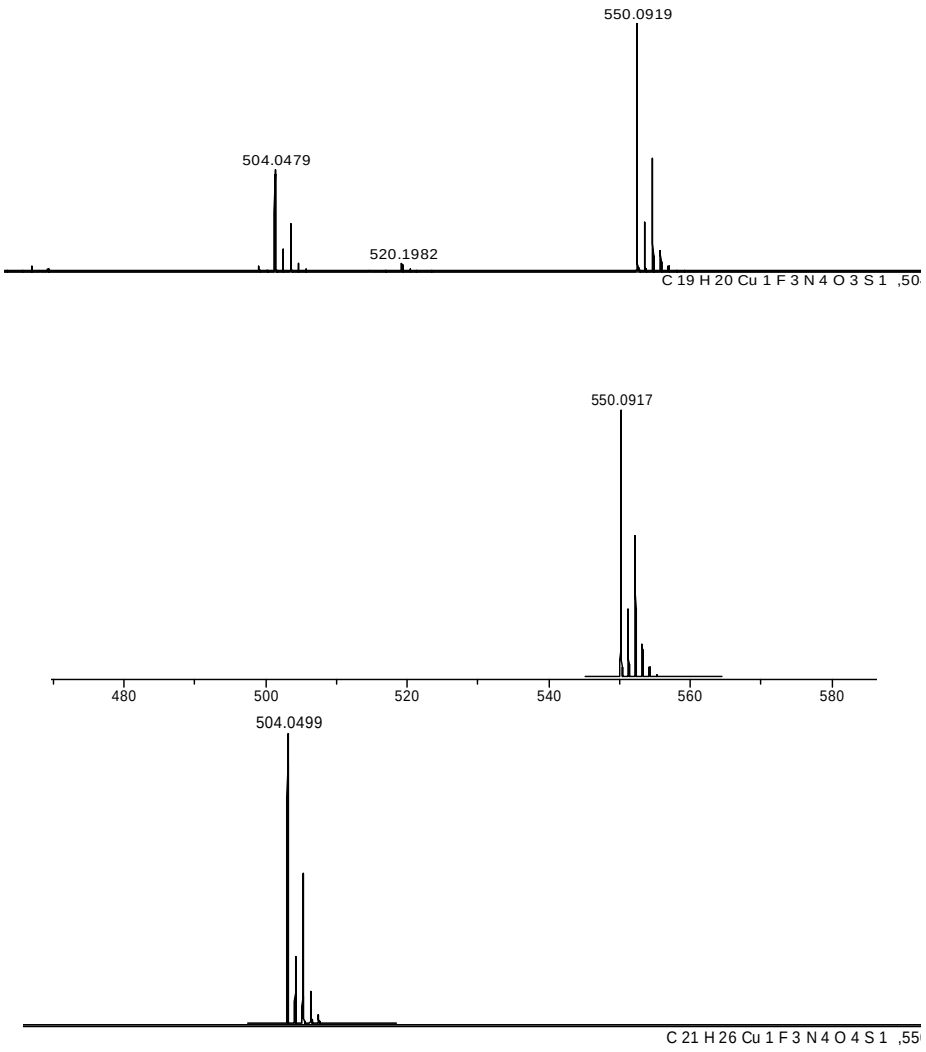

Fig. 3.3.12 Mass spectra of the Cu(9a)$(OTf)_2$ complex prepared in ethanol, comparing the actual spectrum (top), the predicted spectrum of the α-amino ether complex (middle), and the predicted spectrum of the complex with no α-amino ether formation (bottom)

The mass spectra show the presence of the complex both with (550.0919 Da for ethanol and 536.0745 Da for methanol) and without (504.0479 Da) the addition of alcohol across one of the imine bonds. Where the solvent was methanol or ethanol, the spectra show that the α-amino ether complex is more abundant than the complex with no alcohol addition, suggesting that the α-amino ether complex is the favoured complex. Noteworthy, that even under refluxing methanol only one alcohol adds across the C=N bond. As expected for a mass spectrum run in CD_3OD, a mass at 539.0925 Da was detected. Presumably, the initially formed N-D is labile and exchanges with free H^+ in the mass spectrometer. However, when isopropanol is the solvent, only a small amount of α-amino ether complex

can be seen in comparison with the complex with no alcohol addition. Also, the single crystal X-ray diffraction data shows no alcohol addition across the imine bond; isopropanol is observed as solvent of crystallisation within the lattice. This suggests that the α-amino ether complex is not the favoured complex.

These three complexes were also analysed by single crystal X-ray diffraction. The crystal structure of Cu(**9a**)$(OTf)_2$ prepared in methanol can be seen in fig. 3.3.13, and a selection of bond lengths and angles are given in table 3.3.7.

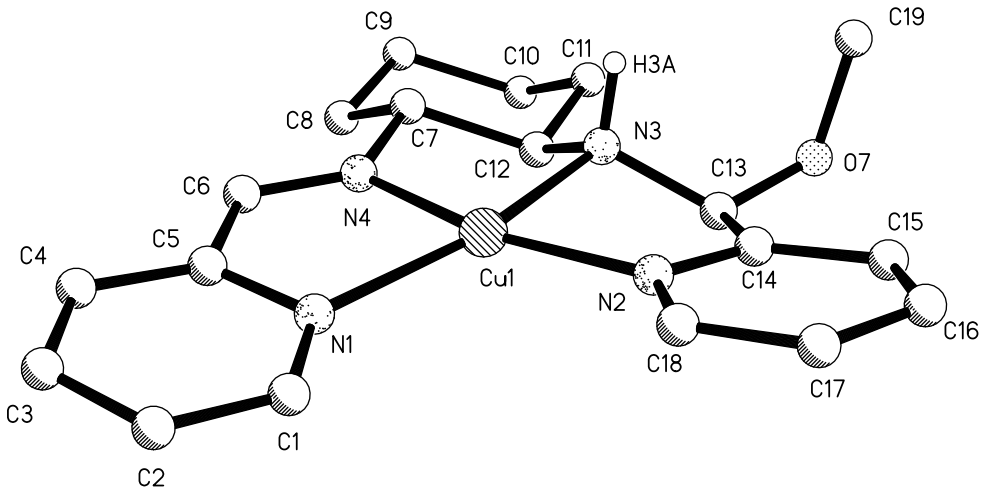

Fig. 3.3.13 Solid-state structure of Cu(9a)$(OTf)_2$ prepared in methanol. All hydrogen atoms {except H(3A)} and triflate counterions have been removed for clarity

Table 3.3.7 A selection of the bond lengths and angles for Cu(9a)$(OTf)_2$ prepared in methanol

Length / Å		**Angle / °**	
Cu(1)-O(1)	2.346(4)	O(1)-Cu(1)-N(4)	85.24(19)
Cu(1)-N(1)	2.054(5)	N(1)-Cu(1)-N(2)	113.1(2)
Cu(1)-N(2)	1.993(5)	N(2)-Cu(1)-N(3)	83.1(2)
Cu(1)-N(3)	2.035(5)	N(3)-Cu(1)-N(4)	83.0(2)
Cu(1)-N(4)	1.955(5)	N(4)-Cu(1)-N(1)	80.9(2)
N(4)-C(6)	1.284(8)	C(6)-N(4)-C(7)	127.2(5)
N(3)-C(13)	1.450(7)	C(12)-N(3)-C(13)	116.9(5)
C(13)-O(7)	1.397(7)	N(3)-C(13)-O(7)	117.7(5)

The data shows that the structure belongs to the triclinic *P*1 space group. The absolute structure parameter is -0.027(13), suggesting that the complex is enantiomerically pure. Interestingly, with the addition of methanol across the C=N double bond, a new chiral centre has been formed at C(13), with an *S* configuration. The data suggests the crystal is 100 % (*S*) at C(13), however this does not necessarily suggest the bulk is. However, the structure has been repeated four times all of which show the (*S*) configuration at C(13). With the absolute structure parameter indicating that the ligand is enantiomerically pure, this also implies that this new chiral centre was formed enantioselectively. The imine bond is adjacent to a chiral centre, so this could account for the enantioselectivity seen with regards to the new chiral centre. The new chiral centre at C(13) is the (*S*) form, presumably this form (*R,R,S*) is of lower energy than the (*R,R,R*) form.

The bond lengths and angles are in agreement with literature values of similar complexes.[12-13] The C(13)-O(7) bond length indicates that this is a single bond, which means that the new functional group formed is an α-amino ether. The N(4)-C(6) bond length is indicative of an imine bond and the N(3)-C(13) of an amine bond. This supports the finding that the alcohol addition across the C=N double bond occurs at just one imine bond, not both. Density functional theory calculations have been employed to study this system, which will be discussed later.

In the solid-state there are two crystallographically unique Cu(II) centres both with a square planar arrangement of nitrogen atoms and a weakly coordinating triflate anion completing the coordination sphere of the metal. For one of the Cu(II) centres the addition of methanol across the imine was 100 % as indicated by the fact that this was fully occupied in the crystal structure. Whereas for the other Cu(II) centre the occupancy of the alcohol group was 40 %. This is exemplified by the N(3)-C(13) distance of 1.450(7) Å, indicative of a nitrogen-carbon single bond, in the fully occupied system. Whilst, in the partially occupied system this distance is 1.358(8) Å; thereby averaging a C-N and C=N bond length. Elemental analysis was consistent with the addition of methanol being the bulk crystallised product and the mass spectrum of the solution after crystallisation and the crystals were identical. A pXRD of the crude product (before recrystallisation) is analogous to that determined from the crystal data,

implying that methanol addition is occurring on a significant scale, with this ligand system. This pXRD can be seen in fig. 3.3.14.

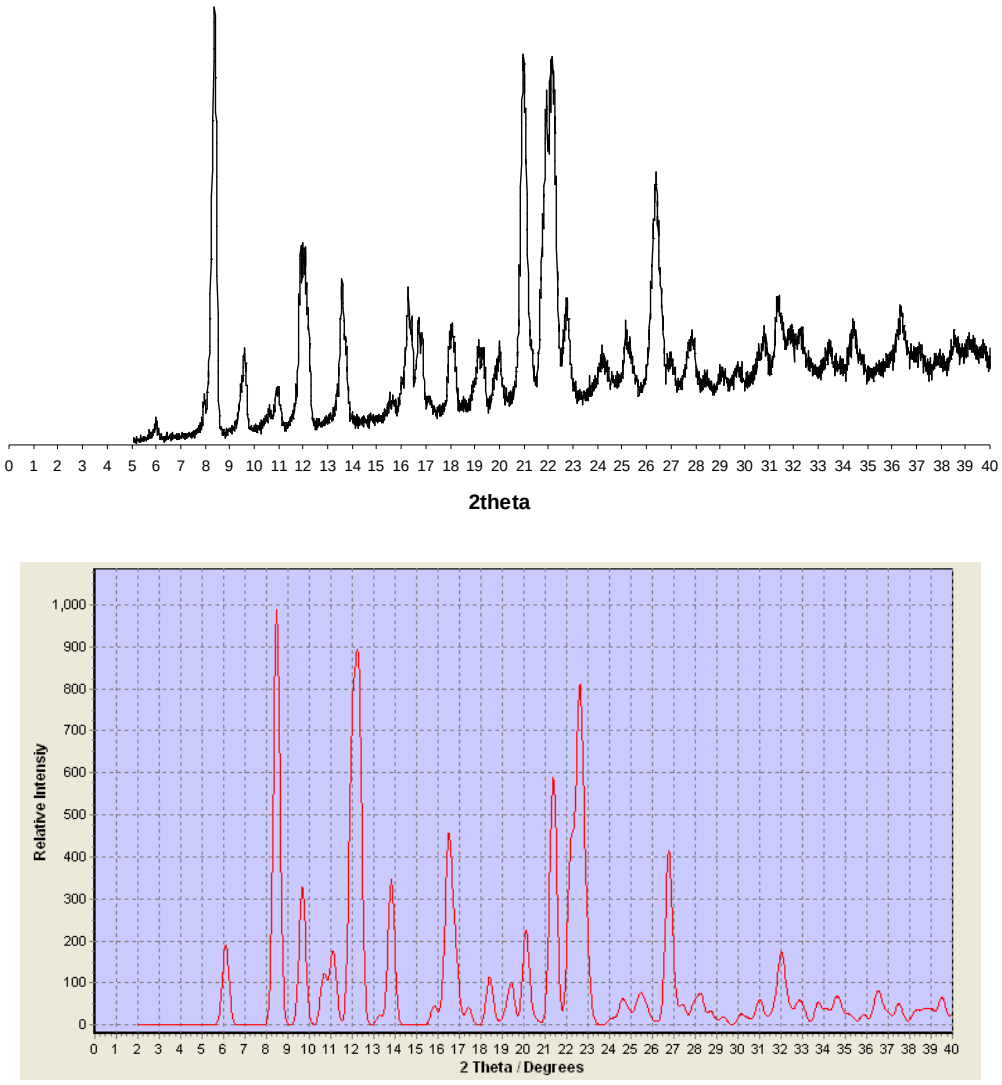

Fig. 3.3.14 pXRD of the crude Cu(9a)$(OTf)_2$ before crystallisation (top). Generated pXRD from the crystal data (bottom)

In an attempt to form the structure in which both alcohols are fully occupied in the solid state the complexation was also performed in a methanol/acetic acid mixture (9:1). As before there were two crystallographically unique Cu(II) centres. The occupancy of the added alcohol was now 100 % for both Cu(II) cations. In this case the N(3)-C(13) bond length was 1.448(5) Å and in the other Cu(II) cation the analogous length was 1.431(6) Å.

The crystal structure of Cu(**9a**)$(OTf)_2$ when prepared in ethanol can be seen in fig. 3.3.15, and a selection of bond lengths and angles are given in table 3.3.8.

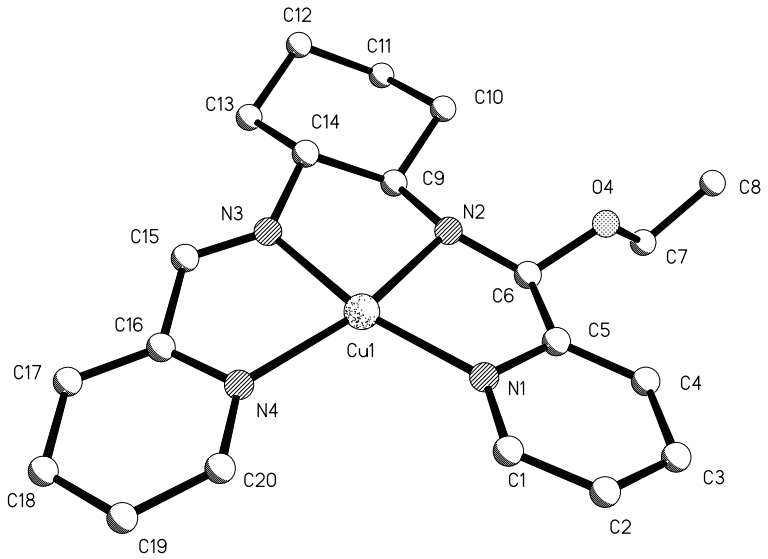

Fig. 3.3.15 Solid-state structure of Cu(9a)$(OTf)_2$ prepared in ethanol. All hydrogen atoms and triflate counterions have been removed for clarity

Table 3.3.8 A selection of bond lengths and angles for Cu(9a)$(OTf)_2$ prepared in ethanol

Length / Å		**Angle / °**	
Cu(1)-N(1)	1.965(15)	N(1)-Cu(1)-N(2)	81.9(6)
Cu(1)-N(2)	1.982(13)	N(2)-Cu(1)-N(3)	84.2(6)
Cu(1)-N(3)	1.927(15)	N(3)-Cu(1)-N(4)	80.2(6)
Cu(1)-N(4)	2.027(15)	N(4)-Cu(1)-N(1)	113.6(6)
N(3)-C(15)	1.25(2)	C(14)-N(3)-C(15)	125.8(15)
N(2)-C(6)	1.505(19)	C(9)-N(2)-C(6)	121.0(13)
C(6)-O(4)	1.374(19)	N(2)-C(6)-O(4)	119.1(13)

The data shows that the structure belongs to the triclinic *P*1 space group. The absolute structure parameter is -0.04(3), suggesting that the complex is enantiomerically pure. As with the case discussed with methanol there are two Cu(II) centres in the asymmetric unit, one with 100 % addition of ethanol and the other with 70 %. A new chiral centre has been formed at C(6), with an *S*

configuration. Again, the imine bond is adjacent to a chiral centre, so this could account for the enantioselectivity seen with regards to the new chiral centre.
The bond lengths and angles are in agreement with literature values of similar complexes.[12-13] The C(6)-O(4) bond length indicates that this is a single bond, which means that the new function group formed is an α-amino ether. This is favoured for reasons previously discussed. The N(3)-C(15) bond length is indicative of an imine bond. The N(2)-C(6) bond length is indicative of an amine bond. Overall, the complex has adopted a square planar geometry with a weakly coordinating triflate counterion, which is indicated by the bond lengths and angles.

The crystal structure of Cu(**9a**)$(OTf)_2$ when prepared in isopropanol is shown in fig. 3.3.16, and a selection of bond lengths and angles are given in table 3.3.9.

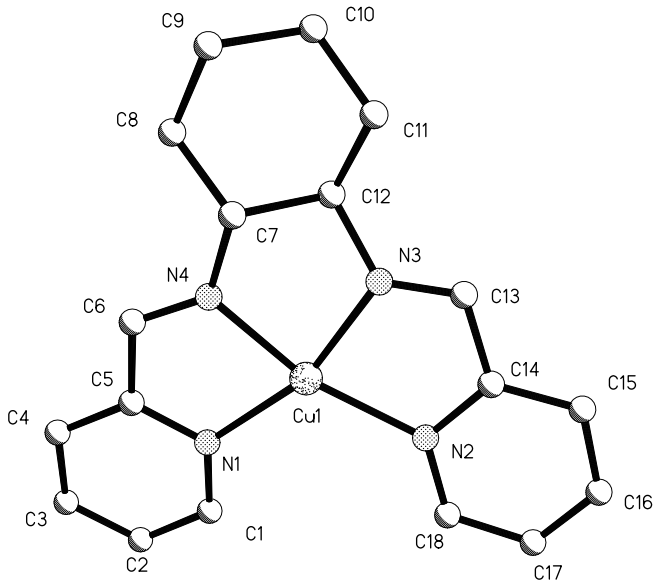

Fig. 3.3.16 Solid-state structure of Cu(9a)$(OTf)_2$ prepared in isopropanol. All hydrogen atoms, triflate counterions and isopropanol solvent have been removed for clarity

Table 3.3.9 A selection of bond lengths and angles for Cu(9a)$(OTf)_2$ prepared in isopropanol

Length / Å		Angle / °	
Cu(1)-N(1)	2.018(1)	N(2)-Cu(1)-N(3)	80.93(2)
Cu(1)-N(2)	2.036(2)	N(1)-Cu(1)-N(2)	116.85(2)
Cu(1)-N(3)	1.965(1)	N(1)-Cu(1)-N(4)	81.11(2)
Cu(1)-N(4)	1.965(2)	N(4)-Cu(1)-N(3)	81.69(2)
N(3)-C(13)	1.266(5)	C(12)-N(3)-C(13)	127.09(3)
N(4)-C(6)	1.268(4)	C(7)-N(4)-C(6)	127.62(4)

The data shows that the structure belongs to the triclinic *P*1 space group. The absolute structure parameter is -0.014(12), suggesting that the complex is enantiomerically pure. The structure suggests that there is no addition of isopropanol across either of the imine bonds. However, it must be noted that the structure did show two molecules of isopropanol within the unit cell, (which are not shown in fig. 3.3.16 for the purpose of clarity). The crystal structure analysis indicates substantial disorder in one of these isopropanol molecules, and potential disorder in the other. The mass spectrometry of this complex showed small amounts of complex where addition of isopropanol across one of the imine bonds had occurred, however this was considerably smaller than with methanol or ethanol. Density functional theory calculations support this, as will be discussed later.

The bond lengths and angles are in agreement with literature values of similar complexes.[12-13] Overall, the complex is square planar. The N(3)-C(13) and N(4)-C(6) bond lengths are indicative of imine bonds, with no significant difference between the two bond lengths. This suggests that there is no addition at all across either of the imine bonds. This may suggest that where addition does occur, the resulting complex does not crystallise as easily as the complex with no addition of isopropanol, which may result in none of the complex with isopropanol addition crystallising. This may explain the discrepancy between the crystal structure and mass spectrometry findings, albeit the major species in the mass spectrum was the solid-state product.

Other alcohols were also employed, to investigate this phenomenon further. These alcohols were 2-methoxyethanol and trifluoroethanol. Analysis by mass spectrometry and single crystal X-ray diffraction suggested that the α-amino ether complex had not formed. Fig. 3.3.17 shows the crystal structure of the Cu(**9a**)$(OTf)_2$ complex prepared in 2-methoxyethanol, with a selection of bond lengths and angles given in table 3.3.10.

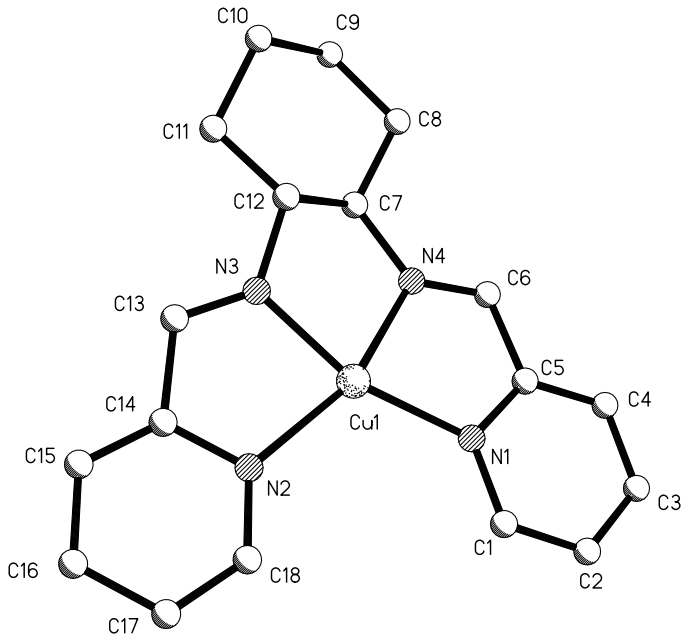

Fig. 3.3.17 Solid-state structure of Cu(9a)$(OTf)_2$ prepared in 2-methoxyethanol. All hydrogen atoms and triflate counterions have been removed for clarity

Table 3.3.10 A selection of bond lengths and angles for Cu(9a)$(OTf)_2$ prepared in 2-methoxyethanol

Length / Å		**Angle / °**	
Cu(1)-N(1)	2.003(7)	N(1)-Cu(1)-N(4)	80.9(3)
Cu(1)-N(4)	1.956(7)	N(4)-Cu(1)-N(3)	81.8(3)
Cu(1)-N(3)	1.933(7)	N(3)-Cu(1)-N(2)	80.7(3)
Cu(1)-N(2)	2.042(8)	N(2)-Cu(1)-N(1)	116.8(3)
N(3)-C(13)	1.275(11)	C(12)-N(3)-C(13)	126.3(7)
N(4)-C(6)	1.267(10)	C(6)-N(4)-C(7)	126.4(7)

The data shows that the structure belongs to the triclinic *P*1 space group. The absolute structure parameter is -0.002(18), suggesting that the complex is enantiomerically pure. The structure suggests that there is no addition of 2-methoxyethanol across either of the imine bonds.

The bond lengths and angles are in agreement with literature values of similar complexes.[12-13] The N(3)-C(13) and N(2)-C(6) bond lengths are indicative of imine bonds, with no significant difference between the two bond lengths. This suggests that there is no addition at all across either of the imine bonds. Overall, the expected square planar geometry is observed.

The crystal structure of the Cu(**9a**)$(OTf)_2$ complex prepared in trifluoroethanol is shown in fig. 3.3.18, and a selection of bond lengths and angles is given in table 3.3.11.

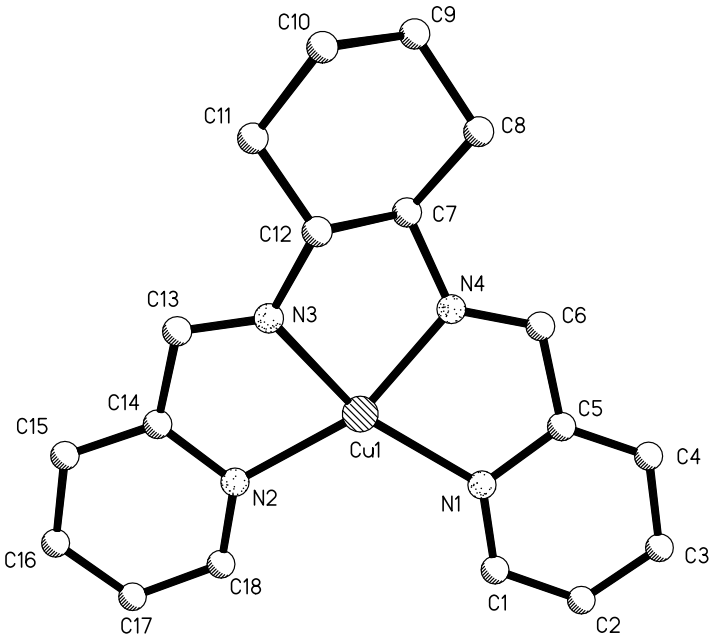

Fig. 3.3.18 Solid-state structure of Cu(9a)$(OTf)_2$ prepared in trifluoroethanol. All hydrogen atoms and triflate counterions have been removed for clarity

Table 3.3.11 A selection of bond lengths and angles for Cu(9a)$(OTf)_2$ prepared in trifluoroethanol

Length / Å		Angle / °	
Cu(1)-N(1)	2.044(10)	N(1)-Cu(1)-N(2)	117.3(5)
Cu(1)-N(2)	2.047(11)	N(2)-Cu(1)-N(3)	80.7(5)
Cu(1)-N(3)	1.964(11)	N(3)-Cu(1)-N(4)	81.7(4)
Cu(1)-N(4)	1.942(10)	N(4)-Cu(1)-N(1)	81.4(4)
N(3)-C(13)	1.275(16)	C(12)-N(3)-C(13)	127.4(11)
N(4)-C(6)	1.276(14)	C(6)-N(4)-C(7)	126.6(10)

The data shows that the structure belongs to the triclinic *P*1 space group. The absolute structure parameter is -0.05(2), suggesting that the complex is enantiomerically pure. The structure suggests that there is no addition of trifluoroethanol across either of the imine bonds.

The bond lengths and angles are in agreement with literature values of similar complexes.[12-13] The N(3)-C(13) and N(4)-C(6) bond lengths are indicative of imine bonds, with no significant difference between the two bond lengths. This suggests that there is no addition at all across either of the imine bonds. Overall, the complex has adopted a square planar geometry, which is indicated by the bond lengths and angles.

Interestingly, if a racemic form of 1-phenyl ethanol was utilised as the solvent then no α-amino ether was detected. However, it is noteworthy that the crystal was chirally enriched, with the solvent of crystallisation being 75 % *S* enantiomer and 25 % *R* enantiomer. This lack of formation of the α-amino ether species is presumably due to the extra steric bulk of this alcohol hindering its formation. The structure is analogous to those previously discussed and therefore is not shown.

It was hypothesised that there are two possible mechanisms of attack on the imine by the alcohol; i) the alcohol dissociates in solution and the anion (RO^-) then attacks the carbon of the imine (with the more acidic alcohols more RO^- will be present in solution), or ii) the alcohol first pre-coordinates to the metal centre and then attacks the imine. When more acidic alcohol solvents where employed

no α-amino ether product was observed which indicates that pre-coordination of the alcohol is potentially involved, and not due to RO^- attacking the imine.

Density functional theory (DFT) calculations were performed with respect to the copper(II) complexes of **9a,** to investigate the relative energetic feasibility of adding an alcohol across the imine bond. DFT is a very powerful computational method to determine the electronic structure of molecules. Table 3.3.12 shows the calculated energy values associated with a number of α-amino ether complexes relative to the Cu(**9a**)$(OTf)_2$ complex with no alcohol addition.

Table 3.3.12 Energy values associated with the α-amino ether complexes, calculated by DFT

α -amino ether	ΔH /kJ mol^{-1}	ΔG / kJ mol^{-1}
None, imine	0	0
Hydroxy	-65.6	-14.6
Methoxy (*S*)	-73.1	-11.3
Methoxy (*R*)	-50.0	+11.6
Dimethoxy	-126.1	-15.9
Ethoxy (*S*)	-56.2	+0.6
Propoxy (*S*)	-48.7	+9.8

These results indicate that the formation of one α-amino ether group is energetically favourable in the presence of methanol (given by the negative value of ΔG), but only where the configuration of the new chiral centre is *S*, as empirically observed. The formation of an α-amino ether group in the presence of ethanol is almost energetically neutral, however the ethanol is present in a massive excess, and so this could explain why the α-amino ether complex is formed in large amounts. In the presence of isopropanol, the formation of the α-amino ether group is not energetically favourable (given by the positive value of ΔG), which supports the experimental findings previously discussed. Interestingly, the addition of methanol across both double bonds is energetically favourable. However, even under reflux conditions after prolonged reaction time (48 h), the α-amino ether complex was not observed. Similarly, the calculations show that the α-amino ether complex should form in the presence of water. Under reflux conditions for a long reaction time, again, this complex was not

observed. Therefore, it is assumed that this species is kinetically not favourable.

The LUMO and SOMO orbitals of the Cu(**9a**)$(OTf)_2$ α-amino ether complex can be seen in figs. 3.3.19 and 3.3.20. DFT has postulated a mechanism for alcohol addition. However, given its limitations, further work could focus on a more robust computational method, for example periodic DFT.

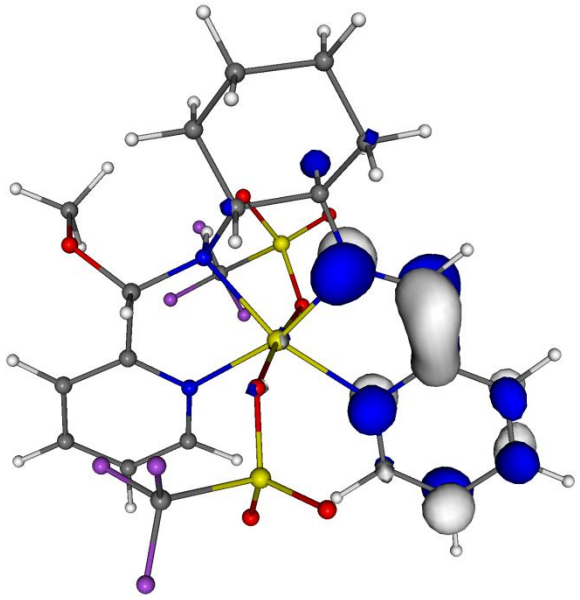

Fig. 3.3.19 LUMO of α-amino ether complex of Cu(9a)$(OTf)_2$, when prepared in methanol

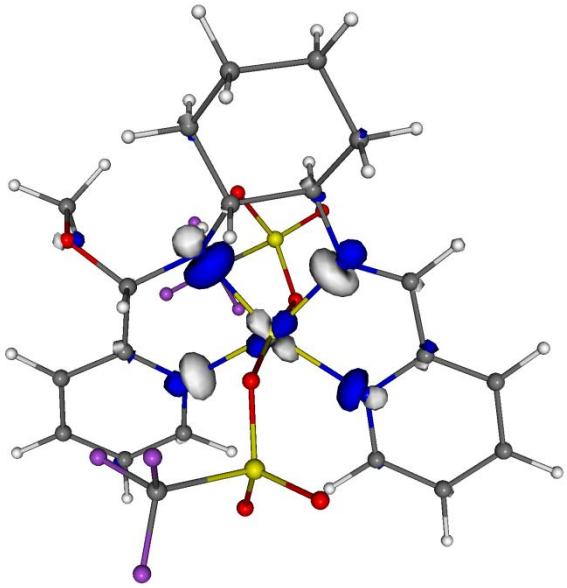

Fig. 3.3.20 SOMO of α-amino ether complex of Cu(9a)$(OTf)_2$, when prepared in methanol

Cu(**9a**)$(OTf)_2$ (methanol), Cu(**9a**)$(OTf)_2$ (ethanol), Cu(**9a**)$(OTf)_2$ (isopropanol) and Cu(**12a**)$(OTf)_2$ were analysed by EPR spectroscopy. Their axial g and A values can be seen in table 3.3.13.

Table 3.3.13 EPR spectroscopy data of complexes Cu(9a)$(OTf)_2$ prepared in methanol, ethanol and isopropanol, and Cu(12a)$(OTf)_2$. Data from the powder, frozen and solution spectra are provided

Complex	Spectrum Type	g⊥	g‖	A⊥ × 10^{-4} cm^{-1}	A‖ × 10^{-4} cm^{-1}
Cu(**9a**)$(OTf)_2$, MeOH	Powder	2.05	2.21	***	***
	Frozen	2.05	2.22	15	176
	Solution	g_{iso} = 2.11		A_{iso} = 72	
Cu(**9a**)$(OTf)_2$, EtOH	Powder	2.05	2.25	***	***
	Frozen	2.05	2.22	15	176
	Solution	g_{iso} = 2.11		A_{iso} = 70	
Cu(**9a**)$(OTf)_2$, IPA	Powder	2.05	2.23	***	***
	Frozen	2.05	2.22	15	184
	Solution	g_{iso} = 2.11		A_{iso} = 72	
Cu(**12a**)$(OTf)_2$	Powder	2.05	2.21	10	173
	Frozen	2.05	2.22	15	182
	Solution	g_{iso} = 2.10		A_{iso} = 80	

*** A values not obtainable, as there was no hyperfine structure detected

These values are in agreement with literature values for similar complexes.[10-11] There are no significant differences in the g and A values between the complexes shown here, or the complexes discussed in section 3.3.1 that were characterised by EPR spectroscopy.

For comparative purposes, the reduced version of this ligand (**9b**) was also complexed to copper(II) triflate. Firstly, this acts as a comparison with the imine complexes in the solid-state. More importantly, these complexes will be utilised catalytically. These complexes either contain two imine linkages to Cu(II) or one imine and one reactive α-amino ether linkage. It would be useful to have an equivalent catalyst that contains two amine moieties, as this could have a substantial effect on the conversions and selectivities observed.

The Cu(**9b**)$(OTf)_2$ complex was analysed by single crystal X-ray diffraction. The crystal structure can be seen in fig. 3.3.21, and a selection of bond lengths and angles are given in table 3.3.14.

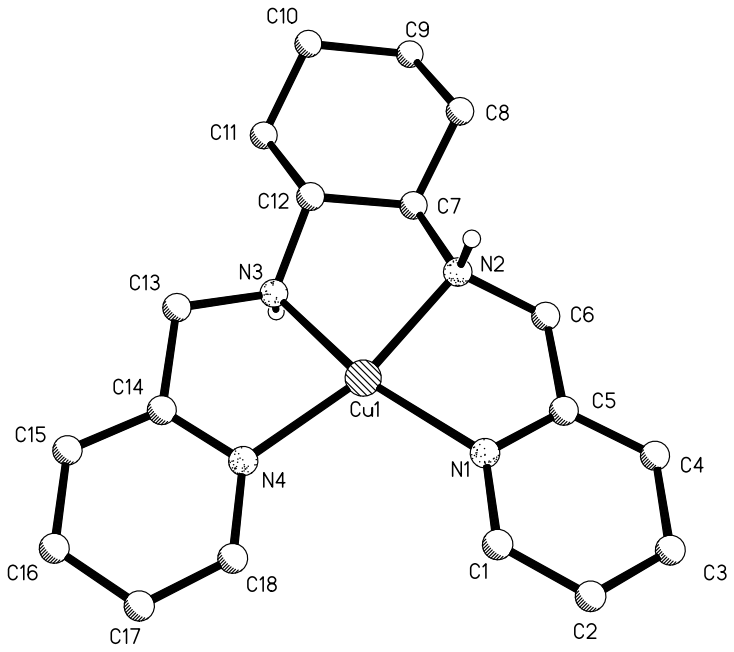

Fig. 3.3.21 Solid-state structure of Cu(9b)$(OTf)_2$. All hydrogen atoms {except those bound to N(2) and N(3)} and triflate counterions have been removed for clarity

Table 3.3.14 A selection of bond lengths and angles for Cu(9b)$(OTf)_2$

Length / Å		**Angle / °**	
Cu(1)-N(1)	1.995(3)	N(1)-Cu(1)-N(2)	82.19(14)
Cu(1)-N(2)	2.002(3)	N(2)-Cu(1)-N(3)	85.02(14)
Cu(1)-N(3)	1.993(3)	N(3)-Cu(1)-N(4)	83.26(14)
Cu(1)-N(4)	2.005(4)	N(4)-Cu(1)-N(1)	110.58(14)
N(3)-C(13)	1.453(5)	C(12)-N(3)-C(13)	116.5(3)
N(2)-C(6)	1.476(5)	C(6)-N(2)-C(7)	116.3(3)

The data shows that the structure belongs to the monoclinic $P2_1$ space group. The absolute structure parameter is -0.002(9), suggesting that the complex is enantiomerically pure. The bond lengths and angles are in agreement with literature values of similar complexes.[12-13]

Overall, the complex has adopted a square planar geometry, which is indicated by the bond lengths and angles. This is favourable, for reasons previously discussed.

Modifications were also made to the ligand, these alternative ligands complexed to copper(II) triflate in the presence of methanol, and the resulting complexes characterised. Such modifications included changing the position of the heteroatom within the pyridine ring, adding extra steric bulk to the ligand in close proximity to the imine groups, and changing the heteroatom itself within the aromatic rings. The results of these modifications will now be discussed.

In ligands **9a** and **9b**, the heteroatom of the pyridine ring is in the 2 (*ortho*) position. On changing this to the 3 (*meta*) position (ligands **10a** and **10b,** previously described in chapter two, section 2.4), characterisation of the resulting copper(II) complex indicated that the complex had successfully formed, but no addition of the methanol across an imine bond was observed. This is likely to be due to a lack of mesomeric stabilisation effects of the intermediate when the heteroatom is in the *meta* position. This is demonstrated in fig. 3.3.22. When the heteroatom is in the *meta* position, the aromaticity of the pyridine ring is disrupted in order to stabilise the intermediate, which is unfavourable. The aromaticity is conserved when the heteroatom is in the *ortho* position on stabilising the intermediate, which is more favourable. In addition, the positive charge is transferred to the nitrogen heteroatom, which given its electronegativity, will attract electron density and stabilise the intermediate further.

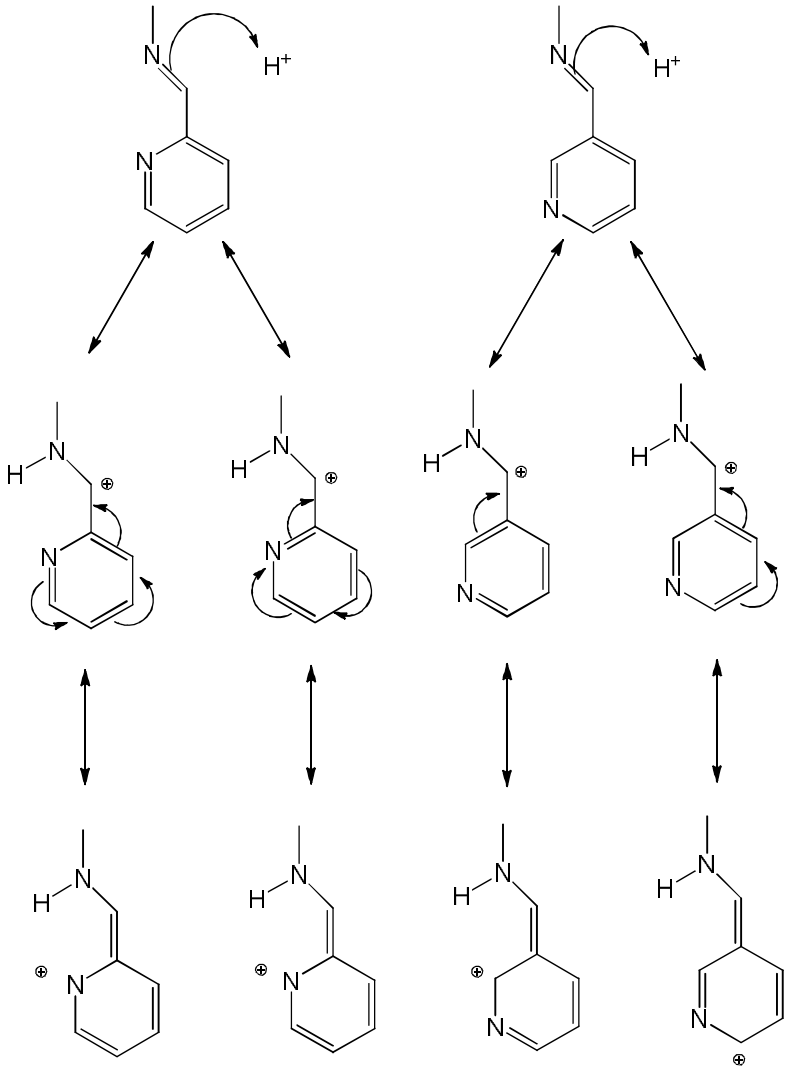

Fig. 3.3.22 Resonance structures (of ligands/complexes relating to 9a and 10a) resulting from electrophilic attack at the imine bond

On changing the position of the heteroatom to the 4-position (ligands **11a** and **11b**), subsequent characterisation revealed that the ligand had broken down, and as a result two molecules of (*R*,*R*)-1,2-diaminocyclohexane had bound to the copper(II) centre. This was shown by the single crystal X-ray diffraction of the complex. The crystal structure is shown in fig. 3.3.23, and a selection of bond lengths and angles are given in table 3.3.15, and is analogous to Cu(**2**)$(OTf)_2$. This is likely to be caused by steric strain produced when the copper(II) attempts to complex with all four chelating nitrogen atoms. The distance between the four chelation sites is simply too great, and so the ligand breaks down at the reactive imine bonds in order for the copper(II) to form a four-coordinate complex without steric strain. Essentially, the complex isolated is Cu(**2**)$(OTf)_2$.

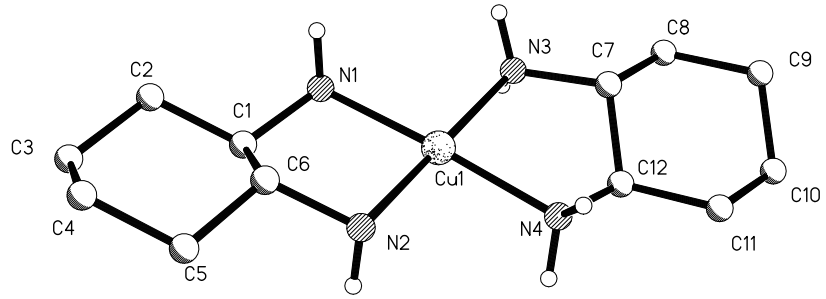

Fig. 3.3.23 Solid-state structure of Cu(11a)(OTf)$_2$. All hydrogen atoms (except those bound to nitrogen) and triflate counterions have been removed for clarity.

Table 3.3.15 A selection of bond lengths and angles for Cu(11a)(OTf)$_2$

Length / Å		**Angle / °**	
Cu(1)-N(1)	2.020(4)	N(1)-Cu(1)-N(2)	84.74(15)
Cu(1)-N(2)	2.009(4)	N(2)-Cu(1)-N(4)	94.15(16)
Cu(1)-N(3)	2.025(4)	N(4)-Cu(1)-N(3)	84.77(16)
Cu(1)-N(4)	2.034(4)	N(3)-Cu(1)-N(1)	96.55(15)

The data shows that the structure belongs to the monoclinic $P2_1$ space group. The absolute structure parameter is -0.020(13), suggesting that the complex is enantiomerically pure.

The structure shows that the ligand has broken down, returning to (*R*,*R*)-1,2-diaminocyclohexane, which is also conducive with mass spectrometry of this complex. This is more than likely due to the position of the pyridine heteroatoms causing too much steric strain on complex formation. A square planar complex is formed, which is favourable for the reasons previously discussed. The bond lengths and angles are in agreement with literature values of similar complexes.[12-13]

Steric bulk was also introduced into the ligand in close proximity to the imine bonds (ligands **12a** and **12b**, fig. 3.3.9). It was thought that this may hinder the addition of an alcohol across these bonds. This may have been the case, as characterisation of the resulting copper(II) complexes (by mass spectrometry and in the solid state) indicated that there had been no formation of an α-amino ether group. This is shown well in the crystal structure of the Cu(**12a**)(OTf)$_2$ complex,

displayed in fig. 3.3.24, with a selection of bond lengths and angles given in table 3.3.16.

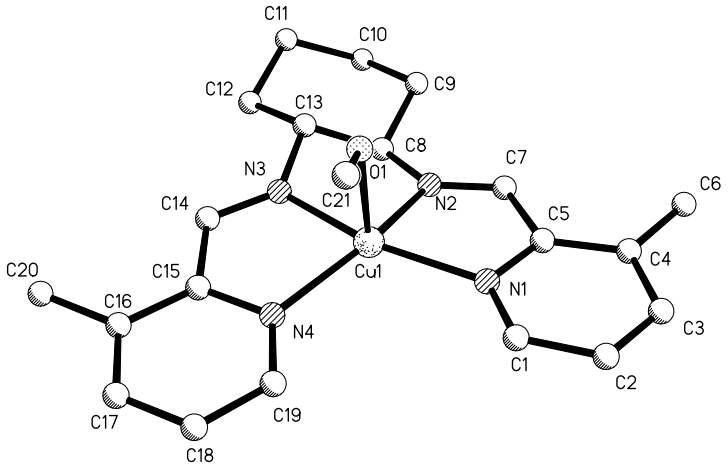

Fig. 3.3.24 Solid-state structure of Cu(12a)$(OTf)_2$. All hydrogen atoms and triflate counterions have been removed for clarity

Table 3.3.16 A selection of bond lengths and angles for Cu(12a)$(OTf)_2$

Length / Å		**Angle / °**	
Cu(1)-O(1)	2.213(3)	O(1)-Cu(1)-N(2)	104.48(13)
Cu(1)-N(1)	2.035(4)	N(1)-Cu(1)-N(2)	81.15(15)
Cu(1)-N(2)	1.957(4)	N(2)-Cu(1)-N(3)	82.01(15)
Cu(1)-N(3)	1.941(3)	N(3)-Cu(1)-N(4)	80.83(14)
Cu(1)-N(4)	2.038(4)	N(4)-Cu(1)-N(1)	114.90(14)
N(3)-C(14)	1.278(5)	C(14)-N(3)-C(13)	128.4(3)
N(2)-C(7)	1.263(5)	C(8)-N(2)-C(7)	127.7(4)

The data shows that the structure belongs to the triclinic *P*1 space group. The absolute structure parameter is -0.004(8), suggesting that the complex is enantiomerically pure. The structure suggests that there is no addition of methanol across either of the imine bonds. In this case the solid-state product included a coordinated MeOH moiety and the imine was left intact. Analysis of the product *via* mass spectrometry indicated there was only a trace amount of the α-amino ether species present. This is presumably related to the extra degree of steric bulk caused by the addition of the *ortho* methyl group on the pyridine ring.

The bond lengths and angles are in agreement with literature values of similar complexes.[12-13] The N(3)-C(14) and N(2)-C(7) bond lengths are indicative of imine bonds, with no significant difference between the two bond lengths. This suggests that there is no addition at all across either of the imine bonds.
Overall, the complex has adopted a square-based pyramidal geometry, which is indicated by the bond lengths and angles. However, if the methanol molecule had not bonded to the metal, a square planar geometry would be observed, which is also favourable, and would be supported by the bond lengths and angles.

The ligand was also varied by changing the heteroatom of the aromatic rings. Sulfur and oxygen were used instead, as previously described in chapter two, section 2.4, ligands **13a**, **13b**, **14a** and **14b**. The resulting copper(II) complexes were prepared as previously outlined, and characterised by mass spectrometry, elemental analysis and IR spectroscopy. The characterisation revealed that the α-amino ether complex was not formed. Bandini prepared the copper(II) complexes of ligands **13a** and **13b**, and did not report any evidence that pointed to the formation of an α-amino ether functionality.[19] He also reported the crystal structure of Cu(**13b**)$(OAc)_2$; the bond lengths and angles were similar to that has been reported here.

3.3.3 Copper(II) Complexes Containing Phosphine Ligands

Ligands **8a**, **8b**, **18a** and **18b** were also complexed to copper(II), using the same experimental methods as have been described for copper(II) complexes. This can be seen in figs. 3.3.25 and 3.3.26. These complexes were analysed by mass spectrometry and elemental analysis. In addition to this, the complex was recrystallised from the minimum amount of methanol, in the presence of air.

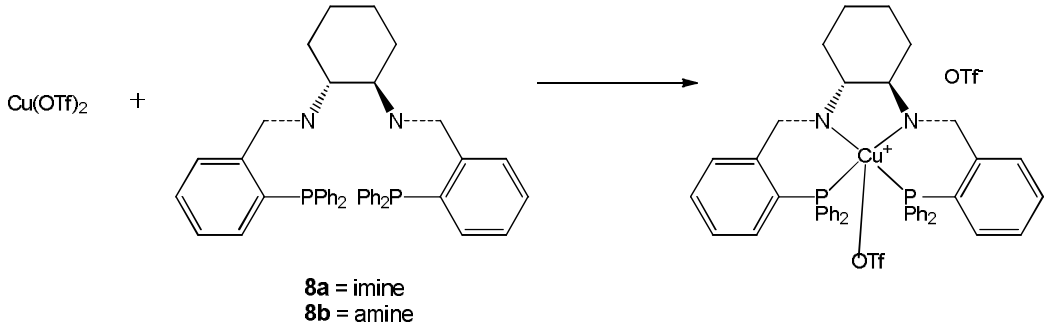

Fig. 3.3.25 Reaction scheme of the preparation of Cu(8a)(OTf)$_2$ and Cu(8b)(OTf)$_2$

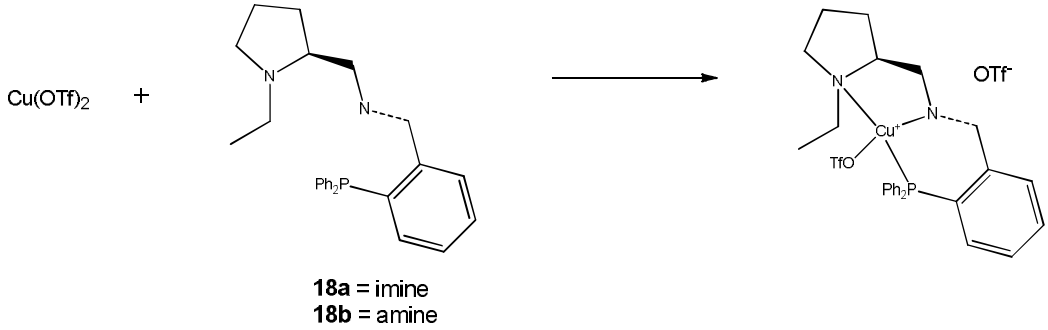

Fig. 3.3.26 Reaction scheme of the preparation of Cu(18a)(OTf)$_2$ and Cu(18b)(OTf)$_2$

Crystals were obtained for the "Cu(**8b**)(OTf)$_2$" complex, which were white in colour. This was highly surprising, as usually copper(II) complexes are blue, green or purple in colour. This suggested that this may in fact not be a copper(II) complex, and that through oxidation of the phosphine ligand, which is common, the copper metal may have been reduced to copper(I).[20-24] Copper(I) is diamagnetic, and can therefore be analysed using NMR spectroscopy. The ^{1}H and ^{31}P{H} spectra of the complex, and the comparisons with the free ligand, can be seen in figs. 3.3.27 and 3.3.28 respectively.

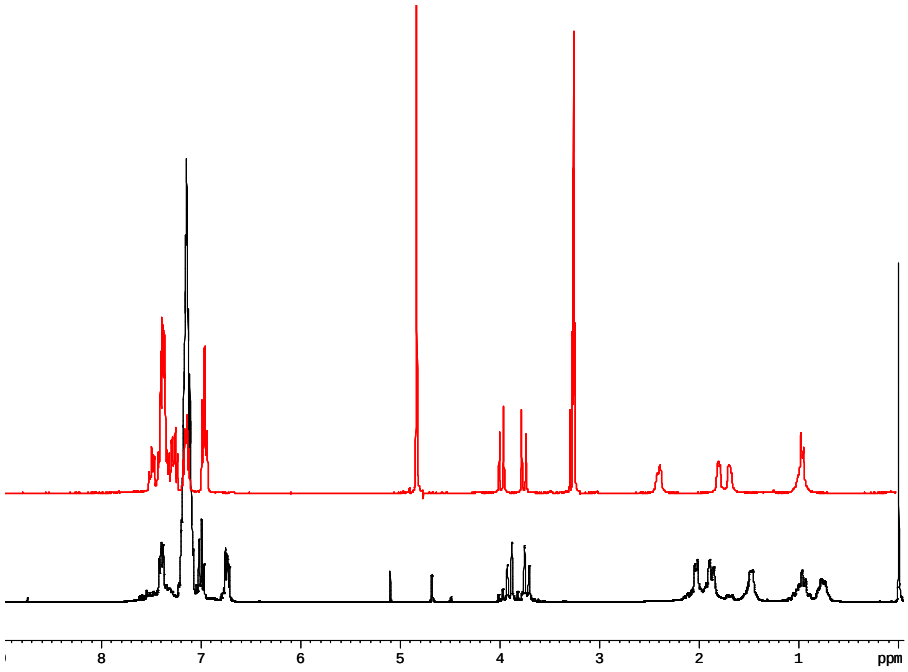

Fig. 3.3.27 ^{1}H NMR spectra of the ligand 8b (black), and its copper(I) complex Cu(8b)(OTf) (red)

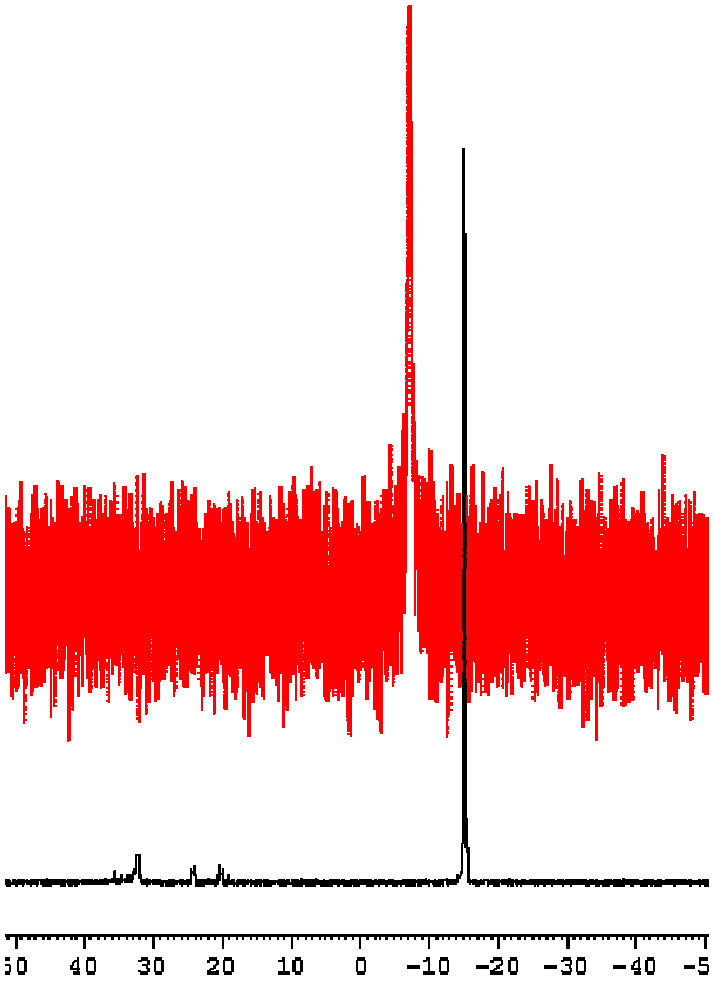

Fig. 3.3.28 ^{31}P{^{1}H} NMR spectra of the ligand 8b (black), and its copper(I) complex Cu(8b)(OTf) (red)

The ^{1}H NMR spectra show no significant differences, which is to be expected. The feature to be noted, is that a clear spectrum with well defined resonances can be obtained for this complex, which would not be possible with a copper(II) complex. The magnetic moment of an unpaired electron is much stronger than that of a proton, and so any signals produced by the protons will be suppressed. Therefore, if this was a copper(II) complex, a spectrum would not be observed. Comparing the $^{31}P\{^{1}H\}$ spectra, the peak has shifted from approximately -15 to -8 ppm, which is brought about by the copper binding to the ligand. Interestingly, there is no additional peak in the spectrum that may correspond to an oxidised phosphine group, which is presumably left in the supernatant liquid upon crystallisation. This in turn suggests that the oxidation of some of the ligand brings about the reduction of copper(II) to copper(I), which complexes with the unoxidised ligand, and forms the crystals that have subsequently been characterised. This also implies that there will be some copper(II) triflate in solution, which is supported by the colour of the solution (blue, even after the majority of this redox process has occurred). In order for the redox process to balance, 20 % of the ligand is oxidised at both phosphine groups. This reduces 80 % of the copper present to copper(I), which complexes with the remaining 80 % of unoxidised ligand. This leaves 20 % of the copper present as copper(II).

The crystal structure for the Cu(**8b**)(OTf) complex can be seen in fig. 3.3.29, and a selection of bond lengths and angles are given in table 3.3.17.

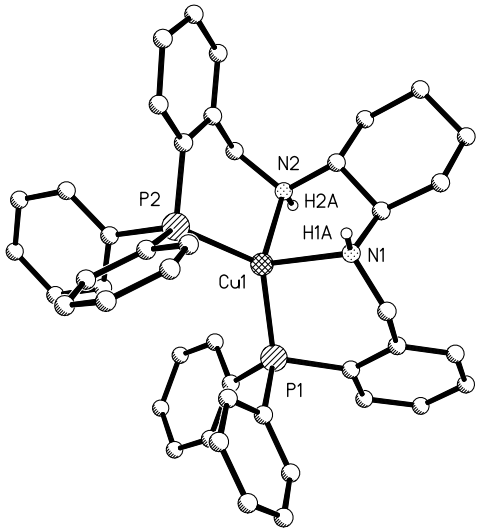

Fig. 3.3.29 Solid-state structure of Cu(8b)(OTf). All hydrogen atoms {except those bound to N(1) and N(2)} and triflate counterion have been removed for clarity

Table 3.3.17 A selection of bond lengths and angles for Cu(8b)(OTf)

Length / Å		Angle / °	
Cu(1)-N(1)	2.1153(13)	N(1)-Cu(1)-N(2)	84.26(5)
Cu(1)-N(2)	2.1025(13)	N(1)-Cu(1)-P(1)	95.58(4)
Cu(1)-P(1)	2.2126(4)	N(2)-Cu(1)-P(2)	97.38(4)
Cu(1)-P(2)	2.2292(4)	P(1)-Cu(1)-P(2)	124.144(16)

The data shows that the structure belongs to the orthorhombic $P2_12_12_1$ space group. The absolute structure parameter is -0.003(5), suggesting that the complex is enantiomerically pure. The bond lengths and angles are in agreement with literature values of similar complexes.[12-13]

By analysis of the crystal structure, and examining the bond angles the complex adopts a highly distorted tetrahedral geometry. The bond angles are very dependent upon the ligand geometry, as previously discussed. When the complex is prepared, copper(II) is used, and analysis by UV-vis spectroscopy suggests that the majority of the initial complex that is formed is copper(II) and this reduces to copper(I) over time. The UV-vis spectroscopy of this complex will be discussed shortly. When the copper(II) complex is formed, a square planar geometry would be favoured, given that the electronic configuration of copper(II) is d^9. However, a copper(I) complex has an electronic configuration of d^{10}, therefore a tetrahedral geometry is preferable. The bond angles suggest a geometry that is somewhere between the two – a "flattened tetrahedron".[25]

As previously mentioned, the copper(II) gives rise to a blue solution; the copper(I) gives a colourless solution. This means that over time, as the copper(II) is reduced to copper(I), the intensity of the colour of the solution will decrease. This can be followed by UV-vis spectroscopy, and the kinetics investigated. The resulting spectra can be seen in fig. 3.3.30.

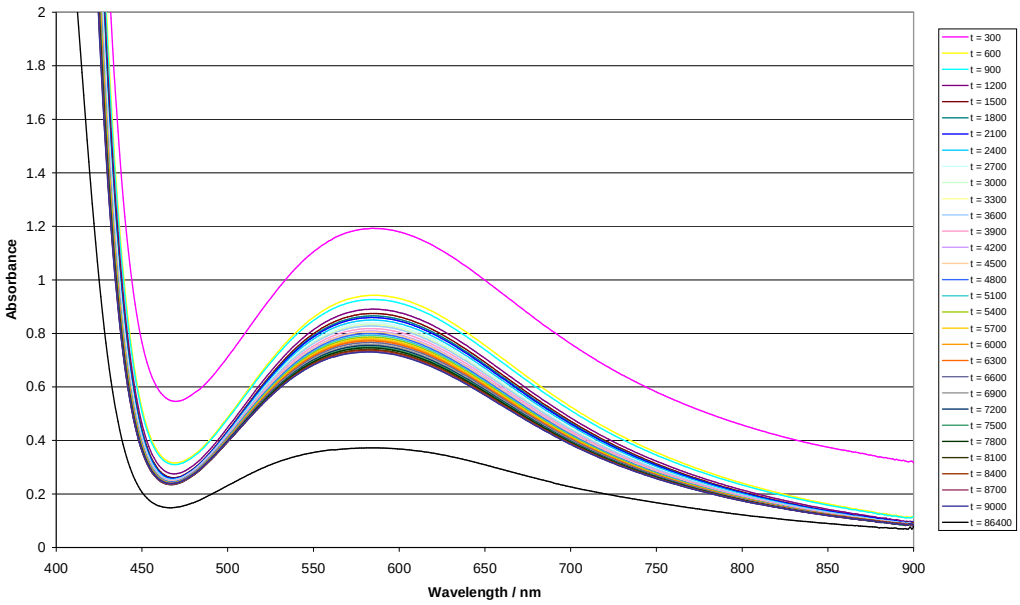

Fig. 3.3.30 UV-vis spectra of Cu(8a)(OTf) at various time intervals, where t = 0 involves mixing a solution of the ligand with a $Cu(OTf)_2$ solution, both of known concentration. t is measured in seconds

The peak due to the copper(II) can clearly be seen at approximately 600 nm, which is where one would expect given a blue compound. The absorbance of this peak as expected, decreases over time. Using the Beer-Lambert law, the concentration can be calculated for each measurement, as follows.

$A = \varepsilon cl$ (where A = absorbance, ε = molar absorption coefficient, c = concentration and l = path length)

So $c = \frac{A}{\varepsilon l}$

At t = 0, c = 0.0228 mol dm^{-3}

Path length = 1 cm

$\varepsilon = \frac{A}{cl} = \frac{1.1924}{(0.0228 \times 1)} = 52.3$ mol^{-1} dm^3 cm^{-1}

The absorbance is measured with each time interval and the molar absorption coefficient and path length remain constant throughout the experiment. Hence, the concentration of copper(II) can be calculated as a function of time. If this process follows a first order process then a plot of $\ln([A]/[A_0])$ vs. time should be linear.

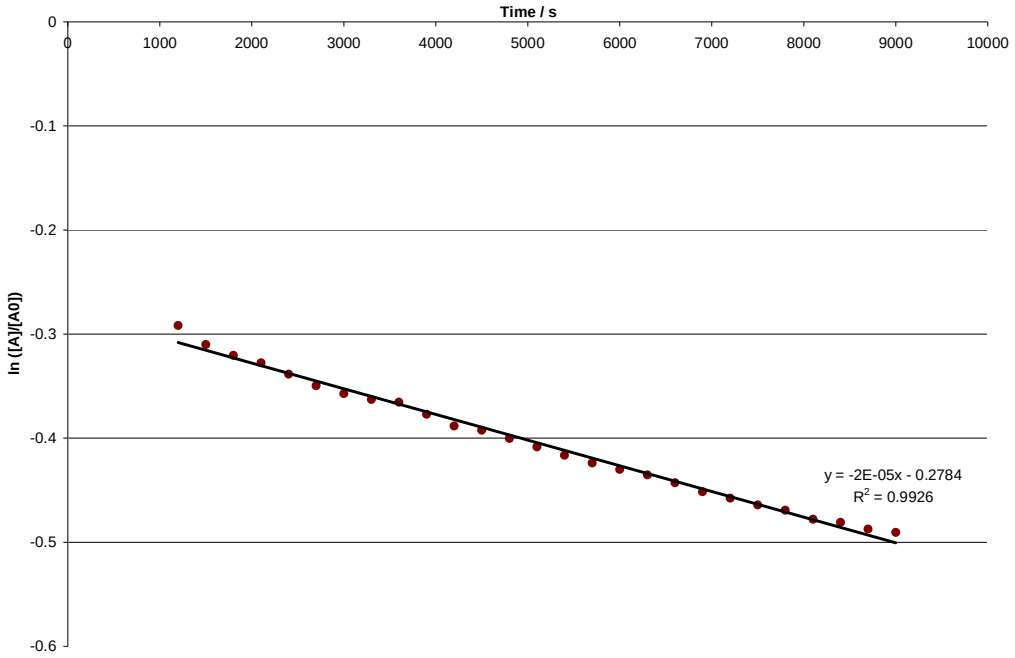

Fig. 3.3.31 Plot of $\ln([A]/[A_0])$ vs time for the conversion of Cu(II) to Cu(I) with ligand 8b

The R^2 value shows that the data correlates almost perfectly with the line of best fit, which suggests that first order kinetics are indeed occurring. The gradient gives the rate constant, therefore $k = 2 \times 10^{-5}$ s^{-1}. The value of k indicates how readily this redox process occurs, and hence provide more information about the stabilities of both the copper(II) and copper(I) complexes. Tisato saw the reduction of copper(II) to copper(I) in the presence of their phosphinoamine ligands.[24] It was found that the ligand stabilised the reduced copper centre, making the formation of the copper(I) complex favourable. The authors speculated that the oxidation of the phosphine moieties was caused by the presence of water. They found that approximately 70 % of the complex formed was the copper(I) complex, which is in accordance with what has been calculated here.

Copper(II) complexes of the ligands **18a** and **18b** were also prepared. However, in this case no reduction of the copper(II) was observed. Single crystal X-ray diffraction of Cu(**18b**)$(OTf)_2$ was performed. The crystal structure can be seen in fig. 3.3.32, and a selection of bond lengths and angles are given in table. 3.3.18.

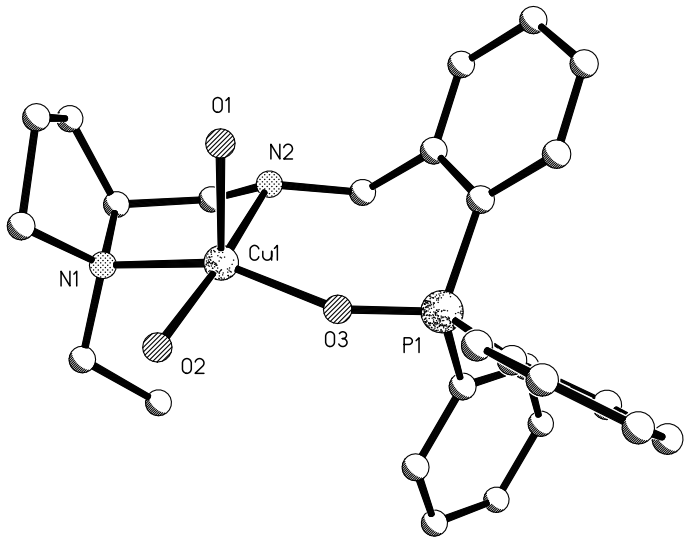

Fig. 3.3.32 Solid-state structure of Cu(18b)$(OTf)_2$. All hydrogen atoms and triflate counterions have been removed for clarity

Table 3.3.18 A selection of bond lengths and angles for Cu(18b)$(OTf)_2$

Length / Å		**Angle / °**	
Cu(1)-N(1)	2.017(5)	N(1)-Cu(1)-N(2)	86.80(19)
Cu(1)-N(2)	2.012(5)	N(1)-Cu(1)-O(2)	89.49(19)
Cu(1)-O(2)	2.017(4)	O(2)-Cu(1)-O(1)	86.5(2)
Cu(1)-O(3)	2.175(4)	O(1)-Cu(1)-N(2)	96.7(2)
Cu(1)-O(1)	1.975(5)	O(3)-Cu(1)-N(2)	92.2(2)
P(1)-O(1)	1.487(5)	Cu(1)-O(1)-P(1)	145.7(3)

The data shows that the structure belongs to the orthorhombic $P2_12_12_1$ space group. The absolute structure parameter is -0.01(2), suggesting that the complex is enantiomerically pure. In this case it was observed that the phosphine was oxidised to the phosphine oxide, presumable caused by oxygen, as no

precautions were taken to remove this, and it is through the oxygen centre that the ligand coordinates to the metal centre.

The bond lengths and angles are in agreement with literature values of similar complexes.[12-13] The P(1)-O(1) bond length matches that of a typical P=O double bond.[26] This, in combination with other characterisation, supports the conclusion that the ligand has been oxidised. However, unlike the Cu(**8b**)(OTf) complex, this has not resulted in the reduction of the metal from copper(II) to copper(I). This results in this complex having a d^9 configuration, which would support a square-based pyramid geometry which is observed here, and supported by the bond angles. If the water molecule {O(1)} was not present and bound to the complex, a square planar geometry would be observed, which would also be favourable, and would also be supported by the bond angles seen here.

3.4 Group (IV) Metal Complexes

As previously discussed, titanium(IV) and zirconium(IV) are hard Lewis acids, and prefer to bond with hard Lewis bases. For this purpose, a series of ligands were prepared containing phenoxide substituents, as previously outlined in chapter two. Some of these ligands have been used in the preparation of titanium(IV) and zirconium(IV) complexes, which will be discussed here.

3.4.1 Titanium(IV) Complexes

A reaction scheme for the preparation of these complexes is given in fig. 3.4.1. The complexes were analysed by NMR spectroscopy and mass spectrometry.

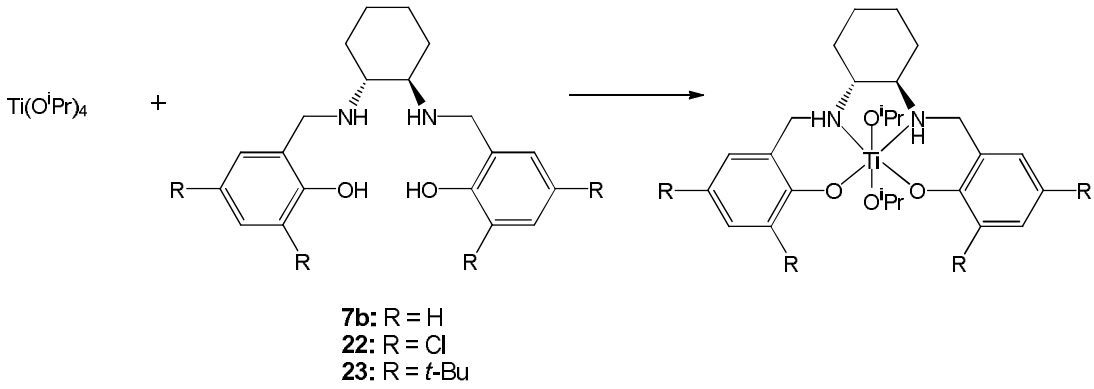

Fig. 3.4.1 Reaction scheme of the preparation of titanium(IV) complexes

Ti(**7b**)(O^iPr)$_2$ was analysed by single crystal X-ray diffraction. The crystal structure can be seen in fig. 3.4.2, and a selection of bond lengths and angles are given in table 3.4.1.

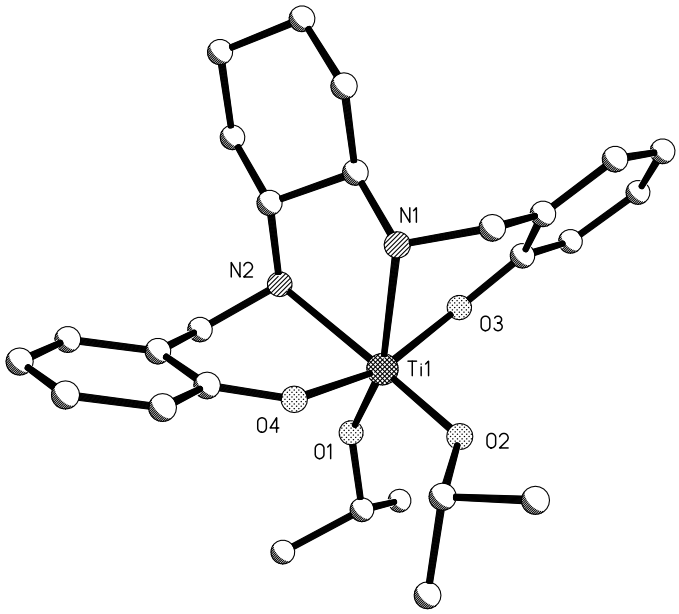

Fig. 3.4.2 Solid-state structure of Ti(7b)(O^iPr)$_2$. All hydrogen atoms have been removed for clarity

Table 3.4.1 A selection of bond lengths and angles for Ti(7b)(O^iPr)$_2$

Length / Å		Angle / °	
Ti(1)-N(1)	2.2832(13)	N(1)-Ti(1)-N(2)	74.82(5)
Ti(1)-N(2)	2.2669(14)	N(2)-Ti(1)-O(1)	84.88(5)
Ti(1)-O(1)	1.8212(12)	O(1)-Ti(1)-O(2)	103.51(6)
Ti(1)-O(2)	1.8046(12)	O(2)-Ti(1)-N(1)	97.72(5)
Ti(1)-O(3)	1.9310(10)	N(1)-Ti(1)-O(3)	78.88(5)
Ti(1)-O(4)	1.9359(11)	N(1)-Ti(1)-O(4)	83.32(5)
		O(2)-Ti(1)-N(2)	167.98(6)
		O(1)-Ti(1)-N(1)	158.36(5)

The data shows that the structure belongs to the orthorhombic $P2_12_12_1$ space group. The absolute structure parameter is -0.023(17), suggesting that the complex is enantiomerically pure. The bond lengths and angles are in agreement with literature values of similar complexes.[27-30]

The complex has adopted a distorted octahedral geometry, which is supported by the bond angles. The distortion is provided by the ligand, in that four of the six metal-ligand bonds involve atoms that are part of the same ligand, and so to a large extent the ligand dictates the bond angles seen in the complex. The bond angles O(2)-Ti(1)-N(2) and O(1)-Ti(1)-N(1) show significant deviation from the expected 180 °, although this is probably due to repulsion of the oxygen atom of this ligand away from the surrounding oxygen atoms.

Ti(**23**)(O^iPr)$_2$ was also analysed by single crystal X-ray diffraction. The crystal structure can be seen in fig. 3.4.3, and a selection of bond lengths and angles are given in table 3.4.2.

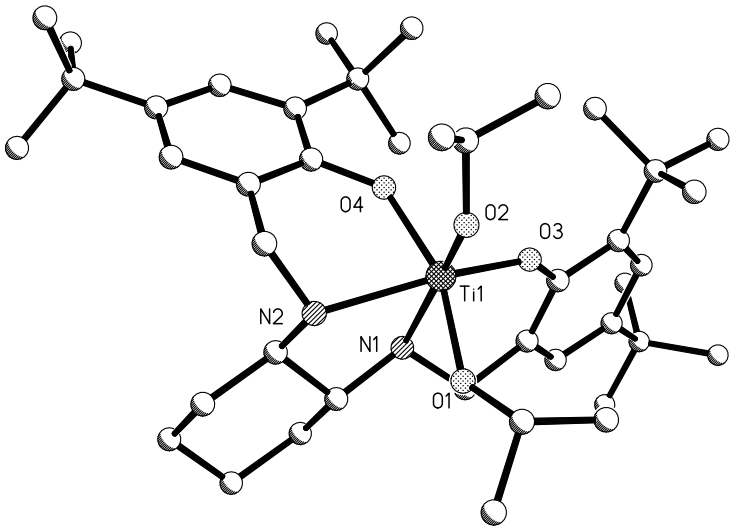

Fig. 3.4.3 Solid-state structure of Ti(23)(O^iPr)$_2$. All hydrogen atoms have been removed for clarity

Table 3.4.2 A selection of bond lengths and angles for Ti(23)(O^iPr)$_2$

Length / Å		**Angle / °**	
Ti(1)-N(1)	2.293(2)	N(1)-Ti(1)-N(2)	75.45(8)
Ti(1)-N(2)	2.224(2)	N(2)-Ti(1)-O(2)	98.02(8)
Ti(1)-O(2)	1.8191(17)	O(2)-Ti(1)-O(3)	103.66(8)
Ti(1)-O(3)	1.8708(16)	O(3)-Ti(1)-N(1)	83.25(7)
Ti(1)-O(1)	1.8655(17)	N(1)-Ti(1)-O(1)	80.16(8)
Ti(1)-O(4)	1.9359(17)	N(1)-Ti(1)-O(4)	89.19(8)
		O(2)-Ti(1)-N(1)	171.65(8)
		O(1)-Ti(1)-O(4)	160.64(8)

The data shows that the structure belongs to the orthorhombic $P2_12_12_1$ space group. The absolute structure parameter is -0.03(2), suggesting that the complex is enantiomerically pure. The bond lengths and angles are in agreement with literature values of similar complexes.[27-30]

The bond lengths, angles and structure geometry are very similar to that of complex Ti(**7b**)(O^iPr)$_2$. The Ti-O bonds are shorter due to the bonds being stronger and more favourable than the Ti-N bonds, and also due to the ligand geometry. The bond angles are supportive of the complex adopting a distorted

octahedral structure. Distortion is likely to be due to ligand geometry, which in turn influences the geometry of the complex, and repulsion between to oxygen atoms within the complex, all as previously discussed.

3.4.2 Zirconium(IV) Complexes

A reaction scheme for the preparation of these complexes is given in fig. 3.4.4.

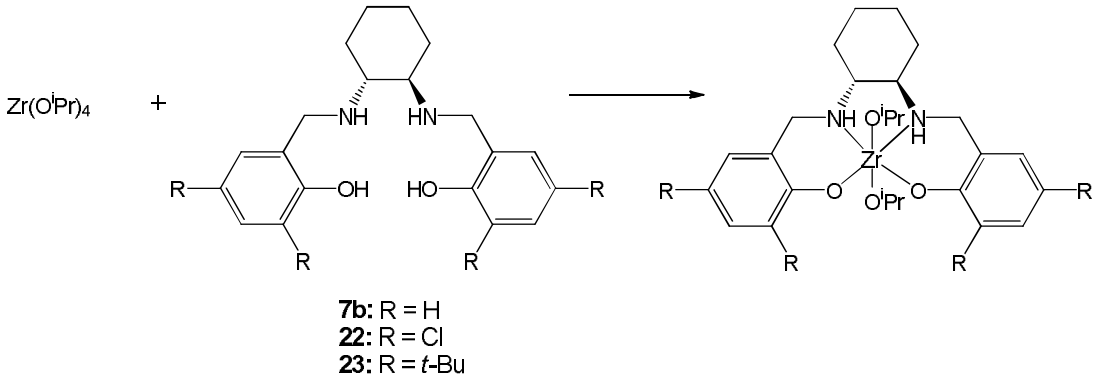

Fig. 3.4.4 Reaction scheme of the preparation of zirconium(IV) complexes

The complexes were analysed by NMR spectroscopy and mass spectrometry. Zr(**7b**)(O^iPr)$_2$ was also analysed by single crystal X-ray diffraction. The crystal structure can be seen in fig. 3.4.5, and a selection of bond lengths and angles are given in table 3.4.3.

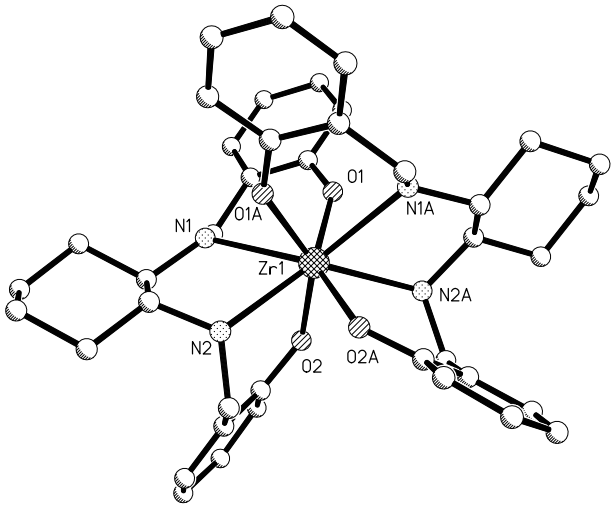

Fig. 3.4.5 Solid-state structure of Zr(7b)(O^iPr)$_2$. All hydrogen atoms have been removed for clarity

Table 3.4.3 A selection of bond lengths and angles for Zr(7b)(O^iPr)$_2$

Length / Å		**Angle / °**	
Zr(1)-N(1)	2.482(6)	N(1)-Zr(1)-N(2)	68.83(19)
Zr(1)-N(2)	2.418(6)	N(2)-Zr(1)-O(2A)	71.99(19)
Zr(1)-N(1A)	2.482(6)	O(2A)-Zr(1)-N(2A)	76.99(19)
Zr(1)N(2A)	2.418(6)	N(2A)-Zr(1)-N(1A)	68.83(19)
Zr(1)-O(1)	2.063(5)	N(1A)-Zr(1)-O(1)	74.1(2)
Zr(1)-O(2A)	2.090(5)	O(1)-Zr(1)-O(1A)	94.1(3)
Zr(1)-O(1A)	2.063(5)	O(2A)-Zr(1)-O(2)	94.4(3)
Zr(1)-O(2)	2.090(5)	O(1A)-Zr(1)-O(2)	144.94(19)

The data shows that the structure belongs to the tetragonal $P3_12_1$ space group. The absolute structure parameter is -0.02(7), suggesting that the complex is enantiomerically pure. The bond lengths and angles are in agreement with literature values of similar complexes.[29,31-32]

The structure shows that this complex is eight-coordinate. This behaviour is not uncommon where 4d metals are concerned.[33] The larger atomic radius enables more ligands to be accommodated around the metal sphere. The electron count of the complex is 16e$^-$. The ligands involved in this complex are π-donor ligands, meaning that there is extra donation of electrons from an occupied ligand orbital

to an unoccupied metal orbital. In these cases, it is energetically favourable to have lower electron counts than the traditional $18e^-$, as this avoids filling antibonding orbitals. It is not uncommon for early transition metal complexes not to have an $18e^-$ count.

The Zr-O bond lengths are significantly shorter than the Zr-N bond lengths, which is to be expected. In a similar fashion to the titanium complexes, zirconium is a "hard" metal and has a +4 oxidation state, so not only does it favour bonding which is more ionic in character, bonding with ligands that can balance the charge on the metal is also favoured, resulting in stronger and hence shorter bonds.

As previously mentioned, this crystal structure showed that two ligands were binding to the zirconium metal. Thus the zirconium complexes involving ligands **7b** and **22** were also prepared using a metal:ligand ratio of 1:2 (rather than 1:1, as used previously). This was not necessary with ligand **23**, as it was thought that the bulky t-Bu groups would cause too much steric hindrance for two ligands to bind to the one zirconium metal centre. These complexes were also analysed by NMR spectroscopy and mass spectrometry.

3.5 Concluding Remarks

A series of iridium(I), rhodium(I), ruthenium(II), platinum(II), palladium(II), copper(II), titanium(IV) and zirconium(IV) complexes have been described here, all of which are novel. Some surprising behaviours have been observed regarding these complexes, which has been discussed in detail. It has been shown that not only can the ligand have a huge input into the characteristics of the complexes, but other factors such as which counterion should be used and what ratio of metal:ligand is appropriate have also been investigated. In explaining this unexpected behaviour, many different areas of chemistry were called upon, that initially one would not necessarily think would be related to this research. This highlights the importance of considering chemistry as a whole

when discussing research, rather than drawing purely upon one relatively small area within this scientific discipline.

3.6 References

(1) Fuentes, J. A.; France, M. B.; Slawin, A. M. Z.; Clarke, M. L. *New J. Chem.* **2009**, *33*, 466.

(2) Murata, K.; Ikariya, T. *J. Org. Chem.* **1999**, *64*, 2186.

(3) Garralda, M. A.; Hernadez, R.; Lbarlucea, L.; Pinilla, E.; Torres, M. R.; Zarandona, M. *Organometallics* **2007**, *26*, 5369.

(4) Dahlenburg, L.; Treffert, H.; Farr, C.; Heinemann, F. W.; Zahl, A. *European Journal of Inorganic Chemistry* **2007**, 1738.

(5) Raja, R.; Thomas, J. M.; Jones, M. D.; Johnson, B. F. G.; Vaughan, D. E. W. *J. Am. Chem. Soc.* **2003**, *125*, 14982.

(6) Beller, M.; Trauthwein, H.; Eichberger, M.; Breindl, C.; Muller, T. E.; Zapf, A. *J. Organomet. Chem.* **1998**, *566*, 277.

(7) Jones, M. D.; Almeida Paz, F. A.; Davies, J. E.; Johnson, B. F. G.; Klinowski, J. *Acta Crystallographica Section E* **2003**, *59*, m1091.

(8) Sen, S.; Saha, M. K.; Mitra, S.; Edwards, A. J.; Clegg, W. *Polyhedron* **2000**, *19*, 1881.

(9) Comba, P.; Hambley, T. W.; Hitchman, M. A.; Stratemeier, H. *Inorg. Chem.* **1995**, *34*, 3903.

(10) Becker, M.; Heinemann, F. W.; Knoch, F.; Donaubauer, W.; Liehr, G.; Schindler, S.; Golub, G.; Cohen, H.; Meyerstein, D. *European Journal of Inorganic Chemistry* **2000**, 719.

(11) Abry, S.; Thibon, A.; Albela, B.; Delichere, P.; Banse, F.; Bonneviot, L. *New J. Chem.* **2009**, *33*, 484.

(12) Rigamonti, L.; Cinti, A.; Forni, A.; Pasini, A.; Piovesana, O. *European Journal of Inorganic Chemistry* **2008**, 3633.

(13) Maxim, C.; Pasatoiu, T. D.; Kravtsov, V. C.; Shova, S.; Muryn, C. A.; Winpenny, R. E. P.; Tuna, F.; Andruh, M. *Inorg. Chim. Acta* **2008**, *361*, 3903.

(14) Albinati, A.; Arz, C.; Pregosin, P. S. *Inorg. Chem.* **1988**, *27*, 2015.

(15) Hoskins, B. F.; Whillans, F. D. *Journal of the Chemical Society a - Inorganic Physical Theoretical* **1970**, 123.

(16) Herrera, A. M.; Kalayda, G. V.; Disch, J. S.; Wikstrom, R. P.; Korendovych, I. V.; Staples, R. J.; Campana, C. F.; Nazarenko, A. Y.; Haas, T. E.; Rybak-Akimova, E. V. *Dalton Trans.* **2003**, 4482.

(17) Dey, S. K.; Mondal, N.; El Fallah, M. S.; Vicente, R.; Escuer, A.; Solans, X.; Font-Bardia, M.; Matsushita, T.; Gramlich, V.; Mitra, S. *Inorg. Chem.* **2004**, *43*, 2427.

(18) Kawamichi, T.; Haneda, T.; Kawano, M.; Fujita, M. *Nature* **2009**, *461*, 633.

(19) Bandini, M.; Piccinelli, F.; Tommasi, S.; Umani-Ronchi, A.; Ventrici, C. *Chem. Commun.* **2007**, 616.

(20) Bowen, R. J.; Coates, J.; Coyanis, E. M.; Defayay, D.; Fernandes, M. A.; Layh, M.; Moutloali, R. M. *Inorg. Chim. Acta* **2009**, *362*, 3172.

(21) Amatore, C.; Carre, E.; Jutand, A.; Mbarki, M. A.; Meyer, G. *Organometallics* **1995**, *14*, 5605.

(22) Matsukawa, S.; Sugama, H.; Imamoto, T. *Tetrahedron Lett.* **2000**, *41*, 6461.

(23) Pilloni, G.; Valle, G.; Corvaja, C.; Longato, B.; Corain, B. *Inorg. Chem.* **1995**, *34*, 5910.

(24) Tisato, F.; Refosco, F.; Bandoli, G.; Pilloni, G.; Corain, B. *J. Chem. Soc.-Dalton Trans.* **1994**, 2471.

(25) Gerloch, M., Constable, E. C. *Transition Metal Chemistry*; VCH, 1994.

(26) Jakob, A.; Ecorchard, P.; Linseis, M.; Winter, R. F.; Lang, H. *J. Organomet. Chem.* **2009**, *694*, 655.

(27) Nielson, A. J.; Waters, J. M. *Polyhedron* **2010**, *29*, 1715.

(28) Wen, X. J.; Dong, J. Y. *Appl. Organomet. Chem.* **2010**, *24*, 503.

(29) Jones, M. D.; Davidson, M. G.; Kociok-Kohn, G. *Polyhedron* **2010**, *29*, 697.

(30) Johnson, A. L.; Davidson, M. G.; Lunn, M. D.; Mahon, M. F. *European Journal of Inorganic Chemistry* **2006**, 3088.

(31) Chmura, A. J.; Cousins, D. M.; Davidson, M. G.; Jones, M. D.; Lunn, M. D.; Mahon, M. F. *Dalton Trans.* **2008**, 1437.

(32) Zhu, H. J.; Wang, M.; Ma, C. B.; Li, B.; Chen, C. N.; Sun, L. C. *J. Organomet. Chem.* **2005**, *690*, 3929.

(33) Nomiya, K., Sakai, Y., Matsunaga, S. *European Journal of Inorganic Chemistry* **2011**, 179.

Preparation of Heterogeneous Catalysts Containing (*R*,*R*)-1,2-diaminocyclohexane Type Imine Ligands

4.1 Introduction

As previously discussed in chapter one, there are two types of bonding that can be utilised to anchor a catalyst to a support, those being covalent or ionic.[1-6] Covalent bonding is irreversible, which is preferred given that leaching is a significant problem in heterogeneous catalysis. Therefore, the synthetic methods discussed here will use covalent bonding to prepare heterogeneous catalysts.

4.2 Preparation of Silica-Supported Ligands Using Covalent Linkages

The covalent technique of attaching the ligand to the support sees the ligand being built up onto the support through a series of synthetic steps. The synthetic methodology can be seen in fig. 4.2.1. There are many reports in the literature of the use of such techniques to prepare heterogeneous catalysts.[7-10] Many reports have utilised the mesoporous material MCM-41.[11-14] However, the synthesis of this material may prove prohibitively expensive for large scale applications. Therefore commercially available porous silica (60 Å, 35-70 micron, surface area of 450 m^2 g^{-1}) was utilised.

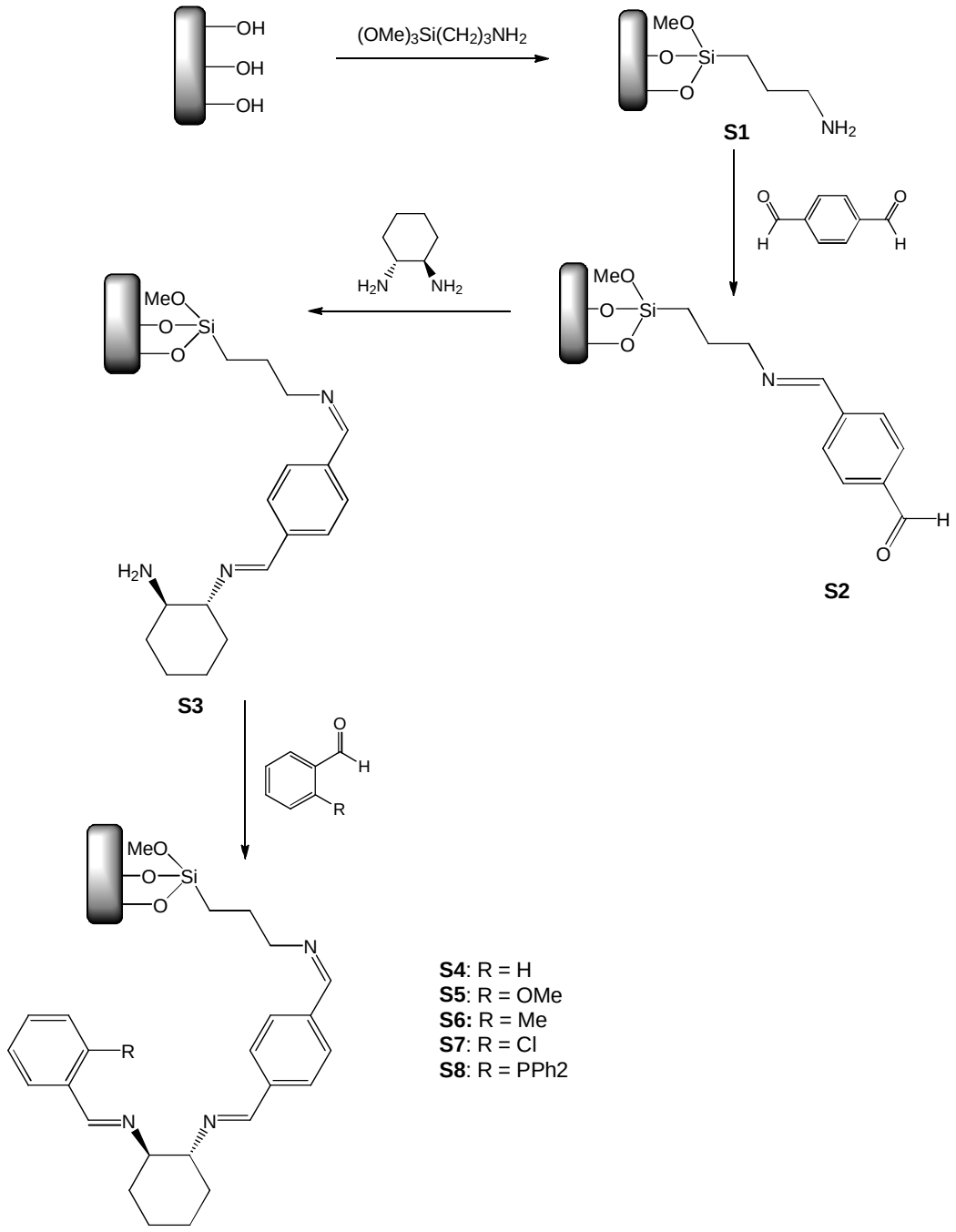

Fig. 4.2.1 Reaction scheme of the preparation of silica-supported imine ligands S4-S8

The precursors to the heterogeneous ligands **S1-S4** were characterised by $^{13}C\{^{1}H\}$ CP/MAS solid state NMR spectroscopy, elemental analysis and thermogravimetric analysis (TGA). Solid-state NMR is more technically challenging than its solution counterpart. This is due to the anisotropic nature of the chemical shift. However, this can be circumvented by spinning the sample at 54.74 ° (the so-called magic angle) which has the effect of averaging the

chemical shift to the isotropic value. The $^{13}C\{^{1}H\}$ CP/MAS (cross polarisation magic angle spinning) NMR spectra for **S1-S4** can be seen in fig. 4.2.2.

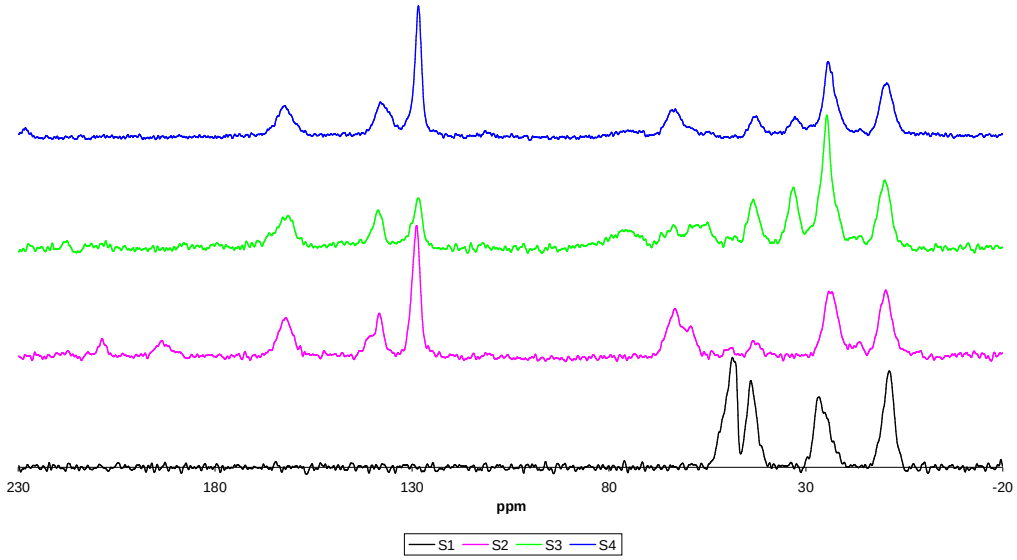

Fig. 4.2.2 $^{13}C\{^{1}H\}$ CP/MAS solid state NMR spectra of S1-S4, previously shown in fig. 4.2.1

The spectrum for **S1** has resonances at 9, 27, 44, 49 ppm respectively. Solid-state pendant type experiments showed the resonance at 49 ppm to arise from the OMe groups still present. The spectrum of **S2** shows a characteristic aldehyde resonance at approximately 200 ppm, indicating that the attachment of terephthalaldehyde was successful. The two aromatic resonances at approximately 130 and 140 ppm and the imine resonance at 165 ppm support this, coupled with the fact that the resonance at 44 ppm ($\mathbf{C}H_2NH_2$) has almost disappeared and a new resonance at 62 ppm is apparent ($\mathbf{C}H_2N{=}CH$). The remaining aliphatic resonances are due to the aminopropyl (now iminopropyl) group from the synthesis of **S1**. On addition of (*R*,*R*)-1,2-diaminocyclohexane (**S3**), the aldehyde resonance is no longer observed, suggesting that the reaction has been successful. This is supported by the addition of new aliphatic resonances to the spectrum, at approximately 35 and 45 ppm, and 75 ppm (CHN), due to cyclohexane carbons. On the addition of benzaldehyde to **S3**, to produce **S4**, the nature of the resonances in the aliphatic region (particularly around the 60 ppm region) change significantly, indicating that a reaction has occurred. If any resonances were to change, this would be the expected resonance, as this carbon atom changes from having an amine group attached to

an imine. Another feature of the **S4** spectrum to notice is the absence of an aldehyde resonance, indicating that any excess aldehyde remaining from the reaction has been completely removed.

Thermogravimetric analysis (TGA) was also used to characterise these samples; the results can be seen in fig. 4.2.3. TGA involves heating a sample, under air, on a sensitive spring balance. As the sample is heated it decomposes and the % weight loss is measured as a function of temperature.

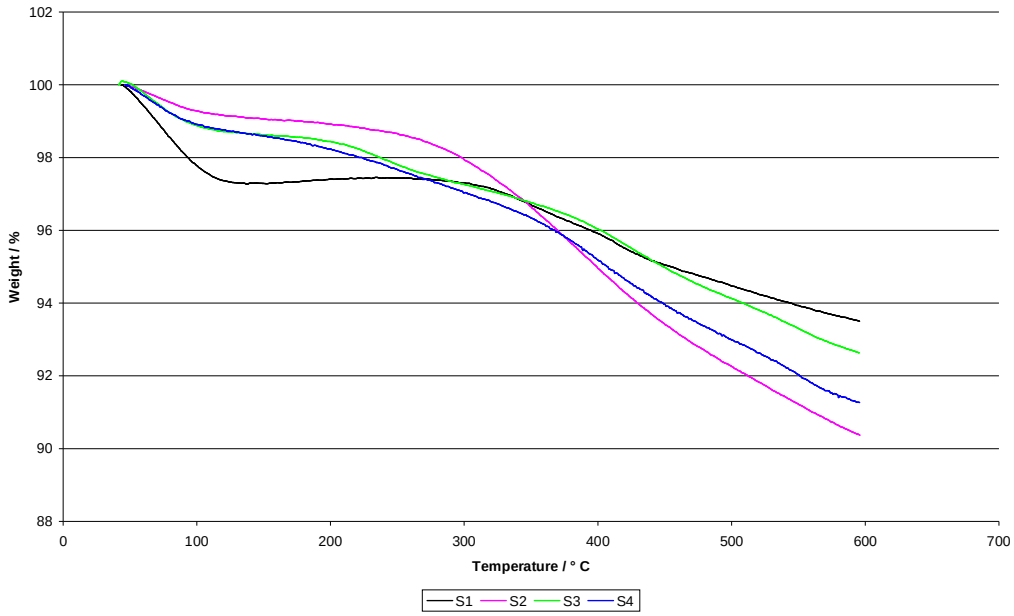

Fig. 4.2.3 TGA of S1-S4, as previously shown in fig. 4.2.1

The TGA data shows that as the ligand is built up onto silica, the percentage weight loss increases. The initial decrease in percentage weight can be attributed to the loss of water in the sample. After this, the percentage weight loss is approximately 8-10 %. This corresponds to the loss of the organic ligand that was bound to the silica – which is also supported by elemental analysis. The elemental analysis also shows that the percent C, H and N values increase accordingly at each reaction stage to produce to heterogeneous precursor **S3**. Together, this characterisation supports the successful "step-wise" synthesis of **S3**.

From the heterogeneous precursor **S3**, a library of heterogeneous ligands were prepared (**S4-S8**). These were characterised by $^{13}C\{^{1}H\}$ CP/MAS solid state NMR, elemental analysis and TGA. The $^{13}C\{^{1}H\}$ NMR spectra can be seen in fig. 4.2.4, and the $^{31}P\{^{1}H\}$ spectrum of **S8** can be seen in fig. 4.2.5.

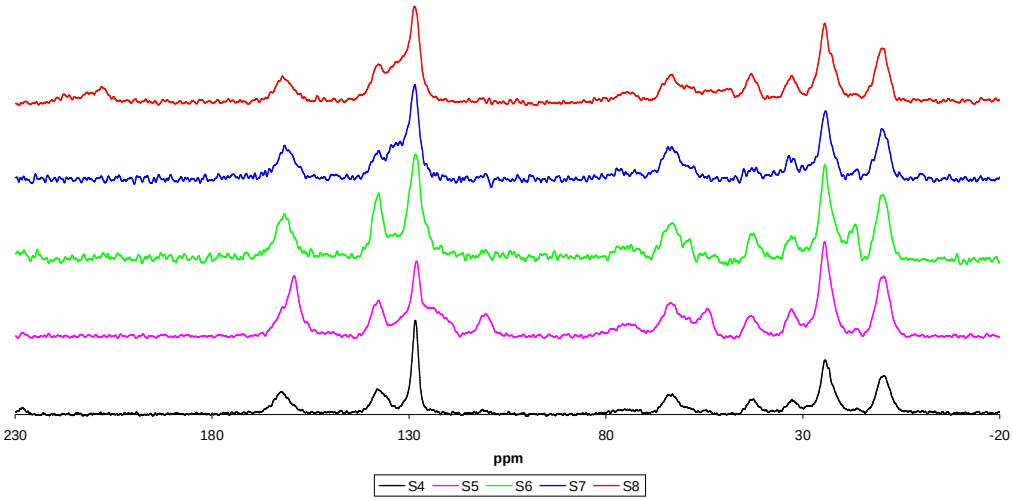

Fig. 4.2.4 $^{13}C\{^{1}H\}$ CP/MAS solid state NMR spectra of silica-supported ligands S4-S8

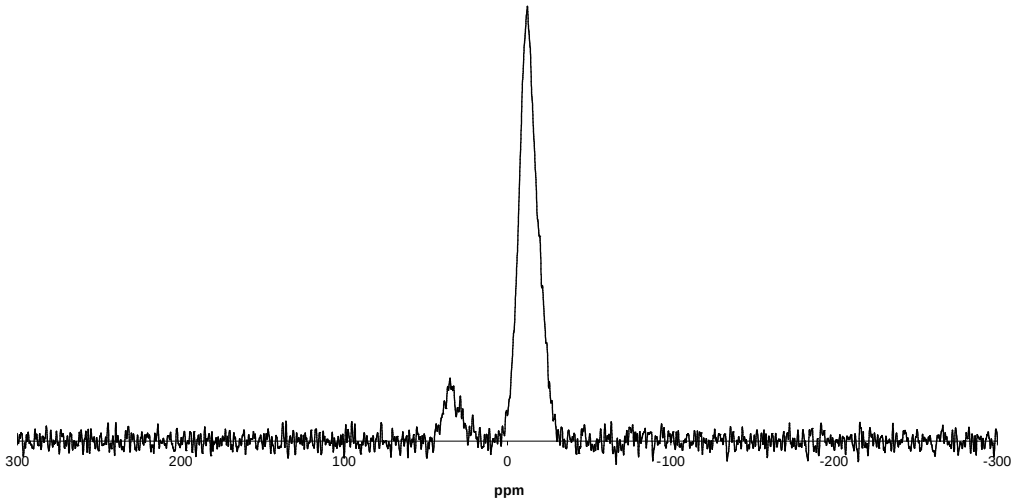

Fig. 4.2.5 $^{31}P\{^{1}H\}$ CP/MAS solid state NMR spectrum of silica-supported ligand S8

Comparing the $^{13}C\{^{1}H\}$ NMR spectra of ligands **S4-S8**, the resonances are very similar in all cases. In the spectrum of **S5** there is an extra resonance at approximately 50 ppm due to the OMe carbon, and in the spectrum of **S6** there is

an extra resonance at approximately 20 ppm due to the Me carbon of the aryl ring. The $^{31}P\{^{1}H\}$ NMR of **S8** shows a major resonance at approximately -20 ppm, and a small resonance at 50 ppm. In combination with its $^{13}C\{^{1}H\}$ NMR spectrum, the evidence suggests that this ligand has been synthesised successfully. The analogous homogeneous phosphine-containing ligand (**8a**) shows a peak at -12.4 ppm in its $^{31}P\{^{1}H\}$ NMR spectrum, which also supports the successful synthesis of **S8**.

TGA analysis of **S4-S8** can be seen in fig. 4.2.6.

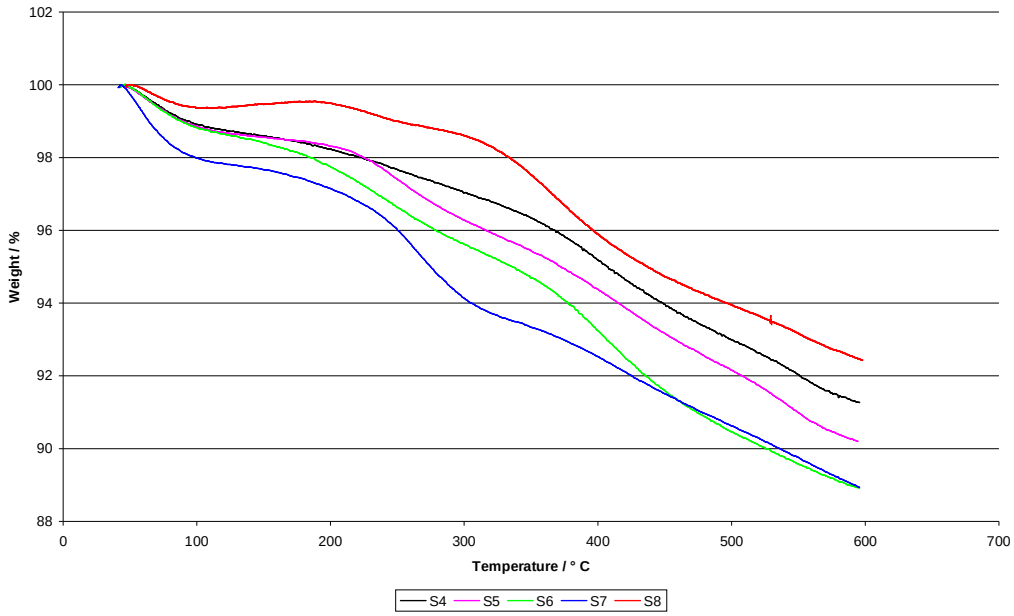

Fig. 4.2.6 TGA of silica-supported ligands S4-S8

The plots of the TGA data are very similar for each of the heterogeneous ligands **S4-S8**. This suggests that the decomposition is similar for ligands **S4-S8**, which would suggest that in terms the mass of organic material present and the structure of this material, the ligands are very similar which is to be expected. In addition to this, the percentage weight loss is approximately 8-10 %, which in conjunction with the elemental analysis of the samples is as expected.

The heterogeneous ligands described so far have encompassed (*R*,*R*)-1,2-diaminocyclohexane as a cyclic amine. In addition to this, a heterogeneous ligand based on (*S*)-(-)-2-aminomethyl-1-ethylpyrrolidine was prepared (**S9**). The corresponding reaction scheme is given in fig. 4.2.7.

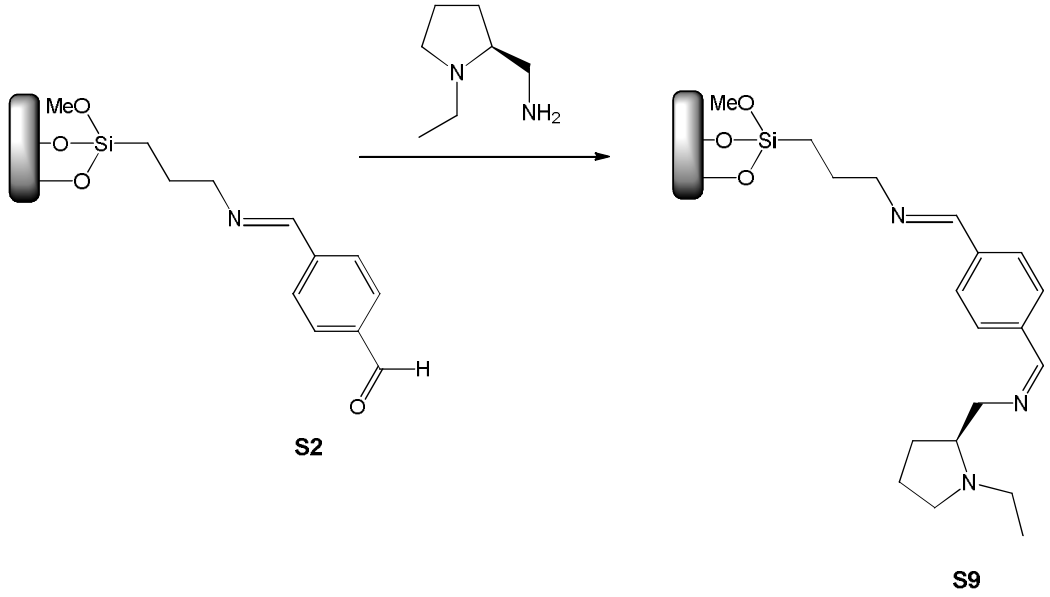

Fig. 4.2.7 Reaction scheme of the preparation of a silica-supported imine ligand (S9) containing (*S*)-(-)-2-aminomethyl-1-ethylpyrrolidine

This was characterised by $^{13}C\{^{1}H\}$ CP/MAS solid state NMR, elemental analysis and TGA. The $^{13}C\{^{1}H\}$ NMR spectrum can be seen in fig. 4.2.8. The spectrum is as expected, and most importantly there is no resonance at approximately 200 ppm, indicating that **S2** has fully reacted with the amine. Furthermore, resonances in the aliphatic region are indicative of successful grafting.

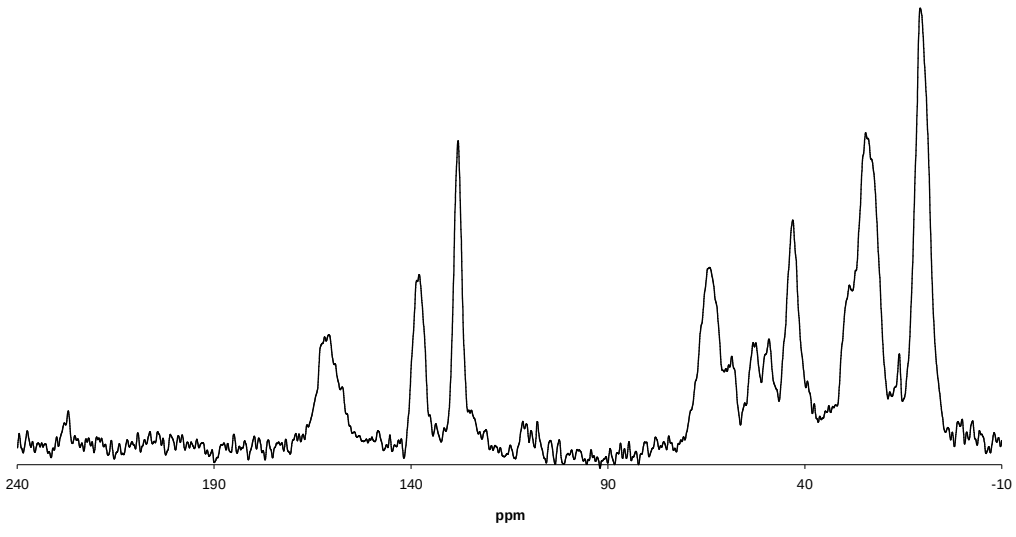

Fig. 4.2.8 $^{13}C\{^{1}H\}$ CP/MAS solid-state NMR spectrum of silica-supported ligand S9, as shown in fig. 4.2.7

The TGA data is very similar to that of **S3**, which was previously displayed in fig. 4.2.3. The two ligands are very similar, and so the decomposition of the ligand would be expected to be similar. The elemental analysis also indicates the successful preparation of **S9**.

Chapter two saw the preparation of various homogeneous ligands containing phenoxide moieties, which were later used to prepare titanium(IV) and zirconium (IV) complexes, as described in chapter three. A heterogeneous ligand containing phenoxide moieties was also prepared; this is shown in fig. 4.2.9.

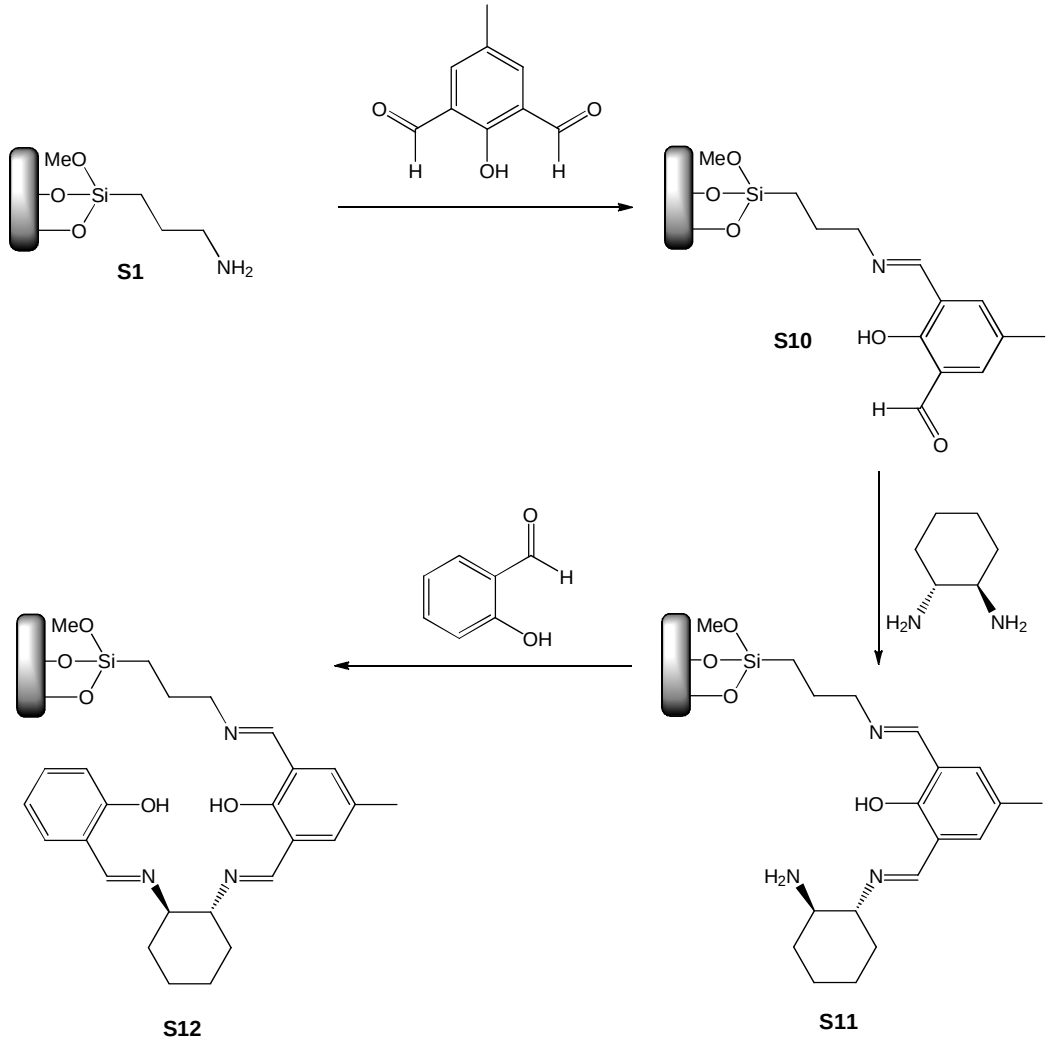

Fig. 4.2.9 Reaction scheme of the preparation of silica-supported ligands (S10-S12) containing phenoxide moieties

S10-S12 were characterised by $^{13}C\{^{1}H\}$ CP/MAS solid-state NMR, elemental analysis and TGA. The $^{13}C\{^{1}H\}$ NMR spectra can be seen in fig. 4.2.10.

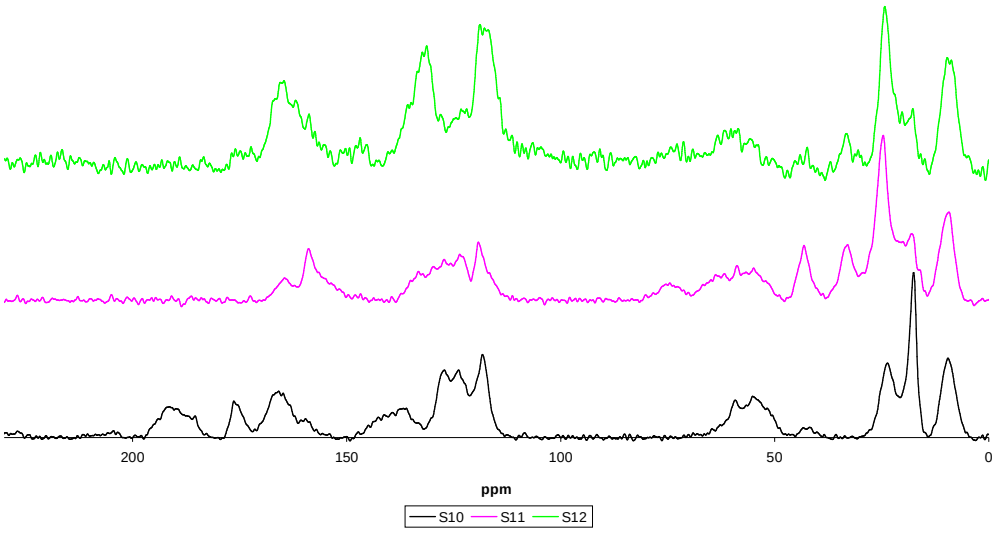

Fig. 4.2.10 $^{13}C\{^{1}H\}$ CP/MAS solid-state NMR spectra of silica-supported ligands S10-S12, as previously shown in fig. 4.2.9

The $^{13}C\{^{1}H\}$ NMR spectrum of **S10** shows resonances in the aromatic region and a resonance at approximately 190 ppm, which can be attributed to the aldehyde functionality. Comparing this to the spectrum of **S11**, the aldehyde resonance is no longer present and there are more resonances in the aliphatic region (0-80 ppm), which indicate that **S10** has reacted completely with (*R*,*R*)-1,2-diaminocyclohexane. The spectrum of **S12** shows significant changes in the aromatic region, which is expected on the addition of salicylaldehyde to **S11**. Furthermore **S10-S12** have an intense yellow colour indicative of salen formation.

The TGA analysis of **S10-S12** can be seen in fig. 4.2.11. In comparison to the other heterogeneous ligands described so far, the initial part of the TGA plots have relatively steep gradients, which is more likely to be due to residual solvent or water that may be present in small quantities. This is likely to be much more prevalent in the compounds **S10-S12**, given the presence of phenoxide groups, which through greater amounts of hydrogen bonding could retain much more solvent and water. Otherwise, the TGA data is similar to previously observed data. In conjunction with the elemental analysis of **S10-S12**, the data suggests that these compounds have been prepared successfully.

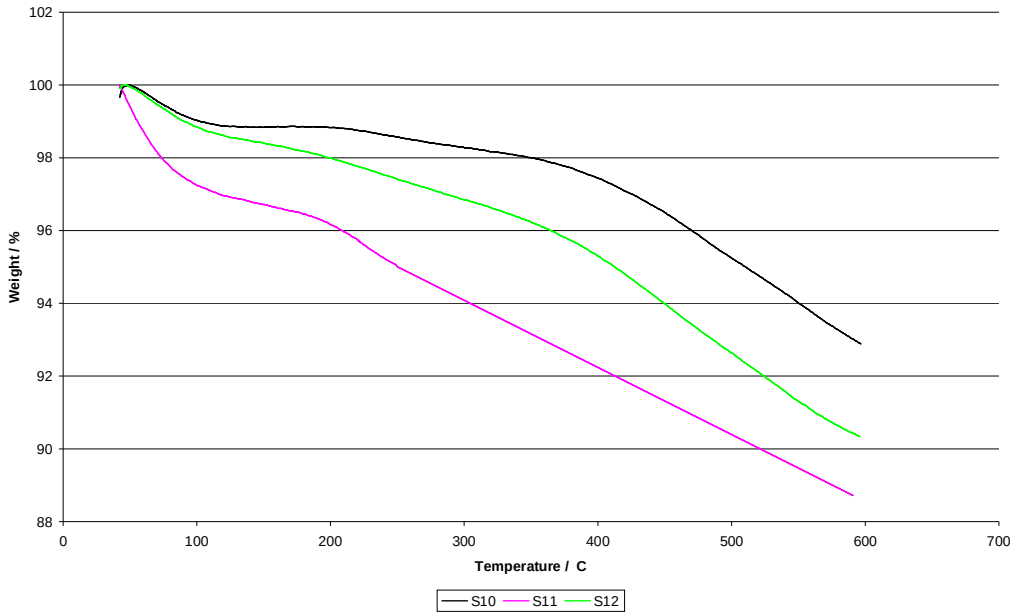

Fig. 4.2.11 TGA of silica-supported ligands S10-S12

4.3 Preparation of Heterogeneous Complexes Using Ligands Prepared Using Covalent Linkages

4.3.1 Precious Group Metal Systems

The heterogeneous complexes were prepared in the same manner as the homogeneous complexes described in chapter three. An example of a typical precious group metal heterogeneous complex is given in fig. 4.3.1. In these examples the BF_4^- salt was employed. It has been shown that the triflate salt will hydrogen bond to the surface.[15-16] Therefore, the use of such has to be avoided to ensure all iridium(I) or rhodium(I) centres are in a chiral environment; thus bound to a heterogenised ligand.

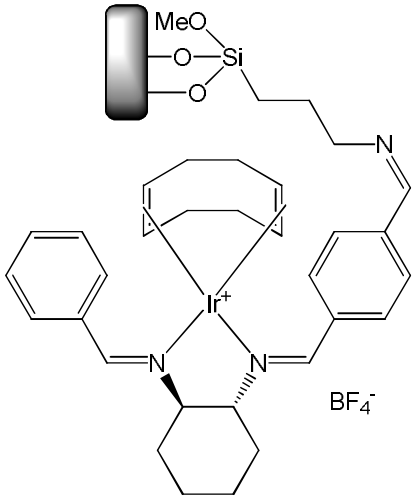

Fig. 4.3.1 A typical heterogeneous iridium(I) system. [Ir(S4)(cod)]BF_4 is displayed here

The resulting complexes were characterised by $^{13}C\{^1H\}$ (and where applicable, $^{31}P\{^1H\}$) solid state NMR, elemental analysis and TGA. Figs. 4.3.2 and 4.3.3 show the $^{13}C\{^1H\}$ and $^{31}P\{^1H\}$ solid state NMR of the iridium(I) and rhodium(I) complexes of **S8**.

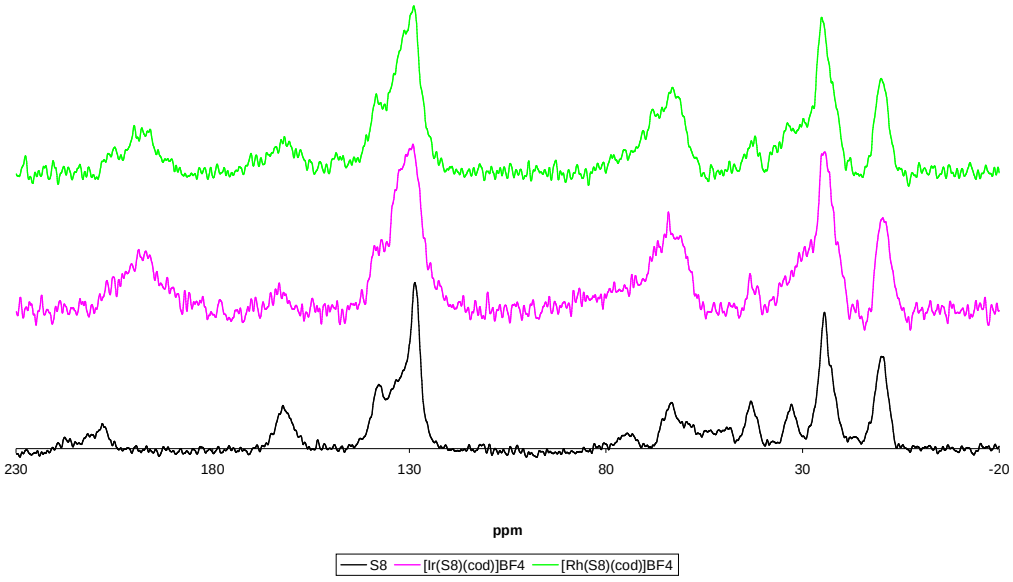

Fig. 4.3.2 $^{13}C\{^1H\}$ CP/MAS solid state NMR spectra of heterogeneous ligand S8, [Ir(S8)(cod)]BF_4 and [Rh(S8)(cod)]BF_4

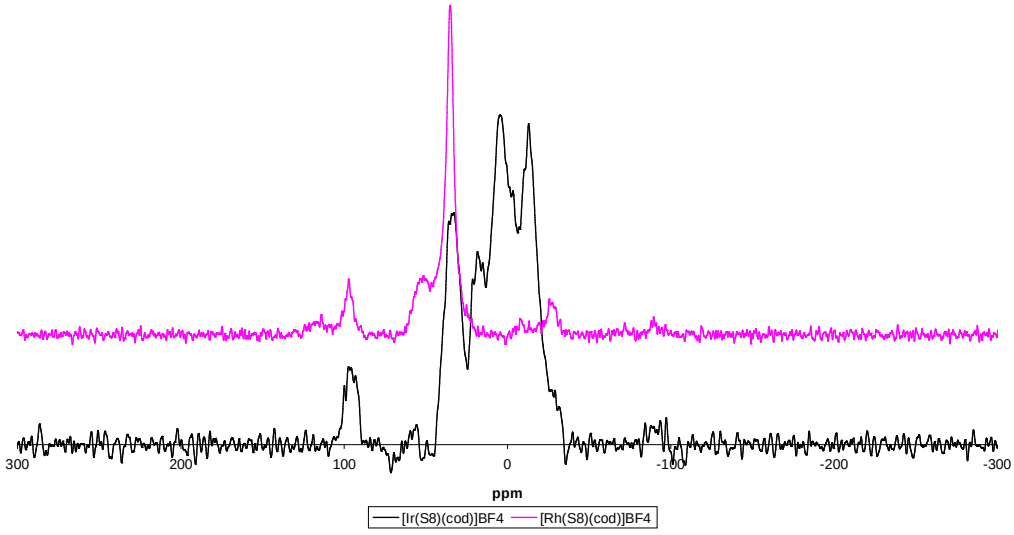

Fig. 4.3.3 $^{31}P\{^{1}H\}$ CP/MAS solid-state NMR of heterogeneous complexes [Ir(S8)(cod)]BF_4 and [Rh(S8)(cod)]BF_4

Fig. 4.3.2 shows broadening of all of the resonances. This is due to a combination of the presence of a heavy metal, and the presence of the cod ligand which would give rise to extra resonances, which may overlap with the existing peaks due to **S8**. Similar behaviour was observed in the analogous homogeneous complexes described in chapter three, as previously discussed. Also, when the metal is complexed to the ligand there will be less mobility in the system. Due to this, resonances in the solid-state tend to be broader. The lack of mobility also gives rise to more intense spinning side bands. The $^{31}P\{^{1}H\}$ spectra shown in fig. 4.3.3 supports the complexing of a metal also. The major phosphine resonance shifts significantly on addition of the metal, indicating a change in the phosphorous atom that affects its electron density. The metal complexing to the ligand would bring about this change. This behaviour is also observed in the analogous homogeneous complexes described in chapter three (for the free ligand, a resonance is observed at -12.4 ppm, in the Ir(I) complex, at 21.2 ppm and in the Rh(I) complex at 45.9 ppm).

These complexes were also analysed by TGA; the results are shown in fig. 4.3.4. The plots are very similar, which indicates the structurally these complexes are also similar. As predicted, the percent weight loss is greater in the cases of the

iridium and rhodium complexes in comparison with the ligand. This is due to the cod ligands present, providing extra organic material for combustion.

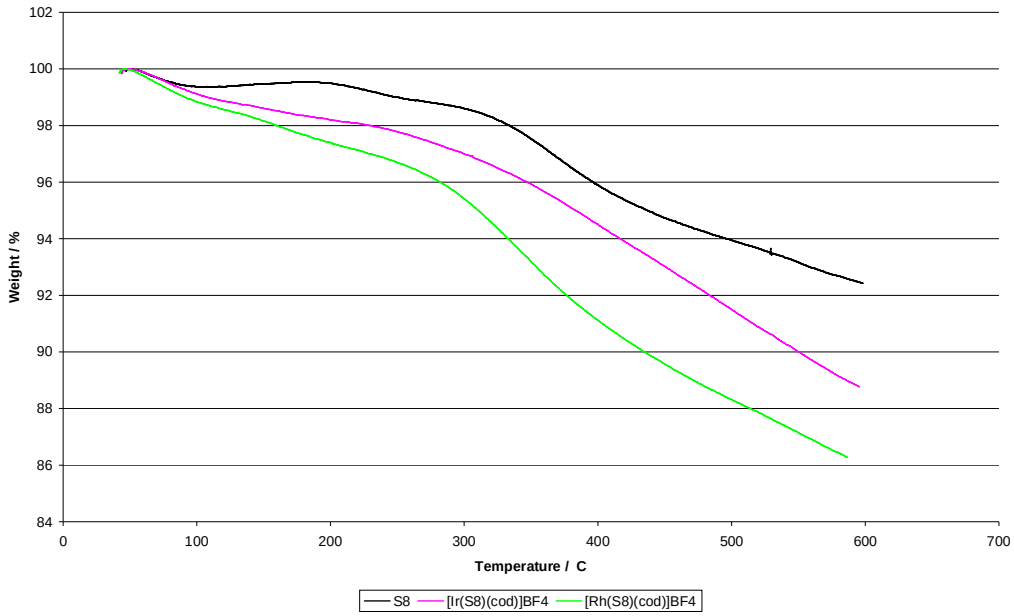

Fig. 4.3.4 TGA of heterogeneous ligand S8, and its complexes [Ir(S8)(cod)]BF_4 and [Rh(S8)(cod)]BF_4

[Ir(**S6**)(cod)]BF_4, [Rh(**S4**)(cod)]BF_4 and [Rh(**S7**)(cod)]BF_4 were also prepared. The differences between the NMR spectra of these complexes and ligands are the same as has been discussed here with respect to the complexes of **S8**. The TGA analysis of these complexes is also very similar to what has been discussed here. This indicates that structurally, the complexes are similar.

4.3.2 Copper(II) Systems

The heterogeneous complexes were prepared in the same manner as the homogeneous complexes described in chapter three. An example of a typical copper(II) heterogeneous complex is given in fig. 4.3.5.

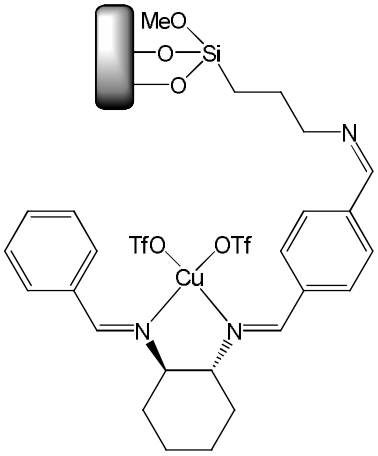

Fig. 4.3.5 A typical silica-supported copper(II) complex. Cu(S4)(OTf)$_2$ is shown here

Copper(II) is paramagnetic, therefore characterisation of these complexes by NMR was not appropriate. The complexes were characterised by TGA and elemental analysis. In addition to this, the heterogeneous complexes were either blue or green in colour, which is an indication of the presence of copper(II) metal. The solid-supported systems were washed with copious amounts of methanol to ensure the full removal of any unbound copper(II).

The TGA data of the complexes is shown in fig. 4.3.6. The plots are very similar, which indicate that structurally, the complexes are very similar. The plots are also similar in terms of % weight loss to the rhodium(I) complexes.

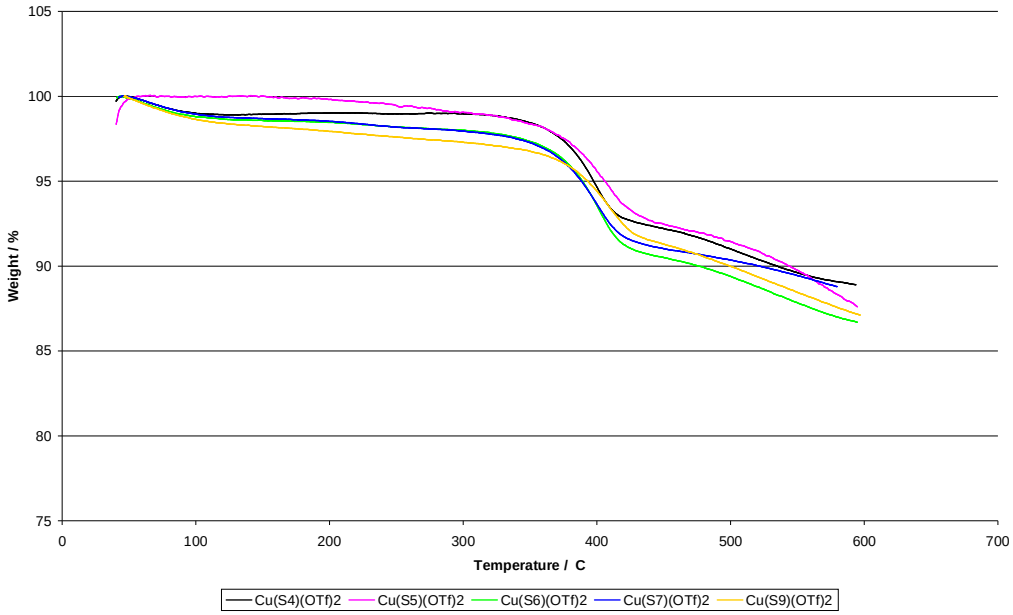

Fig. 4.3.6 TGA of the copper(II) complexes of silica-supported ligands S4-S8

Cu(**S5**)$(OTf)_2$ and Cu(**S6**)$(OTf)_2$ were also characterised by EPR spectroscopy. Both complexes had the same parameters of g⊥ = 2.05, g|| = 2.25 and A⊥ = 23.0 × 10^{-4} cm^{-1}, A|| = 191.2 × 10^{-4} cm^{-1}. These values are in agreement with the homogeneous copper(II) complexes previously described in chapter three, which were in agreement with literature precedent.[17-18]

4.3.3 Group(IV) Metal Systems

The heterogeneous complexes were prepared in the same manner as the homogeneous complexes described in chapter three. An example of a typical group (IV) metal heterogeneous complex is given in fig. 4.3.7.

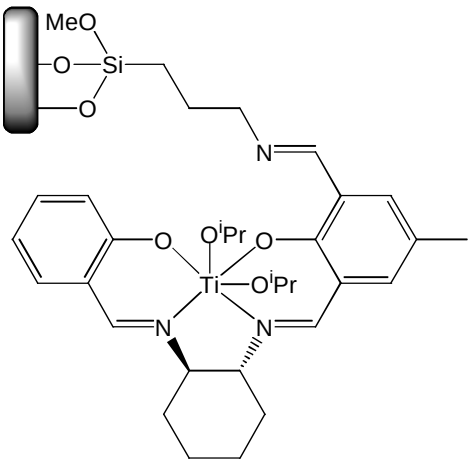

Fig. 4.3.7 A typical silica-supported group(IV) complex. Ti(S12)$(O^iPr)_2$ is shown here

The resulting complexes were characterised by $^{13}C\{^1H\}$ solid state NMR, elemental analysis and TGA. Fig. 4.3.8. shows the $^{13}C\{^1H\}$ solid state NMR spectra of Ti(**S12**)$(O^iPr)_2$, Zr(**S12**)$(O^iPr)_2$ and **S12**.

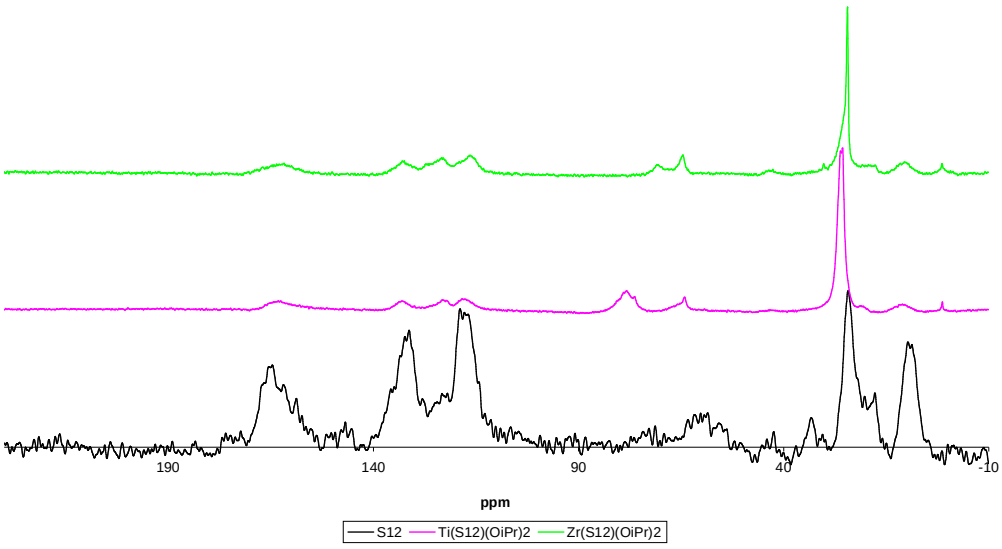

Fig. 4.3.8 $^{13}C\{^{1}H\}$ CP/MAS solid-state NMR spectra of heterogeneous ligand S12, and its group(IV) complexes Ti(S12)($O^{i}Pr$)$_2$ and Zr(S12)($O^{i}Pr$)$_2$

The spectra show significant differences between the complexes and the ligand, indicating that a reaction has occurred, with a significant resonance at 25 ppm for the CH_3 group of the isoproxide. In conjunction with elemental analysis and TGA, the characterisation suggests that the formation of these group(IV) metal complexes has been successful.

4.4 Preparation of Silica-Supported Ligands Using the "Tether Group" Technique

In parallel to the methodology detailed in section 4.2, a technique that has been used by many research groups is to prepare the ligand "outside" of the support, and then attach it.[19-22] The technique involves functionalising the support, and then introducing an appropriate functional group in the ligand or complex, that subsequently will react cleanly in one step with the functionalised support. In this research, silica was functionalised with amine groups, and the chiral ligands synthesised to contain a methylchloro group, which will be discussed in more detail.

The introduction of the tether group on the ligand prior to heterogenising involved synthesising non-symmetrical ligands. Previously, Nguyen has reported the use of hydrochloric acid in protecting (*R*,*R*)-1,2-diaminocyclohexane to achieve this.[23] This method is employed herein. The reaction schemes can be seen in fig. 4.4.1.

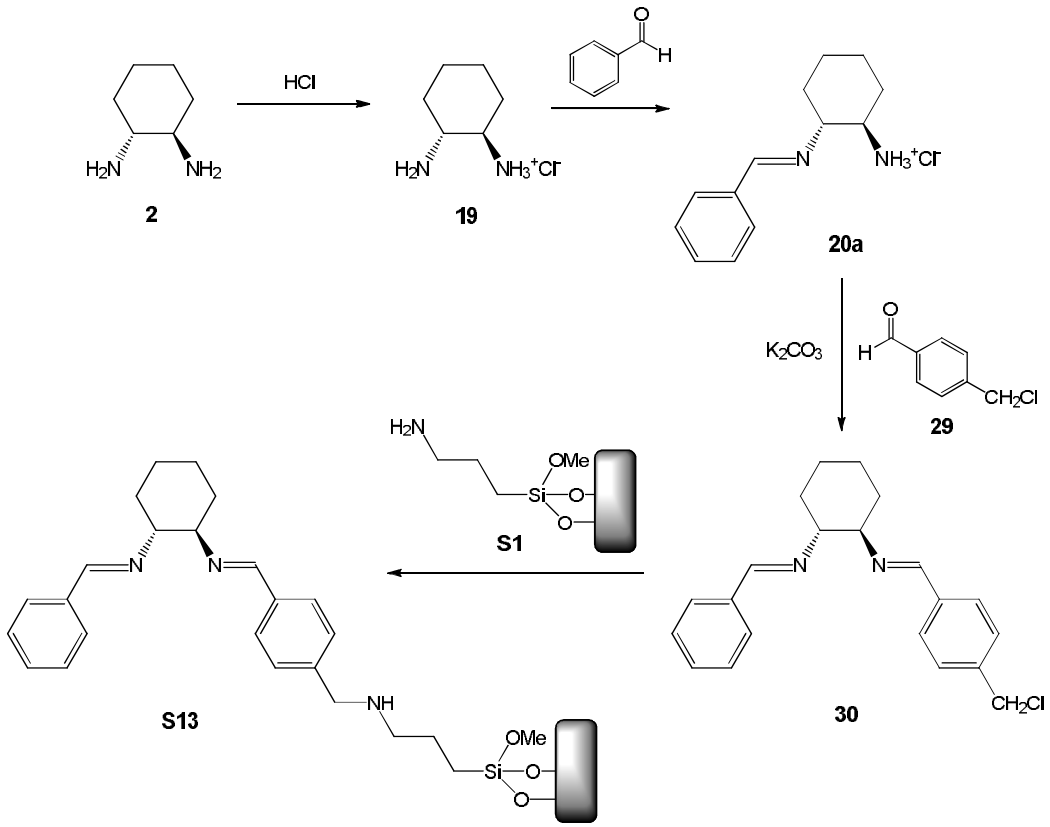

Fig. 4.4.1 Reaction scheme of the preparation of silica-supported ligands prepared using the "tether group" technique

The synthesis of the non-symmetrical ligand was achieved in good yield up to **20a**. However, the addition of 4-methylchlorobenzaldehyde in the presence of potassium carbonate saw a substantial reduction in the reaction ligand (51 % was the highest yield achieved for the reaction of **20a** to **30**). The major problem was imine "scrambling" of the aryl groups of each imine and in the mass spectrometry, peaks for the unsymmetrical imine and both homosymmetrical imines were observed. Although, the major peak was for the unsymmetrical imine. On changing the base from potassium carbonate to triethylamine, the purity was not improved.

This ligand was tethered to *n*-propylamine functionalised silica, as can be seen in fig. 4.4.1. **S13** was characterised by solid-state NMR spectroscopy, elemental analysis and TGA. This data will be discussed in conjunction with its resulting heterogeneous complexes in section 4.5.

4.5 Preparation of Heterogeneous Complexes Using Ligands Prepared Using the "Tether Group" Technique

[Rh(**S13**)(cod)]BF_4 and Cu(**S13**)$(OTf)_2$ were prepared using the synthetic methods previously described. Elemental analysis and TGA were used to characterise the complexes. $^{13}C\{^1H\}$ NMR spectroscopy was also used to characterise [Rh(**S13**)(cod)]BF_4; the spectrum can be seen in fig. 4.5.1. As expected, **S13** is qualitatively comparable to **S4** (shown in fig. 4.2.4).

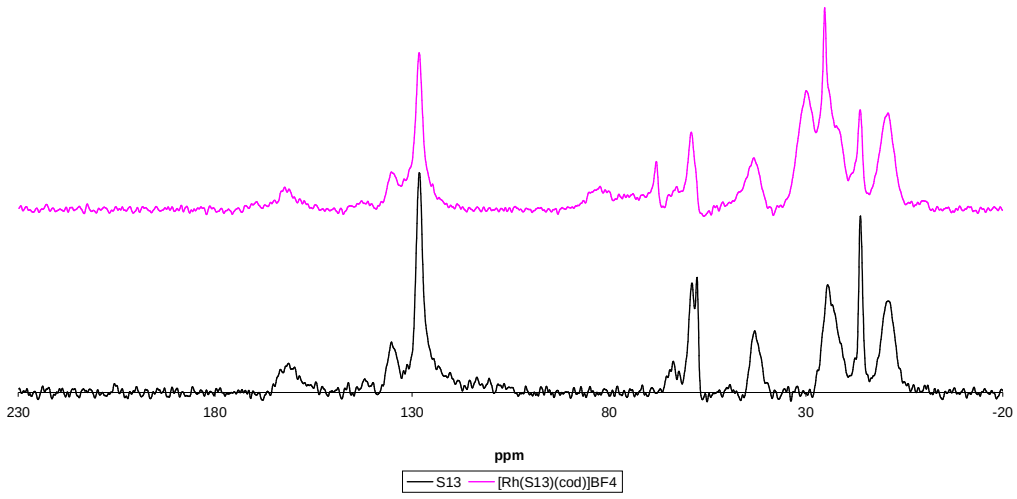

Fig. 4.5.1 $^{13}C\{^1H\}$ CP/MAS solid-state NMR spectra of heterogeneous ligand S13, and its rhodium(I) complex [Rh(S13)(cod)]BF_4

Comparing the rhodium complex with its ligand, the spectra are very similar. The extra resonances in the spectrum of the rhodium complex are due to the presence of cod, and this is analogous to that obtained for [Rh(**S4**)(cod)]BF_4.

TGA of **S13** was also performed; the results can be seen in fig. 4.5.2. The plots corresponding to **S13** and its rhodium complex are very similar, with a greater weight loss observed in the rhodium complex, which is expected due to the cod ligand. The plot corresponding to the copper(II) complex is very different, indicating that the decomposition behaviour of the copper(II) complex is very different. However, on comparing this complex to other heterogeneous copper(II) complexes described in this chapter, the shape of the plots are very similar, indicating that it is the presence of copper(II) that encourages this decomposition behaviour rather than the ligand. In addition, the sharp decrease is always seen at approximately the same temperature of 400 °C. One possible reason for this is the formation of copper oxide at this temperature, which could be catalysing the rapid decomposition of the organic material present.

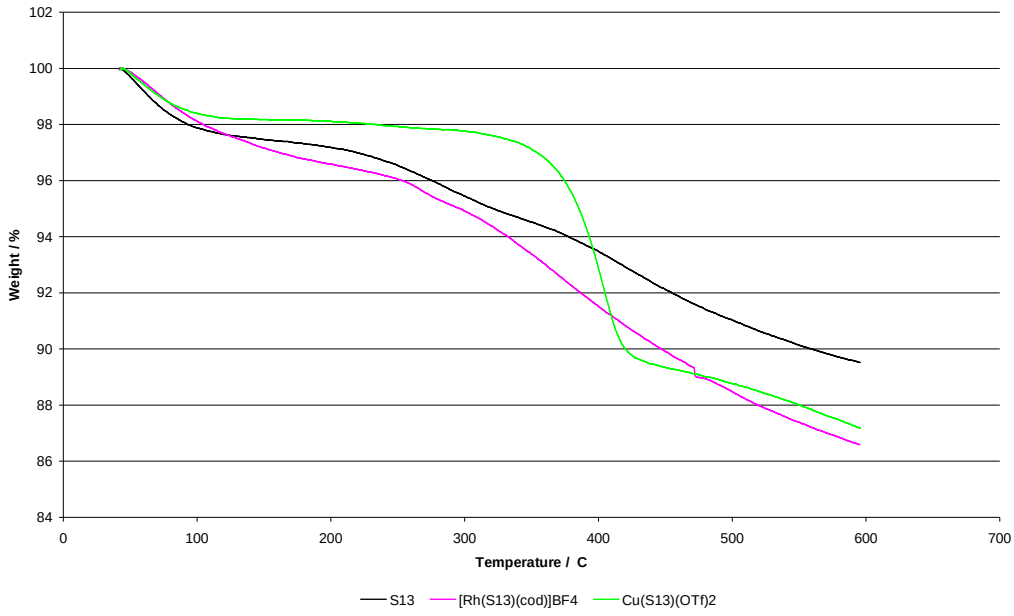

Fig. 4.5.2 TGA of heterogeneous ligand S13, and its complexes [Rh(S13)(cod)]BF_4 and Cu(S13)$(OTf)_2$

4.6 Preparation of Silsesquioxane-Supported Complexes

A number of silsesquioxane-supported complexes have been prepared, for comparative purposes as model compounds.[25-27] As previously discussed, silsesquioxanes are useful as they simulate a ligand or complex being supported by a silica-based material, whilst still being soluble in many solvents, making analysis and characterisation of these materials much simpler.

The preparation of the silsesquioxane-supported ligands can be seen in fig. 4.7.1. As with the silica-supported ligands, the covalent linkages synthetic methodology was employed; this was the best method with respect to these particular ligands, as previously discussed.

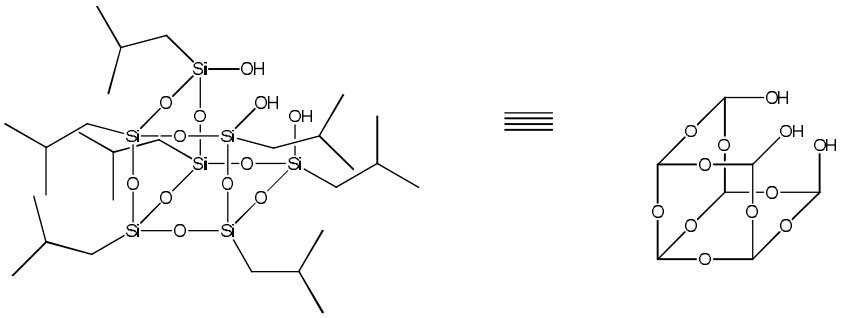

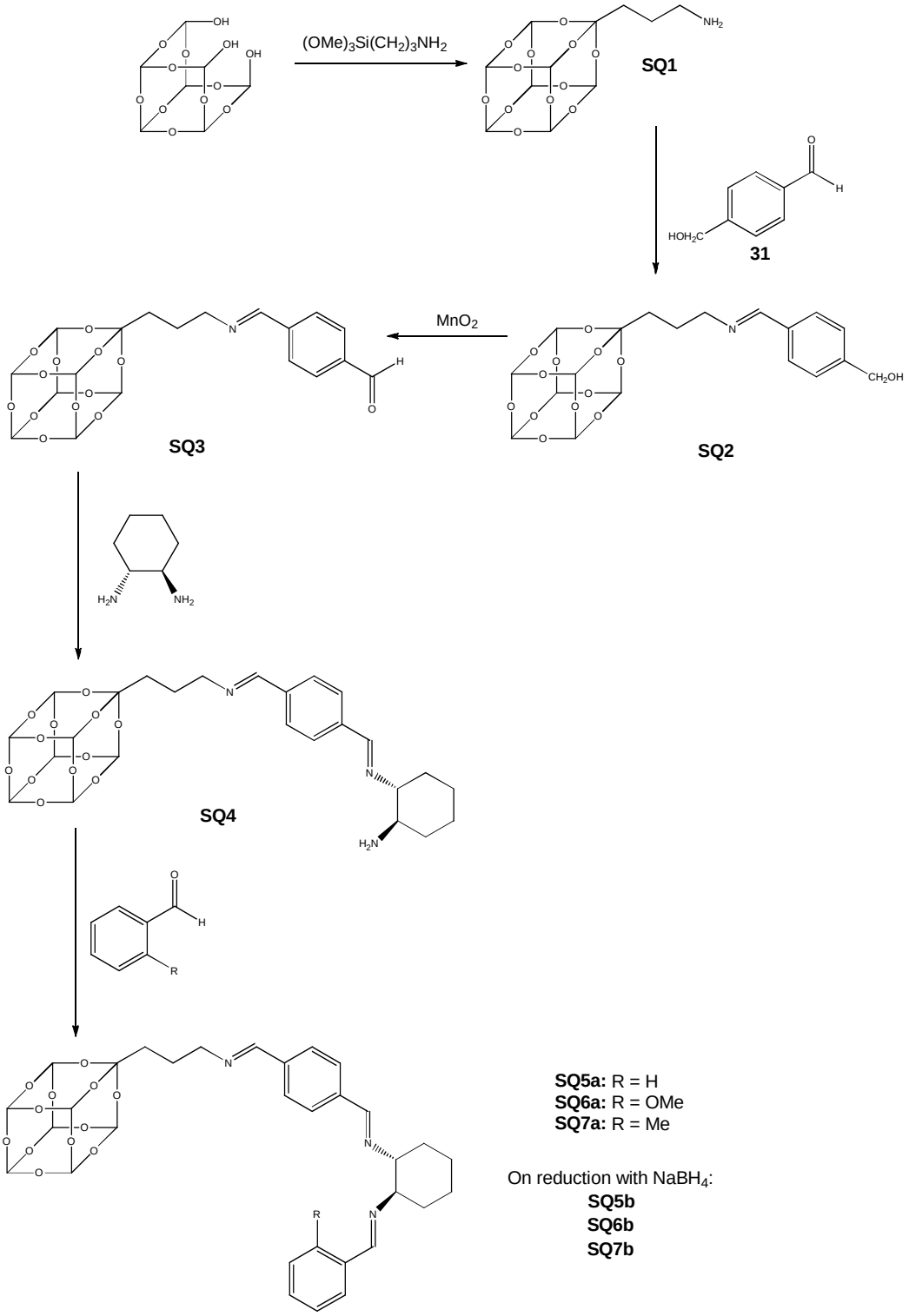

Fig. 4.7.1 Reaction scheme of the preparation of silsesquioxane-supported imine ligands

The ligands **SQ1-SQ7** were characterised by multinuclear NMR spectroscopy. At first glance, the NMR spectra indicated the successful preparation of these ligands, with resonances in the spectra of **SQ5** and **SQ6** that indicated the presence of methoxy and methyl groups respectively. However, on examining

the integrals in the spectra of **SQ4-SQ7**, there were some small discrepancies in the aliphatic region concerning the cyclohexane protons. The integrals were not consistent. This may be due to dimerisation of the ligand on reaction from **SQ3** to **SQ4**, producing the by-product shown in fig. 4.7.2.

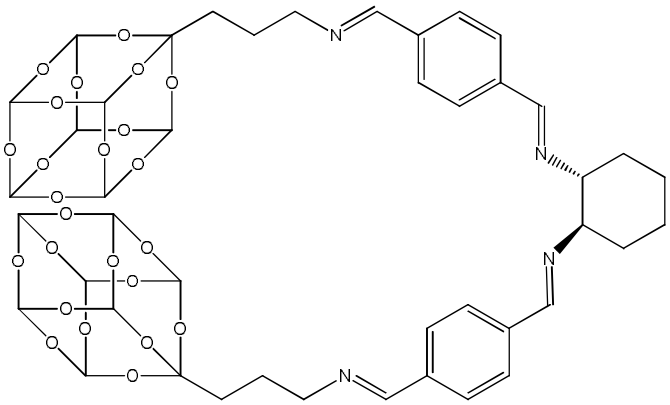

Fig. 4.7.2 Silsesquioxane-supported dimerised ligand

Separation of the two products proved non-trivial. In addition, the dimer is so similar in structure to the desired ligand that the resonance in the NMR due to the dimer and the desired ligand overlap substantially, so quantifying the proportion of dimer proved troublesome. Therefore, silsesquioxane-supported ligands were prepared using a "tether group" methodology, as previously discussed. The reaction scheme for this can be seen in fig. 4.7.3.

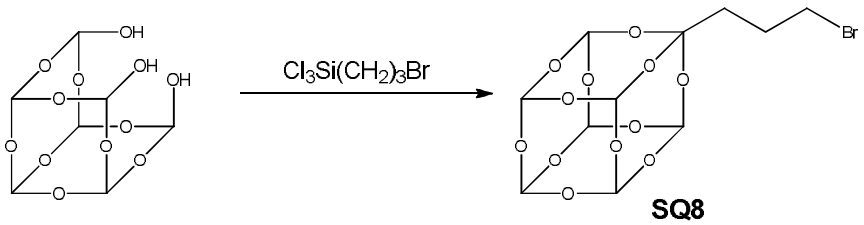

SQ8

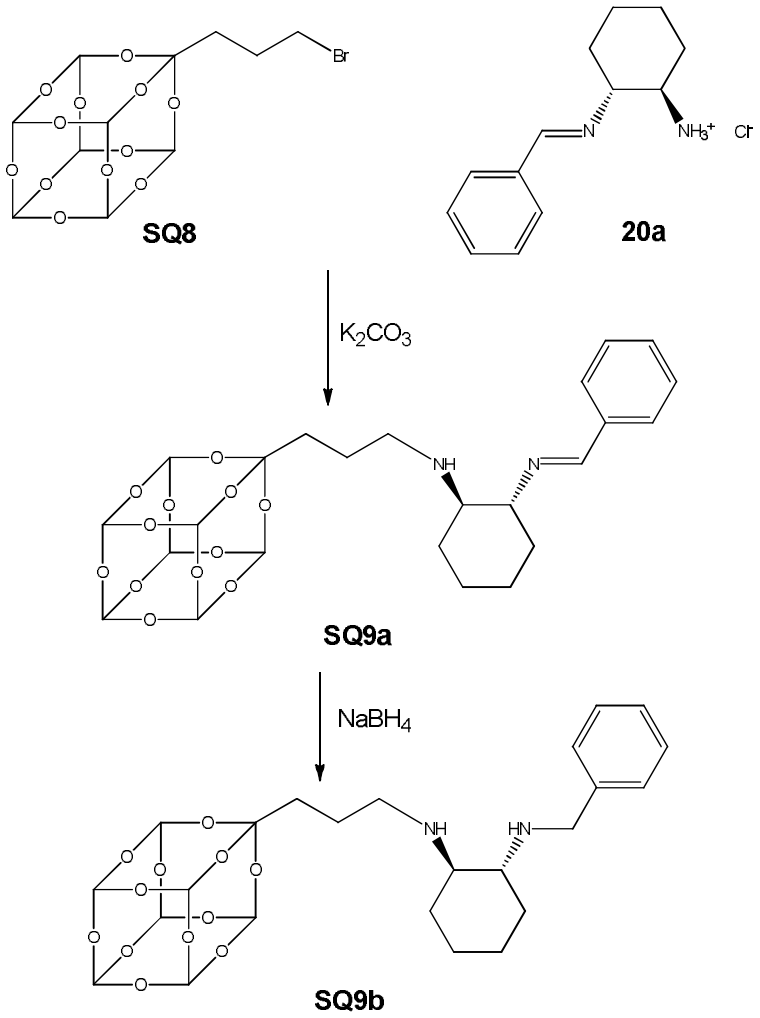

Fig. 4.7.3 Reaction scheme of the preparation of silsesquioxane-supported ligands using the "tether group" technique

These ligands were characterised by multinuclear NMR spectroscopy. In the ^{1}H NMR spectra, the integrations were as expected. **SQ8** was also characterised by mass spectrometry, which showed that this ligand had been successfully prepared. In addition to this, the solid state NMR of the analogous silica-supported **S13** is similar to the $^{13}C\{^{1}H\}$ NMR of **SQ9a**.

Rhodium(I) and copper(II) complexes ([Rh(**SQ9b**)(cod)]BF_4 and Cu(**SQ9b**)$(OTf)_2$ respectively) were prepared. [Rh(**SQ9b**)(cod)]BF_4 was characterised by multinuclear NMR, which showed extra resonances corresponding to the cod ligand, and suggested that the complex had been successfully prepared. NMR spectroscopy was unsuitable for the characterisation of Cu(**SQ9b**)$(OTf)_2$, hence this complex was characterised by

mass spectrometry. The complex was detected in the mass spectrum, which not only indicated a successful complex preparation, but also suggests that the ligand **SQ9b** has been successfully synthesised.

4.7 Concluding Remarks

In conclusion, a number of heterogeneous silica-supported complexes have been prepared. The resulting iridium(I), rhodium(I), copper(II), titanium(IV) and zirconium(IV) complexes have all been successfully characterised, and are ready to be utilised to catalyse a multitude of reactions. Having said this, the subsequent heterogeneous catalysis discussed in chapter five is provided to highlight potential applications of these heterogeneous complexes, and should be looked upon from this point of view, rather than definitive catalytic results. Further characterisation of the heterogeneous complexes would be required to be able to discuss the catalytic results in depth, for example surface area and pore diameter measurements would be essential.

Two different synthetic methods to prepare these heterogeneous complexes have been employed and discussed. In addition, some silsesquioxane-supported complexes have been prepared as model compounds and discussed.

4.8 References

(1) Raytchev, P. D., Bendjeriou, A., Dutasta, J. P., Martinez, A., Dufand,V. *Adv. Synth. Catal.* **2011**, *353*, 2067.

(2) Dimroth, J., Keilitz, J., Schedler, U., Schomacker, R., Haag, R. *Adv. Synth. Catal.* **2010**, *352*, 2497.

(3) de la Torre, M. D. L., Guijarro, M. *Eur. J. Org. Chem.* **2010**, 5147.

(4) Chen, X. Z., Luo, H., Qian, C., He, C. H. *Reaction Kinetics Mechanisms and Catalysis* **2011**, *104*, 163.

(5) Huang, T., Huang, W., Huang, J., Ji, P. *Fuel Processing Technology* **2011**, *92*, 1868.

(6) Sanchez, M. A., Mazzieri, V. A., Grau, J. M., Yori, J. C., Pieck, C. L. *Journal of Chemical Technology and Biotechnology* **2011**, *86*, 1198.

(7) Corma, A., Fuerte, A., Iglesias, M., Sanchez, F. *Journal of Molecular Catalysis A: Chemical* **1996**, *107*, 225.

(8) Sarkar, B. R., Mukhopadhyay, K., Chaudhari, R. V., *Catalysis Communications* **2007**, *8*, 1386.

(9) Huang, L., Kawi, S. *Journal of Molecular Catalysis A: Chemical* **2004**, *211*, 23.

(10) Gao, H. R., Angelici, R. J. *Journal of Molecular Catalysis A: Chemical* **1999**, *149*, 63.

(11) Kresge, C. T., Leonowicz, M. E., Roth, W. J., Vartuli, J. C., Beck, J. S. *Nature* **1992**, *359*, 710.

(12) Rao, Y. V. S., DeVos, D. E., Bein, T., Jacobs, P. A. *Chem. Commun.* **1997**, 355.

(13) Maschmeyer, T., Oldroyd, R. D., Sankar, G., Thomas, J. M., Shannon, I. J., Klepetko, J. A., Masters, A. F., Beattie, J. K., Catlow, C. R. A. *Angew. Chem.-Int. Edit.* **1997**, *36*, 1639.

(14) Bleloch, A., Johnson, B. F. G., Ley, S. V., Price, A. J., Shephard, D. S., Thomas, A. W. *Chem. Commun.* **1999**, 1907.

(15) Bianchini, C., Dal Santo, V., Meli, A., Oberhauser, W., Psaro, R., Vizza, F. *Organometallics* **2000**, *19*, 2433.

(16) Bianchini, C., Dal Santo, V., Meli, A., Moneti, S., Moreno, M., Oberhauser, W., Psaro, R., Sordelli, L., Vizza, F. *J. Catal.* **2003**, *213*, 47.

(17) Becker, M.; Heinemann, F. W.; Knoch, F.; Donaubauer, W.; Liehr, G.; Schindler, S.; Golub, G.; Cohen, H.; Meyerstein, D. *European Journal of Inorganic Chemistry* **2000**, 719.

(18) Abry, S.; Thibon, A.; Albela, B.; Delichere, P.; Banse, F.; Bonneviot, L. *New J. Chem.* **2009**, *33*, 484.

(19) Anand, N.; Reddy, K. H. P.; Swapna, V.; Rao, K. S. R.; Burri, D. R. *Microporous Mesoporous Mat.* **2011**, *143*, 132.

(20) Lemus-Yegres, L. J.; Perez-Cadenas, M.; Roman-Martinez, M. C.; de Lecea, C. S. M. *Microporous Mesoporous Mat.* **2011**, *139*, 164.

(21) Chrisey, L. A.; Lee, G. U.; Oferrall, C. E. *Nucleic Acids Res.* **1996**, *24*, 3031.

(22) Miao, S. J.; Shanks, B. H. *J. Catal.* **2011**, *279*, 136.

(23) Campbell, E. J.; Nguyen, S. T. *Tetrahedron Lett.* **2001**, *42*, 1221.

(24) Caplan, N. A., Hancock, F. E., Page, P. C. B., Hutchings, G. J. *Angew. Chem.-Int. Edit.* **2004**, *43*, 1685.

(25) Lorenz, V., Edelmann, A., Giessmann, S., Hrib, C. G., Blaurock, S., Edelmann, F. T. *Zeitschrift Fur Anorganische Und Allgemeine Chemie* **2010**, *636*, 2172.

(26) Quadrelli, E. A.; Basset, J. M. *Coord. Chem. Rev.* **2010**, *254*, 707.

(27) Feher, F. J.; Newman, D. A.; Walzer, J. F. *J. Am. Chem. Soc.* **1989**, *111*, 1741.

Catalytic Screening of Various Asymmetric Organic Transformations

5.1 Introduction

This chapter will discuss the application of these complexes in a number of asymmetric organic transformations, many of which were introduced in chapter one. Chapters three and four detailed the preparation of a number homogeneous and heterogeneous complexes, respectively. The homogeneous complexes were extensively characterised, and their structural properties discussed at length. The heterogeneous complexes were characterised to ensure to the ligand had bound to the support, and that the metal had bound to the heterogenised ligand. However, further characterisation would be required to develop a deeper structural knowledge of these heterogeneous catalysts, for example determining the surface are and pore diameter. Hence the discussion of the heterogeneous catalysis in this chapter must be viewed with a degree of speculation, and is given to highlight the potential catalytic applications of the heterogeneous complexes.

5.2 Catalysing the Asymmetric Hydrogenation Reaction

The hydrogenation reaction is crucial within organic synthesis, and has been discussed in chapter one.[1-11] There are two types of hydrogenation; direct and transfer. Direct hydrogenation utilises H_2 gas as a source of hydrogen, whereas transfer hydrogenation utilises hydrogen from a source other than H_2, often a secondary alcohol. Transfer hydrogenation is often seen as the more attractive option, given that it eliminates the use of explosive hydrogen gas.[12] However, heterogeneous catalysts for transfer hydrogenation reactions are uncommon,[12] leaving a niche in this area of research. Precious metal complexes are often used as catalysts in the hydrogenation of ketones and alkenes. Rhodium(I), iridium(I), platinum(II), palladium(II) and some ruthenium(II) catalysts have previously been utilised for this purpose.[9,12-17] A selection of precious metal homogeneous

and heterogeneous catalysts described in chapters three and four respectively were used to catalyse the asymmetric hydrogenation of ketones. Direct and transfer hydrogenation methods were employed. The results of this catalysis will be discussed shortly. However, prior to this, the mechanisms of direct and transfer hydrogenation will be examined, in order to gain more insight into the results reported herein.

The mechanism for the direct hydrogenation of ketones is given in fig. 5.2.1.[18] First, H_2 oxidatively adds to the Rh(I) species generating a hydride complex, which is now Rh(III). This is followed by coordination of the ketone, and migratory insertion of a hydride into the C=O bond. The final step is reductive elimination, generating the alcohol and the catalytically active starting material.

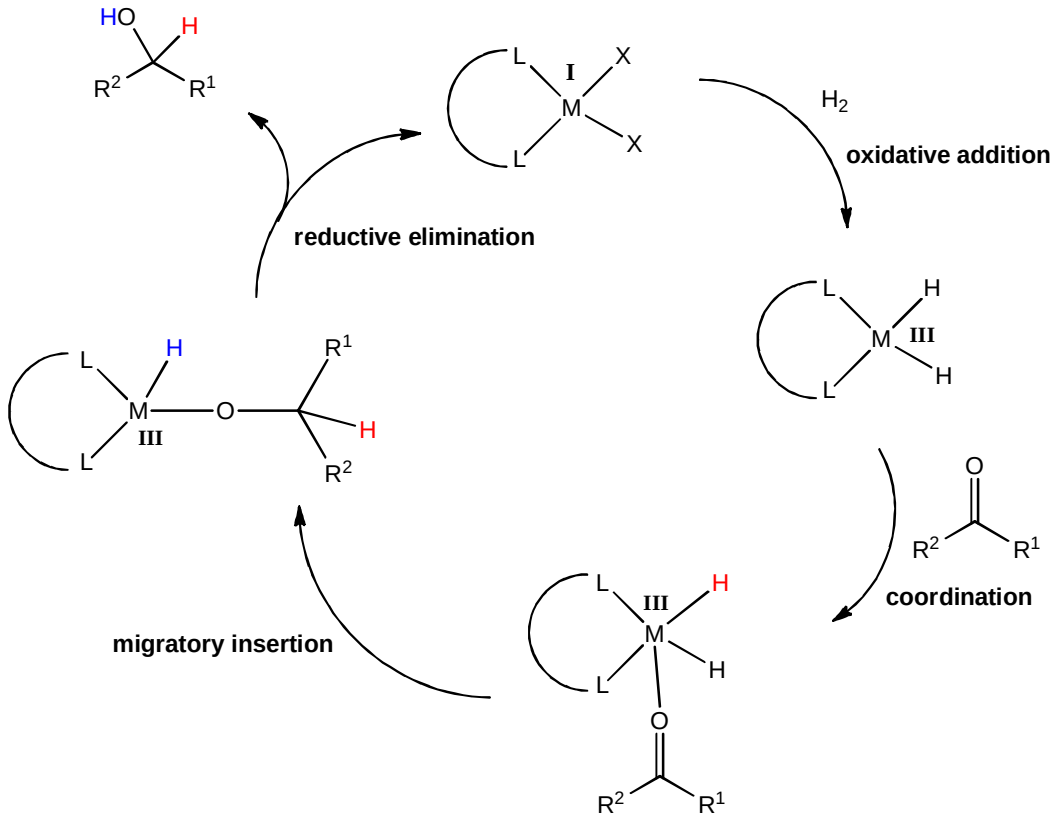

Fig. 5.2.1 Catalytic mechanism for the direct hydrogenation of ketones using a Rh(I) system. X corresponds to a solvent molecule

The mechanism for the transfer hydrogenation of ketones is slightly different. It is represented pictorially in fig. 5.2.2.[18] The ketone coordinates, and the first

hydride addition occurs as described in the direct hydrogenation mechanism. However, the second H moiety is provided by isopropanol. Following the first hydride migration, the catalyst is coordinatively unsaturated. At this point the isopropanol coordinates. A hydride species yielded by isopropanol hydrogenates the ketone which then leaves, and the isopropanol remains coordinated to the metal centre. A second hydride species migrates from the isopropanol to the metal centre. Acetone is generated which leaves, regenerating the coordinatively unsaturated metal hydride complex, ready for the next catalytic cycle.

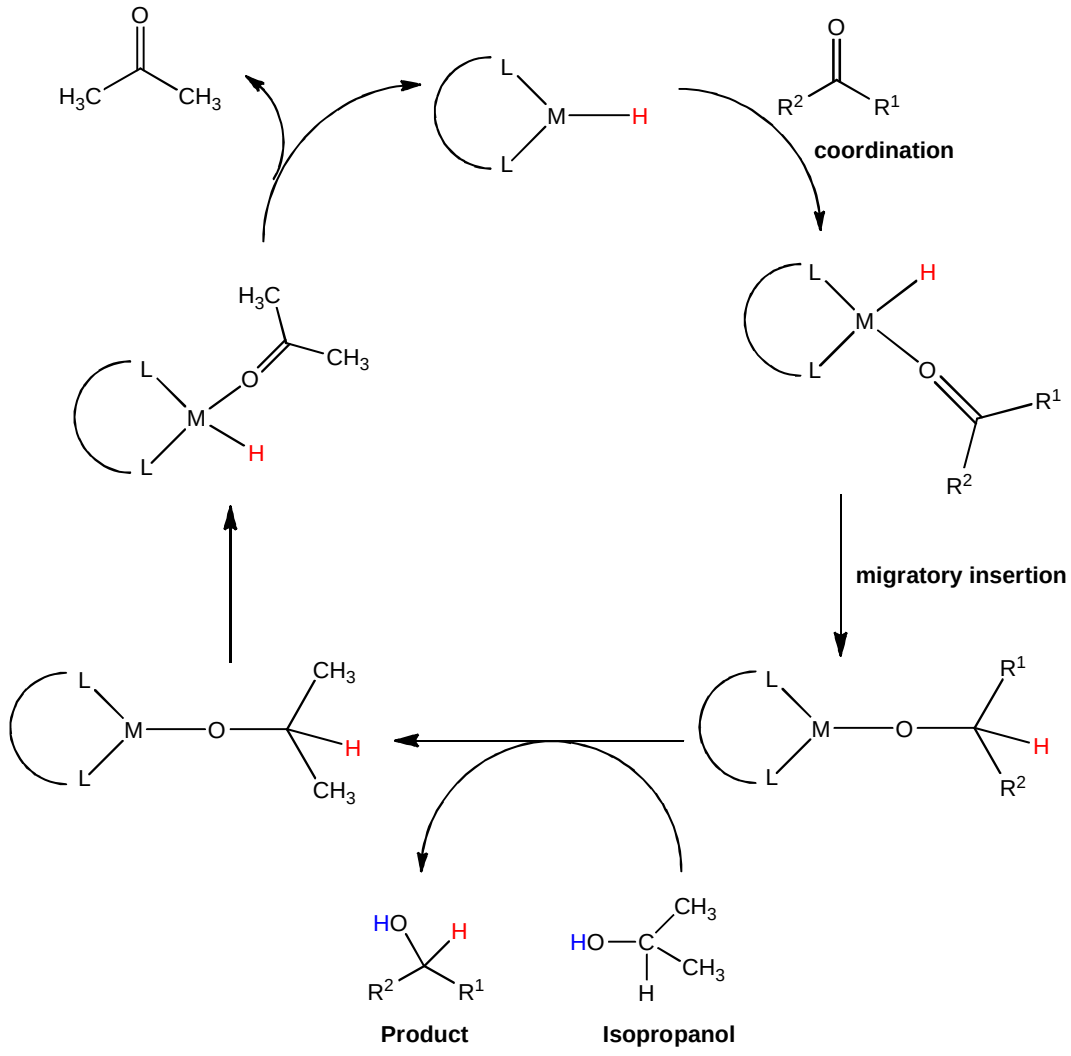

Fig. 5.2.2 Generic catalytic mechanism of transfer hydrogenation of ketones

5.2.1 Homogeneous Catalysis

A number of the precious metal complexes described in chapter three were used to catalyse the asymmetric hydrogenation of ketones, in particular acetophenone and methyl benzoyl formate. Table 5.2.1 shows the results of the direct hydrogenation of methyl benzoyl formate.

Table 5.2.1 Results of homogeneously catalysed direct hydrogenation of methyl benzoyl formate

Catalyst	Time / h	Conv[a] / %	TON[c] / × 10^5	ee[b] / %
[Ir(**3b**)(cod)]OTf	24	60	12	3
[Ir(**4b**)(cod)]OTf	24	37	7.4	3
[Ir(**8a**)(cod)]OTf	24	0	0	-
[Ir(**15**)(cod)]OTf	24	20	4.0	4
[Ir(**6b**)(cod)]BF_4	24	0	0	-
[Rh(**8a**)(cod)]BF_4	24	11	2.2	-
Ru(**3b**)(*p*-cym)Cl_2	24	13	2.6	0

- with no conversion, enantiomeric excess is not applicable

[a]conversion determined by ^{1}H NMR spectroscopy. [b]ee determined by chiral HPLC. [c]TON is calculated with respect to 1 mole of catalyst.

Conditions: 1:100 catalyst:substrate, 20 bar H_2, methanol as solvent, room temperature, 24 h.

A range of conversions are observed. In the cases where there is no conversion, the ligand contains an electron withdrawing group. In the complexes of the other ligands, there is either no significant electron withdrawing or donating effect, or in the case of ligand **4b**, electron donating. An electron withdrawing effect will slightly remove electron density from the metal centre, which may then affect the ability of the dihydrogen to coordinate to the metal centre. The mechanism previously displayed in fig. 5.2.1 shows that at this stage, the metal is oxidised from M(I) to M(III), so at this stage, less electron density at M(I) may cause this oxidation process to occur less readily. This highlights the importance of being able to easily fine tune the electronic properties of the chiral imine ligands to achieve optimum catalytic properties.

Unfortunately, in all cases, enantiomeric excess was low. Jacobsen[19] showed that the combination of bulky chiral ligands with restricted rotation around the chirotopic carbons is required for high enantiomeric excess. Therefore steric constraints are very important in asymmetric catalysis. It may be the case that transfer hydrogenation, which is a much bulkier hydrogen source coordinated to the metal centre, would provide more steric hindrance around the metal centre during hydrogenation, which in combination with the chiral ligand could force the ketone to adopt a specific position. Therefore transfer hydrogenation could give rise to higher enantioselectivities.

Direct hydrogenation of acetophenone was also performed. The results are given in table 5.2.2.

Table 5.2.2 Results of homogeneously catalysed direct hydrogenation of acetophenone

Catalyst	Time / h	Conv[a] / %	[c]TON / 10^5	ee[b] / %
[Ir(**8a**)(cod)]OTf	24	26	5.2	1
[Ir(**8a**)(cod)]BF_4	24	41	8.2	1
[Rh(**3b**)(cod)]BF_4	24	56	11.2	0
Ru(**4b**)(*p*-cym)Cl_2	24	16	3.2	14
Pt(**3b**)Cl_2	24	65	13	0
Pt(**9a**)Cl_2	24	43	8.6	1
Pd(**3b**)Cl_2	24	100	20	0
Pd(**9a**)Cl_2	24	27	5.4	1

[a]conversion determined by ^{1}H NMR spectroscopy. [b]ee determined by chiral HPLC. [c]TON is calculated with respect to 1 mole of catalyst.

Conditions: 1:100 catalyst:substrate, 20 bar H_2, methanol as solvent, room temperature, 24 h.

As with methyl benzoyl formate, a range of conversions were observed, with the same pattern – if electron withdrawing substituents are present in the ligand, conversion is lower, for the reason previously discussed. A blank reaction gave a conversion of approximately 10 %. Therefore, it can be concluded that the lack of enantiomeric excess is due to the lack of chiral induction caused by the

catalyst. Poor enantioselectivities are also observed with methyl benzoyl formate.

The homogeneous catalysts were also used in the transfer hydrogenation of acetophenone. The results are shown in table 5.2.3.

Table 5.2.3 Results of homogeneously catalysed transfer hydrogenation of acetophenone

Catalyst	Conv[a] / %	[c]TON / 10^5	ee[b] / %
[Ir(**8a**)(cod)]OTf	92	18.4	39
[Ir(**8a**)(cod)]BF_4	100	20	5
[Rh(**3b**)(cod)]BF_4	95	19	63
[Rh(**3b**)(nbd)]BF_4	73	14.6	64
[Rh(**4b**)(cod)]BF_4	0	0	-
[Rh(**5b**)(cod)]BF_4	21	4.2	29
[Rh(**6b**)(cod)]BF_4	0	0	-
[Rh(**8a**)(cod)]OTf	31	6.2	0
[Rh(**9b**)(cod)]BF_4	0	0	-
[Rh(**15**)(cod)]BF_4	0	0	-
[Rh(**16**)(cod)]BF_4	5	1	-
Ru(**4b**)(*p*-cym)Cl_2	28	5.6	4
Pt(**3b**)Cl_2	0	0	-
Pt(**9a**)Cl_2	0	0	-
Pd(**3b**)Cl_2	0	0	-
Pd(**9a**)Cl_2	0	0	-

- with no conversion, enantiomeric excess is not applicable

[a]conversion determined by ^{1}H NMR spectroscopy. [b]ee determined by chiral HPLC. [c]TON is calculated with respect to 1 mole of catalyst.

Conditions: 100:1:1 substrate:catalyst:KOH, 4.29×10^{-5} mol dm^{-3} KOH in isopropanol solution, room temperature, 72 h.

A wide range of conversions were observed. The platinum and palladium complexes showed no conversion, which is in agreement with literature, which shows these to be poor catalysts.[20] However, when the same catalysts were

employed in the direct hydrogenation of acetophenone, good conversions were seen. This indicates that this method of hydrogenation is unsuitable to use in conjunction with platinum and palladium complexes. The isopropanol solution contains potassium hydroxide at a low concentration of 4.29×10^{-5} mol dm^{-3}. It is possible that the presence of a strong base such as hydroxide will encourage decomposition of the complex, rendering it catalytically inactive. Interestingly, the iridium complexes gave high conversions. As discussed in chapter three, it was presumed that these complexes were prone to decomposition.

Interestingly [Rh(**3b**)(cod)]BF_4 shows a significantly higher conversion than [Rh(**3b**)(nbd)]BF_4, which has been observed previously by Jones[15]

In general, enantioselectivities have improved. This was predicted when discussing the poor enantioselectivities observed with the direct hydrogenation. A hydrogen source which is more sterically demanding would force the ketone substrate to adopt a specific position during catalysis, which is likely to be the cause for the improvement in enantioselectivity seen here.

Transfer hydrogenation was also carried out using 2'-methylacetophenone and 2'-chloroacetophenone. No conversion was observed with 2'-methylacetophenone. The results of the catalysis with 2'-chloroacetophenone are shown in table 5.2.4.

Table 5.2.4 Results of homogeneously catalysed transfer hydrogenation of 2'-chloroacetophenone

Catalyst	Time / h	Conv[a] / %	[c]TON / 10^5	ee[b] / %
[Rh(**3b**)(cod)]BF_4	96	5	1	-
[Rh(**4b**)(cod)]BF_4	96	0	0	-
[Rh(**5b**)(cod)]BF_4	24	0	0	-
[Rh(**6b**)(cod)]BF_4	24	5	1	-
[Rh(**8a**)(cod)]OTf	24	59	11.8	10
[Rh(**15**)(cod)]BF_4	96	0	0	-
Ru(**5b**)(*p*-cym)Cl_2	96	0	0	-

- with no conversion, enantiomeric excess is not applicable

[a]conversion determined by ^{1}H NMR spectroscopy. [b]ee determined by chiral HPLC. [c]TON is calculated with respect to 1 mole of catalyst.

Conditions: 100:1:1 substrate:catalyst:KOH, 4.29×10^{-5} mol dm^{-3} KOH in isopropanol solution, room temperature.

Poor conversions were observed with the exception of [Rh(**8a**)(cod)]OTf. This is the only catalyst tested here with a triflate counterion, which in combination with this particular substrate may be yielding the reasonable conversion observed. The other distinguishing feature of this catalyst is the presence of the phosphine groups.

The homogeneous catalysts were also used in the transfer hydrogenation of acetophenone in the presence of hydrogen gas. The results are shown in table 5.2.5.

Table 5.2.5 Results of homogeneously catalysed transfer hydrogenation of acetophenone in the presence of H_2

Catalyst	Time / h	Conv[a] / %	[c]TON / 10^5	ee[b] / %
[Ir(**6b**)(cod)]BF_4	24	10	2	15
[Ir(**8a**)(cod)]OTf	24	38	7.6	2
[Ir(**8a**)(cod)]OTf	72	76	15.2	31
[Ir(**8a**)(cod)]BF_4	24	24	4.8	1
[Ir(**15**)(cod)]BF_4	24	4	0.8	-
[Rh(**3b**)(cod)]BF_4	24	28	5.6	18
[Rh(**3b**)(cod)]BF_4	72	31	6.2	10
[Rh(**6b**)(cod)]BF_4	24	16	3.2	0
[Rh(**8a**)(cod)OTf	24	0	0	-
[Rh(**8a**)(cod)]BF_4	24	11	2.2	0
[Rh(**8a**)(cod)]BF_4	72	25	5	0
Ru(**4b**)(p-cym)Cl_2	24	5	1	-
Ru(**15**)(p-cym)Cl_2	24	3	0.6	-

- with no conversion, enantiomeric excess is not applicable

[a]conversion determined by ^{1}H NMR spectroscopy. [b]ee determined by chiral HPLC. [c]TON is calculated with respect to 1 mole of catalyst.

Conditions: 100:1:1 substrate:catalyst:KOH, 4.29×10^{-5} mol dm^{-3} KOH in isopropanol solution, 20 bar H_2, room temperature.

The conversion is higher when the reaction is performed for 72 hours, with [Ir(**8a**)(cod)]OTf. However, with the rhodium(I) complexes only a marginal increase was observed. This may imply that the rhodium(I) complexes become deactivated during the catalysis. When the rhodium complexes were used as catalysts, the presence of electron withdrawing substituents within the ligand is associated with lower conversions, as previously discussed. However, when the iridium complexes were screened, the opposite effect is observed. However, if the iridium complexes which contain triflate counterions are not considered, the conversions of the remaining iridium complexes are relatively low, and so the differences in conversions are not great enough to form conclusions with respect to catalytic behaviour.

When triflate is used as a counterion, conversions are higher compared with their BF_4^- counterparts. This suggests that conversions are enhanced in the presence of triflate. It is hypothesised that the triflate is coordinating to the metal centre potentially stabilising the iridium centre during the catalytic cycle

Homogeneous catalysis was also performed at an increased reaction temperature of 40 °C. The reactions were both carried out under argon. The reaction vessel was either sealed (a closed system) or open to argon (open system). The results are shown in table 5.2.6.

Table 5.2.6 Results of homogeneously catalysed transfer hydrogenation of acetophenone, at 40 °C, in either an open or closed vessel

Catalyst	System	Conv[a] / %	[c]TON / 10^5	ee[b] / %
[Rh(**3b**)(cod)]BF_4	Open	82	16.4	51
[Rh(**3b**)(cod)]BF_4	Closed	74	14.8	17
[Rh(**4b**)(cod)]BF_4	Open	82	16.4	36
[Rh(**4b**)(cod)]BF_4	Closed	69	13.8	27
[Rh(**5b**)(cod)]BF_4	Open	47	9.4	17
[Rh(**5b**)(cod)]BF_4	Closed	43	8.6	2
[Rh(**6b**)(cod)]BF_4	Open	14	2.8	15
[Rh(**6b**)(cod)]BF_4	Closed	35	7.0	2
[Rh(**9b**)(cod)]BF_4	Open	33	6.6	12
[Rh(**9b**)(cod)]BF_4	Closed	92	18.4	0
[Rh(**16**)(cod)]BF_4	Open	91	18.2	28
[Rh(**16**)(cod)]BF_4	Closed	59	11.8	7
Ru(**3b**)(*p*-cym)Cl_2	Open	14	2.8	0
Ru(**3b**)(*p*-cym)Cl_2	Closed	5	1.0	0

[a]conversion determined by ^{1}H NMR spectroscopy. [b]ee determined by chiral HPLC. [c]TON is calculated with respect to 1 mole of catalyst.

Conditions: 100:1:1 substrate:catalyst:KOH, 4.29×10^{-5} mol dm^{-3} KOH in isopropanol solution, 40 °C, 72 h.

In general, the conversions and enantioselectivities are significantly higher in an open reaction system. This can be explained by examining the transfer hydrogenation mechanism. On generating the hydride sources, isopropanol is converted to acetone. In an open reaction system, the acetone can be removed during the catalysis. The removal of the acetone means that the further generation of more acetone by yielding hydride is not restricted, and the equilibrium favours the products. In the closed system, the acetone generated cannot escape, which greatly hinders the production of further acetone, therefore the generation of hydride species is reduced, and the rate of reaction slows. This gives rise to a considerable decrease in conversion. In addition, if the acetone is not allowed to escape, it is highly likely that the acetone will coordinate to the metal centre, blocking coordination of the acetophenone. Essentially, the acetone is competitively binding to the metal centre hindering the approach of acetophenone and thus reducing the conversion. In general, these results support the transfer hydrogenation mechanism, and not only highlight the importance of understanding the catalytic mechanism, but also the importance of tailoring each reaction condition to suit the other conditions, substrates and catalysts.

5.2.2 Heterogeneous Catalysis

A number of the heterogeneous complexes described in chapter four were also used to catalyse the hydrogenation of acetophenone. The results from the direct hydrogenation can be seen in table 5.2.7.

Table 5.2.7 Results of heterogeneously catalysed direct hydrogenation of acetophenone

Catalyst	[c]Metal Loading / × 10^{-4} mol	Conv[a] / %	[d]TON / × 10^5	ee[b] / %
[Ir(**S8**)(cod)]BF_4	3.76	50	70.7	0
[Ir(**S6**)(cod)]BF_4	4.26	78	86.0	1
[Rh(**S4**)(cod)]BF_4	4.24	88	97.9	0
[Rh(**S7**)(cod)]BF_4	3.90	39	51.3	0
[Rh(**S8**)(cod)]BF_4	3.76	41	58.0	0

[a]conversion determined by ^{1}H NMR spectroscopy. [b]ee determined by chiral HPLC. [c]Metal loading corresponds to the amount of metal in 1 gram of catalyst. [d]TON is calculated with respect to one mole of metal.

Conditions: 50 mg catalyst, 20 bar H_2, methanol as solvent, room temperature, 24 h.

The results show that the conversions (and turnover numbers) are relatively high in comparison to the homogeneous catalysts. As discussed in chapter one, it is not uncommon to observe higher conversions in heterogeneous catalysts compared with their homogeneous counterparts. However, no enantioselectivity is observed. The enantioselectivities in the homogeneously catalysed direct hydrogenations were also very poor, so this is likely to be due to the type of hydrogenation being unsuitable for this combination of catalyst, substrate and reaction conditions.

The heterogeneous catalysis of the transfer hydrogenation of acetophenone was also carried out. The results are shown in table 5.2.8.

Table 5.2.8 Results of heterogeneously catalysed transfer hydrogenation of acetophenone

Catalyst	[c]Metal Loading / $\times 10^{-4}$ mol	Conv[a] / %	[d]TON / $\times 10^{5}$	ee[b] / %
[Ir(**S8**)(cod)]BF_4	3.76	0	0	-
[Ir(**S6**)(cod)]BF_4	4.26	0	0	-
[Rh(**S4**)(cod)]BF_4	4.24	0	0	-
[Rh(**S7**)(cod)]BF_4	3.90	0	0	-
[Rh(**S8**)(cod)]BF_4	3.76	0	0	-

- with no conversion, enantiomeric excess is not applicable

[a]conversion determined by ^{1}H NMR spectroscopy. [b]ee determined by chiral HPLC. [c]Metal loading corresponds to the amount of metal in 1 gram of catalyst. [d]TON is calculated with respect to one mole of metal.

Conditions: 50 mg catalyst, 1:1 substrate:KOH, 4.29×10^{-5} mol dm^{-3} KOH in isopropanol solution, room temperature, 24 h.

The results show that there was no conversion. This is not uncommon for silica support systems for catalytic transfer hydrogenation. In silica, silanol (acidic) groups are still present which will react with added KOH, which is essential for the catalysis to be successful. As previously discussed in chapter one, often these silanol groups are capped to remove these reactive moieties – which could be attempted in future research to optimise the performance of these catalysts.

The heterogeneous rhodium(I) system prepared using the "tether group" technique was also screened for the transfer hydrogenation of acetophenone. However, no conversion was observed. The analogous silsesquioxane-supported rhodium(I) system, also prepared using the tether group technique, was also screened for this reaction. No conversion was observed.

The heterogeneous catalysis of the transfer hydrogenation of acetophenone in the presence of hydrogen gas was also performed. The results are shown in table 5.2.9.

Table 5.2.9 Results of heterogeneously catalysed transfer hydrogenation of acetophenone, in the presence of H_2

Catalyst	[c]Metal Loading / × 10^{-4} mol	Conv[a] / %	[d]TON / × 10^5	ee[b] / %
[Ir(**S8**)(cod)]BF_4	3.76	85	120.2	1
[Ir(**S6**)(cod)]BF_4	4.26	23	25.3	4
[Rh(**S4**)(cod)]BF_4	4.24	63	70.1	2
[Rh(**S7**)(cod)]BF_4	3.90	66	86.8	0
[Rh(**S8**)(cod)]BF_4	3.76	43	60.8	0

[a]conversion determined by ^{1}H NMR spectroscopy. [b]ee determined by chiral HPLC. [c]Metal loading corresponds to the amount of metal in 1 gram of catalyst. [d]TON is calculated with respect to one mole of metal.

Conditions: 50 mg catalyst, 1:1 substrate:KOH, 4.29 × 10^{-5} mol dm^{-3} KOH in isopropanol solution, 20 bar H_2, room temperature, 24 h.

The conversions are moderate to good. They do not differ too significantly from the heterogeneous catalysis of the direct hydrogenation. As previously discussed, these conversions and turnover numbers are higher than those observed for the homogeneous catalysis, however higher conversions in heterogeneous catalysis are not uncommon. Unfortunately, the enantioselectivities are very poor. They are much lower than those observed in the analogous homogeneous catalysis. As previously discussed in chapter one, enantioselectivities are often lower in heterogeneous catalysis, particularly with silica-supported catalysts. In conclusion, good conversions for the hydrogenations have been achieved. However, the enantiomeric excesses have proved disappointing. Therefore, these ligands and complexes have been applied to other reactions, detailed in the following section.

5.2.3 Hydrogenation of Imines

The transfer hydrogenation of imines was also investigated. Fig 5.2.3. shows the reaction scheme for the hydrogenation of *N*-benzylidenemethylamine.

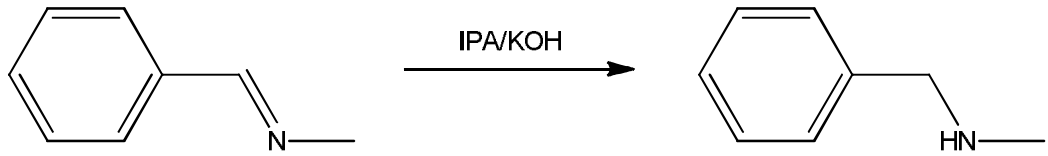

Fig. 5.2.3 Reaction scheme of the transfer hydrogenation of *N*-benzylidenemethylamine

The product of the reaction is not chiral, hence this is not an asymmetric process. However, the imines that would yield a chiral product on hydrogenation are very expensive. Therefore this imine was used to test the concept of hydrogenating imines. The results of this can be seen in table 5.2.10.

Table 5.2.10 Results of the catalysed transfer hydrogenation of *N*-benzylidenemethylamine

Catalyst	Conv[a] / %	TON[b] / 10^5
[Rh(**3b**)(cod)]BF_4	0	0
[Rh(**6b**)(cod)]BF_4	0	0
[Rh(**5b**)(cod)]BF_4	0	0
[Rh(**S4**)(cod)]BF_4	0	0
[Rh(**S7**)(cod)]BF_4	0	0
[Rh(**S8**)(cod)]BF_4	0	0

[a]conversion determined by ^{1}H NMR spectroscopy. [b]TON is calculated with respect to one mole of catalyst.

Conditions: For homogeneous catalysis: 100:1:1 substrate:catalyst:KOH, 4.29×10^{-5} mol dm^{-3} KOH in isopropanol solution, room temperature, 24 h. For heterogeneous catalysis: 50 mg catalyst, 1:1 substrate:KOH, 4.29×10^{-5} mol dm^{-3} KOH in isopropanol solution, room temperature, 24 h.

No conversion was observed, in either the homogeneous or heterogeneous catalysis of this reaction. This suggests that this combination of catalyst type, substrate and reaction conditions were not compatible. The transfer hydrogenation of phenyl-1(1-phenylethylidene) amine was also tested; this substrate was chosen as it was the only commercially available imine that would yield a chiral product. The reaction scheme is shown in fig. 5.2.4.

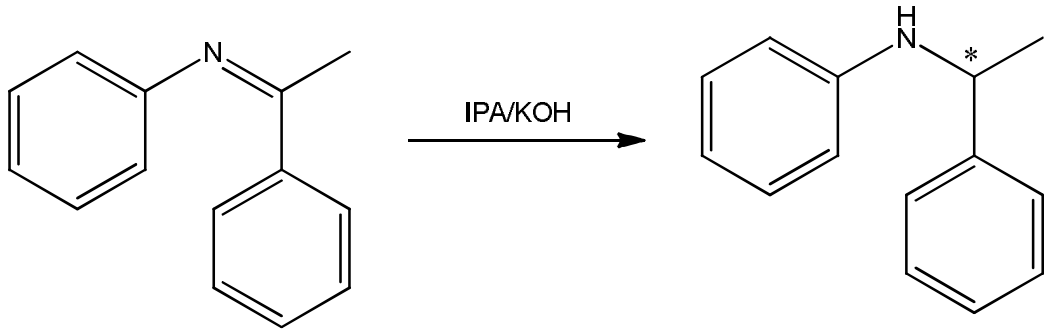

Fig. 5.2.4 Reaction scheme of the transfer hydrogenation of phenyl-1(1-phenylethylidene) amine

In this case, the product was chiral. The catalytic results can be seen in table 5.2.11.

Table 5.2.11 Results of the catalysed transfer hydrogenation of phenyl-1(1-phenylethylidene) amine

Catalyst	Conv[a] / %	TON[b] / 10^5
[Rh(**3b**)(cod)]BF_4	0	0
[Rh(**6b**)(cod)]BF_4	0	0
[Rh(**5b**)(cod)]BF_4	0	0
[Rh(**S4**)(cod)]BF_4	0	0
[Rh(**S7**)(cod)]BF_4	0	0
[Rh(**S8**)(cod)]BF_4	0	0

[a]conversion determined by ^{1}H NMR spectroscopy. [b]TON is calculated with respect to one mole of catalyst.

Conditions: For homogeneous catalysis: 100:1:1 substrate:catalyst:KOH, 4.29×10^{-5} mol dm^{-3} KOH in isopropanol solution, room temperature, 24 h. For heterogeneous catalysis: 50 mg catalyst, 1:1 substrate:KOH, 4.29×10^{-5} mol dm^{-3} KOH in isopropanol solution, room temperature, 24 h.

The results show that no conversion was achieved. On examining the imine, there is significant steric bulk around the imine bond, which may have hindered the coordination of the imine to the metal centre, which is essential for the mechanism. When *N*-benzylidenemethylamine was hydrogenated, steric hindrance could also have prevented coordination to the metal centre. However, there was much less steric bulk surrounding the imine of *N*-

benzylidenemethylamine, therefore it is expected that some conversion would have been observed. The fact that no conversion whatsoever was observed with either imine suggests that the transfer hydrogenation of imines is not compatible with the types of catalysts used here.

5.3 Catalysing the Asymmetric Nitroaldol Reaction

An example of the nitroaldol reaction can be seen in fig. 5.3.1.

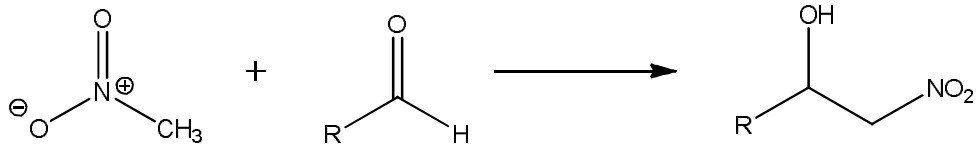

Fig. 5.3.1 Reaction scheme of the nitroaldol reaction of nitromethane and an aldehyde

The nitroaldol reaction is important for carbon-carbon bond formation, and also provides much scope for subsequent conversion of the nitro moiety into other functional groups. Often, copper(II) complexes are used to catalyse this reaction, which was discussed in chapter one. However, many of the catalysts that have been developed require high catalyst loadings[21] or are too substrate specific.[22] Thus, it is clear that there is a niche for an efficient, more generally applicable catalyst in this area. This reaction is not limited to copper(II), for example zinc(II),[23] chromium(III),[24-25] lanthanide(III)[26-27] and cobalt(II)[28-29] have all been utilised. The use of heterogeneous catalysts for this process remains limited. However, there have been successes with catalysts supported on PEG polymers, Wang type resins and dendrimers.[30-32]

In order to rationalise the catalysis of this reaction, the mechanism must be studied in depth. Fig. 5.3.2 shows the catalytic mechanism of the nitroaldol reaction.

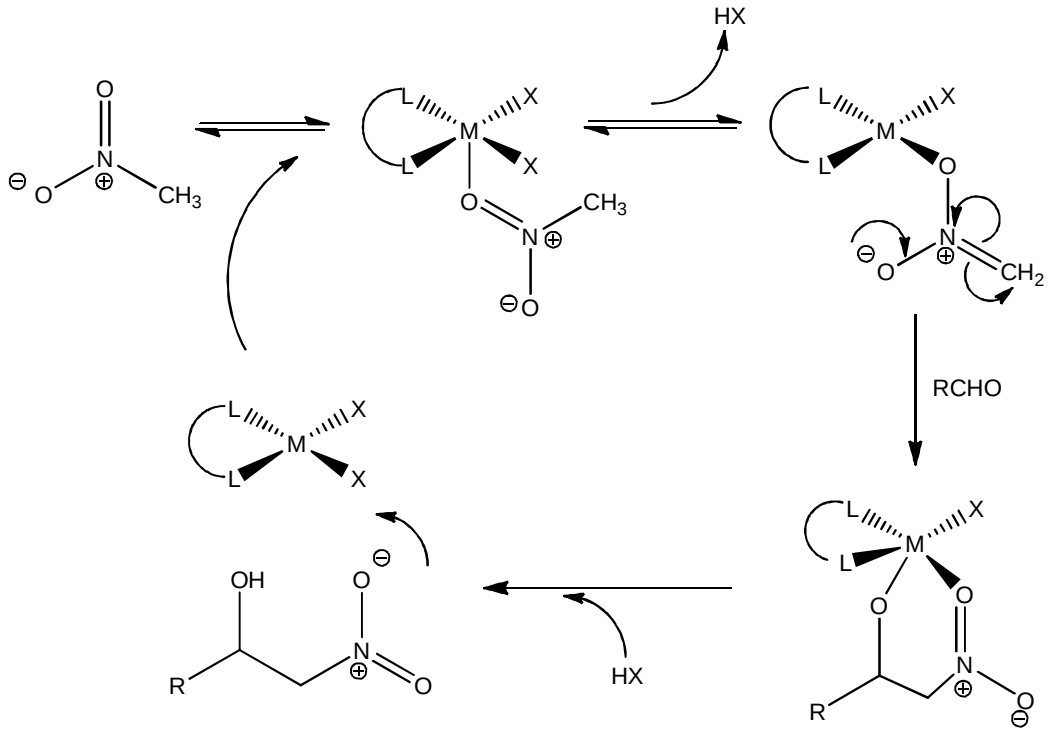

Fig. 5.3.2[33] Catalytic mechanism of the nitroaldol reaction, where X = base (for example triethylamine)

This mechanism highlights the importance of the presence of a base (**X**). The base facilitates the deprotonation of the nitroalkane, which is necessary for the subsequent addition of the nitroalkane to the pseudo-positive (δ+) carbon of the aldehyde. There have been a few examples of the successful catalysis of the nitroaldol reaction without the addition of a base.[34-37] However, the ligands used in these cases usually contain basic moieties. For example, Khan used diaminocyclohexane-based salan ligands in conjunction with copper(II) acetate to catalyse the asymmetric nitroaldol reaction.[38] No base was added to facilitate the reaction. However, the amine functionalities within the ligand are basic and will deprotonate the nitroalkane, removing the need for the addition of a base to the reaction. Good yields (30-82 %) and enantiomeric excesses (27-86 %) were observed.

The ligands reported in this research also contain basic functionalities, therefore a base may not be necessary, therefore it was also hoped that the complexes containing amine moieties might be successful in the absence of base. Also, the base itself and the relative amounts used may have a significant influence on the

catalytic results. The substrates employed and the reaction temperature were also varied, and will be discussed herein.

5.3.1 Optimisation by Varying the Reagents

5.3.1.1 Homogeneous Catalysis

A number of the copper(II) complexes described in chapter three were screened as catalysts in the nitroaldol reaction of nitromethane and benzaldehyde. The results can be seen in table. 5.3.1. In general, moderate conversions and enantioselectivities were observed, with no remarkable differences between the complexes with bichelating (ligands **2-6b**, ligand **17**) and tetrachelating (ligands **9a-14b**) ligands. It had been thought previously that a tetrachelating complex would provide a more rigid complex, therefore improvements in enantioselectivity might be observed. However, this has not been the case, in fact enantioselectivities have decreased.

Table 5.3.1 Results of the homogeneously catalysed nitroaldol reaction of nitromethane and benzaldehyde

Catalyst	Conv[a] / %	[c]TON / × 10^5	ee[b] / %
Cu(**2**)$_2$(OTf)$_2$	68	2.7	0
Cu(**3b**)$_2$(OTf)$_2$	90	3.6	60
Cu(**4b**)$_2$(OTf)$_2$	20	0.8	72
Cu(**5b**)$_2$(OTf)$_2$	26	1.0	78
Cu(**6b**)$_2$(OTf)$_2$	71	2.8	8
Cu(**9a**)(OTf)$_2$ MeOH	50	2.0	42
Cu(**9a**)(OTf)$_2$ EtOH	40	1.6	33
Cu(**9a**)(OTf)$_2$ IPA	27	1.1	19
Cu(**9b**)(OTf)$_2$	98	3.9	4
Cu(**10a**)(OTf)$_2$	82	3.3	26
Cu(**10b**)(OTf)$_2$	95	3.8	26
Cu(**11a**)(OTf)$_2$	74	3.0	1
Cu(**11b**)(OTf)$_2$	95	3.8	46
Cu(**12a**)(OTf)$_2$	18	0.7	2
Cu(**12b**)(OTf)$_2$	44	1.8	5
Cu(**13b**)(OTf)$_2$	94	3.8	37
Cu(**14b**)(OTf)$_2$	96	3.8	57
Cu(**17**)$_2$(OTf)$_2$	76	3.0	36

[a]conversion determined by ^{1}H NMR spectroscopy. [b]ee determined by chiral HPLC. [c]TON is calculated with respect to 1 mole of catalyst.

Conditions: 0.05 mmol catalyst, 1.0 mmol benzaldehyde, 10 mmol nitromethane, 0.13 mmol triethylamine, reaction solvent is ethanol (unless otherwise stated), room temperature, 6 h.

The results show that on the whole, if electron withdrawing substituents are present within the ligand the conversions are higher, and likewise if electron donating substituents are present the conversions are much lower. For example, in comparing Cu(**4b**)$_2$(OTf)$_2$ (OMe substituent) and Cu(**6b**)$_2$(OTf)$_2$ (Cl substituent), the conversion is significantly lower (20 %) when the electron

donating OMe substituent is present than when the Cl substituent is present (71 %).

Another pattern that can be seen is that the more basic the ligands, the greater the enantioselectivity. When electron donating groups are present in the ligand (for example, Cu(**5b**)$_2$(OTf)$_2$), there is more electron density present at the amine groups than when electron withdrawing groups are present (for example Cu(**6b**)$_2$(OTf)$_2$). The increased electron density at the amine group increases its basicity. The amine complexes show greater enantiomeric excesses than the imine complexes, as amines are more basic than imines. However, some complexes show close to no enantioselectivity, for example the complexes containing primary amines, such as Cu(**2**)$_2$(OTf)$_2$ and Cu(**11a**)(OTf)$_2$ (due to ligand decomposition, as discussed in chapter three). In all these cases it was necessary to add base to facilitate the catalysis. The very low enantioselectivities may be due to the ligand not playing a part in the deprotonation of the nitroalkane, as in these cases the triethylamine would have been the strongest base present. In fact a blank reaction with no catalyst gave a yield of approximately 10 %. Because of this the complex may have less of an influence over the coordination of the nitroalkane and subsequently the aldehyde, which in turn may have reduced the enantiomeric excess. This also supports the pattern in the enantioselectivities being related to basicity – the greater the basicity of the ligand, the more the ligand will be deprotonating the nitroalkane rather than the triethylamine, therefore the more influence the chiral ligand will have over the catalytic process.

Comparing the Cu(**9a**)(OTf)$_2$ complexes in methanol, ethanol and isopropanol, significantly lower conversions and enantiomeric excesses were observed when the complex was prepared and the catalysis performed in isopropanol. Firstly, varying the reaction solvent can have a significant effect of catalytic behaviour, as previously described in chapter one. In addition to this, the complexes prepared in methanol and ethanol have an additional chiral centre due to the α-amino ether group, as previously discussed in chapter three, which can help to explain the higher enantioselectivities observed compared to isopropanol.

Table 5.3.2. shows the catalytic data when nitromethane and 4-nitrobenzaldehyde are used as substrates. On changing benzaldehyde to 4-nitrobenzaldehyde, the conversions have dramatically improved. The presence of the nitro group will increase the magnitude of δ^+ on the carbonyl carbon, increasing its susceptibility to nucleophilic attack from the deprotonated nitromethane.

Table 5.3.2 Results of the homogeneously catalysed nitroaldol reaction of nitromethane and 4-nitrobenzaldehyde

Catalyst	Conv[a] / %	TON[c] / × 10^5	ee[b] / %
Cu(**2**)$_2$(OTf)$_2$	98	3.9	2
Cu(**3b**)$_2$(OTf)$_2$	98	3.9	20
Cu(**4b**)$_2$(OTf)$_2$	98	3.9	18
Cu(**5b**)$_2$(OTf)$_2$	98	3.9	15
Cu(**6b**)$_2$(OTf)$_2$	100	4.0	22
Cu(**9a**)(OTf)$_2$ MeOH	62	2.5	0
Cu(**9a**)(OTf)$_2$ EtOH	18	0.7	14
Cu(**9a**)(OTf)$_2$ IPA	36	1.4	2
Cu(**9b**)(OTf)$_2$	98	3.9	13
Cu(**10a**)(OTf)$_2$	99	4.0	2
Cu(**10b**)(OTf)$_2$	98	3.9	31
Cu(**11a**)(OTf)$_2$	99	4.0	2
Cu(**11b**)(OTf)$_2$	98	3.9	21
Cu(**12a**)(OTf)$_2$	80	3.2	17
Cu(**12b**)(OTf)$_2$	99	4.0	9
Cu(**13b**)(OTf)$_2$	98	3.9	8
Cu(**14b**)(OTf)$_2$	98	3.9	30
Cu(**17**)$_2$(OTf)$_2$	89	3.6	28

[a]conversion determined by ^{1}H NMR spectroscopy. [b]ee determined by chiral HPLC. [c]TON is calculated with respect to 1 mole of catalyst.

Conditions: 0.05 mmol catalyst, 1.0 mmol 4-nitrobenzaldehyde, 10 mmol nitromethane, 0.13 mmol triethylamine, reaction solvent is ethanol (unless otherwise stated), room temperature, 6 h.

When nitroethane and benzaldehyde were used as substrates, a diastereomeric product was formed. The reaction scheme for this can be seen in fig. 5.3.3.

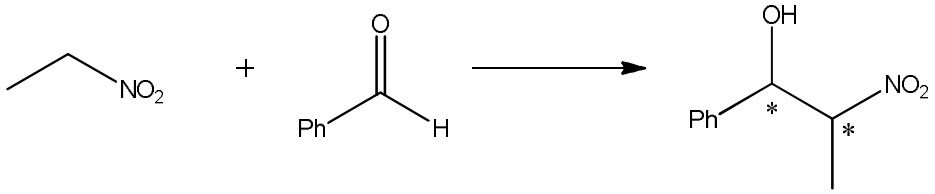

Fig. 5.3.3 Reaction scheme for the nitroaldol reaction of nitroethane and benzaldehyde

The results can be seen in table 5.3.3. Good conversions were seen with these two substrates. In terms of comparisons with the other nitroaldol reactions reported here, there are no significant differences. The pattern in enantioselectivities is very similar to the other nitroaldol reactions reported here – that where electron donating substituents are present, basicity at the amine groups in the ligand is increased which in turn improves enantioselectivity. Unfortunately, the diastereoselectivities observed are low. On examination of the mechanism, the two chiral centres are formed when both substrates are coordinated to the metal centre. Hence, steric hindrance around the metal centre will largely control the diastereoselectivity. Because of this, it is expected that complexes with smaller ligands (such as Cu(**2**)$_2$(OTf)$_2$ and Cu(**17**)$_2$(OTf)$_2$) and ligands with greater degrees of freedom (i.e. amines rather than imines) that can rearrange themselves more easily around the metal centre would encourage higher diastereoselectivities. To a large extent, this can be seen in the results.

Table 5.3.3 Results of the homogeneously catalysed nitroaldol reaction of nitroethane and benzaldehyde

Catalyst	Conv[a] / %	TON[c] / × 10^5	de[a] / %	ee[b] / %
Cu(**2**)$_2$(OTf)$_2$	78	3.1	25	2, 0
Cu(**3b**)$_2$(OTf)$_2$	85	3.4	13	2, 41
Cu(**4b**)$_2$(OTf)$_2$	88	3.5	5	14, 15
Cu(**5b**)$_2$(OTf)$_2$	86	3.4	10	23, 13
Cu(**6b**)$_2$(OTf)$_2$	80	3.2	4	6, 2
Cu(**9a**)(OTf)$_2$ MeOH	80	3.2	2	33, 34
Cu(**9a**)(OTf)$_2$ EtOH	31	1.2	8	10, 9
Cu(**9a**)(OTf)$_2$ IPA	61	2.4	5	11, 0
Cu(**9b**)(OTf)$_2$	97	3.9	26	32, 25
Cu(**10a**)(OTf)$_2$	99	4.0	5	10, 12
Cu(**10b**)(OTf)$_2$	95	3.8	17	7, 38
Cu(**11a**)(OTf)$_2$	96	3.8	8	5, 18
Cu(**11b**)(OTf)$_2$	95	3.8	2	10, 37
Cu(**12a**)(OTf)$_2$	73	2.9	21	13, 7
Cu(**12b**)(OTf)$_2$	79	3.2	43	36, 41
Cu(**13b**)(OTf)$_2$	87	3.5	8	20, 50
Cu(**14b**)(OTf)$_2$	90	3.6	8	33, 8
Cu(**17**)$_2$(OTf)$_2$	78	3.1	29	36, 40

[a]conversion and de determined by ^{1}H NMR spectroscopy. Major diastereomer is *anti* isomer. [b]ee determined by chiral HPLC. [c]TON is calculated with respect to 1 mole of catalyst.

Conditions: 0.05 mmol catalyst, 1.0 mmol benzaldehyde, 10 mmol nitroethane, 0.13 mmol triethylamine, reaction solvent is ethanol (unless otherwise stated), room temperature, 6 h.

The nitroaldol reaction was also performed using nitroethane and 4-nitrobenzaldehyde. The results can be seen in table 5.3.4. When 4-nitrobenzaldehyde and nitromethane were used as previously described, a significant increase in conversion was observed. An analogous trend is observed here, which is due to the nitro functionality increasing the susceptibility of the

aldehyde to nucleophilic attack. The diastereoselectivities show a significant decrease on changing the aldehyde from benzaldehyde to 4-nitrobenzaldehyde; from the mechanism this is expected due to the electron withdrawing nature of the nitro group.

Table 5.3.4 Results of the homogeneously catalysed nitroaldol reaction of nitroethane and 4-nitrobenzaldehyde

Catalyst	Conv[a] / %	TON[c] / × 10^5	de[a] / %	ee[b] / %
Cu(**2**)$_2$(OTf)$_2$	99	4.0	4	1, 0
Cu(**3b**)$_2$(OTf)$_2$	95	3.8	7	5, 22
Cu(**4b**)$_2$(OTf)$_2$	98	3.9	4	13, 5
Cu(**5b**)$_2$(OTf)$_2$	96	3.8	5	7, 8
Cu(**6b**)$_2$(OTf)$_2$	94	3.8	11	12, 24
Cu(**9a**)(OTf)$_2$ MeOH	95	3.8	12	21, 8
Cu(**9a**)(OTf)$_2$ EtOH	93	3.7	8	5, 3
Cu(**9a**)(OTf)$_2$ IPA	78	3.1	9	7, 3
Cu(**9b**)(OTf)$_2$	99	4.0	18	26, 8
Cu(**10a**)(OTf)$_2$	98	3.9	15	5, 5
Cu(**10b**)(OTf)$_2$	99	4.0	1	16, 20
Cu(**11a**)(OTf)$_2$	98	3.9	5	1, 1
Cu(**11b**)(OTf)$_2$	97	3.9	10	14, 16
Cu(**12a**)(OTf)$_2$	97	3.9	3	0, 4
Cu(**12b**)(OTf)$_2$	98	3.9	17	14, 16
Cu(**13b**)(OTf)$_2$	94	3.8	6	2, 3
Cu(**14b**)(OTf)$_2$	94	3.8	4	27, 32
Cu(**17**)$_2$(OTf)$_2$	97	3.9	13	17, 10

[a]conversion and de determined by ^{1}H NMR spectroscopy. Major diastereomer is *anti* isomer. [b]ee determined by chiral HPLC. [c]TON is calculated with respect to 1 mole of catalyst.

Conditions: 0.05 mmol catalyst, 1.0 mmol 4-nitrobenzaldehyde, 10 mmol nitroethane, 0.13 mmol triethylamine, reaction solvent is ethanol (unless otherwise stated), room temperature, 6 h.

5.3.1.2Heterogeneous Catalysis

A selection of the heterogeneous complexes described in chapter four were screened for the catalysis of the nitroaldol reaction. The results of using nitromethane and benzaldehyde as substrates are shown in table 5.3.5.

Table 5.3.5 Results of the heterogeneously catalysed (silica based) nitroaldol reaction of nitromethane and benzaldehyde

Catalyst	Metal Loading[c] / 10^{-5} mol	Conv[a] / %	Selectivity[a] / %	TON[d] / $\times 10^5$	ee[b] / %
Cu(**S4**)$(OTf)_2$	8.48	99	64	1.4	0
Cu(**S4**)$(OTf)_2$	4.24	95	78	5.3	5
Cu(**S5**)$(OTf)_2$	7.95	86	70	1.4	31
Cu(**S5**)$(OTf)_2$	3.98	80	82	5.1	22
Cu(**S6**)$(OTf)_2$	8.52	99	72	1.4	34
Cu(**S6**)$(OTf)_2$	4.26	76	73	4.2	25
Cu(**S7**)$(OTf)_2$	7.81	100	0	1.6	-
Cu(**S7**)$(OTf)_2$	3.90	100	0	6.6	-
Cu(**S8**)$(OTf)_2$	7.52	31	97	0.5	2
Cu(**S8**)$(OTf)_2$	3.76	44	74	3.1	17
Cu(**S9**)$(OTf)_2$	9.43	43	100	0.5	12
Cu(**S9**)$(OTf)_2$	4.71	15	100	0.7	2

- with no conversion, enantiomeric excess is not applicable

[a]conversion and selectivity determined by ^{1}H NMR spectroscopy. [b]ee determined by chiral HPLC. [c]Metal loading corresponds to the amount of metal present in the heterogeneous catalyst used during the reaction. [d]TON is calculated with respect to 1 mole of metal being used.

Conditions: 200 or 100 mg catalyst, 1.0 mmol benzaldehyde, 10 mmol nitromethane, 0.13 mmol triethylamine, reaction solvent is ethanol, room temperature, 24 h.

At first glance, the conversions are impressively high. However, on closer inspection of the ^{1}H NMR spectra of the catalytic residues, it appears that this conversion is not full conversion to the desired product, due to the presence of

by-products. The undesirable product was 1,3-dinitro-2-phenyl propane, shown in fig. 5.3.4.

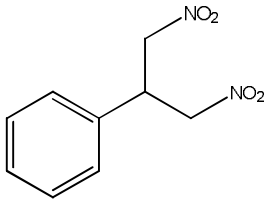

Fig. 5.3.4 1,3-dinitro-2-phenyl propane, the undesirable by-product of the heterogeneously catalysed nitroaldol reaction of nitromethane and benzaldehyde

This results from the product from the nitroaldol reaction reacting further, shown in fig. 5.3.5. 1,3-dinitro alkanes have been shown to be key building blocks in the synthesis of HIV-protease inhibitors and other biologically important intermediates.[39] These alkanes have been shown to be produced from heterogeneous primary amine/tertiary amine catalysts.[40] Significantly, acid surfaces have been shown to enhance the activity via a cooperative mechanism involving free amines on the surface and potentially by activating the intermediate β-nitrostyrene to attack by nitromethane.[40] This is presumably a possible explanation for the observation of this by-product in this case, as the support is acidic. Although not the main thrust of this work it should be noted that the formation of 1,3-dinitro alkanes is typically performed at elevated temperatures.[41] In this work the catalysis is performaed at room temperature.

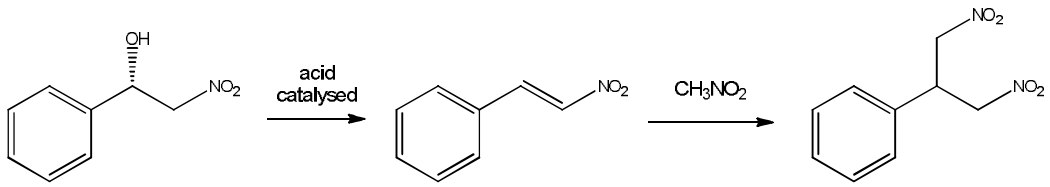

Fig. 5.3.5 Reaction scheme showing the further reaction of the nitroaldol product to the undesired 1,3-dinitro alkane

Selectivity for the desired product is higher when less catalyst is used, which is sensible as the nitroalkene is formed by the acid catalysed dehydration of the desired nitroalcohol.

Another interesting feature to notice is the stereochemistry of the products. In all cases (homogeneous and heterogeneous), the (*R*,*R*) enantiomer of the catalyst is used, and would be expected to produce the (*S*) form of the product, as Bandini et al.[21] observe the (*S*) enantiomer produced from their nitroaldol reactions using similar chiral ligands to the ligands used here, of (*R*,*R*) configuration. When using their amine ligands, the product was of (*S*) configuration, and when using their imine ligands, the (*R*) enantiomer was observed. This suggests that either enantiomer of the product can be obtained by simply choosing to use the imine or amine forms of the ligand. This is a very useful tool to possess in asymmetric catalysis. In our homogeneous case the (*S*) configuration was observed with the amines, but with the heterogeneous (imines), the (*R*) configuration was observed.

The heterogeneous catalysis was also carried out using nitromethane and 4-nitrobenzaldehyde as substrates. The catalytic results can be seen in table 5.3.6.

Table 5.3.6 Results of the heterogeneously catalysed (silica based) nitroaldol reaction of nitromethane and 4-nitrobenzaldehyde

Catalyst	Metal Loading[c] / 10^{-5} mol	Conv[a] / %	Selectivity[a] / %	TON[d] / 10^5	ee[b] / %
Cu(**S4**)$(OTf)_2$	8.48	97	67	1.3	0
Cu(**S4**)$(OTf)_2$	4.24	92	78	5.1	0
Cu(**S5**)$(OTf)_2$	7.95	96	60	1.5	0
Cu(**S5**)$(OTf)_2$	3.98	96	71	6.1	0
Cu(**S6**)$(OTf)_2$	8.52	98	63	1.4	0
Cu(**S6**)$(OTf)_2$	4.26	98	73	5.4	1
Cu(**S7**)$(OTf)_2$	7.81	75	64	1.2	0
Cu(**S7**)$(OTf)_2$	3.90	96	72	6.3	1
Cu(**S8**)$(OTf)_2$	7.52	29	100	0.5	3
Cu(**S8**)$(OTf)_2$	3.76	36	100	2.5	0
Cu(**S9**)$(OTf)_2$	9.43	37	100	0.4	2
Cu(**S9**)$(OTf)_2$	4.71	31	100	1.4	5

[a]conversion and selectivity determined by ^{1}H NMR spectroscopy. [b]ee determined by chiral HPLC. [c]Metal loading corresponds to the amount of metal

present in the heterogeneous catalyst used during the reaction. [d]TON is calculated with respect to 1 mole of metal being used.

Conditions: 200 or 100 mg catalyst, 1.0 mmol 4-nitrobenzaldehyde, 10 mmol nitromethane, 0.13 mmol triethylamine, reaction solvent is ethanol, room temperature, 24 h.

For the complexes of the ligands **S4**-**S7**, the conversions are excellent. However, the selectivities were poor due to the nitroaldol product reacting further, as previously discussed. In complete contrast, the enantiomeric excesses are very poor, with no enantioselectivity observed in most cases. This implies that in asymmetric catalysis, the reaction cannot be deemed as successful, as only a racemic mixture of products was obtained. A common method used to improve enantioselectivity is to reduce the reaction temperature, which was previously discussed in chapter one. This may also increase selectivity for the same reasons. The effect of temperature on the nitroaldol reaction will be examined in more detail in section 5.3.3.

The nitroaldol reaction was also performed using nitroethane and benzaldehyde as substrates, yielding a diastereomeric product as previously discussed in section 5.3.1.1. The results can be seen in table 5.3.7. The results of the heterogeneous catalysis are similar to that of the homogeneous catalysis described in section 5.3.1.1. The enantiomeric excesses observed here are significantly higher than the other heterogeneously catalysed nitroaldol reactions described. They are also significantly higher than that of the homogeneously catalysed nitroaldol reaction of the same substrates and reaction conditions. The specificity of catalysts in asymmetric synthesis was discussed at length in chapter one. This describes what is observed here – a particular set of similar heterogeneous catalysts have shown promising results in the catalysis of the nitroaldol reaction of nitroethane and benzaldehyde, at room temperature for 24 hours with 0.13 equivalents of triethylamine, specifically. If any of these factors were altered, the results completely change; the effect of basicity and reaction temperature will be discussed in more detail later.

Table 5.3.7 Results of the heterogeneously catalysed (silica based) nitroaldol reaction of nitroethane and benzaldehyde

Catalyst	Metal Loading[c] / 10^{-5} mol	Conv[a] / %	Selectivity[a] / %	TON[d] / × 10^5	de[a] / %	ee[b] / %
Cu(**S4**)$(OTf)_2$	8.48	84	48	1.2	6	13, 8
Cu(**S4**)$(OTf)_2$	4.24	94	49	5.2	13	0, 5
Cu(**S5**)$(OTf)_2$	7.95	72	48	1.1	11	22, 8
Cu(**S5**)$(OTf)_2$	3.98	78	49	4.9	6	37, 7
Cu(**S6**)$(OTf)_2$	8.52	65	47	0.9	12	34, 15
Cu(**S6**)$(OTf)_2$	4.26	75	47	4.1	7	7, 5
Cu(**S7**)$(OTf)_2$	7.81	33	48	0.5	8	54, 65
Cu(**S7**)$(OTf)_2$	3.90	30	50	2.0	14	46, 46
Cu(**S8**)$(OTf)_2$	7.52	58	100	1.0	#	57, 25
Cu(**S8**)$(OTf)_2$	3.76	12	100	0.8	10	63, 49
Cu(**S9**)$(OTf)_2$	9.43	44	100	0.5	#	0, 16
Cu(**S9**)$(OTf)_2$	4.71	7	100	0.3	#	46, 36

could not be determined due to broadness of resonance

[a]conversion, selectivity and de determined by ^{1}H NMR spectroscopy. [b]ee determined by chiral HPLC. [c]Metal loading corresponds to the amount of metal present in the heterogeneous catalyst used during the reaction. [d]TON is calculated with respect to 1 mole of metal being used.

Conditions: 200 or 100 mg catalyst, 1.0 mmol benzaldehyde, 10 mmol nitroethane, 0.13 mmol triethylamine, reaction solvent is ethanol, room temperature, 24 h.

The heterogeneous catalysts were also screened in the nitroaldol reaction of nitroethane and 4-nitrobenzaldehyde, the results of which can be seen in table 5.3.8. It should be noted that for catalysts Cu(**S8**)$(OTf)_2$ and Cu(**S9**)$(OTf)_2$, the conversions are much lower than that of the other similar heterogeneous catalysts. However, for these catalysts selectivity is 100 %, hence the conversions are to the nitroaldol product. However, these conversions are very low, and in combination with the poor enantioselectivities observed, these results show that these two catalysts are not effective in conjunction with these

particular substrates, in these reaction conditions. However, it has been observed that using the same catalysts, in changing substrates or reaction conditions (which will be discussed in more detail later), conversions and enantioselectivities can be significantly improved.

Table 5.3.8 Results of the heterogeneously catalysed (silica based) nitroaldol reaction of nitroethane and 4-nitrobenzaldehyde

Catalyst	Metal Loading[c] / 10^{-5} mol	Conv[a] / %	Selectivity[a] / %	TON[d] / × 10^5	de[a] / %	ee[b] / %
Cu(**S4**)$(OTf)_2$	8.48	89	51	1.2	19	2, 0
Cu(**S4**)$(OTf)_2$	4.24	96	51	5.3	11	0, 2
Cu(**S5**)$(OTf)_2$	7.95	98	47	1.6	19	1, 3
Cu(**S5**)$(OTf)_2$	3.98	94	48	5.9	12	1, 3
Cu(**S6**)$(OTf)_2$	8.52	92	48	1.3	19	2, 0
Cu(**S6**)$(OTf)_2$	4.26	92	48	5.1	20	2, 0
Cu(**S7**)$(OTf)_2$	7.81	88	48	1.4	17	3, 5
Cu(**S7**)$(OTf)_2$	3.90	79	49	5.2	20	2, 0
Cu(**S8**)$(OTf)_2$	7.52	14	100	0.2	61	3, 2
Cu(**S8**)$(OTf)_2$	3.76	12	100	0.8	92	3, 1
Cu(**S9**)$(OTf)_2$	4.71	65	100	2.9	24	9, 10

[a]conversion, selectivity and de determined by ^{1}H NMR spectroscopy. [b]ee determined by chiral HPLC. [c]Metal loading corresponds to the amount of metal present in the heterogeneous catalyst used during the reaction. [d]TON is calculated with respect to 1 mole of metal being used.

Conditions: 200 or 100 mg catalyst, 1.0 mmol 4-nitrobenzaldehyde, 10 mmol nitroethane, 0.13 mmol triethylamine, reaction solvent is ethanol, room temperature, 24 h.

The heterogeneous copper(II) system prepared using the "tether group" technique was also screened for the reaction of nitromethane and benzaldehyde. No conversion was observed. The analogous silsesquioxane-supported copper(II) complex, also prepared using the tether group technique, was also tested for this reaction, and gave no conversion.

5.3.2 Optimisation by Varying the Base

As previously mentioned, the presence of a base is crucial to the success of the nitroaldol reaction, as it deprotonates the nitroalkane, and is the first step of the mechanism. However, it has been shown by other research groups that if the ligand itself is basic enough to perform this role, the addition of extra base into the reaction is not necessary. The results shown in section 5.3.1.1 indicate that the basicity of the ligands within the complexes have an effect of the catalytic results, resulting in higher enantioselectivities with higher basicities. One explanation would be that the greater basicity allows the chiral ligand to participate more in this first stage of the catalytic process, thus having more influence over substrate, and improving enantioselectivity. This would suggest two things. Firstly, that the ligand is performing the deprotonation step, therefore in the absence of any additional base, conversion would still be observed. Secondly, on increasing the amount of additional achiral base, enantioselectivity would decrease dramatically, as there would be a greater proportion of this first step of the catalytic cycle that would be facilitated in an achiral manner. These two hypotheses will be discussed here.

Table 5.3.9. shows the results from varying the amount of triethylamine present in the nitroaldol reaction of nitromethane and benzaldehyde. The results clearly show that with greater amounts of triethylamine, substantial reductions in enantiomeric excesses are observed. This supports the results described in section 5.3.1.1, and the hypothesis discussed here, that with a greater contribution of an achiral base to the reaction, enantioselectivity is reduced. Conversions are significantly higher when a greater quantity of base is used, which is not surprising. On reducing the equivalents of triethylamine from 0.25 to 0.13, the conversions decreased from 59 % to 20 % when using the Cu(**4b**)$_2$(OTf)$_2$ complex. This huge difference in conversion suggests that an optimum amount of additional base must be added, in order to achieve good conversions and enantioselectivities. Incidently, when no triethylamine was added, conversions were observed (approximately 10 %). This suggests that although the ligand can perform the deprotonation step, it is not basic enough to avoid the use of additional base altogether.

Table 5.3.9 Results of the homogeneously catalysed nitroaldol reaction of nitromethane and benzaldehyde, with various quantities of triethylamine

Catalyst	Time / h	Triethylamine / mmol	Conv[a] / %	TON[c] / × 10^5	ee[b] / %
Cu(**2**)$_2$(OTf)$_2$	6	0.25	68	2.7	0
Cu(**3b**)$_2$(OTf)$_2$	6	0.25	10	0.4	60 (*S*)
Cu(**4b**)$_2$(OTf)$_2$	4	0.5	75	3.0	43 (*S*)
Cu(**4b**)$_2$(OTf)$_2$	6	0.25	59	2.4	68 (*S*)
Cu(**4b**)$_2$(OTf)$_2$	6	0.13	20	0.8	72 (*S*)
Cu(**5b**)$_2$(OTf)$_2$	4	0.5	71	2.8	37 (*S*)
Cu(**5b**)$_2$(OTf)$_2$	6	0.25	26	1.0	78 (*S*)
Cu(**17**)$_2$(OTf)$_2$	4	0.5	76	3.0	36 (*R*)

[a]conversion determined by ^{1}H NMR spectroscopy. [b]ee determined by chiral HPLC. [c]TON is calculated with respect to 1 mole of catalyst.

Conditions: 0.05 mmol catalyst, 1.0 mmol benzaldehyde, 10 mmol nitromethane, reaction solvent is ethanol, room temperature.

The base itself was also varied, in the nitroaldol reaction of nitromethane and benzaldehyde. The results can be seen in table 5.3.10. In general, the catalysis with triethylamine shows the lowest conversions and highest enantiomeric excesses. Of the three bases, triethylamine is the least basic, and so this supports the other observations that have been made with respect to basicity, as previously discussed. In general, there are no significant differences between the catalysis seen in the presence of diisopropylamine (DIPA) and 1-methyl pyrrolidine. The difference is basicity is relatively small, which could explain the similar catalytic results.

Table 5.3.10 Results of the catalysed nitroaldol reaction of nitromethane and benzaldehyde, with various bases

Catalyst	Triethylamine		DIPA		1-methyl pyrrolidine	
	Conv[a] / %	ee[b] / %	Conv[a] / %	ee[b] / %	Conv[a] / %	ee[b] / %
Cu(**3b**)$_2$(OTf)$_2$	90	60	93	39	78	12
Cu(**4b**)$_2$(OTf)$_2$	20	72	91	43	97	55
Cu(**5b**)$_2$(OTf)$_2$	26	78	90	9	84	37
Cu(**6b**)$_2$(OTf)$_2$	71	8	90	27	78	6
Cu(**8a**)(OTf)$_2$	12	8	100	2	60	2
Cu(**8b**)(OTf)$_2$	80	62	89	75	100	70
Cu(**16**)(OTf)$_2$	87	54	84	21	97	54
Cu(**16**)$_2$(OTf)$_2$	54	22	50	0	58	12
Cu(**18a**)(OTf)$_2$	25	46	20	37	20	46
Cu(**18b**)(OTf)$_2$	26	5	24	0	24	3
Cu(**S4**)(OTf)$_2$	95 (78 sel)	5	51	25	2	12

[a]conversion determined by ^{1}H NMR spectroscopy. [b]ee determined by chiral HPLC.

Conditions: For homogeneous catalysis, 0.05 mmol catalyst, for heterogeneous catalysis, 200 mg catalyst, 1.0 mmol benzaldehyde, 10 mmol nitromethane, 0.13 mmol base, reaction solvent is ethanol, room temperature, 6 h for homogeneous catalysis, 24 h for heterogeneous catalysis.

5.3.3 Optimisation by Varying the Temperature

As previously discussed, reducing the reaction temperature is a common technique used to improve enantioselectivity. This technique was employed in the research described here; the reaction temperature was reduced from 25 °C to 0 °C, for the combination of substrates previously described. Table 5.3.11 shows the results of the nitroaldol reaction of nitromethane and benzaldehyde.

Table 5.3.11 Results of the homogeneously catalysed nitroaldol reaction of nitromethane and benzaldehyde at 0 °C

Catalyst	Conv[a] / %	TON[c] / × 10^5	ee[b] / %
Cu(**3b**)$_2$(OTf)$_2$	90	3.6	75
Cu(**9a**)(OTf)$_2$ MeOH	35	1.4	34
Cu(**9a**)(OTf)$_2$ EtOH	0	0	-
Cu(**9a**)(OTf)$_2$ IPA	0	0	-
Cu(**9b**)(OTf)$_2$	25	1.0	0
Cu(**10a**)(OTf)$_2$	82	3.3	4
Cu(**10b**)(OTf)$_2$	94	3.8	82
Cu(**11b**)(OTf)$_2$	46	1.8	25
Cu(**13b**)(OTf)$_2$	94	3.8	80
Cu(**14b**)(OTf)$_2$	95	3.8	84
Cu(**17**)$_2$(OTf)$_2$	65	2.6	58

- when no conversion is observed, enantiomeric excess is not applicable

[a]conversion determined by ^{1}H NMR spectroscopy. [b]ee determined by chiral HPLC. [c]TON was calculated with respect to 1 mole of catalyst.

Conditions: 0.05 mmol catalyst, 1.0 mmol benzaldehyde, 10 mmol nitromethane, 0.13 mmol triethylamine, reaction solvent is ethanol (unless otherwise stated), room temperature, 6 h.

The enantiomeric excesses show a marked improvement on reducing the temperature. A decrease in conversion is observed, as expected. Although the results shown here do show the common reduction in conversion, the reduction is only mild in comparison to the dramatic increase in enantioselectivity.

Table 5.3.12 shows the results of reducing the temperature to 0 °C in the nitroaldol reaction of nitromethane and 4-nitrobenzaldehyde. In this case, although no significant changes in conversion are observed, no significant changes in enantioselectivity are seen either. This shows that even though many asymmetric catalytic processes benefit from a reduction in reaction temperature, there are exceptions. This also highlights the importance of tailoring the catalyst, substrates and reaction conditions very carefully and in conjunction with each other. This could be investigated further in future research. In addition, the

kinetics of the reaction could be investigated, as this could provide insight into the effect of temperature on the reaction, and why no significant changes in conversion and enantioselectivity are observed in these results.

Table 5.3.12 Results of the homogeneously catalysed nitroaldol reaction of nitromethane and 4-nitrobenzaldehyde at 0 °C

Catalyst	Conv[a] / %	TON[c] / × 10^5	ee[b] / %
Cu(**3b**)$_2$(OTf)$_2$	97	3.9	28
Cu(**9a**)(OTf)$_2$ MeOH	19	0.8	3
Cu(**9b**)(OTf)$_2$	98	3.9	15
Cu(**10b**)(OTf)$_2$	88	3.5	3
Cu(**11b**)(OTf)$_2$	84	3.4	1
Cu(**13b**)(OTf)$_2$	87	3.5	1
Cu(**14b**)(OTf)$_2$	84	3.4	1
Cu(**17**)$_2$(OTf)$_2$	88	3.5	36

[a]conversion determined by ^{1}H NMR spectroscopy. [b]ee determined by chiral HPLC. [c]TON was calculated with respect to 1 mole of catalyst.

Conditions: 0.05 mmol catalyst, 1.0 mmol 4-nitrobenzaldehyde, 10 mmol nitromethane, 0.13 mmol triethylamine, reaction solvent is ethanol (unless otherwise stated), room temperature, 6 h.

The results shown in table 5.3.13 correspond to the nitroaldol reaction of nitroethane and benzaldehyde at 0 °C. As seen with nitromethane and benzaldehyde, a significant increase in enantiomeric excess can be seen, along with an increase in diastereoselectivity at the lower temperature.

Table 5.3.13 Results of the homogeneously catalysed nitroaldol reaction of nitroethane and benzaldehyde at 0 °C

Catalyst	Conv[a] / %	TON[c] / × 10^5	de[a] / %	ee[b] / %
Cu(**3b**)$_2$(OTf)$_2$	60	2.4	23	6, 18
Cu(**9a**)(OTf)$_2$ MeOH	38	1.5	17	18, 21
Cu(**9b**)(OTf)$_2$	86	3.4	58	52, 12
Cu(**10b**)(OTf)$_2$	72	2.9	34	46, 30
Cu(**11b**)(OTf)$_2$	14	0.6	9	65, 1
Cu(**13b**)(OTf)$_2$	77	3.1	40	46, 28
Cu(**14b**)(OTf)$_2$	87	3.5	28	14, 9
Cu(**17**)$_2$(OTf)$_2$	64	2.6	30	35, 28

[a]conversion and de determined by ^{1}H NMR spectroscopy. [b]ee determined by chiral HPLC. [c]TON was calculated with respect to 1 mole of catalyst.

Conditions: 0.05 mmol catalyst, 1.0 mmol benzaldehyde, 10 mmol nitroethane, 0.13 mmol triethylamine, reaction solvent is ethanol (unless otherwise stated), room temperature, 6 h.

The reaction temperature was also reduced in the heterogeneous catalysis of the nitroaldol reaction of nitromethane and 4-nitrobenzaldehyde; the results can be seen in table 5.3.14. In the homogeneous catalysis of this particular reaction at reduced temperature, no significant improvement in enantioselectivity was observed. Similar behaviour is observed in the heterogeneous case. It was previously thought that a reduction in reaction temperature may also increase the selectivity to the desired product. This has been observed, as the selectivity for the desired nitroaldol product is now 100 %, for all of the catalysts tested. Therefore although the reduction in temperature has not improved the poor enantioselectivities, it has resulted in obtaining a purer product in general.

Table 5.3.14 Results of the heterogeneously catalysed nitroaldol reaction of nitromethane and 4-nitrobenzaldehyde at 0 °C

Catalyst	Metal Loading[c] / × 10^{-5} mol	Conv[a] / %	TON[d] / × 10^5	ee[b] / %
Cu(**S4**)$(OTf)_2$	4.24	61	3.4	2
Cu(**S5**)$(OTf)_2$	3.98	90	5.7	2
Cu(**S6**)$(OTf)_2$	4.26	32	1.8	1
Cu(**S7**)$(OTf)_2$	3.90	79	5.2	0
Cu(**S8**)$(OTf)_2$	3.76	19	1.3	7
Cu(**S9**)$(OTf)_2$	4.71	25	1.1	0

[a]conversion determined by ^{1}H NMR spectroscopy. [b]ee determined by chiral HPLC. [c]Metal loading corresponds to the amount of metal present in the heterogeneous catalyst used during the reaction. [d]TON is calculated with respect to 1 mole of metal being used.

Conditions: 100 mg catalyst, 1.0 mmol 4-nitrobenzaldehyde, 10 mmol nitromethane, 0.13 mmol triethylamine, reaction solvent is ethanol, room temperature, 24 h.

5.4 Catalysing the Asymmetric Aldol Reaction

The aldol reaction was discussed in depth in chapter one. It is a widely used carbon-carbon bond forming reaction in organic synthesis. The aldol reaction is very similar to the nitroaldol reaction, which has been discussed at length in section 5.3. The metal-catalysed reaction mechanism for the aldol reaction can be seen in fig. 5.4.1.

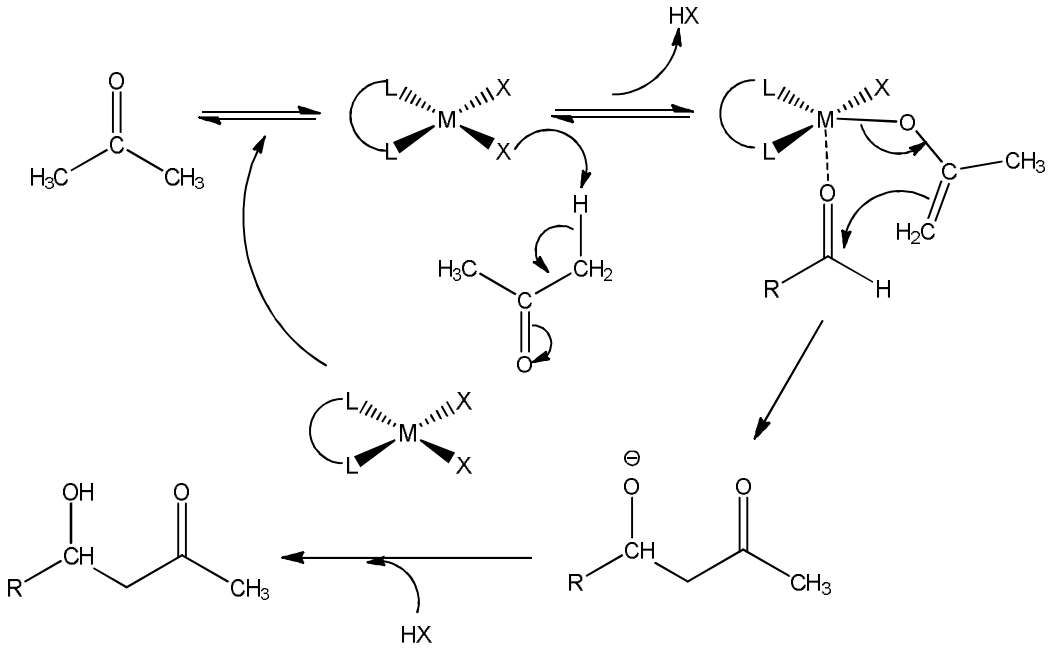

Fig. 5.4.1 Catalytic mechanism of the metal-catalysed aldol addition reaction

Metal-free catalysts have been extensively employed in this asymmetric reaction, more specifically derivatives of proline.[43-49] In metal-free catalysis, the aldol reaction is typically either base-catalysed or acid catalysed. Where metal-free catalysis has been reported, there will be a Bronsted base or acid group within the catalyst. The base- and acid-catalysed metal-free reaction mechanisms can be seen in fig. 5.4.2.

Base Catalysed:

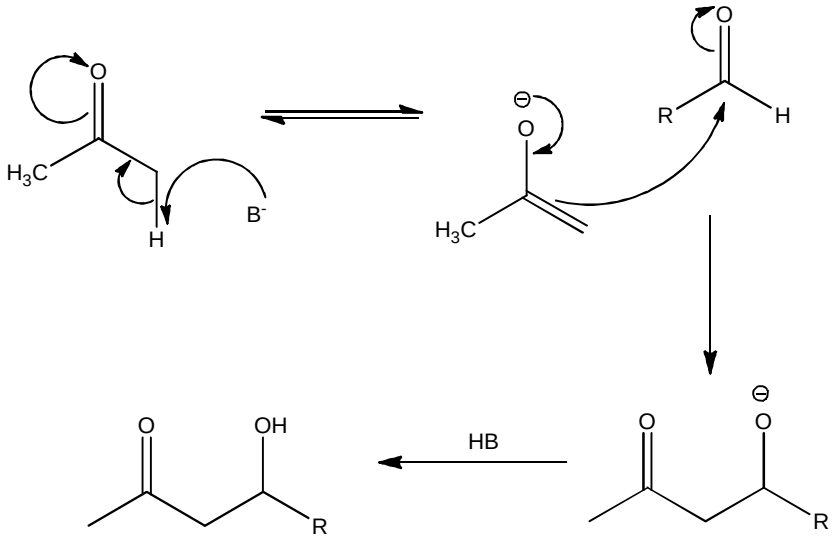

Acid Catalysed:

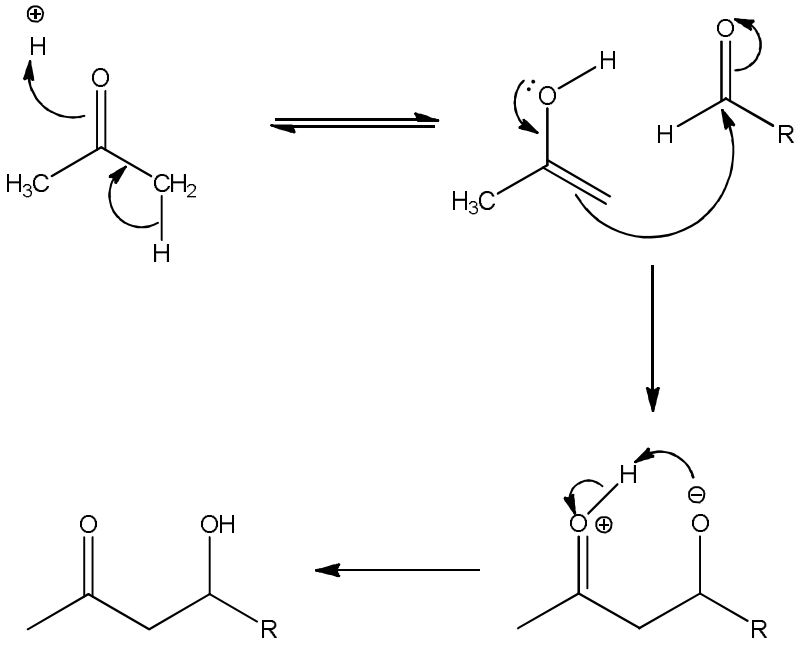

Fig. 5.4.2 Catalytic mechanisms of the base and acid catalysed aldol addition reaction

There is often a competing reaction – known as the aldol condensation – occurring simultaneously. It involves the aldol addition product reacting further. It is widely accepted that the aldol addition and aldol condensations occur alongside each other, although in many circumstances, one of these products is favoured depending on the catalyst used and the reaction conditions employed. Therefore in analysing the products of an aldol reaction, often either the products from the addition or condensation reaction are observed – it is uncommon for both sets of products to be observed in significant quantities. The reaction mechanism for the aldol condensation can be seen in fig. 5.4.3.

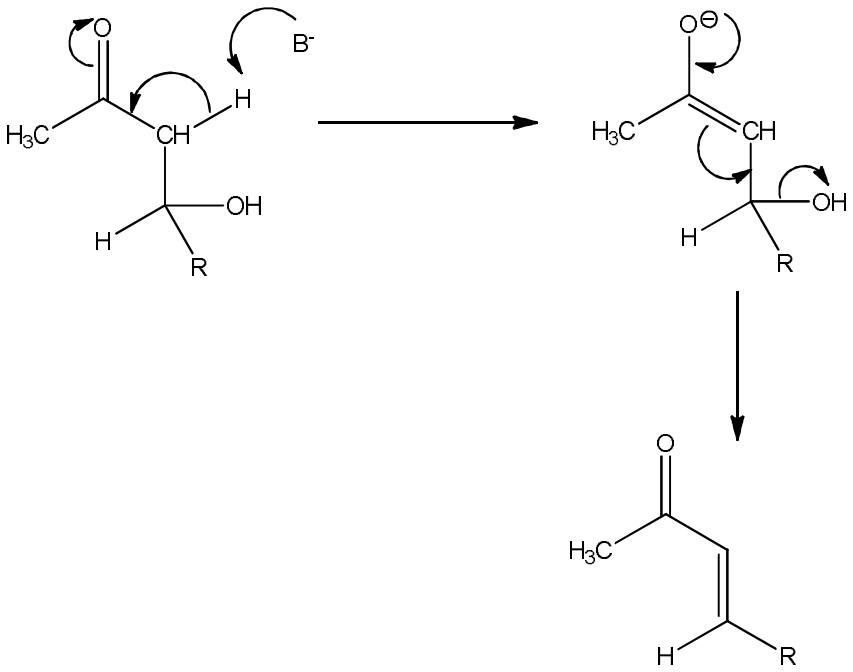

Fig. 5.4.3 Mechanism of the aldol condensation reaction

A number of homogeneous and heterogeneous ligands and some of their copper(II) complexes were used to catalyse the asymmetric aldol reaction of acetone and benzaldehyde, either in the presence or absence of additional quantities of acid. The results will be discussed herein.

The ligands **3b-7b** were used as catalysts in the asymmetric aldol reaction of benzaldehyde and acetone, either in the presence or absence of acetic acid (20 mol %). The reaction scheme for this reaction is given in fig. 5.4.4.

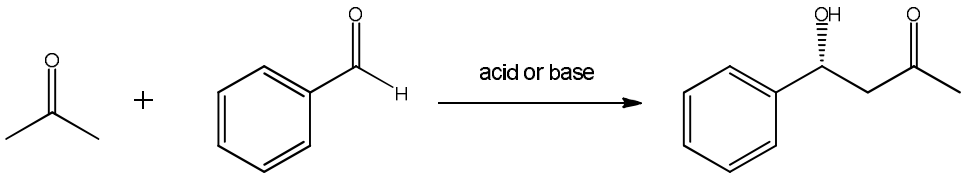

Fig. 5.4.4 Reaction scheme of the aldol addition reaction of acetone and benzaldehyde

Post-reaction, the reaction mixture was analysed by ^{1}H NMR spectroscopy and high performance liquid chromatography (HPLC). Where the amine ligands **3b-7b** are used, no reaction was observed. The ^{1}H NMR spectra indicated the sole presence of benzaldehyde and ligand.

When the imine ligands **3a-7a** were screened, the results were very different. The results of the catalysis with ligands **3a-7a** in the absence of additional acetic acid, over 72 h are given in table 5.4.1.

Table 5.4.1 Results of the aldol addition reaction of acetone and benzaldehyde, catalysed by homogeneous imine ligands, in the absence of acetic acid

Catalyst	Conv[a] / %	Selectivity[a] / %	ee[b] / %
3a	19	100	51
4a	36	44	31
5a	21	40	3
6a	21	35	12
7a	0	-	-

- with no conversion, selectivity and enantiomeric excess are not applicable

[a]conversion and selectivity determined by ^{1}H NMR spectroscopy. [b]ee determined by chiral HPLC.

Conditions: 1.0 mmol catalyst, **5**.0 mmol benzaldehyde, 10 ml acetone, room temperature, 72 h.

Ligand **7a** showed no conversion. Of the five ligands, **7a** is the least basic (at the nitrogen atoms). For the remaining ligands, conversions were low. The interesting feature of the results is selectivity. Fig. 5.4.5 shows the ^{1}H NMR spectrum of the products of the reaction catalysed by **4a**. This NMR spectrum is typical for ligands **4a-6a** under these reaction conditions.

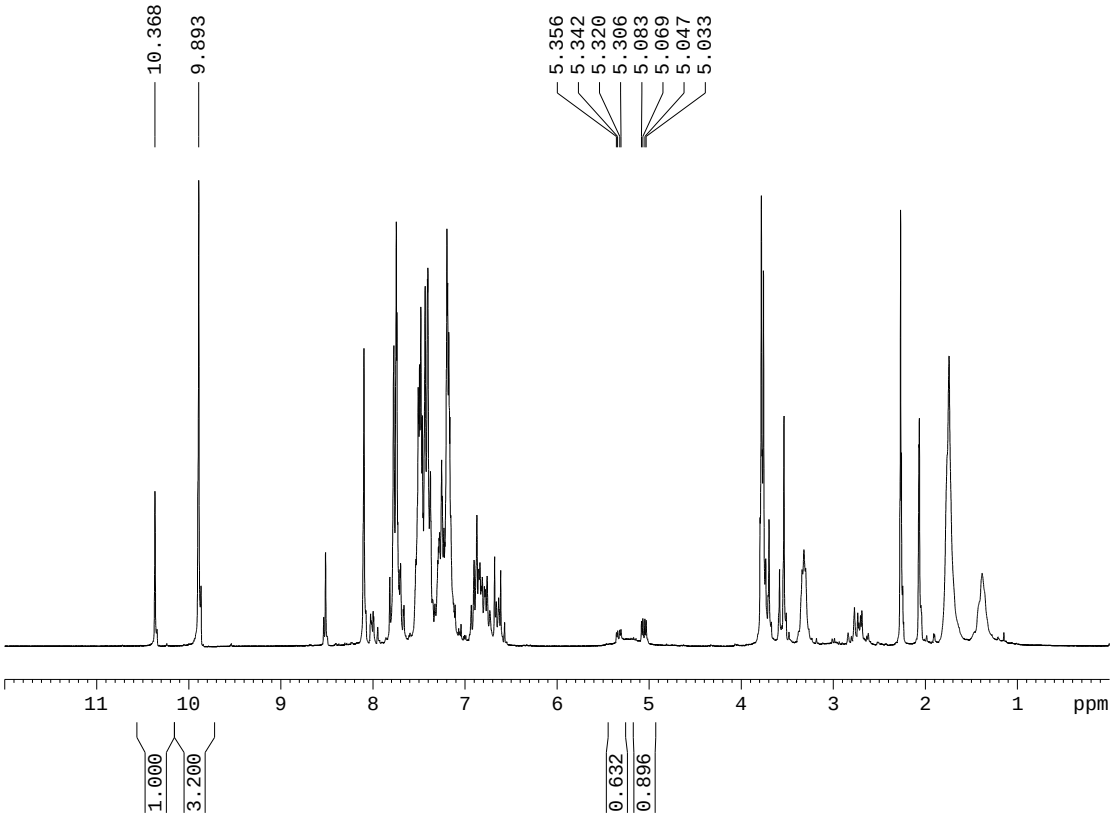

5.4.5 ^{1}H NMR spectrum of the products catalysed by ligand 4a

The resonance at 9.89 ppm corresponds to benzaldehyde (starting material), and the resonance at 5.05 ppm corresponds to the product of the aldol addition reaction. However, there is a significant resonance at 10.27 ppm, and an additional resonance at 5.34 ppm. As previously mentioned, the aldol condensation often competes with the aldol addition reaction. The product of the aldol condensation contains a ketone and an alkene, with the alkene group in the β-position with respect to the ketone. The resonance at 5.34 is more than likely due to this alkene group. It is entirely feasible that the aldol condensation product could break down at the alkene bond (which may be catalysed by the ligand), yielding an aldehyde (most probably ethanal). As previously mentioned, usually either the aldol addition or condensation reaction is much more favoured than the other – it is rare to see significant quantities of product from both reactions. Unfortunately, ethanal has a low boiling point, therefore it is likely that in removing the acetone from the reaction mixture post-reaction, the ethanal was also removed. Hence, quantifying the proportion of condensation product that decomposes is not possible. Also, the resonances at 5.05 and 5.34 would be compared to quantify the relative amounts of aldol addition and condensation

products, but if a significant proportion of the condensation product is decomposing (which cannot be quantified), this comparison between resonances would yield errors in the selectivity.

This finding is important, as there is some ambiguity regarding the aldol condensation reaction.[50] Uncertainty surrounds whether the condensation reaction is occurring alongside the addition reaction, or if the addition reaction occurs and then the condensation reaction occurs as a "further reaction" of the addition product.[51] This is often difficult to investigate, as significant amounts of both products are not usually observed. This has deeper implications also, as the kinetics of the reaction cannot be fully investigated and an accurate mechanism determined, until the nature of the condensation reaction is understood. Schmid observed significant quantities of the two products by ^{1}H NMR spectroscopy, and hence investigated the kinetics of the catalytic process.[51] It was determined that the condensation reaction occurs as a competing reaction.

The ligands **3a-7a** were also screened for the aldol reaction in the presence of additional acetic acid, over 72h. On analysing the products with ^{1}H NMR spectroscopy, the spectra indicated that the ligands had broken down. The imine bonds present in the ligands are very reactive, and so the decomposition of the ligands although unexpected, is not unfeasible. The spectra did not show a peak due to benzaldehyde. However, this does not imply 100 % conversion has been achieved. On the decomposition of the ligand, the benzaldehyde may have reacted with resulting compounds generated. The exception to this behaviour was ligand **7a**, where the NMR spectrum showed resonances corresponding to benzaldehyde and ligand **7a**, intact. This may imply that the decomposition of the ligand is the catalyst's active form.

The heterogeneous ligands **S4-S7** and **S12** were also screened for the aldol reaction, both in the presence and absence of acetic acid, for 72h. Where no additional acid was present, no reaction was observed. A reaction was observed however when acetic acid was present; the results can be seen in table 5.4.2.

Table 5.4.2 Results of the aldol addition reaction of acetone and benzaldehyde, catalysed by heterogeneous(silica-supported) imine ligands, in the presence of acetic acid

Catalyst	Conv[a] / %	ee[b] / %
S4	42	49
S5	54	58
S6	42	74
S7	58	64
S12	0	-

- with no conversion, selectivity and enantiomeric excess are not applicable

[a]conversion determined by ^{1}H NMR spectroscopy. [b]ee determined by chiral HPLC.

Conditions: 1.0 mmol catalyst, **5**.0 mmol benzaldehyde, 10 ml acetone, 1.0 mmol glacial acetic acid, room temperature, 72 h.

The conversions and enantioselectivities are good. Ideally, the enantiomeric excesses would be higher for a successful asymmetric catalytic reaction. Usually, the reaction temperature would be reduced to achieve this, as previously discussed. However, often a decrease in conversion accompanies this. The conversions here are not high enough for a drop in conversion to be an acceptable compromise to achieve greater enantioselectivity, especially as the reaction time is already long (72 hours), with large amounts of catalyst being used. This is a common problem within the asymmetric catalysis of aldol reactions, which has been previously discussed in chapter one.[43-47] The acid was changed from acetic acid the trifluoroacetic acid (TFA), in order to observe the effect of the acid on catalytic results. However, no reaction was observed. TFA is a much stronger acid than acetic acid. It is feasible that rather than catalysing the aldol reaction, it interacted with the ligand in some way, either through reaction or binding to the silica support. The ligands were also screened for the aldol reaction with additional base, rather than acid. The base used for this purpose was triethylamine, and the reaction was allowed to proceed for 5 hours. However, only low conversions were observed (5 %) for ligands **S4**-**S7**, with no reaction occurring for ligand **S12**. Again, the base may have bound to the silica support rather contributing towards the aldol reaction.

Copper(II) complexes have also been widely used in the asymmetric catalysis of the aldol reaction.[52-56] A selection of the homogeneous and heterogeneous copper(II) complexes described in chapters three and four respectively were used to catalyse the aldol reaction. However, despite using relatively large amounts of catalyst, either in the presence or absence of acid, no reaction was observed.

5.5 Catalysing the Asymmetric Allylic Oxidation Reaction

The asymmetric allylic oxidation of alkenes is a useful reaction in organic synthesis. Numerous groups have carried out catalytic research with this reaction. For example, Katsuki used copper(II) trisoxazolines,[57] Gokhale used copper(I) bisoxazolines[58] as did Andrus,[59] and Ramalingam used copper bisimidazolines.[60] An example of the reaction scheme can be seen in fig. 5.5.1.[61]

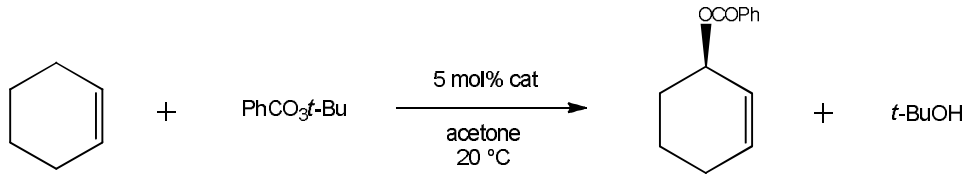

Fig. 5.5.1 Reaction scheme of the allylic oxidation of cyclohexene

Commonly, copper(I) is used to catalyse this reaction, although it is not unheard of for copper(II) to be an effective catalyst for the allylic oxidation. Following the success of other groups in this area, a number of the homogeneous complexes reported in chapter three were screened in this reaction. Cu(**9a**)$(OTf)_2$ prepared in methanol, ethanol and ispropanol, Cu(**9b**)$(OTf)_2$ and Cu(**12a**)$(OTf)_2$ were used as catalysts in the allylic oxidation of cyclohexene, using the same oxidant (*tert*-butyl perbenzoate), stoichiometries and reaction conditions as Tan.[61] The products were analysed using gas chromatography-mass spectrometry (GC-MS), due to problems encountered in the work-up. A typical GC spectrum is shown in fig. 5.5.2.

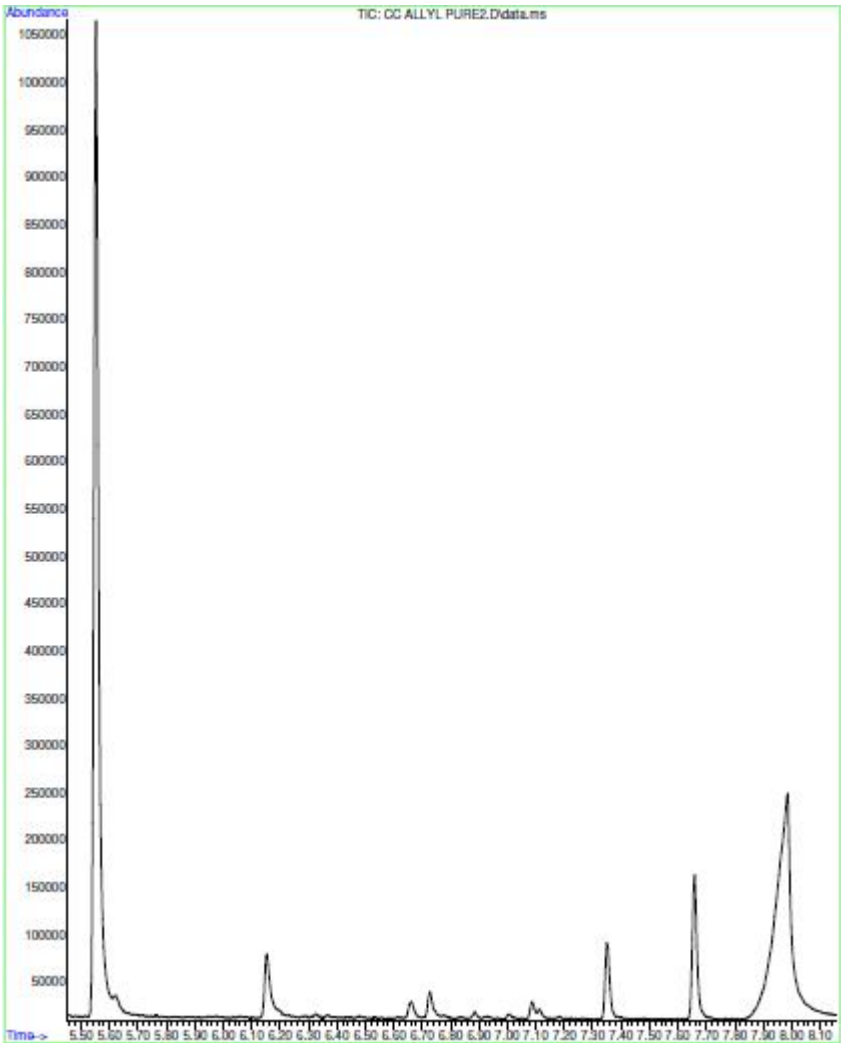

Fig. 5.5.2 GC spectrum of the allylic oxidation of cyclohexene using Cu(9b)$(OTf)_2$ as a catalyst, tert-butyl perbenzoate as an oxidant, at 5 min reaction time

The major peak at approximately 5.55 min corresponds to 2,5-hexanedione. This suggests that a ring-opening reaction has occurred, and that the reaction has been over-oxidised. The other peaks are due to various other by-products of the oxidation of cyclohexene or breakdown products of *tert*-butyl perbenzoate, for example the peak at 6.15 min corresponds to phenol, the peak at 7.35 min corresponds a methyl ester of benzoic acid, the peak at 7.66 min corresponds to 1-(cyclohex-1-en-1-yl)propan-2-one and the peak at 7.95 min corresponds to benzoic acid. Crucially, there is no peak that corresponds to the starting material, which suggests that a full conversion has been achieved, but with low selectivity. The reaction is complete within five minutes – the spectrum seen in fig. 5.5.2 was obtained five minutes after adding the oxidant to the reaction mixture, and

the peaks observed and their relative intensities do not change over 48 hours of reaction time.

If the reaction is occurring very quickly and the starting material being over-oxidised, the obvious factor in the reaction to change would be the oxidant. However, the oxidants which were weaker than *tert*-butyl perbenzoate and suitable for this reaction were alkali-metal nitrates, such as potassium nitrate. Other oxidants which were weaker than *tert*-butyl perbenzoate were transition metal-based. This would have been unsuitable, because if successful catalysis had occurred, it would have been unknown how the reaction was taking place, and what was actually catalysing the reaction.

Potassium nitrate requires the presence of water to dissolve. However, this was not possible with the allylic oxidation of cyclohexene; even with the addition of relatively small amounts of water, the cyclohexene precipitated. And so potassium nitrate was suspended in the reaction mixture, which was refluxed at 50 °C for 96 hours. No conversion was observed, which is likely to be due to the oxidant being insoluble. It was concluded that the asymmetric catalysis of the allylic oxidation of cyclohexene using the combination of catalyst, oxidant and reaction conditions described here was unsuccessful with the catalysts described.

If future research were to be carried out with regards to this organic transformation, the amount of oxidant used with respect to the amount of substrate could be reduced.

5.6 Catalysing the Asymmetric Epoxidation Reaction

As previously discussed in chapter one, the ligand design of many of the ligands described here was based on Jacobsen's ligand.[62] Jacobsen had great success in catalysing a variety of asymmetric transformations, but the reaction that he was most famous for contributing to was the asymmetric epoxidation reaction. The

majority of this catalysis was performed using manganese(III) and chromium(III) complexes of this ligand set.[19,63-65] Other research groups have built on the success of Jacobsen's work, again using manganese and chromium complexes.[66-67] However, there are not as many examples of the use of titanium(IV) complexes in conjunction with Jacobsen's ligand.[68] For this reason, Ti(**7b**)(O^iPr)$_2$ and Ti(**S12**)(O^iPr)$_2$ complexes were used to catalyse the asymmetric epoxidation of styrene. The corresponding reaction scheme can be seen in fig. 5.6.1.

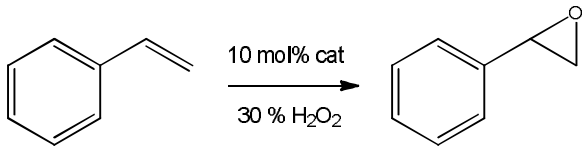

Fig. 5.6.1 Reaction scheme of the epoxidation of styrene

The products of the reaction was analysed by ^{1}H NMR spectroscopy. Where Ti(**7b**)(O^iPr)$_2$ was used as a catalyst, the NMR spectrum indicated that the reaction was being overcatalysed. Encouragingly, no styrene was observed in the spectrum, however, multiple products were observed. It is likely that the epoxide was formed, and then a ring-opening reaction occurred. There is water present due to the hydrogen peroxide being present as part of a 30 % aqueous solution, which in the presence of titanium have catalysed the ring opening of the product. In addition, the oxidation of the ring-opened product was observed, which is not surprising given that hydrogen peroxide is such a strong oxidant. Many of the oxidants that could be used in epoxidations exist as part of an aqueous solution. There are weaker oxidants such as potassium nitrate, but water is often required to encourage these oxidants to dissolve. Hence, it was decided that this catalyst was unsuitable for use in the asymmetric epoxidation reaction.

In contrast, the NMR spectrum of the products of the heterogeneous Ti(**S12**)(O^iPr)$_2$ catalysed reaction showed no reaction whatsoever. The aim of this research in general was to prepare catalysts for use in a variety of asymmetric organic transformations. In terms of the epoxidation reactions reported here, the heterogeneous catalysts described in herein are unsuitable, as no conversion was observed. Changing the oxidant, solvent or reaction

temperature may improve this, but it is unlikely that a significant enough increase in conversion will be observed to class this reaction as being a success.

5.7 Catalysing the Stereoselective Polymerisation of *rac*-lactide

The ring opening polymerisation of *rac*-lactide is of particular interest currently, as polylactic acid (PLA) is a suitable replacement for many of the plastic materials used today, which is also obtained from a sustainable source. In the past, plastics have been prepared using materials from fossil fuels, the sources of which are now limited.[69] In 2007, the waste plastic from consumer use was estimated at 24.6 million tonnes across the EU, according to PlasticsEurope.[69] A considerable proportion of this plastic is deposited in landfill, where it remains for hundreds of years. PLA is biodegradable,[70-72] so it will decompose more rapidly than many other plastics, which is better for the environment in terms of landfill. Fig. 5.7.1 shows *rac*-lactide.

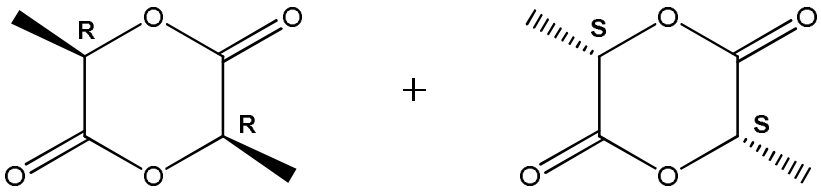

Fig. 5.7.1 *rac*-lactide

The stereochemistry of PLA is influential in its mechanical and physical properties, as well as the rate of degradation.[70] In particular, isotactic PLA is favourable, as the mechanical and physical properties are the most preferable for commercial applications, such as packaging. Especially if PLA is to be used as a replacement for plastics such as polyethylene and polypropylene, as the properties of isotactic PLA match these plastics more so than atactic PLA, for example.[73-75] Isotactic PLA is shown in fig. 5.7.2, along with heterotactic and atactic PLA, the other varieties of PLA obtainable from *rac*-lactide.

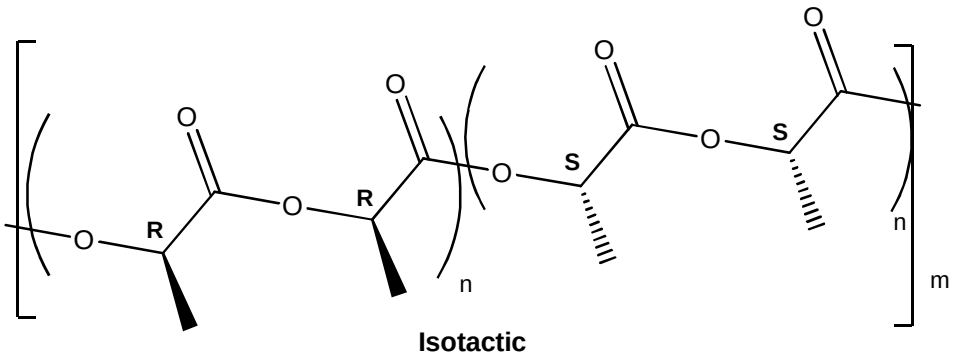

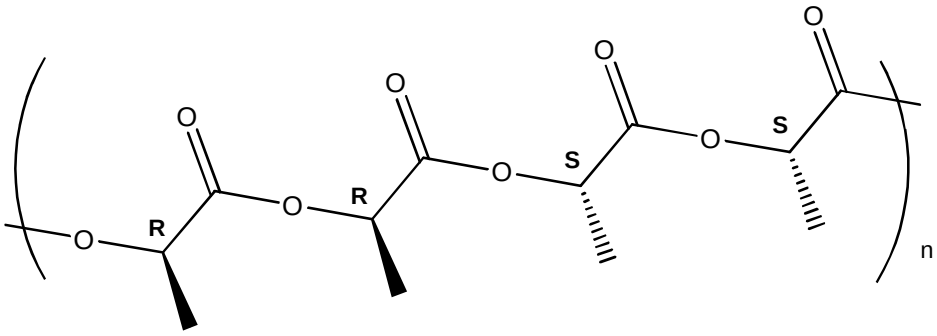

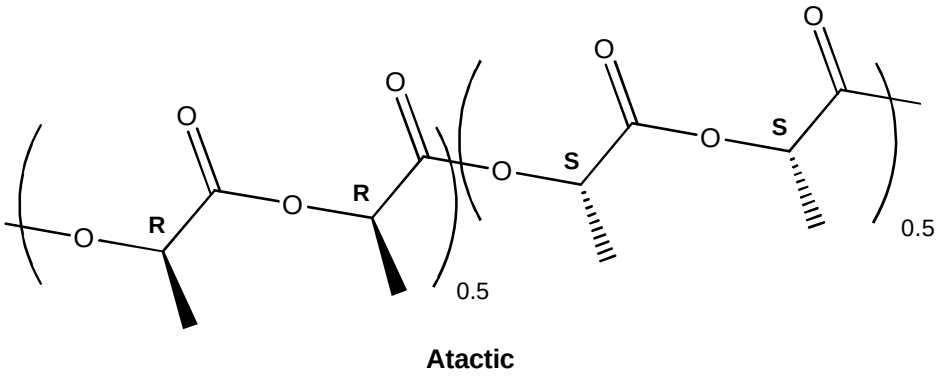

Fig. 5.7.2 Isotactic, heterotactic and atactic PLA, produced from *rac*-lactide

Various metal-catalysts have been employed in the stereoselective ring opening polymerisation of PLA. Such catalysts have involved Zn(II)[70,76-78], Al(III),[79-85] Ca(II),[86] Mg(II),[70,76] Ba(II),[87] lanthanides[88-89] and group IV metals,[90-105] i.e. Ti(IV), Zr(IV) and Hf(IV). Polymerisations are commonly performed under melt or solution conditions, with the most successful results (in terms of conversion, M_n and tacticity – either isotactic or heterotactic) observed under melt conditions.

The homogenous and heterogeneous titanium(IV) and zirconium(IV) complexes described in chapters three and four respectively were used to catalyse the stereoselective ring opening polymerisation of *rac*-lactide. The results from the homogeneously catalysed polymerisation under melt conditions can be seen in table 5.7.1.

Table 5.7.1 Results of the homogeneously catalysed polymerisation of *rac*-lactide, under melt conditions

Catalyst	M_n[a]	Conv[b] / %	PDI[a]	P_r[c]
Ti(**7b**)(O^iPr)$_2$	24220	100	1.22	0.50
Ti(**22**)(O^iPr)$_2$	41165	100	1.63	0.54
Ti(**23**)(O^iPr)$_2$	16774	100	1.06	0.48
Zr(**7b**)(O^iPr)$_2$	23452	100	1.49	0.42
Zr(**22**)(O^iPr)$_2$	29285	100	1.80	0.50
Zr(**23**)(O^iPr)$_2$	5445	7	1.28	0.29

[a]determined by GPC. [b]determined by ^{1}H NMR spectroscopy. [c]determined from ^{1}H NMR for analysis of the methane resonance of the ^{1}H NMR spectrum.

Conditions: 0.02 mmol catalyst, 6.9 mmol recrystallised *rac*-lactide, 130 °C, 2h

The results show high M_n values on the use of all catalysts with the exception of Zr(**23**)(O^iPr)$_2$, which still indicates the formation of a polymer; however with the other catalysts, the chain length of the PLA is significantly greater. Of the titanium(IV) and zirconium(IV) catalysts, those containing the electron withdrawing Cl substituents gave the greatest M_n value. The lowest M_n values were provided by the catalysts containing the electron donating *t*-Bu groups. Significantly higher PDI values were observed with the Ti(**22**)(O^iPr)$_2$ and Zr(**22**)(O^iPr)$_2$ catalysts. This indicates that the chain lengths of the polymer were not as uniform as with the other catalysts tested. This may be due to the polymerisation occurring so rapidly that the polymerisation was not as controlled, yielding higher PDIs. The lowest PDI values were observed with the Ti(**23**)(O^iPr)$_2$ and Zr(**23**)(O^iPr)$_2$, which also had the lowest M_n values. This supports the explanation of higher PDIs being due to a more rapid, less controlled polymerisation, as a slower, more controlled polymerisation would yield lower PDIs, as had been observed.

The P_r values indicate the probability that the PLA is heterotactic in character. A P_r value of 1 indicates that the PLA is perfectly heterotactic, and a P_r value of 0 indicates that the PLA is perfectly isotactic in character. A P_r value of 0.5 indicates that the PLA is atactic. The P_r values shown in table 5.7.1 indicate that all of the PLA is atactic in character, with the exception of the PLA produced with Zr(**23**)(O^iPr)$_2$, which is more isotactic in character. However, the PLA produced in this case was not high molecular weight, relative to the other polymers, due to the conversion being poor. It may be the case that if a higher conversion was observed, the P_r value would have increased. In all other cases a P_r value of 0.5 was observed indicating no chiral induction occurs during the polymerisation.

These catalysts were also used to catalyse the polymerisation of *rac*-lactide under solution conditions. The results can be seen in table 5.7.2.

Fig. 5.7.2 Results of the homogeneously catalysed polymerisation of *rac*-lactide, under solution conditions

Catalyst	M_n[a]	Conv[b] / %	PDI[a]
Ti(**7b**)(O^iPr)$_2$	-	0	-
Ti(**22**)(O^iPr)$_2$	#	13	#
Ti(**23**)(O^iPr)$_2$	-	0	-
Zr(**7b**)(O^iPr)$_2$	-	0	-
Zr(**22**)(O^iPr)$_2$	411	28	1.19
Zr(**23**)(O^iPr)$_2$	-	0	-

- GPC not performed, no conversion

GPC showed no polymer

[a]determined by GPC. [b]determined by ^{1}H NMR spectroscopy.

Conditions: 0.02 mmol catalyst, 2.3 mmol recrystallised *rac*-lactide, toluene, 80 °C, 2h

The conversions observed under solution conditions were poor. The only catalysts that showed conversion were Ti(**22**)(O^iPr)$_2$ and Zr(**22**)(O^iPr)$_2$, which were the most active catalysts under melt conditions. However, analysis by Gel

Permeation Chromatography (GPC) revealed that polymeric material was not present, and only oligomeric material was observed.

The heterogeneous titanium(IV) and zirconium(IV) systems were also used to catalyse the polymerisation of *rac*-lactide. The results of the polymerisation under melt conditions are shown in table 5.7.3.

Table 5.7.3 Results of the heterogeneously catalysed polymerisation of *rac*-lactide, under melt conditions

Catalyst	M_n[a]	Conv[b] / %	PDI[a]
Ti(**S12**)(O^iPr)$_2$	6355	100	1.62
Zr(**S12**)(O^iPr)$_2$	#	14	#

GPC showed no polymer

[a]determined by GPC. [b]determined by ^{1}H NMR spectroscopy.

Conditions: 50 mg catalyst, 6.9 mmol recrystallised *rac*-lactide, 130 °C, 2h

Polymeric material was only observed when the heterogeneous titanium(IV) system was used to catalyse the polymerisation. GPC analysis revealed an M_n value of 6355 g mol^{-1}, which was much lower than has previously been observed under these conditions. In addition, 100 % conversion was observed. This indicates that although all of the monomeric *rac*-lactide has reacted, this catalyst encourages a shorter chain length than the other catalysts observed. This may be due to the acidic nature of the support terminating the polymer before the chains can grow significantly. This is not particularly useful for the applications previously described.

These heterogeneous systems were also used to catalyse the polymerisation of *rac*-lactide under solution conditions. The results can be seen in table 5.7.4.

Table 5.7.4 Results of the heterogeneously catalysed polymerisation of *rac*-lactide, under solution conditions

Catalyst	M_n[a]	Conv[b] / %	PDI[a]
Ti(**S12**)(O^iPr)$_2$	476	35	1.58
Zr(**S12**)(O^iPr)$_2$	-	0	-

- GPC not performed, no conversion

[a]determined by GPC. [b]determined by ^{1}H NMR spectroscopy.

Conditions: 50 mg catalyst, 2.3 mmol recrystallised *rac*-lactide, toluene, 80 °C, 2h

No conversion was observed when Zr(**S12**)(O^iPr)$_2$ was used as a catalyst. In the case of Ti(**S12**)(O^iPr)$_2$, analysis by GPC revealed that polymeric material was not present. In general, the homogeneous catalysts have been much more successful in the polymerisation of *rac*-lactide than the heterogeneous catalysts.

5.8 Concluding Remarks

A number of the homogeneous complexes described in chapter three have been used to catalyse a variety of asymmetric transformations, with varying degrees of success. The greatest success has been observed in the hydrogenation of ketones, the nitroaldol reaction and the aldol reaction. The results are supported by the catalytic mechanisms that have previously been established with regards to these reactions. In addition, these results show promise for further development of the catalysis of these reactions, in order to improve the impressive results that have already been observed. Of particular importance would be to investigate the kinetics of the catalytic reactions. By assessing the kinetics, information regarding the catalytic mechanism, in particular the rate determining step and hence the behaviour of the catalyst, can be uncovered. With this information, future research can be focussed on developing the catalysts to yield improvements specifically at this point in the catalytic mechanism, which will then give rise to dramatic improvements in catalytic performance.

From the catalytic results described here, it is not practical to select which catalysts showed the best performance. It was found that for each organic transformation investigated, on varying the substrate, reagents and reaction conditions, catalytic performance was greatly affected. For the purposes of future research, it would be more practical to take the organic transformations where the strongest catalytic results were observed in general, and then assess which catalysts to optimise to suit the substrates and preferred reaction conditions chosen. This conclusion is common in the area of asymmetric catalysis, as was discussed at length during chapter one. The performance of a catalyst often varies according to the substrates and reaction conditions employed.

As previously discussed, the heterogeneous catalysis described here should be viewed with a reflective nature. Thus any future research in this area should firstly focus on characterising these heterogeneous complexes in greater depth. Having said this, some promise has been shown in the heterogeneous catalysts described here, particularly in the asymmetric hydrogenation and nitroaldol reactions. Future research with respect to the heterogeneous catalysis could also involve the use of different supports, such as zeolites, carbon and polymers.

5.9 References

(1) Knowles, W. S.; Sabacky, M. J. *Chem. Commun.* **1968**, 1445.

(2) Fan, Q. H.; Li, Y. M.; Chan, A. S. C. *Chem. Rev.* **2002**, *102*, 3385.

(3) Osborn, J. A.; Jardine, F. H.; Young, J. F.; Wilkinso.G *Journal of the Chemical Society a -Inorganic Physical Theoretical* **1966**, 1711.

(4) Miyashita, A.; Yasuda, A.; Takaya, H.; Toriumi, K.; Ito, T.; Souchi, T.; Noyori, R. *J. Am. Chem. Soc.* **1980**, *102*, 7932.

(5) Ohta, T.; Takaya, H.; Kitamura, M.; Nagai, K.; Noyori, R. *J. Org. Chem.* **1987**, *52*, 3174.

(6) Ohta, T.; Takaya, H.; Noyori, R. *Inorg. Chem.* **1988**, *27*, 566.

(7) Kitamura, M.; Kasahara, I.; Manabe, K.; Noyori, R.; Takaya, H. *J. Org. Chem.* **1988**, *53*, 708.

(8) Kitamura, M.; Tokunaga, M.; Ohkuma, T.; Noyori, R. *Tetrahedron Lett.* **1991**, *32*, 4163.

(9) Fuentes, J. A.; France, M. B.; Slawin, A. M. Z.; Clarke, M. L. *New J. Chem.* **2009**, *33*, 466.

(10) Ikariya, T.; Blacker, A. J. *Accounts of Chemical Research* **2007**, *40*, 1300.

(11) Noyori, R.; Hashiguchi, S. *Accounts of Chemical Research* **1997**, *30*, 97.

(12) Song, C. E.; Lee, S. G. *Chem. Rev.* **2002**, *102*, 3495.

(13) David, J. M., Wenbin, L. *Angew. Chem.-Int. Edit.* **2008**, *47*, 6229.

(14) Brethon, A., Moreau, J. J. E., Man, M. W. C. *Tetrahedron: Asymmetry* **2004**, *15*, 495.

(15) Jones, M. D.; Raja, R.; Thomas, J. M.; Johnson, B. F. G.; Lewis, D. W.; Rouzaud, J.; Harris, K. D. M. *Angew. Chem.-Int. Edit.* **2003**, *42*, 4326.

(16) James, B. R., Pacheco, A., Rettig, S. J., Thorburn, I. S., Ball, R. G., Ibers, J. A. *Journal of Molecular Catalysis* **1987**, *41*, 147.

(17) Mestroni, G., Zassinovich, G., Camus, A. *J. Organomet. Chem.* **1977**, *140*, 63.

(18) Clapham, S. E., Hadzovic, A., Morris, R. H. *Coord. Chem. Rev.* **2004**, *248*, 2201.

(19) Jacobsen, E. N.; Zhang, W.; Muci, A. R.; Ecker, J. R.; Deng, L. *J. Am. Chem. Soc.* **1991**, *113*, 7063.

(20) Costa, M., Pelagatti, P., Pelizzi, C., Rogolino, D. *Journal of Molecular Catalysis A: Chemical* **2002**, *178*, 21.

(21) Bandini, M.; Piccinelli, F.; Tommasi, S.; Umani-Ronchi, A.; Ventrici, C. *Chem. Commun.* **2007**, 616.

(22) Ginotra, S. K.; Singh, V. K. *Org. Biomol. Chem.* **2007**, *5*, 3932.

(23) Trost, B. M.; Yeh, V. S. C.; Ito, H.; Bremeyer, N. *Org. Lett.* **2002**, *4*, 2621.

(24) Kowalczyk, R.; Sidorowicz, L.; Skarzewski, J. *Tetrahedron: Asymmetry* **2007**, *18*, 2581.

(25) Zulauf, A.; Mellah, M.; Schulz, E. *J. Org. Chem.* **2009**, *74*, 2242.

(26) Arai, T.; Yamada, Y. M. A.; Yamamoto, N.; Sasai, H.; Shibasaki, M. *Chem.-Eur. J.* **1996**, *2*, 1368.

(27) Bhatt, A. P.; Pathak, K.; Jasra, R. V.; Kureshy, R. I.; Khan, N. U. H.; Abdi, S. H. R. *J. Mol. Catal. A-Chem.* **2006**, *244*, 110.

(28) Kogami, Y.; Nakajima, T.; Ikeno, T.; Yamada, T. *Synthesis* **2004**, 1947.

(29) Park, J.; Lang, K.; Abboud, K. A.; Hong, S. *J. Am. Chem. Soc.* **2008**, *130*, 16484.

(30) Bandini, M.; Benaglia, M.; Sinisi, R.; Tommasi, S.; Umani-Ronchi, A. *Org. Lett.* **2007**, *9*, 2151.

(31) Gaab, M.; Bellemin-Laponnaz, S.; Gade, L. H. *Chem.-Eur. J.* **2009**, *15*, 5450.

(32) Kehat, T.; Portnoy, M. *Chem. Commun.* **2007**, 2823.

(33) Evans, D. A.; Seidel, D.; Rueping, M.; Lam, H. W.; Shaw, J. T.; Downey, C. W. *J. Am. Chem. Soc.* **2003**, *125*, 12692.

(34) Ozturk, G.; Colak, M.; Demirel, N. *Chirality* **2011**, *23*, 374.

(35) Bandini, M.; Cabiddu, S.; Cadoni, E.; Olivelli, P.; Sinisi, R.; Umani-Ronchi, A.; Usai, M. *Chirality* **2009**, *21*, 239.

(36) Didier, D.; Magnier-Bouvier, C.; Schulz, E. *Adv. Synth. Catal.* **2011**, *353*, 1087.

(37) Yang, W.; Du, D. M. *Eur. J. Org. Chem.* **2011**, 1552.

(38) Khan, N. U.; Prasetyanto, E. A.; Kim, Y. K.; Ansari, M. B.; Park, S. E. *Catal. Lett.* **2010**, *140*, 189.

(39) Ballini, R.; Barboni, L.; Fiorini, D.; Giarlo, G.; Palmieri, A. *Chem. Commun.* **2005**, 2633.

(40) Motokura, K.; Tada, M.; Iwasawa, Y. *Angew. Chem.-Int. Edit.* **2008**, *47*, 9230.

(41) Komura, K.; Kawamura, T.; Sugi, Y. *Catalysis Communications* **2007**, *8*, 644.

(42) Barnard, C. F. J.; Rouzaud, J.; Stevenson, S. H. *Org. Process Res. Dev.* **2005**, *9*, 164.

(43) List, B.; Lerner, R. A.; Barbas, C. F. *J. Am. Chem. Soc.* **2000**, *122*, 2395.

(44) Seebach, D.; Beck, A. K.; Badine, D. M.; Limbach, M.; Eschenmoser, A.; Treasurywala, A. M.; Hobi, R.; Prikoszovich, W.; Linder, B. *Helv. Chim. Acta* **2007**, *90*, 425.

(45) Enders, D.; Grondal, C. *Angew. Chem.-Int. Edit.* **2005**, *44*, 1210.

(46) Tokuda, O.; Kano, T.; Gao, W. G.; Ikemoto, T.; Maruoka, K. *Org. Lett.* **2005**, *7*, 5103.

(47) Bogevig, A.; Kumaragurubaran, N.; Jorgensen, K. A. *Chem. Commun.* **2002**, 620.

(48) Tang, Z.; Jiang, F.; Yu, L. T.; Cui, X.; Gong, L. Z.; Mi, A. Q.; Jiang, Y. Z.; Wu, Y. D. *J. Am. Chem. Soc.* **2003**, *125*, 5262.

(49) Samanta, S.; Liu, J. Y.; Dodda, R.; Zhao, C. G. *Org. Lett.* **2005**, *7*, 5321.

(50) de Maria, P. D., Bracco, P., Castelhano, L. F., Bargeman, G. *ACS Catalysis* **2011**, *1*, 70.

(51) Schmid, M. B., Zeitler, K., Gschwind, R. M. *J. Org. Chem.* **2011**, *76*, 3005.

(52) Gathergood, N.; Juhl, K.; Poulsen, T. B.; Thordrup, K.; Jorgensen, K. A. *Org. Biomol. Chem.* **2004**, *2*, 1077.

(53) Xu, Z. H.; Daka, P.; Budik, I.; Wang, H.; Bai, F. Q.; Zhang, H. X. *Eur. J. Org. Chem.* **2009**, 4581.

(54) Evans, D. A.; Burgey, C. S.; Kozlowski, M. C.; Tregay, S. W. *J. Am. Chem. Soc.* **1999**, *121*, 686.

(55) Mandoli, A.; Arnold, L. A.; de Vries, A. H. M.; Salvadori, P.; Feringa, B. L. *Tetrahedron: Asymmetry* **2001**, *12*, 1929.

(56) Langner, M.; Remy, P.; Bolm, C. *Chem.-Eur. J.* **2005**, *11*, 6254.

(57) Kawasaki, K., Tsumura, S., Katsuki, T. *Synlett* **1995**, 1245.

(58) Gokhale, A. S., Minidis, A. B. E., Pfaltz, A. *Tetrahedron Lett.* **1995**, *36*, 1831.

(59) Andrus, M. B., Argade, A. B., Chen, X. Pamment, M. G. *Tetrahedron Lett.* **1995**, *36*, 2945.

(60) Ramalingam, B., Neuburger, M., Pfaltz, A. *Synthesis* **2007**, 572.

(61) Tan, Q. H., M. *Adv. Synth. Catal.* **2008**, *350*, 2639.

(62) Larrow, J. F.; Jacobsen, E. N.; Gao, Y.; Hong, Y. P.; Nie, X. Y.; Zepp, C. M. *J. Org. Chem.* **1994**, *59*, 1939.

(63) Zhang, W.; Loebach, J. L.; Wilson, S. R.; Jacobsen, E. N. *J. Am. Chem. Soc.* **1990**, *112*, 2801.

(64) Jacobsen, E. N. *Accounts of Chemical Research* **2000**, *33*, 421.

(65) Brandes, B. D.; Jacobsen, E. N. *Synlett* **2001**, 1013.

(66) Daly, A. M.; Renehan, M. F.; Gilheany, D. G. *Org. Lett.* **2001**, *3*, 663.

(67) Irie, R.; Noda, K.; Ito, Y.; Matsumoto, N.; Katsuki, T. *Tetrahedron Lett.* **1990**, *31*, 7345.

(68) Sawada, Y., Matsumoto, K., Kondo, S., Watanabe, H., Ozawa, T., Suzuki, K., Saito, B., Katsuki, T. *Angew. Chem.-Int. Edit.* **2006**, *45*, 3478.

(69) Hopewell, J.; Dvorak, R.; Kosior, E. *Philos. Trans. R. Soc. B-Biol. Sci.* **2009**, *364*, 2115.

(70) Chamberlain, B. M.; Cheng, M.; Moore, D. R.; Ovitt, T. M.; Lobkovsky, E. B.; Coates, G. W. *J. Am. Chem. Soc.* **2001**, *123*, 3229.

(71) Zhang, X. Q.; Schneider, K.; Liu, G. M.; Chen, J. H.; Bruning, K.; Wang, D. J.; Stamm, M. *Polymer* **2011**, *52*, 4141.

(72) Du, H. Z.; Velders, A. H.; Dijkstra, P. J.; Zhong, Z. Y.; Chen, X. S.; Feijen, J. *Macromolecules* **2009**, *42*, 1058.

(73) Suesat, J.; Phillips, D. A. S.; Wilding, M. A.; Farrington, D. W. *Polymer* **2003**, *44*, 5993.

(74) Agrawal, A. K.; Bhalla, R. *J. Macromol. Sci.-Polym. Rev* **2003**, *C43*, 479.

(75) Dorgan, J. R.; Lehermeier, H. J.; Palade, L. I.; Cicero, J. *Macromol. Symp.* **2001**, *175*, 55.

(76) Chisholm, M. H.; Gallucci, J. C.; Phomphrai, K. *Inorg. Chem.* **2005**, *44*, 8004.

(77) Jones, M. D.; Davidson, M. G.; Keir, C. G.; Hughes, L. M.; Mahon, M. F.; Apperley, D. C. *European Journal of Inorganic Chemistry* **2009**, 635.

(78) Rieth, L. R.; Moore, D. R.; Lobkovsky, E. B.; Coates, G. W. *J. Am. Chem. Soc.* **2002**, *124*, 15239.

(79) Du, H. Z.; Velders, A. H.; Dijkstra, P. J.; Sun, J. R.; Zhong, Z. Y.; Chen, X. S.; Feijen, J. *Chem.-Eur. J.* **2009**, *15*, 9836.

(80) Ma, H. Y.; Melillo, G.; Oliva, L.; Spaniol, T. P.; Englert, U.; Okuda, J. *Dalton Trans.* **2005**, 721.

(81) Nomura, N.; Akita, A.; Ishii, R.; Mizuno, M. *J. Am. Chem. Soc.* **2010**, *132*, 1750.

(82) Nomura, N.; Ishii, R.; Akakura, M.; Aoi, K. *J. Am. Chem. Soc.* **2002**, *124*, 5938.

(83) Nomura, N.; Ishii, R.; Yamamoto, Y.; Kondo, T. *Chem.-Eur. J.* **2007**, *13*, 4433.

(84) Schwarz, A. D.; Chu, Z. Y.; Mountford, P. *Organometallics* **2010**, *29*, 1246.

(85) Zhong, Z. Y.; Dijkstra, P. J.; Feijen, J. *Angew. Chem.-Int. Edit.* **2002**, *41*, 4510.

(86) Chisholm, M. H.; Gallucci, J. C.; Phomphrai, K. *Inorg. Chem.* **2004**, *43*, 6717.

(87) Davidson, M. G.; O'Hara, C. T.; Jones, M. D.; Keir, C. G.; Mahon, M. F.; Kociok-Kohn, G. *Inorg. Chem.* **2007**, *46*, 7686.

(88) Ma, H. Y.; Spaniol, T. P.; Okuda, J. *Dalton Trans.* **2003**, 4770.

(89) Skvortsov, G. G.; Yakovenko, M. V.; Castro, P. M.; Fukin, G. K.; Cherkasov, A. V.; Carpentier, J. F.; Trifonov, A. A. *European Journal of Inorganic Chemistry* **2007**, 3260.

(90) Chmura, A. J.; Cousins, D. M.; Davidson, M. G.; Jones, M. D.; Lunn, M. D.; Mahon, M. F. *Dalton Trans.* **2008**, 1437.

(91) Chmura, A. J.; Davidson, M. G.; Frankis, C. J.; Jones, M. D.; Lunn, M. D. *Chem. Commun.* **2008**, 1293.

(92) Chmura, A. J.; Davidson, M. G.; Jones, M. D.; Lunn, M. D.; Mahon, M. F.; Johnson, A. F.; Khunkamchoo, P.; Roberts, S. L.; Wong, S. S. F. *Macromolecules* **2006**, *39*, 7250.

(93) Gendler, S.; Segal, S.; Goldberg, I.; Goldschmidt, Z.; Kol, M. *Inorg. Chem.* **2006**, *45*, 4783.

(94) Jones, M. D.; Davidson, M. G.; Kociok-Kohn, G. *Polyhedron* **2010**, *29*, 697.

(95) Gregson, C. K. A.; Blackmore, I. J.; Gibson, V. C.; Long, N. J.; Marshall, E. L.; White, A. J. P. *Dalton Trans.* **2006**, 3134.

(96) Whitelaw, E. L.; Jones, M. D.; Mahon, M. F. *Inorg. Chem.* **2010**, *49*, 7176.

(97) Sarazin, Y.; Howard, R. H.; Hughes, D. L.; Humphrey, S. M.; Bochmann, M. *Dalton Trans.* **2006**, 340.

(98) Schwarz, A. D.; Thompson, A. L.; Mountford, P. *Inorg. Chem.* **2009**, *48*, 10442.

(99) Chen, H. Y.; Liu, M. Y.; Sutar, A. K.; Lin, C. C. *Inorg. Chem.* **2010**, *49*, 665.

(100) Sergeeva, E.; Kopilov, J.; Goldberg, I.; Kol, M. *Inorg. Chem.* **2010**, *49*, 3977.

(101) Hsieh, K. C.; Lee, W. Y.; Hsueh, L. F.; Lee, H. M.; Huang, J. H. *European Journal of Inorganic Chemistry* **2006**, 2306.

(102) Hu, M. G.; Wang, M.; Zhu, H. J.; Zhang, L.; Zhang, H.; Sun, L. C. *Dalton Trans.* **2010**, *39*, 4440.
(103) Kim, S. H.; Lee, J.; Kim, D. J.; Moon, J. H.; Yoon, S.; Oh, H. J.; Do, Y.; Ko, Y. S.; Yim, J. H.; Kim, Y. *J. Organomet. Chem.* **2009**, *694*, 3409.
(104) Krauzy-Dziedzic, K.; Ejfler, J.; Szafert, S.; Sobota, P. *Dalton Trans.* **2008**, 2620.
(105) Romain, C.; Brelot, L.; Bellemin-Laponnaz, S.; Dagorne, S. *Organometallics* **2010**, *29*, 1191.

Experimental

6.1 General Procedures

All solvents were purchased from Fisher. Where dry solvents were used, these were obtained using a solvent purification system (MBraun SPS). All reagents were purchased from Sigma Aldrich or Fisher unless otherwise stated. (*R*)-(+)-1,1'-binaphthalene-2,2'-diamine was purchased from Strem Chemicals. $[IrCl(cod)]_2$ and $[RhCl(cod)]_2$ and $[RuCl_2(p\text{-cymene})]_2$ were generously donated from Johnson Matthey.

NMR spectroscopy – solution state

NMR spectra were recorded on Bruker 250, 300 and 400 MHz instruments. Young's NMR tubes were used for air sensitive products, otherwise Wilmad 5 mm NMR tubes were used. Spectra were referenced to residual solvent peaks (for example for $CDCl_3$, 7.26 ppm in an ^1H NMR and 77.0 ppm in an $^{13}C\{^1H\}$ NMR spectrum). The ^1H NMR spectrum for [Rh(**3b**)(cod)]BF_4 was recorded at 233 K. All other spectra were recorded at room temperature, unless otherwise stated. All samples were dissolved in appropriate deuterated solvents. The calculations used to determine conversion, selectivity and diastereomeric excess given in chapter five are shown below.

To obtain conversion:

$$\text{Conv} = \frac{\Sigma \text{ (integral of product resonances)}}{\Sigma \text{ (integral of starting material and product resonances)}} \times 100$$

To obtain selectivity:

$$\text{Sel} = \frac{\Sigma \text{ (integral of desired product resonances)}}{\Sigma \text{ (integral of desired product and by-product resonances}} \times 100$$

To obtain diastereomeric excess:

$$de = \frac{(\text{integral of peak\{diastereomer A\}} - \text{integral of peak\{diastereomer B\}})}{(\text{integral of peak\{diasteromer A\}} + \text{integral of peak\{diastereomer B\})} \times 100$$

NMR spectroscopy – solid state

Spectra were recorded using a Varian VNMRS 400MHz instrument, operating at 100.56 MHz for ^{13}C and 161.87 MHz for ^{31}P, at Durham University. A spin rate of 10000 Hz was used. A cross-polarisation pulse sequence of contact time of 3.0 ms and recycle delay of 1.0 s was used, with TPPM decoupling. $^{13}C\{^{1}H\}$ spectra were referenced with respect to tetramethylsilane. $^{31}P\{^{1}H\}$ spectra were referenced with respect to a solution of 85 % H_3PO_4. All spectra were recorded at room temperature.

EPR spectroscopy

All measurements were performed using a Bruker EMX instrument, at X-band 9.4 GHz and K-band 24.0 GHz, at Manchester University. Samples were measured as powders at 290 K and 120 K, fluid solutions at 290 K and frozen solutions at 120 K. Simulations of the spectra were performed using Bruker XSophe computer simulation software (version 1.1.4).

Mass spectrometry include MALDI-TOF

Samples were analysed using ESI (electro-spray ionisation) on a Bruker micrOTOF (ESI-TOF) instrument. Positive ESI mode was used. Appropriate polar solvents were used. Where MALDI-TOF was used, this was carried out via the EPSRC mass spectrometry service. A Voyager-DE-STR instrument was used.

Single crystal X-ray diffraction

Single crystal X-Ray diffraction data were collected on a Nonius KappaCCD diffractometer with Mo-Kα radiation (λ = 0.71073 Å at 150(2)K). Data for $[Cu(\mathbf{5b})_2](OTf)_2$ was collected on a Xcalibur Atlas diffractometer with CuKα radiation (λ = 1.54184Å at 100(2)K). Suitable single crystals were mounted on

glass fibre using oil. The structures were solved with direct methods, and unless otherwise stated, refined by full-matrix least squares on F^2 using SHELXL-97. Hydrogen atoms were included in idealised positions and refined using the riding model. The data was collected at a temperature of 150(2) K. The data was collected and solved by Dr Matthew Jones, Dr Mary Mahon, Dr Gabriele Kociok-Köhn at the University of Bath.

Powder X-ray diffraction

Patterns were recorded on a Bruker D8 powder diffractometer with CuK_α (λ = 1.54 Å) radiation (50 kV, 20 mA) 0.025 ° step size and 1 s step time.

Elemental Analysis

Elemental analysis was performed by Mr Alan Carver at the University of Bath. ICP measurements were recorded by Medac Ltd.

Thermogravimetric Analysis (TGA)

Thermogravimetric analysis was performed by Mr Russel Barlow at the University of Bath, on a Perkin Elmer TGA 4000 instrument. The samples were heated from 50-600 °C at 10 °C per minute, under an atmosphere of air.

UV-vis spectroscopy

UV-vis spectroscopy was performed using a Perkin Elmer Lambda S50 UV-vis Spectrometer. Data was collected for 900 to 200 nm, with a scan speed of 750 nm min^{-1}. A data interval of 1.00 nm and an integration time of 0.04 s were used. Slit width was 2.00 nm, and path length was 1 cm.

Chiral High Performance Liquid Chromatography (HPLC)

Samples were created by dissolving 1 mg of the material to be analysed in 1 ml HPLC grade isopropanol. The samples were then filtered using through syringe filters (Millex GS filter unit, 0.22 μm, MF Millipore MCE membrane). HPLC analysis was performed on an Agilent Technologies 1120 Compact LC instrument. All solvents used were HPLC grade.

Analysis of hydrogenation products: a chiral Daicel OD-H column was used. A wavelength of 254 nm was used. A flow rate of 0.5 ml min^{-1} was used with a

solvent mixture of 90:10 hexane:isopropanol. Enantiomers seen at 12.1 and 13.6 min.

Analysis of nitroaldol products: an OD-H Daicel chiral column was used. Where the substrates were benzaldehyde and nitromethane, a wavelength of 230 nm and a flow rate of 1.0 ml min^{-1} was used with a solvent mixture of 90:10 hexane:isopropanol. Enantiomers seen at 16.6 and 20.5 min. Where the substrates were nitrobenzaldehyde and nitromethane, a wavelength of 254 nm and a flow rate of 1.0 ml min^{-1} was used with a solvent mixture of 90:10 hexane:isopropanol. Enantiomers seen at 31.1 and 39.4 min. Where the substrates were benzaldehyde and nitroethane, a wavelength of 230 nm and a flow rate of 1.0 ml min^{-1} was used with a solvent mixture of 90:10 hexane:isopropanol. Peaks observed at 35.3 and 55.4, and 46.2 and 57.9 min. Where the substrates were nitrobenzaldehyde and nitroethane, a wavelength of 230 nm and a flow rate of 0.7 ml min^{-1} was used with a solvent mixture of 98:2 hexane:isopropanol. Peaks observed at 174.4 and 233.7, and 254.4 and 287.3 min.

Analysis of aldol products: a chiral Daicel OJ-H column was used. A wavelength of 250 nm and a flow rate of 1.0 ml min^{-1} was used with a solvent mixture of 90:10 hexane:isopropanol. Enantiomers seen at 21.4 and 24.6 min.

To obtain enantiomeric excess:

$$ee = \frac{(\text{integral of peak\{enantiomer A\}} - \text{integral of peak\{enantiomer B\}})}{(\text{integral of peak\{enantiomer A\}} + \text{integral of peak\{enantiomer B\}})} \times 100$$

Gel Permeation Chromatography (GPC)

Samples were created by dissolving 2 mg of the material to be analysed in 1 ml GPC grade THF. The samples were left to fully dissolve for 24h before being filtered using through syringe filters (Millex GS filter unit, 0.22 μm, MF Millipore MCE membrane). Analysis was performed using a Polymer Laboratories PL-GPC 50 instrument. GPC grade THF was the solvent used, with a flow rate of 1.0 ml min^{-1}. Analysis was carried out at a temperature of 308 K. Samples were referenced to polystyrene standards.

Gas-Chromatography-Mass Spectrometry (GC-MS)

GC-MS was performed on an Agilent 7890 GC-MS instrument with a FID and MS detector. Samples were injected on a HP-5 column. The oven was held at 50 °C for 5 min and heated at 5 °C per minute until a temperature of 270 °C at which point the temperature remained constant for a further 10 minutes.

6.2 Experimental from Chapter Two

Synthesis of 1

This compound was synthesised as described by Jacobsen et al.[1] L-(+)-tartaric acid (150g, 1.0 mol) was dissolved in distilled water (400 ml) and a mixture of cis/trans 1,2-diaminocyclohexane added (240 ml, 2.0 mol) so that the reaction temperature reached 70 °C. To this glacial acetic acid was added (100 ml, 1.8 mol) so that the reaction temperature reached 90 °C. The resulting slurry was stirred for a further 2 h, and then cooled to 5 °C for 2 h. The resulting precipitate was collected by vacuum filtration and washed with 5 °C distilled water (2 × 50 ml) and then methanol (5 × 100 ml). The crude product was then recrystallised by dissolving the compound in distilled water at 90 °C and leaving to cool to room temperature overnight. The purified product was collected by vacuum filtration and dried under reduced pressure. 51 % yield.

^{1}H (D_2O) 1.39 (m, 4H), 1.79 (m, 2H), 2.13 (m, 2H), 3.33 (m, 2H, C**H**NH_3^+), 4.29 (s, 2H, C**H**OH). $^{13}C\{^{1}H\}$ (D_2O) 23.2 (CH_2), 29.8 (CH_2), 52.5 (CH), 74.3 (CHOH), 178.9 (COOH). Mass spec: HR-ESI Calc for [M^+] 115.1235 found 115.1241

Synthesis of 2

This compound was synthesised as described by Rafii et al.[2] **1** (26.4 g, 100 mmol) was dissolved in water (80 ml) and dichloromethane (100 ml). To this a cooled solution of sodium hydroxide (9.6 g in 80 ml water, 3 mol dm^{-3}) was added dropwise. Sodium chloride was added (6 g, 103 mmol), and then the reaction mixture was stirred for 30 minutes. Following this the aqueous phase

was decanted and extracted with chloroform (3 × 20 ml), with the combined organic layers being dried over magnesium sulphate. The mixture was filtered and the solvent removed by rotary evaporation. The product was dried under reduced pressure and stored at -20 °C. 49 % yield.

^{1}H ($CDCl_3$) 1.04 (m, 2H), 1.19 (m, 2H), 1.60 (m, 2H), 1.76 (m, 2H), 2.18 (m, 2H). $^{13}C\{^{1}H\}$ ($CDCl_3$) 25.8 (CH_2), 35.9 (CH_2), 58.1 (CH). Mass spec: HR-ESI Calc for [M^+] 115.1235 found 115.1243

Synthesis of 3a

2 (1.0 g, 8.8 mmol) was dissolved in methanol (50 ml), and benzaldehyde added (1.8 ml, 17.6 mmol). The reaction mixture was stirred continuously at room temperature for 3h, before the solvent was removed by rotary evaporation. The product dried under reduced pressure. 75 % yield.

^{1}H ($CDCl_3$) 1.49 (m, 2H), 1.86 (m, 6H), 3.42 (m, 2H), 7.32 (m, 6H), 7.57 (m, 4H), 8.21 (s, 2H C**H**N imine). $^{13}C\{^{1}H\}$ ($CDCl_3$) 24.5 (CH_2), 33.0 (CH_2), 73.9 (CHN cyclohexane), 128.0 (CH Ar), 128.4 (CH Ar), 130.3 (CH Ar), 136.4 (C Ar), 161.1 (CHN imine). Mass spec: HR-ESI Calc for [M^+] 291.1861 found 291.1856

Single Crystal X-Ray Diffraction:

Empirical formula	$C_{20}H_{22}N_2$	
Formula weight	290.40	
Temperature	150(2) K	
Wavelength	0.71073 Å	
Crystal system	Orthorhombic	
Space group	$P2_12_12_1$	
Unit cell dimensions	a = 8.9440(2) Å	α = 90°
	b = 9.3940(2) Å	β = 90°
	c = 19.9660(4) Å	γ = 90°
Volume	1677.54(6) Å^3	
Z	4	
Density (calculated)	1.150 Mg/m^3	
Absorption coefficient	0.067 mm^{-1}	
F(000)	624	
Crystal Size	0.20 × 0.20 × 0.20 mm	
Theta range for data collection	3.75 to 24.00°	

Limiting indices	-10<=h<=10, -10<=k<=10, -22<=l<=22
Reflections collected	15637
Independent reflections	2609 [R(int) = 0.0978]
Completeness to theta = 24.00°	98.2 %
Absorption correction	None
Max. and Min. transmission	0.9866 and 0.9866
Refinement method	Full-matrix least-squares on F^2
Data / restraints / parameters	2609 / 0 / 199
Goodness-of-fit on F^2	1.064
Final R indices [I>2sigma(I)]	R1 = 0.0362, wR2 = 0.0803
R indices (all data)	R1 = 0.0423, wR2 = 0.0832
Absolute structure parameter	0(3)
Largest diff. peak and hole	0.115 and -0.175 e.$Å^{-3}$

Synthesis of 3b

2 (1.0 g, 8.8 mmol) was dissolved in methanol (50 ml), and benzaldehyde added (1.8 ml, 17.6 mmol). The reaction mixture was stirred continuously at room temperature for 3h, before sodium borohydride was added (1.0 g, 26.4 mmol). This was stirred continuously at room temperature for a further 3h. The solvent was removed by rotary evaporation, and the residue dissolved in 50:50 dichloromethane:water. The organic layer was decanted off, and the aqueous layer washed three times with dichloromethane. The organic layers were combined and dried over magnesium sulphate. The mixture was gravity filtered, and the solvent removed from the filtrate by rotary evaporation. The resulting product was dried under reduced pressure. 68 % yield.

^{1}H ($CDCl_3$) 0.92 (m, 2H), 1.14 (m, 2H), 1.63 (m, 2H), 1.79 (m, 2H), 2.17 (m, 2H) 3.61 (d J = 13 Hz, 2H, C**H$_2$**NH), 3.80 (d J = 13 Hz, 2H, C**H$_2$**NH), 7.30 (m, 10H). ^{13}C{^{1}H} ($CDCl_3$) 25.5 (CH_2), 32.0 (CH_2), 51.3 (CH_2NH), 61.4 (CHNH), 127.1 (CH), 128.5 (CH), 128.7 (CH), 141.5 (C). Mass spec: HR-ESI Calc for [M^+] 295.2174 found 295.2166

Synthesis of 4a

2 (1.0 g, 8.8 mmol) was dissolved in methanol (50 ml), and 2-methoxybenzaldehyde added (2.40 g, 17.6 mmol). The reaction mixture was stirred continuously at room temperature for 3h, before the solvent was removed

by rotary evaporation. The product was dried under reduced pressure. 83 % yield.

^{1}H ($CDCl_3$) 1.42 (m, 2H, CH_2), 1.78 (m, 6H), 3.36 (m, 2H, CHN cyclohexane), 3.64 (s, 6H, OCH_3), 6.76 (m, 4H), 7.20 (m, 2H), 7.74 (m, 2H), 8.54 (s, 2H CHN imine). ^{13}C{^{1}H} ($CDCl_3$) 24.8 (CH_2), 33.2 (CH_2), 55.5 (OCH_3), 74.0 (CHN cyclohexane), 110.8 (CH), 120.7 (CH), 124.8 (C), 127.4 (CH), 131.2 (CH), 157.4 (CHN imine), 158.7 (**C**OMe). Mass spec: HR-ESI Calc for [M^+] 351.2073 found 351.2161

Synthesis of 4b

2 (1.0 g, 8.8 mmol) was dissolved in methanol (50 ml), and 2-methoxybenzaldehyde added (2.40 g, 17.6 mmol). The reaction mixture was stirred continuously at room temperature for 3h, before sodium borohydride was added (1.0 g, 26.4 mmol). This was stirred continuously at room temperature for a further 3h. The solvent was removed by rotary evaporation, and the residue dissolved in 50:50 dichloromethane:water. The organic layer was decanted off, and the aqueous layer washed three times with dichloromethane. The organic layers were combined and dried over magnesium sulphate. The mixture was gravity filtered, and the solvent removed from the filtrate by rotary evaporation. The resulting product was dried under reduced pressure. 72 % yield.

^{1}H ($CDCl_3$) 1.07 (m, 2H), 1.21 (m, 2H), 1.69 (m, 2H), 2.12 (m, 2H), 2.25 (m, 2H), 3.66 (d J = 13 Hz, 2H, C**H$_2$**NH), 3.74 (s, 6H, CH_3), 3.88 (d J = 13 Hz, 2H, C**H$_2$**NH), 6.89 (m, 4H), 7.26 (m, 4H). ^{13}C{^{1}H} ($CDCl_3$) 25.5 (CH_2), 32.0 (CH_2), 46.4 (CH_2NH), 55.5 (OCH_3), 61.4 (CHNH), 110.5 (CH), 120.7 (CH), 128.2 (CH), 129.7 (CH), 129.8 (C), 158.0 (C). Mass spec: HR-ESI Calc for [M^+] 355.2386 found 355.2375

Synthesis of 5a

2 (1.0 g, 8.8 mmol) was dissolved in methanol (50 ml), and 2-methylbenzaldehyde added (2.0 ml, 17.6 mmol). The reaction mixture was stirred continuously at room temperature for 3h, before the solvent was removed by rotary evaporation. The product was dried under reduced pressure. 60 % yield.

^{1}H ($CDCl_3$) 1.44 (m, 2H CH_2), 1.78 (m, 6H, CH_2), 2.20 (s, 6H CH_3), 3.35 (m, 2H CHN cyclohexane), 7.05 (m, 6H), 7.66 (m, 2H), 8.42 (s, 2H CHN imine). ^{13}C{^{1}H} ($CDCl_3$) 19.0 (CH_3), 24.5 (CH_2), 33.0 (CH_2), 74.3 (CHN cyclohexane), 126.0 (CH), 127.2 (CH), 129.9 (CH), 130.5 (CH), 134.5 (C), 137.4 (C), 159.8 (CHN imine). Mass spec: HR-ESI Calc for [M^+] 319.2174 found 319.2266

Synthesis of 5b

2 (1.0 g, 8.8 mmol) was dissolved in methanol (50 ml), and 2-methylbenzaldehyde added (2.0 ml, 17.6 mmol). The reaction mixture was stirred continuously at room temperature for 3h, before sodium borohydride was added (1.0 g, 26.4 mmol). This was stirred continuously at room temperature for a further 3h. The solvent was removed by rotary evaporation, and the residue dissolved in 50:50 dichloromethane:water. The organic layer was decanted off, and the aqueous layer washed three times with dichloromethane. The organic layers were combined and dried over magnesium sulphate. The mixture was gravity filtered, and the solvent removed from the filtrate by rotary evaporation. The resulting product was dried under reduced pressure. 51 % yield.

^{1}H ($CDCl_3$) 1.00 (q, 2H), 1.19 (m, 2H), 1.67 (t, 4H), 1.68 (m, 2H), 2.22 (s, 6H, CH_3), 3.53 (d J = 13 Hz, 2H, C**H$_2$**NH), 3.76 (d J = 13 Hz, 2H, C**H$_2$**NH), 7.05 (m J = 1.5 Hz, 6H), 7.16 (m J = 1.5 Hz, 2H). ^{13}C{^{1}H} ($CDCl_3$) 19.4 (CH_3), 25.6 (CH_2), 32.1 (CH_2), 49.3 (CH_2NH), 61.9 (CHNH), 126.3 (CH), 127.3 (CH), 128.9 (CH), 130.6 (CH), 136.8 (C), 139.3 (C). Mass spec: HR-ESI Calc for [M^+] 323.2487 found 323.2480

Synthesis of 6a

2 (1.0 g, 8.8 mmol) was dissolved in methanol (50 ml), and 2-chlorobenzaldehyde added (2.0 ml, 17.6 mmol). The reaction mixture was stirred continuously at room temperature for 3h, before the solvent was removed by rotary evaporation. The product was dried under reduced pressure. 80 % yield.

^{1}H ($CDCl_3$) 1.09 (m, 2H), 1.29 (m, 2H), 1.69 (m, 4H), 2.84 (m, 2H), 7.19 (m, 6H), 7.84 (d, 2H), 8.70 (s, 2H, CHN imine). ^{13}C{^{1}H} ($CDCl_3$) 24.7 (CH_2), 33.1 (CH_2), 73.8 (CHN cyclohexane), 126.8 (CH), 128.4 (CH), 129.5 (CH), 131.5

(CH), 133.4 (C), 135.1 (C), 157.8 (CHN imine). Mass spec: HR-ESI Calc for $[M^+]$ 359.1082 found 359.1190

Synthesis of 6b

2 (1.0 g, 8.8 mmol) was dissolved in methanol (50 ml), and 2-chlorobenzaldehyde added (2.0 ml, 17.6 mmol). The reaction mixture was stirred continuously at room temperature for 3h, before sodium borohydride was added (1.0 g, 26.4 mmol). This was stirred continuously at room temperature for a further 3h. The solvent was removed by rotary evaporation, and the residue dissolved in 50:50 dichloromethane:water. The organic layer was decanted off, and the aqueous layer washed three times with dichloromethane. The organic layers were combined and dried over magnesium sulphate. The mixture was gravity filtered, and the solvent removed from the filtrate by rotary evaporation. The resulting product was dried under reduced pressure. 69 % yield.

^{1}H ($CDCl_3$) 1.03 (m, 4H), 1.62 (m, 2H), 2.17 (m, 4H), 3.67 (d J = 14 Hz, 2H, C**H$_2$**NH), 3.85 (d J = 14 Hz, 2H, C**H$_2$**NH), 7.18 (m, 8H). ^{13}C{^{1}H} ($CDCl_3$) 25.4 (CH_2), 32.1 (CH_2), 48.8 (CH_2NH), 61.4 (CHNH), 127.1 (CH), 128.4 (CH), 129.8 (CH), 130.4 (CH), 134.1 (C), 138.8(C). Mass spec: HR-ESI Calc for $[M^+]$ 363.1395 found 363.1385

Synthesis of 7a

2 (1.0 g, 8.8 mmol) was dissolved in methanol (50 ml), and salicylaldehyde added (1.9 ml, 17.6 mmol). The reaction mixture was stirred continuously at room temperature for 3h, before the solvent was removed by rotary evaporation. The product was dried under reduced pressure. 73 % yield.

^{1}H ($CDCl_3$) 1.42 (m, 2H CH_2), 1.62 (m, 2H CH_2), 1.82 (m, 4H CH_2), 3.24 (m, 2H CHN cyclohexane), 6.67 (m, 4H), 7.12 (m, 4H), 8.22 (s, 2H CHN imine). ^{13}C{^{1}H} ($CDCl_3$) 24.2 (CH_2), 33.1 (CH_2), 72.7 (CHN cyclohexane), 116.8 (CH), 118.6 (CH), 118.7 (C), 131.5 (CH), 132.2 (CH), 161.0 (COH), 164.7 (CHN imine). Mass spec: HR-ESI Calc for $[M^+]$ 323.1760 found 323.1757

Synthesis of 7b

2 (1.0 g, 8.8 mmol) was dissolved in methanol (50 ml), and salicylaldehyde added (1.9 ml, 17.6 mmol). The reaction mixture was stirred continuously at room temperature for 3h, before sodium borohydride was added (1.0 g, 26.4 mmol). This was stirred continuously at room temperature for a further 3h. The solvent was removed by rotary evaporation, and the residue dissolved in dichloromethane. This was gravity filtered, and the solvent removed from the filtrate by rotary evaporation. The resulting product was dried under reduced pressure. 65 % yield.

^{1}H (MeOD) 1.20 (m, 4H), 1.70 (m, 2H), 2.17 (m, 2H), 2.45 (m, 2H), 3.91 (d J = 14 Hz, 2H, C**H$_2$**NH), 4.03 (d J = 14 Hz, 2H, C**H$_2$**NH), 6.81 (m, 4H), 7.00 (m, 2H), 7.19 (m, 2H). ^{13}C{^{1}H} (MeOD) 24.5 (CH_2), 30.6 (CH_2), 50.1 (CH_2NH), 60.1 (CHNH), 116.9 (CH), 119.6 (CH), 123.3 (C), 128.7 (CH), 129.2 (CH), 158.3 (COH). Mass spec: HR-ESI Calc for [M^+] 327.2073 found 327.2078

Synthesis of 8a

2 (39 mg, 0.34 mmol) and 2-(diphenylphosphino)benzaldehyde (0.2 g, 0.69 mmol) were placed in a round bottomed flask, which was then repeatedly degassed and backfilled with argon. To this, dry dichloromethane was added (50 ml), and the reaction mixture stirred continuously at room temperature for 3h. The solvent was removed by rotary evaporation, and the product dried under reduced pressure. 69 % yield.

^{1}H ($CDCl_3$) 1.30 (m, 6H), 1.56 (m, 2H), 3.05 (m, 2H), 6.74 (m, 2H), 7.16 (m, 24H), 7.66 (m, 2H), 8.61 (d, 2H). ^{13}C{^{1}H} ($CDCl_3$) 23.3 (CH_2), 31.5 (CH_2), 72.6 (CH), 127.5 (CH), 128.7 (CH), 132.2 (CH), 132.9 (CH), 136.1 (C), 139.0 (C), 158.4 (CHN). ^{31}P{^{1}H} ($CDCl_3$) -12.4 (PPh_2). Mass spec: HR-ESI Calc for [M^+] 659.2745 found 659.2739

Synthesis of 8b

2 (39 mg, 0.34 mmol) and 2-(diphenylphosphino)benzaldehyde (0.2 g, 0.69 mmol) were placed in a round bottomed flask, which was then repeatedly degassed and backfilled with argon. To this, methanol was added (50 ml), and the reaction mixture stirred continuously at room temperature for 3h. At this point, sodium borohydride was added (39 mg, 1.02 mmol), and the reaction mixture was stirred continuously at room temperature for a further 3h. The

solvent was removed by rotary evaporation, and the residue dissolved in dichloromethane. This was gravity filtered, and the solvent removed from the filtrate by rotary evaporation. The resulting product was dried under reduced pressure. 38 % yield.

^{1}H ($CDCl_3$) 0.77 (m, 2H CH_2), 0.96 (m, 2H CH_2), 1.48 (m, 2H CH_2), 1.88 (m, 2H CH_2), 2.03 (m, 2H CHN cyclohexane), 3.74 (d J = 14 Hz, 2H, C**H$_2$**NH), 3.91 (d J = 14 Hz, 2H, C**H$_2$**NH), 7.12 (m, 28H). $^{13}C\{^{1}H\}$ ($CDCl_3$) 24.1 (CH_2), 30.3 (CH_2), 48.3 (CH_2NH), 60.0 (CHNH), 126.2 (CH), 128.3 (CH), 129.6 (CH), 130.7 (CH), 132.0 (CH), 134.3 (C), 135.9 (C), 144.1 (C). $^{31}P\{^{1}H\}$ ($CDCl_3$) -15.1 (PPh_2). Mass spec: HR-ESI Calc for [M^+] 664.3136 found 664.3116

Synthesis of 9a

2 (0.5 g, 4.4 mmol) was dissolved in methanol (50 ml), and 2-pyridinecarboxaldehyde (0.84 ml, 8.8 mmol) added. The reaction mixture was stirred for 3h at room temperature, before the solvent was removed by rotary evaporation. The product was dried under reduced pressure. 91 % yield.

^{1}H ($CDCl_3$) 1.49 (m, 2H), 1.83 (m, 6H), 3.53 (m, 2H, CHN cyclohexane), 7.18 (m, 2H), 7.58 (t, 2H), 7.84 (d, 2H), 8.29 (s, 2H CHN imine), 8.52 (d, 2H). $^{13}C\{^{1}H\}$ ($CDCl_3$) 24.4 (CH_2), 32.7 (CH_2), 73.6 (CHN cyclohexane), 121.3 (CH), 124.5 (CH), 136.4 (CH), 149.2 (CHN Ar), 154.6 (C Ar), 161.5 (CHN imine). Mass spec: HR-ESI Calc for [M^+] 293.1766 found 293.1757

Synthesis of 9b

2 (0.5 g, 4.4 mmol) was dissolved in methanol (50 ml), and 2-pyridinecarboxaldehyde (0.84 ml, 8.8 mmol) added. The reaction mixture was stirred for 3h at room temperature, upon which sodium borohydride was added (0.5 g, 13.2 mmol). Following a further 3h reaction time, the solvent was removed by rotary evaporation and a 50:50 water:dichloromethane mix was added to the product. The organic layer was decanted off, and the remaining aqueous layer washed three times with dichloromethane. The organic layers were combined, dried over magnesium sulphate and gravity filtered. The solvent was then removed by rotary evaporation before the product was dried under reduced pressure. 80 % yield.

^{1}H ($CDCl_3$) 1.04 (m, 2H), 1.20 (m, 2H), 1.69 (m, 2H), 2.11 (m, 2H), 2.27 (m, 2H), 3.81 (d J = 14 Hz, 2H, CH_2NH), 3.99 (d J = 14 Hz, 2H, CH_2NH), 7.11 (m, 2H), 7.47 (d, 2H), 7.70 (t, 2H), 8.55 (d, 2H). $^{13}C\{^{1}H\}$ ($CDCl_3$) 24.0 (CH_2), 30.9 (CH_2), 53.2 (CH_2NH amine), 60.3 (CHN cyclohexane), 120.8 (CH), 135.4 (CH), 148.0 (CHN Ar), 159.5 (C Ar). Mass spec: HR-ESI Calc for [M^+] 297.2079 found 297.2068

Synthesis of 10a

2 (0.5 g, 4.4 mmol) was dissolved in methanol (50 ml), and 3-pyridinecarboxaldehyde (0.83 ml, 8.8 mmol) added. The reaction mixture was stirred for 3h at room temperature, before the solvent was removed by rotary evaporation. The product was dried under reduced pressure. 82 % yield.

^{1}H ($CDCl_3$) 1.44 (m, 2H), 1.81 (m, 6H), 3.39 (m, 2H, CHN cyclohexane), 7.19 (m, 2H), 7.91 (m, 2H, CH Ar), 8.17 (s, 2H, CHN imine), 8.49 (d, 2H, CH**CH**N Ar), 8.69 (s, 2H, C**CH**N Ar). $^{13}C\{^{1}H\}$ ($CDCl_3$) 24.3 (CH_2), 32.7 (CH_2), 74.1 (CHN cyclohexane), 123.5 (CH), 131.7 (C), 134.4 (CH), 149.9 (CHN Ar), 151.3 (CHN Ar), 158.0 (CHN imine). Mass spec: HR-ESI Calc for [M^+] 293.1766 found 293.1774.

Synthesis of 10b

2 (0.5 g, 4.4 mmol) was dissolved in methanol (50 ml), and 3-pyridinecarboxaldehyde (0.83 ml, 8.8 mmol) added. The reaction mixture was stirred for 3h at room temperature, upon which sodium borohydride was added (0.5 g, 13.2 mmol). Following a further 3h reaction time, the solvent was removed by rotary evaporation and a 50:50 water:dichloromethane mix was added to the product. The organic layer was decanted off, and the remaining aqueous layer washed three times with dichloromethane. The organic layers were combined, dried over magnesium sulphate and gravity filtered. The solvent was then removed by rotary evaporation before the product was dried under reduced pressure. 72 % yield.

^{1}H ($CDCl_3$) 1.02 (m, 2H), 1.16 (m, 2H), 1.67 (m, 2H), 2.14 (m, 6H), 3.62 (d J = 13.5 Hz, 2H, CH_2NH), 3.86 (d J = 13.5 Hz, 2H, CH_2NH), 7.19 (m, 2H), 7.58 (m, 2H), 8.46 (m, 4H). $^{13}C\{^{1}H\}$ ($CDCl_3$) 24.9 (CH_2), 31.5 (CH_2), 48.3 (CH_2NH

amine), 61.0 (CHN cyclohexane), 123.4 (CH), 135.7 (CH), 136.23 (C), 148.4 (CH) 149.6 (CH). Mass spec: HR-ESI Calc for [M^+] 297.2079 found 297.2055

Synthesis of 11a

2 (0.5 g, 4.4 mmol) was dissolved in methanol (50 ml), and 4-pyridinecarboxaldehyde (0.83 ml, 8.8 mmol) added. The reaction mixture was stirred for 3h at room temperature, before the solvent was removed by rotary evaporation. The product was dried under reduced pressure. 81 % yield.

^{1}H ($CDCl_3$) 1.36 (m, 2H), 1.73 (m, 6H), 3.32 (m, 2H), 7.32 (d, 4H), 8.03 (s, 2H, CHN imine), 8.46 (d, 4H, CHN Ar). $^{13}C\{^1H\}$ ($CDCl_3$) 24.2 (CH_2), 32.6 (CH_2), 73.8 (CHN cyclohexane), 120.4 (CH), 142.9 (C), 150.3 (CHN Ar), 159.1 (CHN imine). Mass spec: HR-ESI Calc for [M^+] 293.1766 found 293.1770.

Synthesis of 11b

2 (0.5 g, 4.4 mmol) was dissolved in methanol (50 ml), and 2-pyridinecarboxaldehyde (0.83 ml, 8.8 mmol) added. The reaction mixture was stirred for 3h at room temperature, upon which sodium borohydride was added (0.5 g, 13.2 mmol). Following a further 3h reaction time, the solvent was removed by rotary evaporation and a 50:50 water:dichloromethane mix was added to the product. The organic layer was decanted off, and the remaining aqueous layer washed three times with dichloromethane. The organic layers were combined and dried over magnesium sulphate. The solvent was then removed by rotary evaporation before the product was dried under reduced pressure. 75 % yield.

^{1}H ($CDCl_3$) 0.97 (m, 2H), 1.15 (m, 2H), 1.66 (m, 2H), 2.10 (m, 4H), 3.65 (d J = 14.5 Hz, 2H, CH_2NH), 3.88 (d J = 14.5 Hz, 2H, CH_2NH), 7.19 (m, 4H), 8.47 (m, 4H). $^{13}C\{^1H\}$ ($CDCl_3$) 23.8 (CH_2), 30.4 (CH_2), 53.1 (CH_2NH amine), 60.1 (CHN cyclohexane), 121.9 (CH Ar), 148.8 (CHN Ar), 149.1 (C Ar). Mass spec: HR-ESI Calc for [M^+] 297.2079 found 297.2034

Synthesis of 12a

2 (0.15 g, 1.3 mmol) was dissolved in methanol (50 ml), and 3-methylpyridine-2-carboxaldehyde (0.3 ml, 2.6 mmol) added. The reaction mixture was stirred for 24h at room temperature. Following this the mixture was filtered and the solvent of the filtrate removed by rotary evaporation. The product was dried under reduced pressure. 66 % yield.

^{1}H ($CDCl_3$) 1.45 (m, 2H), 1.79 (m, 6H), 2.31 (s, 6H), 3.46 (m, 2H), 7.02 (m, 2H), 7.32 (m, 2H), 8.4 (d, 2H, CHN Ar) 8.42 (s, 2H, CHN imine). $^{13}C\{^{1}H\}$ ($CDCl_3$) 20.0 (CH_3), 24.2 (CH_2), 32.9 (CH_2), 74.9 (CHN cyclohexane), 123.9 (CH Ar), 133.5 (C, Ar), 139.5 (CH Ar), 147.5 (CHN imine), 152.1 (C), 161.5 (CHN imine). Mass spec: HR-ESI Calc for [M^+] 321.2079 found 321.2076.

Synthesis of 12b

2 (0.3 g, 2.6 mmol) was dissolved in methanol (50 ml), and 3-methylpyridine-2-carboxaldehyde (0.60 ml, 5.2 mmol) added. The reaction mixture was stirred for 3h at room temperature, upon which sodium borohydride was added (0.3 g, 7.9 mmol). Following a further 3h reaction time, the solvent was removed by rotary evaporation and a 50:50 water:dichloromethane mix was added to the product. The organic layer was decanted off, and the remaining aqueous layer washed three times with dichloromethane. The organic layers were combined, dried over magnesium sulphate and gravity filtered. The solvent was then removed by rotary evaporation before the product was dried under reduced pressure. 52 % yield.

^{1}H ($CDCl_3$) 1.17 (m, 2H), 1.67 (m, 2H), 2.32 (s, 6H, CH_3), 2.35 (br m, 6H), 3.78 (d J = 14 Hz, 2H, CH_2NH), 4.04 (d J = 14 Hz, 2H, CH_2NH), 7.06 (m, 2H), 7.25 (m, 2H), 7.38 (m, 2H), 8.33 (m, 2H). $^{13}C\{^{1}H\}$ ($CDCl_3$) 18.1 (CH_3), 25.0 (CH_2), 31.6 (CH_2), 121.8 (CH Ar), 131.3 (C, Ar), 137.6 (CH Ar), 146.2 (CH Ar). Mass spec: HR-ESI Calc for [M^+] 325.2392 found 325.2376

Synthesis of 13a

2 (0.5 g, 4.4 mmol) was dissolved in methanol (50 ml), and 2-thiophenecarboxaldehyde (0.83 ml, 8.8 mmol) added. The reaction mixture was stirred for 3h at room temperature. Following this the mixture was filtered and the solvent of the filtrate removed by rotary evaporation. The product was dried under reduced pressure. 54 % yield.

^{1}H ($CDCl_3$) 1.38 (m, 2H), 1.75 (m, 4H), 3.22 (m, 2H), 6.98 (m, 2H), 7.06 (d, 2H), 7.20 (m, 2H), 8.20 (s, 2H, CHN imine). $^{13}C\{^{1}H\}$ ($CDCl_3$) 24.4 (CH_2), 33.0 (CH_2), 73.8 (CHN cyclohexane), 127.1 (CH Ar), 128.5 (CH Ar), 130.0 (CH Ar), 142.3 (C), 154.4 (CHN imine). Mass spec: HR-ESI Calc for [M^+] 303.0988 found 303.0998.

Single Crystal X-Ray Diffraction:

Empirical formula	$C_{16}H_{18}N_2S_2$	
Formula weight	302.44	
Temperature	150(2) K	
Wavelength	0.71073 Å	
Crystal system	Monoclinic	
Space group	$P2_1$	
Unit cell dimensions	a = 8.7420(2) Å	α = 90°
	b = 9.2670(2) Å	β = 113.831(2)°
	c = 10.7390(2) Å	γ = 90°
Volume	795.81(3) Å^3	
Z	2	
Density (calculated)	1.262 Mg/m^3	
Absorption coefficient	0.326 mm^{-1}	
F(000)	320	
Crystal Size	0.30 × 0.25 × 0.20 mm	
Theta range for data collection	3.88 to 27.49°	
Limiting indices	-11<=h<=11, -12<=k<=12, -13<=l<=13	
Reflections collected	13308	
Independent reflections	3602 [R(int) = 0.0303]	
Completeness to theta = 27.49°	99.0 %	
Absorption correction	None	
Max. and Min. transmission	0.9376 and 0.9085	
Refinement method	Full-matrix least-squares on F^2	
Data / restraints / parameters	3602 / 1 / 181	
Goodness-of-fit on F^2	1.019	
Final R indices [I>2sigma(I)]	R1 = 0.0254, wR2 = 0.0677	
R indices (all data)	R1 = 0.0274, wR2 = 0.0697	
Absolute structure parameter	-0.01(5)	
Largest diff. peak and hole	0.150 and -0.219 e.Å^{-3}	

Synthesis of 13b

2 (0.5 g, 4.4 mmol) was dissolved in methanol (50 ml), and 2-thiophenecarboxaldehyde (0.83 ml, 8.8 mmol) added. The reaction mixture was

stirred for 3h at room temperature, upon which sodium borohydride was added (0.5 g, 13.2 mmol). Following a further 3h reaction time, the solvent was removed by rotary evaporation and a 50:50 water:dichloromethane mix was added to the product. The organic layer was decanted off, and the remaining aqueous layer washed three times with dichloromethane. The organic layers were combined, dried over magnesium sulphate and gravity filtered. The solvent was then removed by rotary evaporation before the product was dried under reduced pressure. 43 % yield.

^{1}H ($CDCl_3$) 1.01 (m, 2H), 1.22 (m, 2H), 1.71 (m, 2H), 2.11 (m, 2H), 2.28 (m, 2H), 3.84 (d J = 14 Hz, 2H, CH_2NH amine), 4.08 (d J = 14 Hz, 2H, CH_2NH amine), 6.93 (m, 4H), 7.18 (m, 2H). ^{13}C{^{1}H} ($CDCl_3$) 25.0 (CH_2), 31.4 (CH_2), 45.4 (CH_2NH amine), 60.3 (CHN cyclohexane), 124.2 (CH Ar), 124.4 (CH Ar), 126.6 (CHS Ar), 145.0 (**C**S Ar). Mass spec: HR-ESI Calc for [M^+] 307.1303 found 307.1311.

Synthesis of 14a

2 (0.5 g, 4.4 mmol) was dissolved in methanol (50 ml), and 5-bromo-2-furaldehyde (1.5 g, 8.8 mmol) added. The reaction mixture was stirred for 3h at room temperature. Following this the mixture was filtered and the solvent of the filtrate removed by rotary evaporation. The product was dried under reduced pressure. 50 % yield.

^{1}H ($CDCl_3$) 1.32 (m, 2H), 1.70 (m, 4H), 3.22 (m, 2H), 6.20 (d, 2H), 6.43 (d, 2H), 7.79 (s, 2H, CHN imine). ^{13}C{^{1}H} ($CDCl_3$) 24.5 (CH_2), 33.0 (CH_2), 74.2 (CHN cyclohexane), 113.2 (CH Ar), 116.0 (CH Ar), 125.5 (C), 148.3 (CHN imine), 153.0 (C). Mass spec: HR-ESI Calc for [M^+] 426.9656 found 426.9650.

Synthesis of 14b

2 (0.5 g, 4.4 mmol) was dissolved in methanol (50 ml), and 5-bromo-2-furaldehyde (1.5 g, 8.8 mmol) added. The reaction mixture was stirred for 3h at room temperature, upon which sodium borohydride was added (0.5 g, 13.2 mmol). Following a further 3h reaction time, the solvent was removed by rotary evaporation and a 50:50 water:dichloromethane mix was added to the product. The organic layer was decanted off, and the remaining aqueous layer washed three times with dichloromethane. The organic layers were combined, dried over

magnesium sulphate and gravity filtered. The solvent was then removed by rotary evaporation before the product was dried under reduced pressure. 39 % yield.

^{1}H ($CDCl_3$) 1.00 (m, 2H), 1.20 (m, 2H), 1.66 (m, 2H), 1.97 (m, 2H), 2.16 (m, 2H), 3.59 (d J = 14.5 Hz, 2H, CH_2NH amine), 3.76 (d J = 14.5 Hz, 2H, CH_2NH amine), 6.12 (d J = 3 Hz, 2H, Ar), 6.17 (d J = 3 Hz, 2H, Ar). ^{13}C{^{1}H} ($CDCl_3$) 24.9 (CH_2), 31.4 (CH_2), 43.6 (CH_2NH amine), 59.1 (CHN cyclohexane), 109.9 (CH Ar), 111.8 (CH Ar), 120.2 (C Ar), 156.8 (**C**Br Ar). Mass spec: HR-ESI Calc for [M^+] 432.9950 found 432.9964.

Synthesis of 15

15 was purchased from Strem Chemicals.

Synthesis of 16

2 (0.5 g, 4.4 mmol) was dissolved in methanol (50 ml), and 2-naphthaldehyde (1.37 g, 8.8 mmol) added. The reaction mixture was stirred for 3h at room temperature, upon which sodium borohydride was added (0.5 g, 13.2 mmol). Following a further 3h reaction time, the solvent was removed by rotary evaporation and a 50:50 water:dichloromethane mix was added to the product. The organic layer was decanted off, and the remaining aqueous layer washed three times with dichloromethane. The organic layers were combined, dried over magnesium sulphate and gravity filtered. The solvent was then removed by rotary evaporation before the product was dried under reduced pressure. 49 % yield.

^{1}H ($CDCl_3$) 0.96 (m, 2H CH_2), 1.12 (m, 2H CH_2), 1.63 (m, 2H CH_2), 1.90 (m, 2H CH_2), 2.20 (m, 2H CHN cyclohexane), 3.68 (d J = 13.5 Hz, 2H CH_2NH), 3.93 (d J = 13.5 Hz, 2H CH_2NH), 7.32 (m, 6H), 7.66 (m, 8H). ^{13}C{^{1}H} ($CDCl_3$) 24.6 (CH_2), 33.1 (CH_2), 73.4 (CHNH cyclohexane), 124.0 (CH Ar), 126.2 (CH Ar), 126.8 (CH Ar), 127.7 (CH Ar), 128.2 (CH Ar), 128.5 (CH Ar), 129.1 (CH Ar), 133.1 (C Ar), 134.0 (C Ar), 134.5 (C Ar), 161.2 (CH_2NH). Mass spec: HR-ESI Calc for [M^+] 395.2487 found 395.2485

Synthesis of 17

17 was purchased from Sigma Aldrich.

Synthesis of 18a

2-(diphenylphosphino)benzaldehyde (0.5 g, 1.72 mmol) was placed in a round bottomed flask which was repeatedly degassed and backfilled with argon. To this, a solution of **17** (0.25 ml, 1.79 mmol) in dichloromethane (50 ml) was added, and the reaction mixture stirred at room temperature for 3h. Following this, the solvent was removed by rotary evaporation and the product dried under reduced pressure. 83 % yield.

^{1}H ($CDCl_3$) 1.14 (t, 3H CH_3), 1.78 (m, 6H), 2.54 (m, 2H), 2.97 (m, 2H), 3.33 (m, 1H, CHN pyrrolidine ring), 7.31 (m, 14H), 8.82 (s, 1H CHN imine). ^{13}C{^{1}H} ($CDCl_3$) 13.7 (CH_3), 22.4 (CH_2), 29.2 (CH_2), 48.8 (CH_2), 52.9 (CH_2), 53.9 (CH_2), 64.4 (CHN pyrrolidine ring), 66.3 (CH_2), 127.6 (CH), 128.6 (CH), 130.1 (CH), 133.2 (CH), 134.2 (CH), 136.4 (C), 137.3 (C), 139.4 (C), 160.2 (CHN imine). ^{31}P{^{1}H} ($CDCl_3$) major peak at -12.8 (PPh_2), minor peak at 31.7 (oxidised PPh_2).Mass spec: HR-ESI Calc for [M^+] 401.2147 found 401.2145

Synthesis of 18b

2-(diphenylphosphino)benzaldehyde (0.5 g, 1.72 mmol) was placed in a round bottomed flask which was repeatedly degassed and backfilled with argon. To this, a solution of **17** (0.25 ml, 1.79 mmol) in methanol (50 ml) was added, and the reaction mixture stirred at room temperature for 3h. At this stage, sodium borohydride was added (0.13 g, 3.44 mmol), and the reaction mixture stirred for a further 3h at room temperature. Following this, the solvent was removed by rotary evaporation and the residue dissolved in dichloromethane (50 ml). This was gravity filtered and the solvent removed by rotary evaporation, before the product was dried under reduced pressure. 46 % yield.

^{1}H ($CDCl_3$) 1.00 (t, 3H CH_3), 1.38 (m, 2H CH_2), 1.60 (m, 4H, 2 × CH_2), 2.03 (m, 2H CH_2), 2.66 (m, 2H CH_2), 3.02 (m, 1H CHN pyrrolidine ring), 3.93 (s, 2H, C**H$_2$**NH(Ar)), 7.26 (m, 14H). ^{13}C{^{1}H} ($CDCl_3$) 13.9 (CH_3), 22.7 (CH_2), 29.2 (CH_2), 48.9 (CH_2), 52.9 (CH_2), 53.7 (CH_2), 64.1 (CHN pyrrolidine ring), 127.1 (CH), 128.6 (CH), 131.9 (CH), 133.7 (CH), 134.0 (CH), 135.5 (C), 136.8 (C), 144.9 (C). ^{31}P{^{1}H} ($CDCl_3$) major peak at -15.4 (PPh_2), minor peak at 32.9. Mass spec: HR-ESI Calc for [M^+] 403.2303 found 403.2432

Synthesis of 19

This reaction was carried out in accordance with that reported by Nguyen et. al.[3] **2** (1.0 g, 8.8 mmol) was dissolved in diethyl ether (30 ml) and anhydrous hydrochloric acid in ether (8.8 ml, 8.8 mmol) added dropwise at 5 °C. The mixture was then stirred for 24h at room temperature. The resulting precipitate was collected by vacuum filtration and washed with diethyl ether. The product was dried under reduced pressure. 68 % yield.

^{1}H (MeOD) 1.35 (m, 4H), 1.79 (m, 2H), 2.01 (m, 2H), 2.61 (m, 2H). ^{13}C[^{1}H} (MeOD) 26.0 (CH_2), 34.3 (CH_2), 56.6 (CH). Mass spec: HR-ESI Calc for [M^+] 115.1235 found 115.1244

Synthesis of 20a

19 (0.3 g, 3.8 mmol) was dissolved in methanol (40 ml) and benzaldehyde added (0.39 ml, 3.8 mmol). The mixture was stirred at room temperature for 3h before the solvent was removed by rotary evaporation. The product dried under reduced pressure. 74 % yield.

^{1}H ($CDCl_3$) 1.40 (m, 4H), 1.70 (m, 3H), 2.07 (m, 1H), 3.21 (m, 2H), 7.36 (m, 3H), 7.72 (m, 2H), 8.39 (s, 1H, CHN). ^{13}C{^{1}H} ($CDCl_3$) 25.4 (CH_2), 30.9 (CH_2), 56.9 (CHN cyclohexane), 72.4 (CHN cyclohexane), 130.1 (CH), 132.9 (CH), 137.5 (C), 166.05 (CH imine). Mass spec: HR-ESI Calc for [M^+] 203.1548 found 203.1540

Synthesis of 20b

19 (0.3 g, 3.8 mmol) was dissolved in methanol (40 ml) and benzaldehyde added (0.39 ml, 3.8 mmol). The reaction mixture was stirred at room temperature for 3h, and then sodium borohydride was added (0.29 g, 7.6 mmol). The reaction mixture was stirred for a further 3h at room temperature before the solvent was removed by rotary evaporation. The residue was dissolved in dichloromethane (50 ml), which was then gravity filtered, and the solvent removed by rotary evaporation. The product was dried under reduced pressure. 38 % yield.

^{1}H ($CDCl_3$) 1.16 (m, 4H), 1.75 (m, 6H), 3.61 (d, J = 13.5 Hz, 1H, C**H$_2$**NH), 3.87 (d, 13.5 Hz, 1H, C**H$_2$**NH), 7.22 (m, 5H). ^{13}C{^{1}H} ($CDCl_3$) 25.3 (CH_2), 31.4 (CH_2), 51.1 (CH_2NH), 55.4 (CHN cyclohexane), 63.2 (CHN cyclohexane), 126.8

(CH), 128.2 (CH), 130.7 (CH), 141.0 (C). Mass spec: HR-ESI Calc for [M^+] 205.1705 found 205.1692

Synthesis of 21a

This reaction was carried out in accordance to that reported by Nguyen et. al.[3] **20b** (0.3 g, 1.25 mmol) and potassium carbonate (0.34 g, 2.46 mmol) were dissolved in methanol (40 ml), and terephthalaldehyde added (0.08 g, 0.60 mmol). The reaction mixture was stirred at room temperature for 24h, before the solvent was removed by rotary evaporation. The residue was dissolved in 50:50 dichloromethane:water, and the organic layer decanted off. The aqueous layer was washed three times with dichloromethane, and the organic layers combined. This was dried over magnesium sulphate, gravity filtered and the solvent removed by rotary evaporation. The product was dried under reduced pressure. 81 % yield.

^{1}H ($CDCl_3$) 1.26 (m, 6H CH_2), 1.67 (m, 10H CH_2), 2.10 (m, 3H CH_3), 2.76 (m, 2H CHN cyclohexane), 3.07 (m, 2H CHN cyclohexane), 3.66 (d J = 13.5 Hz, 2H C**H$_2$**NH), 3.82 (d J = 13.5 Hz, 2H C**H$_2$**NH), 7.19 (m, 14H), 8.34 (s, 2H, CHN imine). ^{13}C{^{1}H} ($CDCl_3$) 23.4 (CH_2), 31.9 (CH_2), 72.8 (CHN cyclohexane), 126.8 (CH Ar), 126.9 (CH Ar), 127.0 (CH Ar), 127.4 (CH Ar), 129.2 (CH Ar), 135.2 (CH Ar), 136.8 (C), 136.9 (C), 159.5 (CHN imine), 160.1 (CHN imine). Mass spec: HR-ESI Calc for [M^+] 507.3488 found 507.3483

Synthesis of 21b

21a (0.2 g, 0.40 mmol) was dissolved in methanol (40 ml), and sodium borohydride added (0.05 g, 1.32 mmol). The reaction mixture was stirred at room temperature for 3h, before the solvent was removed by rotary evaporation. The residue was dissolved in 50:50 dichloromethane:water, and the organic layer decanted off. The aqueous layer was washed three times with dichloromethane, and the organic layers combined. This was dried over magnesium sulphate, gravity filtered and the solvent removed by rotary evaporation. The product was dried under reduced pressure. 62 % yield.

^{1}H ($CDCl_3$) 0.98 (m, 5H), 1.15 (m, 5H), 2.17 (m, 10H), 3.57 (dd, 4H), 3.82 (dd, 4H), 7.23 (m, 14H). ^{13}C{^{1}H} ($CDCl_3$) 25.1 (CH_2), 49.3 (CH_2NH), 126.8 (CH

Ar), 128.1 (CH Ar), 128.4 (CH Ar). Mass spec: HR-ESI Calc for [M^+] 511.3801 found 511.3849

Synthesis of 22

2 (1.0 g, 8.8 mmol) was dissolved in methanol (50 ml), and 3,5-dichlorosalicylaldehyde (3.35 g, 17.6 mmol) added. The reaction mixture was stirred for 3h at room temperature, upon which sodium borohydride was added (1.0 g, 26.4 mmol). The reaction mixture was stirred for a further 3h, and then the solvent was removed by rotary evaporation. The residue was dissolved in dichloromethane, which was gravity filtered and the solvent removed by rotary evaporation. The product was dried under reduced pressure. 49 % yield.

^{1}H ($CDCl_3$) 1.68 (m, 3H, CH_2), 1.77 (m, 2H, CH_2), 2.02 (m, 3H, CH_2), 2.27 (m, 1H CHN cyclohexane), 2.39 (m, 1H CHN cyclohexane), 3.88 (m, 4H C**H$_2$**NH), 5.26 (s, 2H OH), 6.84 (s, 2H CH), 7.21 (s, 2H CH). ^{13}C{^{1}H} ($CDCl_3$) 24.1 (CH_2), 30.7 (CH_2), 49.0 (CH_2NH), 59.8 (CHN cyclohexane), 126.6 (CH), 128.7 (CH). Mass spec: HR-ESI Calc for [M^+] 463.0514 found 463.0583

Synthesis of 23

2 (1.0 g, 8.8 mmol) was dissolved in methanol (50 ml), and 3,5-dichlorosalicylaldehyde (4.10 g, 17.6 mmol) added. The reaction mixture was stirred for 3h at room temperature, upon which sodium borohydride was added (1.0 g, 26.4 mmol). The reaction mixture was stirred for a further 3h, and then the solvent was removed by rotary evaporation. The residue was dissolved in dichloromethane, which was gravity filtered and the solvent removed by rotary evaporation. The product was dried under reduced pressure. 89 % yield.

^{1}H ($CDCl_3$) 1.26 (m, 36H, CH_3 $_t$Bu), 1.70 (m, 6H CH_2), 2.14 (m, 2H, CH_2), 2.40 (m, 2H CHN cyclohexane), 3.83 (d J = 13.5 Hz, 2H C**H$_2$**NH), 4.00 (d, J = 13.5 Hz, 2H C**H$_2$**NH), 6.80 (m, 2H CH), 7.16 (m, 2H CH), 10.64 (br s, 2H OH). ^{13}C{^{1}H} ($CDCl_3$) 24.5 (CH_2), 31.7 (CH_3 $_t$Bu), 34.9 (CH_2), 50.9 (CH_2NH), 59.9 (CHN cyclohexane), 122.4 (C), 123.1 (CH), 126.1 (CH), 136.0 (C), 140.6 (C), 154.4 (COH). Mass spec: HR-ESI Calc for [M^+] 551.4577 found 551.4630

Synthesis of 24

This oxidation was carried out in accordance with that reported by Ise et.al.[4] 2,6-bis(hydroxymethyl)-*p*-cresol (5.0g, 29.7 mmol) was dissolved in dry THF (200 ml), and 8 equivalents of activated manganese(IV) oxide added (20.7g, 238 mmol). The reaction mixture was refluxed at 70 °C for 3.5 days, before being gravity filtered twice. The solvent was removed by rotary evaporation, and the product dried under reduced pressure. 58 % yield.

^{1}H ($CDCl_3$) 2.24 (s, 3H C**H**$_3$), 7.66 (s, 2H Ar), 10.10 (s, 2H C**H**O), 11.35 (s, 1H O**H**). ^{13}C{^{1}H} ($CDCl_3$) 19.2 (**C**H$_3$), 121.9 (**C**H), 128.5 (**C**CH$_3$), 136.9 (**C**CHO), 160.7 (**C**OH), 191.2 (**C**HO). Mass spec: HR-ESI Calc for [M^+] 165.0552 found 165.0542

6.3 Experimental from Chapter Three

The following iridium(I) and rhodium(I) complexes were prepared as reported by Jones et. al.[5] The following ruthenium(II) complexes were prepared as reported by Raja et. al.[6] The preparation of the following copper(II) complexes were based on that reported by Reedijk et. al.[7] Titanium and Zirconium complexes were prepared in accordance with that reported by Whitelaw et. al.[8]

Preparation of [Ir(3b)(cod)]OTf

[IrCl(cod)]$_2$ (100 mg, 0.15 mmol) was placed in a schlenk flask which was repeatedly degassed and backfilled with argon. This was dissolved in dry THF (10 ml), and AgOTf added (90 mg, 0.34 mmol). The reaction mixture was stirred for 30 mins before being filtered. **3b** (90 mg, 0.30 mmol) was added to the filtrate and this was stirred for a further 30 mins. Following this hexane was added and decanted off once the precipitate had settled. The resulting complex was dried under reduced pressure.

^{1}H (MeOD) 1.26 (m, 4H), 1.70 (m, 4H), 2.08 (m, 2H), 3.34 (m, 4H), 3.90 (m, 4H), 4.33 (m, 4H), 7.46 (m, 10H). ^{13}C{^{1}H} (MeOD) 24.1 (CH_2), 26.9 (CH_2), 33.1 (CH_2), 69.3 (CH cod), 130.3 (CH), 130.7 (CH). Mass spec: HR-ESI Calc for [M^+] 595.2664 found 595.2632

Preparation of [Ir(4b)(cod)]OTf

$[IrCl(cod)]_2$ (100 mg, 0.15 mmol) was placed in a schlenk flask which was repeatedly degassed and backfilled with argon. This was dissolved in dry THF (10 ml), and AgOTf added (90 mg, 0.34 mmol). The reaction mixture was stirred for 30 mins before being filtered. **4b** (110 mg, 0.30 mmol) was dissolved in dry THF (5 ml), which was added to the filtrate, and this was stirred for a further 30 mins. Following this hexane was added and decanted off once the precipitate had settled. The resulting complex was dried under reduced pressure.

^1H (MeOD) 0.74 (m, 8H), 1.18 (m, 8H), 1.67 (m, 2H), 2.96 (d J = 13 Hz, 2H, C**H$_2$**NH), 3.09 (d J = 13 Hz, 2H, C**H$_2$**NH), 4.28 (s, 6H, OCH_3), 6.87 (m, 8H). $^{13}C\{^1H\}$ (MeOD) 26.4 (CH_2), 32.7 (CH_2), 56.5 (OCH_3), 68.2 (CH cod), 112.6 (CH), 122.3 (CH), 125.8 (C), 131.3 (CH), 133.4 (CH), 160.1 (**C**OMe). Mass spec: HR-ESI Calc for $[M^+]$ 655.2876 found 655.2865

Preparation of [Ir(8a)(cod)]OTf

$[IrCl(cod)]_2$ (100 mg, 0.15 mmol) was placed in a schlenk flask which was repeatedly degassed and backfilled with argon. This was dissolved in dry THF (10 ml), and AgOTf added (90 mg, 0.34 mmol). The reaction mixture was stirred for 30 mins before being filtered. **8a** (190 mg, 0.30 mmol) was added to the filtrate and this was stirred for a further 30 mins. Following this hexane was added and decanted off once the precipitate had settled. The resulting complex was dried under reduced pressure.

^1H (CD_2Cl_2) 1.28 (m, 6H), 1.54 (m, 2H), 1.75 (m, 8H, cod), 2.07 (m, 2H), 5.46 (m, 4H, cod), 6.93-7.76 (br m), 8.59 (s, 2H, CHN imine). $^{13}C\{^1H\}$ (CD_2Cl_2) 21.9 (CH_2), 23.5 (CH_2), 24.8 (CH_2), 27.2, 30.8 (CH_2), 127.7 (CH), 128.1 (CH), 128.5 (CH), 130.2 (CH), 131.6 (CH), 132.5 (C), 133.2 (CH), 133.5 (C). $^{31}P\{^1H\}$ (CD_2Cl_2) 21.2 (PPh_2). Mass spec: HR-ESI Calc for $[M^+]$-cod 851.2269 found 851.2348

Preparation of [Ir(15)(cod)]OTf

$[IrCl(cod)]_2$ (100 mg, 0.15 mmol) was placed in a schlenk flask which was repeatedly degassed and backfilled with argon. This was dissolved in dry THF (10 ml), and AgOTf added (90 mg, 0.34 mmol). The reaction mixture was

stirred for 30 mins before being filtered. **15** (90 mg, 0.32 mmol) was added to the filtrate and this was stirred for a further 30 mins. Following this hexane was added and decanted off once the precipitate had settled. The resulting complex was dried under reduced pressure.

^{1}H (CD_2Cl_2) 1.46 (m, 4H, CH_2 cod), 2.05 (m, 4H, CH_2 cod), 3.76 (m, 2H, CH cod), 4.26 (m, 2H, CH cod), 6.95 (d J = 8 Hz, 2H, Ar-H), 7.22 (m, 2H, Ar-H), 7.43 (m, 2H, Ar-H), 7.53 (d J = 8.5 Hz, 2H, Ar-H), 7.90 (d J = 8 Hz, 2H, Ar-H), 7.98 (d J = 8.5 Hz, 2H, Ar-H). ^{13}C{^{1}H} (CD_2Cl_2) 31.8 (CH_2 cod), 66.1 (CH cod), 120.4 (C Ar), 120.9 (CH Ar), 126.0 (CH Ar), 126.8 (CH Ar), 128.5 (CH Ar), 129.3 (CH Ar), 132.2 (CH Ar), 132.9 (C Ar), 133.7 (C Ar), 137.0 (C Ar). ^{19}F{^{1}H} (CD_2Cl_2) -79.0 (OTf). Mass spec: HR-ESI Calc for [M^+] 585.1882 found 585.1859

Single Crystal X-Ray Diffraction:

Empirical formula	$C_{30.50}H_{29}N_2ClF_6IrO_6S_2$	
Formula weight	925.33	
Temperature	150(2) K	
Wavelength	0.71073 Å	
Crystal system	Orthorhombic	
Space group	$P22_12_1$	
Unit cell dimensions	a = 10.13600(10) Å	α = 90°
	b = 15.09700(10) Å	β = 90°
	c = 21.2430(2) Å	γ = 90°
Volume	3250.67(5) Å^3	
Z	4	
Density (calculated)	1.891 Mg/m^3	
Absorption coefficient	4.400 mm^{-1}	
F(000)	1816	
Crystal Size	0.10 × 0.10 × 0.10 mm	
Theta range for data collection	3.84 to 27.51°	
Limiting indices	-13<=h<=13, -19<=k<=19, -27<=l<=27	
Reflections collected	72163	
Independent reflections	7448 [R(int) = 0.1001]	
Completeness to theta = 27.51°	99.5 %	
Absorption correction	Sortav	
Max. and Min. transmission	0.6674 and 0.6674	
Refinement method	Full-matrix least-squares on F^2	
Data / restraints / parameters	7448 / 4 / 535	

Goodness-of-fit on F^2	1.087
Final R indices [I>2sigma(I)]	R1 = 0.0328, wR2 = 0.0747
R indices (all data)	R1 = 0.0371, wR2 = 0.0768
Absolute structure parameter	-0.007(7)
Largest diff. peak and hole	1.987 and -2.084 e.Å^{-3}

Preparation of [Ir(3b)(cod)]BF_4

$[IrCl(cod)]_2$ (100 mg, 0.15 mmol) was placed in a schlenk flask which was repeatedly degassed and backfilled with argon. This was dissolved in dry THF (10 ml), and $AgBF_4$ added (60 mg, 0.31 mmol). The reaction mixture was stirred for 30 mins before being filtered. **3b** (90 mg, 0.30 mmol) was added to the filtrate and this was stirred for a further 30 mins. Following this hexane was added and decanted off once the precipitate had settled. The resulting complex was dried under reduced pressure.

^{1}H (MeOD) 0.60-2.70 (br m), 3.25 (m), 3.60-4.30 (br m), 4.80 (m), 7.10-7.70 (br m). $^{13}C\{^1H\}$ (MeOD) 25.9 (CH_2), 29.9 (CH_2), 30.4 (CH_2), 70.4 (CH cod), 130.4 (CH), 134.1 (C). Mass spec: HR-ESI Calc for [M^+] 595.2664 found 595.2635

Preparation of [Ir(6b)(cod)]BF_4

$[IrCl(cod)]_2$ (100 mg, 0.15 mmol) was placed in a schlenk flask which was repeatedly degassed and backfilled with argon. This was dissolved in dry THF (10 ml), and $AgBF_4$ added (60 mg, 0.31 mmol). The reaction mixture was stirred for 30 mins before being filtered. **6b** (110 mg, 0.30 mmol) was dissolved in dry THF (5 ml), which was added to the filtrate, and stirred for a further 30 mins. Following this hexane was added and decanted off once the precipitate had settled. The resulting complex was dried under reduced pressure.

^{1}H (CD_2Cl_2) 1.09 (br m, 2H), 1.26 (br m, 4H), 1.59 (br m, 4H), 2.06 (br m, 2H), 2.31 (br m, 2H), 2.49 (br m, 2H), 2.61 (br m, 2H), 3.79 (br m, 4H), 4.61 (br m, 4H), 7.37 (br m, 8H). $^{13}C\{^1H\}$ (CD_2Cl_2) 23.4 (CH_2), 31.8 (CH_2), 68.5 (CH cod), 126.1 (CH), 128.7 (CH), 131.2 (CH), 132.3 (CH), 135.1 (C). Mass spec: HR-ESI Calc for [M^+] 663.1885 found 663.1869

Preparation of [Ir(8a)(cod)]BF_4

$[IrCl(cod)]_2$ (100 mg, 0.15 mmol) was placed in a schlenk flask which was repeatedly degassed and backfilled with argon. This was dissolved in dry THF (10 ml), and $AgBF_4$ added (60 mg, 0.31 mmol). The reaction mixture was stirred for 30 mins before being filtered. **8a** (190 mg, 0.30 mmol) was added to the filtrate and this was stirred for a further 30 mins. Following this hexane was added and decanted off once the precipitate had settled. The resulting complex was dried under reduced pressure.

^1H (MeOD) 0.71 (m, 2H), 1.03 (m, 2H), 1.30 (m, 2H), 1.49 (m, 4H), 1.77 (m, 8H, cod), 3.65 (m, 4H, cod), 7.03-7.74 (br m), 8.33 (s, 2H, CHN imine). $^{13}C\{^1H\}$ (CD_2Cl_2) 23.5 (CH_2), 30.8 (CH_2), 127.8 (CH), 128.5 (CH), 130.2 (CH), 131.6 (CH), 132.5 (C), 133.5 (C). $^{31}P\{^1H\}$ (CD_2Cl_2) 21.2 (PPh_2). Mass spec: HR-ESI Calc for $[M^+]$-cod 851.2269 found 851.2337

Preparation of [Ir(15)(cod)]BF_4

$[IrCl(cod)]_2$ (100 mg, 0.15 mmol) was placed in a schlenk flask which was repeatedly degassed and backfilled with argon. This was dissolved in dry THF (10 ml), and $AgBF_4$ added (60 mg, 0.31 mmol). The reaction mixture was stirred for 30 mins before being filtered. **15** (90 mg, 0.32 mmol) was added to the filtrate and this was stirred for a further 30 mins. Following this hexane was added and decanted off once the precipitate had settled. The resulting complex was dried under reduced pressure.

^1H (MeOD) 2.11 (m, 8H, cod), 3.75 (m, 4H, cod), 6.93 (m, 2H), 7.21 (m, 2H), 7.45 (m, 4H), 8.00 (m, 4H). $^{13}C\{^1H\}$ (MeOD) 31.9 (CH_2 cod), 66.8 (CH cod), 122.0 (CH Ar), 127.0 (CH Ar), 128.0 (CH Ar), 128.7 (CH Ar), 130.0 (CH Ar), 132.3 (CH Ar), 133.4 (C Ar), 133.9 (C Ar), 135.4 (C Ar). Mass spec: HR-ESI calc 585.1882 for $[M^+]$, found 615.1944 when solvent is methanol, found 629.2121 when solvent is ethanol, found 643.2330 when solvent is isopropanol. Corresponds to [complex]+OCH_3, [complex]+OCH_2CH_3 and [complex]$OCH(CH_3)_2$, respectively.

Preparation of [Ir(9a)(cod)]BF_4

$[IrCl(cod)]_2$ (100 mg, 0.15 mmol) was placed in a schlenk flask which was repeatedly degassed and backfilled with argon. This was dissolved in dry THF

(10 ml), and $AgBF_4$ added (60 mg, 0.31 mmol). The reaction mixture was stirred for 30 mins before being filtered. **9a** (87 mg, 0.30 mmol) was added to the filtrate and this was stirred for a further 30 mins. Following this hexane was added and decanted off once the precipitate had settled. The resulting complex was dried under reduced pressure.

^1H ($CDCl_3$) 1.28-2.09 (br m, 14H), 2.25 (m, 4H), 3.73 (m, 4H, cod), 7.53 (m, 4H, Ar), 8.03 (m, 4H, Ar), 8.27 (s, 2H, CHN imine). $^{13}C\{^1H\}$ ($CDCl_3$) 30.6 (CH_2), 31.7 (CH_2 cod), 69.6 (CH cod), 76.4 (CHN cyclohexane), 135.5 (CH), 148.4 (CH), 160.4 (CHN imine). Mass spec: HR-ESI Calc for $[M^+]$ 593.2256 found 593.2311

Preparation of [Rh(8a)(cod)]OTf

$[RhCl(cod)]_2$ (100 mg, 0.20 mmol) was placed in a schlenk flask which was repeatedly degassed and backfilled with argon. This was dissolved in dry THF (10 ml), and AgOTf added (104 mg, 0.41 mmol). The reaction mixture was stirred for 30 mins before being filtered. **8a** (270 mg, 0.43 mmol) was added to the filtrate and this was stirred for a further 30 mins. Following this hexane was added and decanted off once the precipitate had settled. The resulting complex was dried under reduced pressure.

^1H (CD_2Cl_2) 1.45 (m, 2H), 2.12 (m, 2H), 2.35 (m, 2H), 2.67 (m, 2H), 3.53 (m, 2H), 6.74 (m, 4H), 6.92 (m, 4H), 7.24 (m, 6H), 7.43 (m, 6H), 7.59 (m, 2H), 7.76 (m, 6H), 8.63 (s, 2H, CHN). $^{13}C\{^1H\}$ (CD_2Cl_2) 23.7 (CH_2), 30.1 (CH_2), 69.6 (CH), 127.3 (CH), 128.7 (CH), 130.0 (CH), 131.8 (CH), 134.9 (C), 136.5 (C), 159.5 (CHN). $^{31}P\{^1H\}$ (CD_2Cl_2) 45.9 (PPh_2). Mass spec: HR-ESI Calc for $[M^+]$-cod 761.1722 found 761.1778

Preparation of [Rh(3b)(cod)]BF_4

$[RhCl(cod)]_2$ (100 mg, 0.20 mmol) was placed in a schlenk flask which was repeatedly degassed and backfilled with argon. This was dissolved in dry THF (10 ml), and $AgBF_4$ added (80 mg, 0.41 mmol). The reaction mixture was stirred for 30 mins before being filtered. **3b** (120 mg, 0.41 mmol) was added to the filtrate and this was stirred for a further 30 mins. Following this hexane was added and decanted off once the precipitate had settled. The resulting complex was dried under reduced pressure.

^{1}H (CD_2Cl_2) 1.51 (m, 8H), 2.31 (m, 8H), 3.00 (m, 1H, C**H**NH), 3.20 (m, 1H, C**H**NH), 3.51 (m, 4H), 4.00 (m, 4H), 7.49 (m, 10H). ^{13}C{^{1}H} (CD_2Cl_2) 25.2 (CH_2), 29.8 (CH_2), 30.5 (CH_2), 83.1 (CH cod), 129.5 (CH). Mass spec: HR-ESI Calc for [M^+] 505.2090 found 505.2688. Elemental analysis: calc C, 57.83; H, 6.58; N, 4.82 found C, 57.5; H, 6.60; N, 4.65

Single Crystal X-Ray Diffraction:

Empirical formula	$C_{28}H_{38}N_2BF_4Rh$	
Formula weight	592.32	
Temperature	150(2) K	
Wavelength	0.71073 Å	
Crystal system	Orthorhombic	
Space group	$P2_12_12_1$	
Unit cell dimensions	a = 10.32500(10) Å	α = 90°
	b = 11.15800(10) Å	β = 90°
	c = 23.0980(2) Å	γ = 90°
Volume	2661.04(4) Å^3	
Z	4	
Density (calculated)	1.478 Mg/m^3	
Absorption coefficient	0.690 mm^{-1}	
F(000)	1224	
Crystal Size	0.15 × 0.15 × 0.10 mm	
Theta range for data collection	3.65 to 27.48°	
Limiting indices	-13<=h<=13, -14<=k<=14, -29<=l<=29	
Reflections collected	44481	
Independent reflections	6104 [R(int) = 0.0624]	
Completeness to theta = 27.48°	99.7 %	
Absorption correction	Multi scan	
Max. and Min. transmission	0.9342 and 0.9036	
Refinement method	Full-matrix least-squares on F^2	
Data / restraints / parameters	6104 / 0 / 369	
Goodness-of-fit on F^2	1.074	
Final R indices [I>2sigma(I)]	R1 = 0.0316, wR2 = 0.0689	
R indices (all data)	R1 = 0.0422, wR2 = 0.0734	
Absolute structure parameter	-0.04(3)	
Largest diff. peak and hole	0.437 and -0.888 e.Å^{-3}	

Preparation of [Rh(3b)(nbd)]BF_4

[RhCl(nbd)]$_2$ (100 mg, 0.22 mmol) was placed in a schlenk flask which was repeatedly degassed and backfilled with argon. This was dissolved in dry THF (10 ml), and $AgBF_4$ added (85 mg, 0.44 mmol). The reaction mixture was stirred for 30 mins before being filtered. **3b** (128 mg, 0.44 mmol) was added to the filtrate and this was stirred for a further 30 mins. Following this hexane was added and decanted off once the precipitate had settled. The resulting complex was dried under reduced pressure.

^{1}H (MeOD) 0.79 (m, 2H), 1.01 (m, 2H), 1.21 (m, 2H), 1.52 (m, 4H), 1.72 (m, 2H), 3.37 (m, 2H), 3.55 (m, 2H), 3.82 (m, 4H), 7.37 (m, 10H, Ar). ^{13}C{^{1}H} (MeOD) 26.0 (CH_2), 28.0 (CH_2), 50.2 (CH), 72.2 (CH_2), 129.0 (CH), 129.6 (CH), 130.0 (CH), 130.4 (CH), 131.3 (CH). Mass spec: HR-ESI Calc for [M^+] 488.1699 found 521.1672. Corresponds to [complex]+methanol (calc 521.2039).

Preparation of [Rh(4b)(cod)]BF_4

[RhCl(cod)]$_2$ (100 mg, 0.20 mmol) was placed in a schlenk flask which was repeatedly degassed and backfilled with argon. This was dissolved in dry THF (10 ml), and $AgBF_4$ added (80 mg, 0.41 mmol). The reaction mixture was stirred for 30 mins before being filtered. **4b** (140 mg, 0.40 mmol) was dissolved in dry THF (5 ml), which was added to the filtrate and stirred for a further 30 mins. Following this hexane was added and decanted off once the precipitate had settled. The resulting complex was dried under reduced pressure. 51 % yield.

^{1}H (CD_2Cl_2) 1.27 (br m, 2H), 1.63 (br m, 8H), 2.29 (br m, 8H), 3.84 (br m, 4H, C**H$_2$**NH), 3.89 (s, 6H, OCH_3), 4.06 (br m, 4H, CH cod), 6.96 (m, 2H), 7.09 (m, 2H), 7.40 (m, 2H), 7.72 (m, 2H). ^{13}C{^{1}H} (CD_2Cl_2) 30.2 (CH_2), 31.4 (CH_2), 56.2 (OCH_3), 83.0 (CH cod), 111.7 (CH), 121.9 (CH), 131.1 (CH). Mass spec: HR-ESI Calc for [M^+] 565.2301 found 565.2309

Preparation of [Rh(5b)(cod)]BF_4

[RhCl(cod)]$_2$ (100 mg, 0.20 mmol) was placed in a schlenk flask which was repeatedly degassed and backfilled with argon. This was dissolved in dry THF (10 ml), and $AgBF_4$ added (80 mg, 0.41 mmol). The reaction mixture was stirred for 30 mins before being filtered. **5b** (131 mg, 0.40 mmol) was dissolved in dry THF (5 ml) added to the filtrate and this was stirred for a further 30 mins.

Following this hexane was added and decanted off once the precipitate had settled. The resulting complex was dried under reduced pressure.

^{1}H (MeOD) 1.66 (br m, 10H), 2.18 (m, 2H), 2.34 (m, 4H), 2.64 (m, 2H), 3.23 (m, 6H, CH_3), 4.01 (m, 4H, C**H$_2$**NH), 4.74 (m, 4H, CH cod), 7.23 (m, 5H), 7.43 (m, 1H), 7.56 (m, 1H), 7.94 (m, 1H). ^{13}C{^{1}H} (MeOD) 20.0 (CH_3), 25.8 (CH_2), 34.7 (CH_2 cod), 45.2 (CH_2), 52.5 (CH_2), 61.6 (CHNH), 83.0 (CH cod), 127.4 (C), 128.1 (CH), 129.2 (CH), 130.4 (CH), 131.4 (C), 132.4 (CH). Mass spec: HR-ESI Calc for [M^+] 533.2403 found 533.2359. Elemental analysis: calc C, 59.11; H, 6.94; N, 4.59 found C, 58.4; H, 6.70; N, 4.40

Preparation of [Rh(6b)(cod)]BF_4

[RhCl(cod)]$_2$ (100 mg, 0.20 mmol) was placed in a schlenk flask which was repeatedly degassed and backfilled with argon. This was dissolved in dry THF (10 ml), and $AgBF_4$ added (80 mg, 0.41 mmol). The reaction mixture was stirred for 30 mins before being filtered. **6b** (150 mg, 0.41 mmol) was dissolved in dry THF (5 ml), which was added to the filtrate and stirred for a further 30 mins. Following this hexane was added and decanted off once the precipitate had settled. The resulting complex was dried under reduced pressure. 48 % yield.

^{1}H (CD_2Cl_2) 1.08 (br m), 1.68 (br m), 2.29 (br m), 3.82 (br m, 2H, C**H$_2$**NH), 4.11 (br m, 4H, CH cod), 7.45 (m, 6H), 7.95 (br m, 2H). ^{13}C{^{1}H} (CD_2Cl_2) 23.7 (CH_2), 29.6 (CH_2), 82.5 (CH cod), 127.2 (CH), 129.3 (CH), 129.7 (CH), 131.2 (CH), 133.5 (C). Elemental analysis: calc C, 51.70; H, 5.58; N, 4.31 found C, 51.1; H, 5.19; N, 3.96

Single Crystal X-Ray Diffraction:

Empirical formula	$C_{29}H_{35}N_2BF_4RhCl_5$	
Formula weight	778.56	
Temperature	150(2) K	
Wavelength	0.71073 Å	
Crystal system	Monoclinic	
Space group	*C*2	
Unit cell dimensions	a = 16.9280(4) Å	α = 90°
	b = 8.5520(2) Å	β = 110.2110(10)°
	c = 23.5890(7) Å	γ = 90°
Volume	3204.67(14) Å^3	

Z	4
Density (calculated)	1.614 Mg/m^3
Absorption coefficient	0.997 mm^{-1}
F(000)	1576
Crystal Size	0.10 × 0.10 × 0.10 mm
Theta range for data collection	3.51 to 25.65°
Limiting indices	-20<=h<=20, -10<=k<=10, -28<=l<=28
Reflections collected	25493
Independent reflections	6086 [R(int) = 0.1052]
Completeness to theta = 25.65°	99.5 %
Absorption correction	None
Max. and Min. transmission	0.9069 and 0.9069
Refinement method	Full-matrix least-squares on F^2
Data / restraints / parameters	6086 / 1 / 340
Goodness-of-fit on F^2	1.071
Final R indices [I>2sigma(I)]	R1 = 0.0766, wR2 = 0.1830
R indices (all data)	R1 = 0.1010, wR2 = 0.2006
Absolute structure parameter	-0.02(8)
Largest diff. peak and hole	1.203 and -1.565 e.$Å^{-3}$

Preparation of [Rh(8a)(cod)]BF_4

$[RhCl(cod)]_2$ (100 mg, 0.20 mmol) was placed in a schlenk flask which was repeatedly degassed and backfilled with argon. This was dissolved in dry THF (10 ml), and $AgBF_4$ added (80 mg, 0.41 mmol). The reaction mixture was stirred for 30 mins before being filtered. **8a** (270 mg, 0.43 mmol) was added to the filtrate and this was stirred for a further 30 mins. Following this hexane was added and decanted off once the precipitate had settled. The resulting complex was dried under reduced pressure.

^1H (CD_2Cl_2) 1.43 (m, 2H), 2.12 (m, 2H), 2.35 (m, 2H), 2.66 (m, 2H), 3.53 (m, 2H), 6.74 (m, 4H), 6.94 (m, 4H), 7.24 (m, 6H), 7.43 (m, 6H), 7.57 (m, 2H), 7.77 (m, 6H), 8.61 (s, 2H, CHN). $^{13}C\{^1H\}$ (CD_2Cl_2) 23.7 (CH_2), 30.1 (CH_2), 69.6 (CH), 127.4 (CH), 128.7 (CH), 130.2 (CH), 131.7 (CH), 134.8 (C), 136.4 (C), 159.5 (CHN). $^{31}P\{^1H\}$ (CD_2Cl_2) 45.9 (PPh_2). Mass spec: HR-ESI Calc for $[M^+]$-cod 761.1722 found 761.1746

Preparation of [Rh(15)(cod)]BF_4

$[RhCl(cod)]_2$ (100 mg, 0.20 mmol) was placed in a schlenk flask which was repeatedly degassed and backfilled with argon. This was dissolved in dry THF (10 ml), and $AgBF_4$ added (80 mg, 0.41 mmol). The reaction mixture was stirred for 30 mins before being filtered. **15** (120 mg, 0.42 mmol) was added to the filtrate and this was stirred for a further 30 mins. Following this hexane was added and decanted off once the precipitate had settled. The resulting complex was dried under reduced pressure. 54 % yield.

^1H (CD_2Cl_2) 0.49 (br m, 2H, CH_2 cod), 1.62 (br m, 3H, CH_2 cod), 2.45 (br m, 3H, CH_2 cod), 4.23 (br m, 4H, CH cod), 7.00 (d, 2H), 7.26 (br m, 5H), 7.93 (br m, 5H). $^{13}C\{^1H\}$ (MeOD) 31.4 (CH_2 cod), 81.6 (CH cod), 121.7 (CH Ar), 126.4 (CH Ar), 128.5 (CH Ar), 130.0 (CH Ar), 132.1 (CH Ar), 135.2 (C Ar). Mass spec: HR-ESI Calc for $[M^+]$ 495.1308 found 495.1340

Preparation of [Rh(16)(cod)]BF_4

$[RhCl(cod)]_2$ (100 mg, 0.20 mmol) was placed in a schlenk flask which was repeatedly degassed and backfilled with argon. This was dissolved in dry THF (10 ml), and $AgBF_4$ added (80 mg, 0.41 mmol). The reaction mixture was stirred for 30 mins before being filtered. **16** (40 mg, 0.10 mmol) was dissolved in dry THF (5 ml), which was added to the filtrate and stirred for a further 30 mins. Following this hexane was added and decanted off once the precipitate had settled. The resulting complex was dried under reduced pressure. 54 % yield.

^1H (MeOD) 1.19 (m, 2H), 1.63 (m, 8H, CH_2 cod), 2.10 (m, 2H), 2.33 (m, 4H), 2.53 (m, 2H), 2.95 (d J = 13.5 Hz, 1H C**H$_2$**NH), 3.61 (m, 2H C**H$_2$**NH), 3.86 (d J = 13.5 Hz, 1H C**H$_2$**NH), 4.74 (m, 4H, CH cod), 7.34-8.06 (m, 14H). $^{13}C\{^1H\}$ (MeOD) 26.1 (CH_2), 30.8 (CH_2 cod), 59.8 (CHNH), 86.0 (CH cod), 128.4 (CH), 129.4 (CH), 130.2 (CH), 131.3 (CH), 132.4 (C), 135.0 (C). Mass spec: HR-ESI Calc for $[M^+]$ 605.2403 found 605.2428

Preparation of [Rh(9a)(cod)]BF_4

$[RhCl(cod)]_2$ (100 mg, 0.20 mmol) was placed in a schlenk flask which was repeatedly degassed and backfilled with argon. This was dissolved in dry THF (10 ml), and $AgBF_4$ added (80 mg, 0.41 mmol). The reaction mixture was stirred for 30 mins before being filtered. **9a** (119 mg, 0.41 mmol) was added to the filtrate and stirred for a further 30 mins. Following this hexane was added and

decanted off once the precipitate had settled. The resulting complex was dried under reduced pressure. 26 % yield.

^{1}H ($CDCl_3$) 0.81 (m, 1H), 1.20 (m, 2H), 1.57 (m, 3H), 1.87 (m, 8H, cod), 2.11 (m, 2H), 2.44 (m, 2H), 4.15 (m, 4H, CH cod), 7.64 (m, 8H, Ar), 8.08 (s, 2H, CHN imine). $^{13}C\{^{1}H\}$ ($CDCl_3$) 28.0 (CH_2 cyclohexane), 128.7 (CH Ar). Mass spec: HR-ESI Calc for [M^+] 503.1682 found 503.1689

Preparation of [Rh(9b)(cod)]BF_4

[RhCl(cod)]$_2$ (100 mg, 0.20 mmol) was placed in a schlenk flask which was repeatedly degassed and backfilled with argon. This was dissolved in dry THF (10 ml), and $AgBF_4$ added (80 mg, 0.41 mmol). The reaction mixture was stirred for 30 mins before being filtered. **9b** (120 mg, 0.41 mmol) was dissolved in dry THF (5 ml), which was added to the filtrate and stirred for a further 30 mins. Following this hexane was added and decanted off once the precipitate had settled. The resulting complex was dried under reduced pressure. 46 % yield.

^{1}H (MeOD) 1.15 (br m), 1.64 (br m), 2.24 (br m), 3.34 (m, C**H**NH cyclohexane), 4.21 (d J = 15.5 Hz, 2H, C**H$_2$**NH), 4.33 (d J = 15.5 Hz, 2H, C**H$_2$**NH)), 4.83 (m, 4H, CH cod), 7.43 (m, 2H), 7.52 (m, 2H), 7.91 (m, 2H), 8.51 (m, 2H). $^{13}C\{^{1}H\}$ (MeOD) 26.2 (CH_2), 32.3 (CH_2), 54.4 (CH_2NH), 64.2 (CHNH cyclohexane), 69.3 (CH_2 cod), 73.8 (CH cod), 124.3 (CH), 125.3 (CH), 139.5 (CH), 151.0 (CHN Ar), 161.1 (C Ar). Mass spec: HR-ESI Calc for [M^+] 507.1995 found 507.2002.

Preparation of [Ru(3b)(*p*-cymene)Cl]Cl

[$RuCl_2$(*p*-cymene)]$_2$ (100 mg, 0.16 mmol) was placed in a schlenk flask which was repeatedly degassed and backfilled with argon. This was dissolved in dry dichloromethane, and **3b** added (100 mg, 0.34 mmol). The reaction mixture was stirred for 1 h before hexane was added, and decanted off once the precipitate had settled. The resulting complex was dried under reduced pressure. 48 % yield.

^{1}H (CD_2Cl_2) 1.37 (m, 6H), 1.47 (m, 3H), 1.69 (m, 4H), 2.19 (m, 1H), 2.60 (m, 6H), 4.01 (m, 4H, C**H$_2$**NH), 7.40 (m, 14H). $^{13}C\{^{1}H\}$ (CD_2Cl_2) 20.4 (CH_3 cym), 21.8 (CH_3 cym), 27.7 (CH_2), 29.3 (CH cym), 31.6 (CH_2), 51.9 (CH_2NH), 60.9 (CHNH), 127.0 (CH), 128.5 (CH), 129.6 (CH), 130.8 (CH), 135.7 (CH), 136.4

(C), 137.0 (C), 137.2 (C). Mass spec: HR-ESI Calc for [M^+] 565.1923 found 565.1913

Preparation of [Ru(4b)(*p*-cymene)Cl]Cl

[$RuCl_2$(*p*-cymene)]$_2$ (100 mg, 0.16 mmol) was placed in a schlenk flask which was repeatedly degassed and backfilled with argon. This was dissolved in dry dichloromethane, and a solution of **4b** added (119 mg, 0.34 mmol in 5 ml dichloromethane). The reaction mixture was stirred for 1 h before hexane was added, and decanted off once the precipitate had settled. The resulting complex was dried under reduced pressure. 67 % yield.

^{1}H (CD_2Cl_2) 0.95 (m, 4H), 1.08 (m, 6H), 1.67 (m, 3H), 2.02 (m, 3H), 2.64 (m, 4H), 4.63 (d, 2H, C**H$_2$**NH), 4.73 (d, 2H, C**H$_2$**NH), 5.26 (s, 6H, OCH_3), 6.97 (m, 12H). ^{13}C{^{1}H} (CD_2Cl_2) 21.2 (CH_3 cym), 22.1 (CH_3 cym), 23.4 (CH_2), 29.4 (CH cym), 31.8 (CH_2), 51.1 (CH_2NH), 60.9 (OCH_3), 64.8 (CHNH), 110.0 (CH), 120.6 (CH), 124.3 (CH), 125.1 (CH), 125.5 (C), 128.1 (CH), 129.1 (CH), 130.4 (C), 132.4 (C), 157.4 (C). Mass spec: HR-ESI Calc for [M^+] 625.2135 found 625.2141

Preparation of [Ru(8a)(*p*-cymene)Cl]Cl

[$RuCl_2$(*p*-cymene)]$_2$ (100 mg, 0.16 mmol) was placed in a schlenk flask which was repeatedly degassed and backfilled with argon. This was dissolved in dry dichloromethane, and **8a** added (210 mg, 0.33 mmol). The reaction mixture was stirred for 1 h before hexane was added, and decanted off once the precipitate had settled. The resulting complex was dried under reduced pressure.

^{1}H (CD_2Cl_2) 1.05 (m, 3H), 1.74 (m, 6H), 3.08 (m, 1H), 4.85 (m, 4H), 5.35 (m, 6H), 7.42 (m, 22H), 7.65 (m, 10H), 8.58 (s, 2H, CHN). ^{13}C{^{1}H} (CD_2Cl_2) 21.0 (CH_3 cym), 21.9 (CH_3 cym), 29.7 (CH_2), 30.8 (CH cym), 31.7 (CH_2), 71.5 (CHNH), 126.9 (CH), 127.1 (CH), 128.6 (CH), 129.4 (CH), 129.5 (CH), 130.0 (C), 134.1 (CH), 134.3 (C).

^{31}P{^{1}H} (CD_2Cl_2) 29.5 (PPh_2). Mass spec: HR-ESI Calc for [M^+] 929.2494 found 929.3569

Preparation of [Ru(15)(*p*-cymene)Cl]Cl

$[RuCl_2(p\text{-cymene})]_2$ (100 mg, 0.16 mmol) was placed in a schlenk flask which was repeatedly degassed and backfilled with argon. This was dissolved in dry dichloromethane, and **15** added (90 mg, 0.32 mmol). The reaction mixture was stirred for 1 h before hexane was added, and decanted off once the precipitate had settled. The resulting complex was dried under reduced pressure.

^{1}H (MeOD) 1.07 (d, 3H cym), 1.21 (d, 3H cym), 1.29 (m, 1H cym), 1.89 (s, 3H cym), 5.53 (d, 1H cym), 5.61 (d, 1H cym), 5.69 (d, 1H cym), 5.75 (d, 1H cym), 6.83 (d, 1H Ar), 7.05 (d, 1H, Ar), 7.18 (d, 1H, Ar), 7.39 (m, 4H, Ar), 7.89 (d, 2H, Ar), 8.01 (d, 2H, Ar), 8.23 (d, 1H, Ar). ^{13}C{^{1}H} (CD_2Cl_2) 18.0 (CH_3 cym), 21.9 (CH_3 cym), 31.6 (CH cym), 119.7 (C), 121.5 (CH), 125.0 (CH), 126.0 (CH), 126.6 (CH), 127.5 (CH), 128.2 (CH), 129.2 (C), 131.9 (C), 132.5 (CH), 133.0 (CH), 133.7 (C), 137.3 (C), 140.6 (C). Mass spec: HR-ESI Calc for $[M^+]$-Cl 519.1465 found 519.0480

Preparation of $[Pt(3b)Cl_2$

$PtCl_2$ (100 mg, 0.38 mmol) and **3b** (111 mg, 0.38 mmol) were dissolved in acetonitrile (20 ml) and methanol (1 ml). The solution was stirred at room temperature for 1 h, upon which the product had precipitated. The product was collected by vacuum filtration and dried under reduced pressure.

^{1}H ($CDCl_3$) 0.95 (m, 4H), 1.42 (m, 4H), 2.27 (m, 2H), 3.95 (m, 1H, C**H**$_2$NH), 4.23 (m, 1H, C**H**$_2$NH), 4.45 (m, 2H, C**H**$_2$NH), 7.27 (m, 7H), 7.54 (m, 1H, CH Ar), 7.70 (m, 1H, CH Ar), 7.93 (m, 1H, CH Ar). ^{13}C{^{1}H} ($CDCl_3$) 24.5 (CH_2), 30.6 (CH_2), 53.9 (CH_2NH), 69.1 (CHNH cyclohexane), 125.5 (CH), 128.9 (CH), 129.2 (CH), 130.6 (CH), 132.3 (CH), 134.7 (C). Mass spec: HR-ESI Calc for $[M^+]$-Cl 489.1744 found 489.1710

Preparation of $[Pt(9a)Cl_2$

$PtCl_2$ (100 mg, 0.38 mmol) and **9a** (110 mg, 0.38 mmol) were dissolved in acetonitrile (20 ml) and methanol (1 ml). The solution was stirred at room temperature for 1 h, upon which the product had precipitated. The product was collected by vacuum filtration and dried under reduced pressure.

^{1}H (MeOD) 1.45 (m, 4H CH_2), 1.79 (m, 4H CH_2), 3.21 (m, 2H), 7.39 (m, 2H), 7.57 (m, 1H), 7.79 (m, 3H), 8.19 (s, 2H CHN imine), 8.41 (m, 2H). ^{13}C{^{1}H} (MeOD) 34.1 (CH_2), 75.4 (CHN cyclohexane), 123.1 (CH), 127.0 (CH), 149.6

(CH), 150.6 (CH), 163.4 (CHN imine). Mass spec: HR-ESI Calc for [M^+] [complex]-Cl 489.1371 found 489.2446

Preparation of [Pd(3b)Cl_2

$PdCl_2$ (100 mg, 0.56 mmol) and **3b** (166 mg, 0.56 mmol) were dissolved in acetonitrile (20 ml) and methanol (1 ml). The solution was stirred at room temperature for 1 h, upon which the product had precipitated. The product was collected by vacuum filtration and dried under reduced pressure.

^{1}H ($CDCl_3$) 0.81 (m, 2H CH2), 1.48 (m, 6H CH2), 2.46 (m, 2H CHN cyclohexane), 3.73 (d J = 13.5 Hz, 2H C**H2**NH), 4.31 (d J = 13.5 Hz, 2H C**H2**NH), 7.45 (m, 10H). $^{13}C\{^1H\}$ ($CDCl_3$) 51.1 (CH_2), 66.4 (CHNH), 128.1 (CH), 128.8 (CH), 130.7 (CH), 135.3 (C). Mass spec: HR-ESI Calc for [M^+] 435.0819 found 435.0833

Preparation of [Pd(9a)Cl_2

$PdCl_2$ (100 mg, 0.56 mmol) and 9a (165 mg, 0.57 mmol) were dissolved in acetonitrile (20 ml) and methanol (1 ml). The solution was stirred at room temperature for 1 h, upon which the product had precipitated. The product was collected by vacuum filtration and dried under reduced pressure. 62 % yield.

^{1}H (MeOD) 1.22 (m, 2H), 1.44 (m, 2H), 1.74 (m, 2H), 2.52 (m, 1H), 2.98 (m, 1H), 3.18 (m, 2H CHN cyclohexane), 7.40 (m, 2H), 7.72 (m, 2H), 7.97 (m, 2H), 8.22 (m, 2H), 8.56 (s, 2H CHN imine). $^{13}C\{^1H\}$ (MeOD) 25.0 (CH_2), 25.8 (CH_2), 130.1 (CH), 130.7 (CH), 143.3 (CH), 152.5 (CH), 160.7 (C), 166.6 (CHN imine). Mass spec: HR-ESI Calc for [M^+] found 434.0719

Preparation of [Cu(2)$_2$](OTf)$_2$

Copper(II) triflate (0.20 g, 0.55 mmol) was placed in a round bottomed flask which was repeatedly degassed and backfilled with argon. To this, a solution of **2** (0.13 g, 1.11 mmol) in methanol (30 ml) was added. The mixture was stirred for 30 mins before the solvent was removed by rotary evaporation. The product was dried under reduced pressure. To encourage crystallisation of the complex, the product was re-dissolved in methanol (10 ml) and diethyl ether (1 ml) and cooled to -20 °C. On recrystallisation of the product the crystals were collected by vacuum filtration and dried under reduced pressure. 60 % yield

Mass spec: HR-ESI Calc for [M^{2+}] 145.5800 found 145.5807. Elemental analysis: Found C, 28.5; H, 4.75; N, 9.49 Expected C, 28.5; H, 4.78; N, 9.50.

Single Crystal X-Ray Diffraction:

Empirical formula	$C_{28}H_{56}N_8F_{12}O_{12}S_4Cu_2$	
Formula weight	1180.13	
Temperature	150(2) K	
Wavelength	0.71073 Å	
Crystal system	Triclinic	
Space group	*P*1	
Unit cell dimensions	a = 8.61400(10) Å	α = 81.7570(10)°
	b = 11.6740(2) Å	β = 87.1130(10)°
	c = 11.7340(2) Å	γ = 89.3440(10)°
Volume	1166.29(3) $Å^3$	
Z	1	
Density (calculated)	1.680 Mg/m^3	
Absorption coefficient	1.201 mm^{-1}	
F(000)	606	
Crystal Size	0.40 × 0.30 × 0.25 mm	
Theta range for data collection	3.53 to 27.48°	
Limiting indices	-11<=h<=11, -15<=k<=14, -15<=l<=15	
Reflections collected	22337	
Independent reflections	10000 [R(int) = 0.0313]	
Completeness to theta = 27.48°	99.5 %	
Absorption correction	Semi-empirical from equivalents	
Max. and Min. transmission	0.7533 and 0.6451	
Refinement method	Full-matrix least-squares on F^2	
Data / restraints / parameters	10000 / 3 / 595	
Goodness-of-fit on F^2	1.051	
Final R indices [I>2sigma(I)]	R1 = 0.0263, wR2 = 0.0614	
R indices (all data)	R1 = 0.0290, wR2 = 0.0627	
Absolute structure parameter	-0.006(5)	
Largest diff. peak and hole	0.332 and -0.624 e.$Å^{-3}$	

Preparation of $[Cu(17)_2](OTf)_2$

Copper(II) triflate (0.20 g, 0.64 mmol) was placed in a round bottomed flask which was repeatedly degassed and backfilled with argon. To this, a solution of **17** (0.18 ml, 1.28 mmol) in methanol (30 ml) was added. The mixture was stirred for 30 mins before the solvent was removed by rotary evaporation. The

product was dried under reduced pressure. To encourage crystallisation of the complex, the product was re-dissolved in methanol (10 ml) and diethyl ether (1 ml) and cooled to -20 °C. On recrystallisation of the product the crystals were collected by vacuum filtration and dried under reduced pressure.

Mass spec: HR-ESI Calc for $[M^{2+}]$ 159.5956 found 159.5954. Elemental analysis: Found C, 30.2; H, 5.38; N, 8.75 Expected C, 30.2; H, 5.39; N, 8.81.

Single Crystal X-Ray Diffraction:

Empirical formula	$C_{16}H_{34}N_4F_6O_7S_2Cu$	
Formula weight	636.13	
Temperature	150(2) K	
Wavelength	0.71073 Å	
Crystal system	Tetragonal	
Space group	$P4_12_12$	
Unit cell dimensions	a = 12.6100(1) Å	α = 90°
	b = 12.6100(1) Å	β = 90°
	c = 16.2480(2) Å	γ = 90°
Volume	2583.63(4) $Å^3$	
Z	4	
Density (calculated)	1.635 Mg/m^3	
Absorption coefficient	1.094 mm^{-1}	
F(000)	1316	
Crystal Size	0.40 × 0.15 × 0.10 mm	
Theta range for data collection	3.61 to 27.46°	
Limiting indices	-16<=h<=16, -16<=k<=16, -21<=l<=21	
Reflections collected	51740	
Independent reflections	2965 [R(int) = 0.0496]	
Completeness to theta = 27.46°	99.6 %	
Absorption correction	Semi-empirical from equivalents	
Max. and Min. transmission	0.8985 and 0.6688	
Refinement method	Full-matrix least-squares on F^2	
Data / restraints / parameters	2965 / 0 / 164	
Goodness-of-fit on F^2	1.079	
Final R indices [I>2sigma(I)]	R1 = 0.0590, wR2 = 0.1399	
R indices (all data)	R1 = 0.0688, wR2 = 0.1444	
Absolute structure parameter	-0.01(3)	
Extinction coefficient	0.0107(16)	
Largest diff. peak and hole	2.867 and -3.666 $e.Å^{-3}$	

Preparation of $[Cu(3b)_2](OTf)_2$

Copper(II) triflate (0.20 g, 0.55 mmol) was placed in a round bottomed flask which was repeatedly degassed and backfilled with argon. To this, a solution of **3b** (0.33 g, 1.11 mmol) in methanol (30 ml) was added. The mixture was stirred for 30 mins before the solvent was removed by rotary evaporation. The product was dried under reduced pressure. To encourage crystallisation of the complex, the product was re-dissolved in methanol (10 ml) and diethyl ether (1 ml) and cooled to -20 °C. On recrystallisation of the product the crystals were collected by vacuum filtration and dried under reduced pressure. 67 % yield

Mass spec: HR-ESI Calc for $[M^{2+}]$ 325.6738 found 325.6739. Elemental analysis: Found C, 52.3; H, 5.44; N, 5.74 Expected C, 53.1; H, 5.51; N, 5.89.

Single Crystal X-Ray Diffraction:

Empirical formula	$C_{42}H_{52}N_4F_6O_6S_2Cu$	
Formula weight	950.54	
Temperature	150(2) K	
Wavelength	0.71073 Å	
Crystal system	Monoclinic	
Space group	$P2_1$	
Unit cell dimensions	a = 11.7300(1) Å	α = 90°
	b = 35.5410(4) Å	β = 114.624(1)°
	c = 11.7290(1) Å	γ = 90°
Volume	4445.10(7) $Å^3$	
Z	4	
Density (calculated)	1.420 Mg/m^3	
Absorption coefficient	0.661 mm^{-1}	
F(000)	1980	
Crystal Size	0.35 × 0.20 × 0.10 mm	
Theta range for data collection	3.53 to 27.44°	
Limiting indices	-15<=h<=15, -46<=k<=46, -15<=l<=15	
Reflections collected	35572	
Independent reflections	35590 [R(int) = 0.0000]	
Reflections observed (>2σ)	33459	
Data completeness	0.942	
Absorption correction	Semi-empirical from equivalents	
Max. and Min. transmission	0.937 and 0.880	
Refinement method	Full-matrix least-squares on F^2	
Data / restraints / parameters	35590 / 1 / 1100	

Goodness-of-fit on F^2	1.140
Final R indices [I>2sigma(I)]	R1 = 0.0467, wR2 = 0.1295
R indices (all data)	R1 = 0.0525, wR2 = 0.1393
Absolute structure parameter	-0.009(9)
Largest diff. peak and hole	0.961 and -0.623 e.Å^{-3}

Preparation of $[Cu(4b)_2](OTf)_2$

Copper(II) triflate (0.20 g, 0.55 mmol) was placed in a round bottomed flask which was repeatedly degassed and backfilled with argon. To this, a solution of **4b** (0.39 g, 1.11 mmol) in methanol (30 ml) was added. The mixture was stirred for 30 mins before the solvent was removed by rotary evaporation. The product was dried under reduced pressure. To encourage crystallisation of the complex, the product was re-dissolved in methanol (10 ml) and diethyl ether (1 ml) and cooled to -20 °C. On recrystallisation of the product the crystals were collected by vacuum filtration and dried under reduced pressure. 68 % yield.

Mass spec: HR-ESI Calc for $[M^{2+}]$ 385.6950 found 385.6950. Elemental analysis: Found C, 51.5; H, 5.63; N, 5.21 Expected C, 51.6; H, 5.65; N, 5.23.

Single Crystal X-Ray Diffraction:

Empirical formula	$C_{46}H_{60}N_4F_6O_{10}S_2Cu$	
Formula weight	1070.64	
Temperature	150(2) K	
Wavelength	0.71073 Å	
Crystal system	Monoclinic	
Space group	$P2_1$	
Unit cell dimensions	a = 11.5320(5) Å	α = 90°
	b = 18.6300(10) Å	β = 102.643(3)°
	c = 11.8630(6) Å	γ = 90°
Volume	2486.9(2) Å^3	
Z	2	
Density (calculated)	1.430 Mg/m^3	
Absorption coefficient	0.605 mm^{-1}	
F(000)	1118	
Crystal Size	0.10 × 0.10 × 0.10 mm	
Theta range for data collection	3.66 to 25.02°	

Limiting indices	-13<=h<=13, -22<=k<=22, -13<=l<=14
Reflections collected	28135
Independent reflections	8617 [R(int) = 0.1397]
Completeness to theta = 25.02°	99.4 %
Absorption correction	Semi-empirical from equivalents
Max. and Min. transmission	0.9420 and 0.9420
Refinement method	Full-matrix least-squares on F^2
Data / restraints / parameters	8617 / 1 / 681
Goodness-of-fit on F^2	1.032
Final R indices [I>2sigma(I)]	R1 = 0.0637, wR2 = 0.1238
R indices (all data)	R1 = 0.1337, wR2 = 0.1518
Absolute structure parameter	-0.010(19)
Largest diff. peak and hole	0.570 and -0.438 e.$Å^{-3}$

Preparation of $[Cu(5b)_2](OTf)_2$

Copper(II) triflate (0.20 g, 0.55 mmol) was placed in a round bottomed flask which was repeatedly degassed and backfilled with argon. To this, a solution of **5b** (0.35 g, 1.11 mmol) in methanol (30 ml) was added. The mixture was stirred for 30 mins before the solvent was removed by rotary evaporation. The product was dried under reduced pressure. To encourage crystallisation of the complex, the product was re-dissolved in methanol (10 ml) and diethyl ether (1 ml) and cooled to -20 °C. On recrystallisation of the product the crystals were collected by vacuum filtration and dried under reduced pressure.

Mass spec: HR-ESI Calc for $[M^+]$ 707.4114 (corresponds to ligand). Elemental analysis: Found C, 53.5; H, 5.88; N, 5.49 Expected C, 54.9; H, 6.01; N, 5.57.

Single Crystal X-Ray Diffraction:

Empirical formula	$C_{93}H_{124}N_8F_{12}O_{13}S_4Cu_2$	
Formula weight	2045.32	
Temperature	100(2) K	
Wavelength	1.54184 Å	
Crystal system	Monoclinic	
Space group	$P2_1$	
Unit cell dimensions	a = 11.4238(7) Å	α = 90°
	b = 32.3577(8) Å	β = 96.545(4)°
	c = 13.0790(4) Å	γ = 90°
Volume	4803.1(3) $Å^3$	
Z	2	

Density (calculated)	1.414 Mg/m^3
Absorption coefficient	2.106 mm^{-1}
F(000)	2144
Crystal Size	0.05 × 0.05 × 0.01 mm
Theta range for data collection	3.67 to 62.26°
Limiting indices	-12<=h<=12, -20<=k<=36, -14<=l<=14
Reflections collected	22418
Independent reflections	10864 [R(int) = 0.0735]
Completeness to theta = 62.26°	98.6 %
Absorption correction	Semi-empirical from equivalents
Max. and Min. transmission	0.9792 and 0.9020
Refinement method	Full-matrix least-squares on F^2
Data / restraints / parameters	10864 / 1 / 1194
Goodness-of-fit on F^2	0.878
Final R indices [I>2sigma(I)]	R1 = 0.0466, wR2 = 0.0789
R indices (all data)	R1 = 0.0812, wR2 = 0.0872
Absolute structure parameter	-0.027(19)
Largest diff. peak and hole	0.533 and -0.329 $e.Å^{-3}$

Preparation of $[Cu(6b)_2](OTf)_2$

Copper(II) triflate (0.20 g, 0.55 mmol) was placed in a round bottomed flask which was repeatedly degassed and backfilled with argon. To this, a solution of **6b** (0.40 g, 1.11 mmol) in methanol (30 ml) was added. The mixture was stirred for 30 mins before the solvent was removed by rotary evaporation. The product was dried under reduced pressure.

Mass spec: HR-ESI Calc for $[M^{2+}]$ 394.5950 found 363.1413 (corresponds to ligand). Copper isotope pattern observed. Elemental analysis: Found C, 45.5; H, 4.41; N, 5.14 Expected C, 46.4; H, 4.45; N, 5.15.

Preparation of $[Cu(9a)](OTf)_2$ in methanol

Copper(II) triflate (0.2 g, 0.55 mmol) was placed into a round bottom flask with a sidearm under argon. To this, **9a** (0.16 g, 0.55 mmol) was added in methanol (30 ml), and the resulting mixture stirred at room temperature for 1h. Following this, the solvent was removed by rotary evaporation and the complex dried under reduced pressure. On later recrystallisation, the complex was dissolved in the minimum amount of methanol and a relatively small amount of diethyl ether added. Crystals were encouraged to form at -20°C.

Mass spec: HR-ESI Calc for [M^+] 504.0499 found 504.0473. Mass spec: HR-ESI Calc for [M^+ + MeOH] 536.0761 found 536.0745. Elemental analysis: calc C, 36.8; H, 3.40; N, 8.28 found C, 36.1; H, 3.24; N, 8.15

Single Crystal X-Ray Diffraction:

Empirical formula	$C_{20.70}H_{22.80}N_4F_6O_{6.70}S_2Cu$	
Formula weight	676.49	
Temperature	150(2) K	
Wavelength	0.71073 Å	
Crystal system	Triclinic	
Space group	*P*1	
Unit cell dimensions	a = 8.8600(5) Å	α = 80.751(3)°
	b = 11.2890(5) Å	β = 86.603(2)°
	c = 14.6510(7) Å	γ = 69.248(3)°
Volume	1352.51(12) $Å^3$	
Z	2	
Density (calculated)	1.661 Mg/m^3	
Absorption coefficient	1.050 mm^{-1}	
F(000)	687	
Crystal Size	0.20 × 0.15 × 0.10 mm	
Theta range for data collection	3.57 to 27.48°	
Limiting indices	-11<=h<=11, -14<=k<=14, -18<=l<=18	
Reflections collected	25918	
Independent reflections	11526 [R(int) = 0.0452]	
Completeness to theta = 27.48°	99.3 %	
Absorption correction	Semi-empirical from equivalents	
Max. and Min. transmission	0.9023 and 0.8175	
Refinement method	Full-matrix least-squares on F^2	
Data / restraints / parameters	11526 / 3 / 750	
Goodness-of-fit on F^2	1.018	
Final R indices [I>2sigma(I)]	R1 = 0.0533, wR2 = 0.1296	
R indices (all data)	R1 = 0.0815, wR2 = 0.1481	
Absolute structure parameter	-0.027(13)	
Largest diff. peak and hole	0.681 and -0.600 e.$Å^{-3}$	

Preparation of [Cu(9a)](OTf)$_2$ in methanol/acetic acid mixture

Copper(II) triflate (0.2 g, 0.55 mmol) was placed into a round bottom flask with a sidearm under argon. To this, **9a** (0.16 g, 0.55 mmol) was added in a methanol/acetic acid mixture (30:3 ml), and the resulting mixture stirred at room

temperature for 1h. Following this, the solvent was removed by rotary evaporation and the complex dried under reduced pressure. Crystals were encouraged to form at -20°C.

Single Crystal X-Ray Diffraction:

Empirical formula	$C_{20.90}H_{23.60}N_4F_6O_{6.90}S_2Cu$	
Formula weight	682.90	
Temperature	150(2) K	
Wavelength	0.71073 Å	
Crystal system	Triclinic	
Space group	*P*1	
Unit cell dimensions	a = 8.8640(4) Å	α = 79.934(5)°
	b = 11.2510(8) Å	β = 86.832(6)°
	c = 14.8000(9) Å	γ = 68.875(3)°
Volume	1355.56(14) $Å^3$	
Z	2	
Density (calculated)	1.673 Mg/m^3	
Absorption coefficient	1.049 mm^{-1}	
F(000)	694	
Crystal Size	0.20 × 0.10 × 0.10 mm	
Theta range for data collection	3.55 to 27.55°	
Limiting indices	-11<=h<=11, -14<=k<=14, -19<=l<=18	
Reflections collected	25952	
Independent reflections	11719 [R(int) = 0.0405]	
Completeness to theta = 27.55°	99.2 %	
Absorption correction	None	
Max. and Min. transmission	0.9023 and 0.8176	
Refinement method	Full-matrix least-squares on F^2	
Data / restraints / parameters	11719 / 3 / 742	
Goodness-of-fit on F^2	1.032	
Final R indices [I>2sigma(I)]	R1 = 0.0440, wR2 = 0.0939	
R indices (all data)	R1 = 0.0576, wR2 = 0.1014	
Absolute structure parameter	-0.019(10)	
Largest diff. peak and hole	0.718 and -0.557e.$Å^{-3}$	

Preparation of [Cu(9a)](OTf)$_2$ in methanol, refluxed

Copper(II) triflate (0.2 g, 0.55 mmol) was placed into a round bottom flask with a sidearm under argon. To this, **9a** (0.16 g, 0.55 mmol) was added in methanol (30 ml), and the resulting mixture refluxed at 65 °C for 24h. Following this, the

solvent was removed by rotary evaporation and the complex dried under reduced pressure.

Mass spec: HR-ESI Calc for [M^+] mono-α-amino ether product 536.0761 found 536.0806. No peak seen for di-α-amino ether product.

Preparation of [Cu(9a)](OTf)$_2$ in ethanol

Copper(II) triflate (0.2 g, 0.55 mmol) was placed into a round bottom flask with a sidearm under argon. To this, **9a** (0.16 g, 0.55 mmol) was added in ethanol (30 ml), and the resulting mixture stirred at room temperature for 1h. Following this, the solvent was removed by rotary evaporation and the complex dried under reduced pressure. On later recrystallisation, the complex was dissolved in the minimum amount of ethanol and a relatively small amount of diethylether added. Crystals were encouraged to form at -20°C.

Mass spec: HR-ESI Calc for [M^+] 504.0499 found 504.0479. Mass spec: HR-ESI Calc for [M^+ + EtOH] 550.0917 found 550.0919. Elemental analysis: calc C, 37.6; H, 3.65; N, 8.08 found C, 37.3; H, 3.52; N, 7.94

Single Crystal X-Ray Diffraction:

Empirical formula	$C_{21.70}H_{25.10}N_4F_6O_{6.85}S_2Cu$	
Formula weight	693.22	
Temperature	150(2) K	
Wavelength	0.71073 Å	
Crystal system	Triclinic	
Space group	*P*1	
Unit cell dimensions	a = 8.8450(11) Å	α = 97.893(6)°
	b = 11.6530(15) Å	β = 93.559(7)°
	c = 14.8310(17) Å	γ = 111.467(6)°
Volume	1398.6(3) Å^3	
Z	2	
Density (calculated)	1.646 Mg/m^3	
Absorption coefficient	1.018 mm^{-1}	
F(000)	706	
Crystal Size	0.10 × 0.10 × 0.05 mm	
Theta range for data collection	4.86 to 24.18°	
Limiting indices	-10<=h<=10, -13<=k<=13, -17<=l<=16	
Reflections collected	8829	

Independent reflections	7161 [R(int) = 0.0774]
Completeness to theta = 24.18°	95.9 %
Absorption correction	Semi-empirical from equivalents
Max. and Min. transmission	0.9509 and 0.9050
Refinement method	Full-matrix least-squares on F^2
Data / restraints / parameters	7161 / 3 / 760
Goodness-of-fit on F^2	1.071
Final R indices [I>2sigma(I)]	R1 = 0.0744, wR2 = 0.1560
R indices (all data)	R1 = 0.1274, wR2 = 0.1861
Absolute structure parameter	-0.04(3)
Largest diff. peak and hole	0.459 and -0.563 e.Å^{-3}

Preparation of [Cu(9a)](OTf)$_2$ in isopropanol

Copper(II) triflate (0.2 g, 0.55 mmol) was placed into a round bottom flask with a sidearm under argon. To this, **9a** (0.16 g, 0.55 mmol) was added in isopropanol (30 ml), and the resulting mixture stirred at room temperature for 1h. Following this, the solvent was removed by rotary evaporation and the complex dried under reduced pressure. On later recrystallisation, the complex was dissolved in the minimum amount of isopropanol and a relatively small amount of diethyl ether added. Crystals were encouraged to form at -20°C. 92 % yield.

Mass spec: HR-ESI Calc for [M^+] 504.0499 found 504.0493. Mass spec: HR-ESI Calc for [M^+ + ^{i}PrOH] 564.1074 found 564.1075. Elemental analysis: calc C, 36.7; H, 3.95; N, 7.84 found C, 36.5; H, 2.81; N, 8.50

Single Crystal X-Ray Diffraction:

Empirical formula	$C_{23}H_{28}N_4F_6O_7S_2Cu$	
Formula weight	714.15	
Temperature	150(2) K	
Wavelength	0.71073 Å	
Crystal system	Triclinic	
Space group	*P*1	
Unit cell dimensions	a = 9.5699(3) Å	α = 76.376(2)°
	b = 11.4168(3) Å	β = 82.0610(10)°
	c = 13.9033(4) Å	γ = 88.3080(10)°
Volume	1462.14(7) Å^3	
Z	2	
Density (calculated)	1.622 Mg/m^3	
Absorption coefficient	0.977 mm^{-1}	

F(000)	730
Crystal Size	0.20 × 0.10 × 0.10 mm
Theta range for data collection	3.54 to 27.49°
Limiting indices	-12<=h<=12, -14<=k<=14, -18<=l<=17
Reflections collected	27768
Independent reflections	12531 [R(int) = 0.0391]
Completeness to theta = 27.49°	99.4 %
Max. and Min. transmission	0.9086 and 0.8286
Refinement method	Full-matrix least-squares on F^2
Data / restraints / parameters	12531 / 8 / 795
Goodness-of-fit on F^2	1.033
Final R indices [I>2sigma(I)]	R1 = 0.0497, wR2 = 0.1116
R indices (all data)	R1 = 0.0723, wR2 = 0.1238
Absolute structure parameter	-0.014(12)
Largest diff. peak and hole	1.058 and -0.425 e.$Å^{-3}$

Preparation of [Cu(9a)](OTf)$_2$ in isopropanol, refluxed

Copper(II) triflate (0.2 g, 0.55 mmol) was placed into a round bottom flask with a sidearm under argon. To this, **9a** (0.16 g, 0.55 mmol) was added in isopropanol (30 ml), and the resulting mixture refluxed at 65 °C for 24h. Following this, the solvent was removed by rotary evaporation and the complex dried under reduced pressure.

Mass spec: HR-ESI Calc for [M^+] mono-α-aminoether product 564.1074 found 564.1070. No peak seen for di-α-aminoether product.

Preparation of [Cu(9a)](OTf)$_2$ in 2-methoxyethanol

Copper(II) triflate (0.2 g, 0.55 mmol) was placed into a round bottom flask with a sidearm under argon. To this, 9a (0.16 g, 0.55 mmol) was added in 2-methoxyethanol (30 ml), and the resulting mixture stirred at room temperature for 1h. Following this, the solvent was removed by rotary evaporation and the complex dried under reduced pressure. On later recrystallisation, the complex was dissolved in the minimum amount of isopropanol and a relatively small amount of diethylether added. Crystals were encouraged to form at -20°C.

Mass spec: HR-ESI Calc for [M^+]-(OTf) 355.0984 found 355.0945.

Single Crystal X-Ray Diffraction:

Empirical formula	$C_{21}H_{22.50}N_4F_6O_{6.50}S_2Cu$	
Formula weight	676.59	
Temperature	150(2) K	
Wavelength	0.71073 Å	
Crystal system	Triclinic	
Space group	*P*1	
Unit cell dimensions	a = 8.8900(2) Å	α = 111.6200(10)°
	b = 11.4790(3) Å	β = 101.1990(10)°
	c = 15.4820(5) Å	γ = 93.6650(10)°
Volume	1424.80(7) $Å^3$	
Z	2	
Density (calculated)	1.577 Mg/m^3	
Absorption coefficient	0.996 mm^{-1}	
F(000)	687	
Crystal Size	0.10 × 0.10 × 0.05 mm	
Theta range for data collection	3.56 to 27.47°	
Limiting indices	-11<=h<=11, -14<=k<=14, -20<=l<=20	
Reflections collected	26438	
Independent reflections	12251 [R(int) = 0.0496]	
Completeness to theta = 27.47°	99.0 %	
Absorption correction	None	
Max. and Min. transmission	0.9519 and 0.9069	
Refinement method	Full-matrix least-squares on F^2	
Data / restraints / parameters	12251 / 5 / 717	
Goodness-of-fit on F^2	1.033	
Final R indices [I>2sigma(I)]	R1 = 0.0585, wR2 = 0.1376	
R indices (all data)	R1 = 0.0922, wR2 = 0.1561	
Absolute structure parameter	-0.02(2)	
Largest diff. peak and hole	1.219 and -0.504 e.$Å^{-3}$	

Preparation of [Cu(9a)](OTf)$_2$ in trifluoroethanol

Copper(II) triflate (0.2 g, 0.55 mmol) was placed into a round bottom flask with a sidearm under argon. To this, **9a** (0.16 g, 0.55 mmol) was added in 2,2,2-trifluoroethanol (30 ml), and the resulting mixture stirred at room temperature for 1h. Following this, the solvent was removed by rotary evaporation and the complex dried under reduced pressure. On later recrystallisation, the complex was dissolved in the minimum amount of isopropanol and a relatively small amount of diethyl ether added. Crystals were encouraged to form at -20°C.

Mass spec: HR-ESI Calc for $[M^+]$-(OTf) 355.0984 found 355.0976

Single Crystal X-Ray Diffraction:

Empirical formula	$C_{22}H_{21}N_4F_9O_7S_2Cu$	
Formula weight	752.09	
Temperature	150(2) K	
Wavelength	0.71073 Å	
Crystal system	Triclinic	
Space group	*P*1	
Unit cell dimensions	a = 9.5450(8) Å	α = 78.636(6)°
	b = 11.4260(10) Å	β = 83.184(5)°
	c = 13.6980(12) Å	γ = 88.992(5)°
Volume	1454.3(2) $Å^3$	
Z	2	
Density (calculated)	1.718 Mg/m^3	
Absorption coefficient	1.001 mm^{-1}	
F(000)	758	
Crystal Size	0.10 × 0.10 × 0.05 mm	
Theta range for data collection	4.16 to 24.16°	
Limiting indices	-10<=h<=10, -13<=k<=13, -15<=l<=15	
Reflections collected	10765	
Independent reflections	7741 [R(int) = 0.0629]	
Completeness to theta = 24.16°	98.2 %	
Absorption correction	Semi-empirical from equivalents	
Max. and Min. transmission	0.9516 and 0.9065	
Refinement method	Full-matrix least-squares on F^2	
Data / restraints / parameters	7741 / 3 / 811	
Goodness-of-fit on F^2	1.048	
Final R indices [I>2sigma(I)]	R1 = 0.0548, wR2 = 0.1137	
R indices (all data)	R1 = 0.0869, wR2 = 0.1313	
Absolute structure parameter	-0.05(2)	
Largest diff. peak and hole	0.419 and -0.447 e.$Å^{-3}$	

Preparation of $[Cu(9a)](OTf)_2$ in water

Copper(II) triflate (0.2 g, 0.55 mmol) was placed into a round bottom flask with a sidearm under argon. To this, **9a** (0.16 g, 0.55 mmol) and water (30 ml) were added, and the resulting mixture stirred at room temperature for 72 h. Following this, a few drops of the solution were taken for analysis by mass spectrometry. Product peaks were not observed in the mass spectrum.

Preparation of [Cu(9b)](OTf)$_2$

Copper(II) triflate (0.2 g, 0.55 mmol) was placed into a round bottom flask with a sidearm under argon. To this, **9b** (0.16 g, 0.55 mmol) was added in methanol (30 ml), and the resulting mixture stirred at room temperature for 1h. Following this, the solvent was removed by rotary evaporation and the complex dried under reduced pressure. On later recrystallisation, the complex was dissolved in the minimum amount of methanol and a relatively small amount of diethyl ether added. Crystals were encouraged to form at -20°C.

Mass spec: HR-ESI Calc for [M^+] 508.0817 found 508.0798. Elemental analysis: calc C, 36.5; H, 3.68; N, 8.51 found C, 36.6; H, 3.70; N, 8.60

Single Crystal X-Ray Diffraction:

Empirical formula	$C_{20}H_{24}N_4F_6O_6S_2Cu$
Formula weight	658.09
Temperature	150(2) K
Wavelength	0.71073 Å
Crystal system	Monoclinic
Space group	$P2_1$
Unit cell dimensions	a = 9.5520(2) Å α = 90°
	b = 27.0250(10) Å β = 97.143(2)°
	c = 10.1510(4) Å γ = 90°
Volume	2600.07(15) Å^3
Z	4
Density (calculated)	1.681 Mg/m^3
Absorption coefficient	1.088 mm^{-1}
F(000)	1340
Crystal Size	0.20 × 0.10 × 0.10 mm
Theta range for data collection	3.86 to 27.50°
Limiting indices	-12<=h<=12, -35<=k<=35, -13<=l<=13
Reflections collected	34139
Independent reflections	11318 [R(int) = 0.0568]
Completeness to theta = 27.50°	99.0 %
Max. and Min. transmission	0.8990 and 0.8118
Refinement method	Full-matrix least-squares on F^2
Data / restraints / parameters	11318 / 1 / 735
Goodness-of-fit on F^2	1.047
Final R indices [I>2sigma(I)]	R1 = 0.0463, wR2 = 0.0968

R indices (all data)	R1 = 0.0712, wR2 = 0.1068
Absolute structure parameter	-0.002(9)
Largest diff. peak and hole	0.419 and -0.698 e.Å^{-3}

Preparation of [Cu(10a)](OTf)$_2$

Copper(II) triflate (0.2 g, 0.55 mmol) was placed into a round bottom flask with a sidearm under argon. To this, **10a** (0.16 g, 0.55 mmol) was added in methanol (30 ml), and the resulting mixture stirred at room temperature for 1h. Following this, the solvent was removed by rotary evaporation and the complex dried under reduced pressure.

Mass spec: HR-ESI Calc for [M$^+$] 504.0504 found 293.1742 – corresponds to ligand (calculated 293.1766). Elemental analysis: calc C, 36.7; H, 3.08; N, 8.57 found C, 35.8; H, 3.22; N, 8.10

Preparation of [Cu(10b)](OTf)$_2$

Copper(II) triflate (0.2 g, 0.55 mmol) was placed into a round bottom flask with a sidearm under argon. To this, **10b** (0.16 g, 0.55 mmol) was added in methanol (30 ml), and the resulting mixture stirred at room temperature for 1h. Following this, the solvent was removed by rotary evaporation and the complex dried under reduced pressure.

Mass spec: HR-ESI Calc for [M$^+$] for [complex]-(OTf) 359.1297 found 359.1304. Elemental analysis: calc C, 36.5; H, 3.68; N, 8.51 found C, 33.3; H, 3.16; N, 7.80

Preparation of [Cu(11a)](OTf)$_2$

Copper(II) triflate (0.2 g, 0.55 mmol) was placed into a round bottom flask with a sidearm under argon. To this, 11a (0.16 g, 0.55 mmol) was added in methanol (30 ml), and the resulting mixture stirred at room temperature for 1h. Following this, the solvent was removed by rotary evaporation and the complex dried under reduced pressure. On later recrystallisation, the complex was dissolved in the minimum amount of methanol and a relatively small amount of diethyl ether added. Crystals were encouraged to form at -20°C. 89 % yield.

Mass spec: HR-ESI Calc for [M^+] 504.0504 found 293.1751 – corresponds to the ligand (calculated 293.1766). Elemental analysis: calc C, 36.7; H, 3.08; N, 8.57 found C, 32.8; H, 3.64; N, 7.47

Single Crystal X-Ray Diffraction:

Empirical formula	$C_{14}H_{32}N_4F_6O_8S_2Cu$	
Formula weight	626.10	
Temperature	150(2) K	
Wavelength	0.71073 Å	
Crystal system	Monoclinic	
Space group	$P2_1$	
Unit cell dimensions	a = 10.0620(2) Å	α = 90°
	b = 10.3490(2) Å	β = 99.3220(10)°
	c = 25.1290(5) Å	γ = 90°
Volume	2582.17(9) $Å^3$	
Z	4	
Density (calculated)	1.611 Mg/m^3	
Absorption coefficient	1.096 mm^{-1}	
F(000)	1292	
Crystal Size	0.20 × 0.20 × 0.10 mm	
Theta range for data collection	3.54 to 27.49°	
Limiting indices	-13<=h<=13, -13<=k<=13, -32<=l<=32	
Reflections collected	33299	
Independent reflections	10657 [R(int) = 0.0529]	
Completeness to theta = 27.49°	97.0 %	
Absorption correction	None	
Refinement method	Full-matrix least-squares on F^2	
Data / restraints / parameters	10657 / 9 / 663	
Goodness-of-fit on F^2	1.027	
Final R indices [I>2sigma(I)]	R1 = 0.0438, wR2 = 0.1057	
R indices (all data)	R1 = 0.0637, wR2 = 0.1188	
Absolute structure parameter	-0.020(13)	
Largest diff. peak and hole	0.403 and -0.618 $e.Å^{-3}$	

Preparation of [Cu(11b)](OTf)$_2$

Copper(II) triflate (0.2 g, 0.55 mmol) was placed into a round bottom flask with a sidearm under argon. To this, **11b** (0.16 g, 0.55 mmol) was added in methanol (30 ml), and the resulting mixture stirred at room temperature for 1h. Following

this, the solvent was removed by rotary evaporation and the complex dried under reduced pressure.

Mass spec: HR-ESI Calc for [M^+] 508.0817 found 297.2058 – (ligand calculated at 297.2079). Copper(II) isotope pattern was observed. Elemental analysis: calc C, 36.5; H, 3.08; N, 8.51 found C, 36.1; H, 3.21; N, 8.01

Preparation of [Cu(12a)](OTf)$_2$

Copper(II) triflate (0.2 g, 0.55 mmol) was placed into a round bottom flask with a sidearm under argon. To this, **12a** (0.18 g, 0.55 mmol) was added in methanol (30 ml), and the resulting mixture stirred at room temperature for 1h. Following this, the solvent was removed by rotary evaporation and the complex dried under reduced pressure. On later recrystallisation, the complex was dissolved in the minimum amount of methanol and a relatively small amount of diethyl ether added. Crystals were encouraged to form at -20°C.

Mass spec: HR-ESI Calc for [M^+] 532.0817 found 532.0767. Elemental analysis: calc C, 38.7; H, 3.54; N, 8.21 found C, 37.8; H, 3.70; N, 8.17

Single Crystal X-Ray Diffraction:

Empirical formula	$C_{23}H_{28}N_4F_6O_7S_2Cu$	
Formula weight	714.15	
Temperature	150(2) K	
Wavelength	0.71073 Å	
Crystal system	Triclinic	
Space group	*P*1	
Unit cell dimensions	a = 9.6290(3) Å	α = 99.918(2)°
	b = 11.7880(5) Å	β = 105.773(2)°
	c = 13.8240(5) Å	γ = 96.2200(10)°
Volume	1467.40(9) Å^3	
Z	2	
Density (calculated)	1.616 Mg/m^3	
Absorption coefficient	0.973 mm^{-1}	
F(000)	730	
Crystal Size	0.20 × 0.20 × 0.20 mm	
Theta range for data collection	3.56 to 27.55°	
Limiting indices	-12<=h<=12, -15<=k<=15, -17<=l<=17	
Reflections collected	29086	

Independent reflections	12630 [R(int) = 0.0335]
Completeness to theta = 27.55°	98.9 %
Absorption correction	None
Max. and Min. transmission	0.8291 and 0.8291
Refinement method	Full-matrix least-squares on F^2
Data / restraints / parameters	12630 / 3 / 805
Goodness-of-fit on F^2	1.042
Final R indices [I>2sigma(I)]	R1 = 0.0341, wR2 = 0.0774
R indices (all data)	R1 = 0.0438, wR2 = 0.0830
Absolute structure parameter	-0.004(8)
Largest diff. peak and hole	0.302 and -0.521 e.Å^{-3}

Preparation of [Cu(12b)](OTf)$_2$

Copper(II) triflate (0.2 g, 0.55 mmol) was placed into a round bottom flask with a sidearm under argon. To this, **12b** (0.18 g, 0.55 mmol) was added in methanol (30 ml), and the resulting mixture stirred at room temperature for 1h. Following this, the solvent was removed by rotary evaporation and the complex dried under reduced pressure.

Mass spec: HR-ESI Calc for [M^+] 536.1130 found 536.1307. Elemental analysis: calc C, 34.1; H, 3.51; N, 7.07 found C, 38.5; H, 4.11; N, 8.17

Preparation of [Cu(13a)](OTf)$_2$

Copper(II) triflate (0.2 g, 0.55 mmol) was placed into a round bottom flask with a sidearm under argon. To this, **13a** (0.17 g, 0.55 mmol) was added in methanol (30 ml), and the resulting mixture stirred at room temperature for 1h. Following this, the solvent was removed by rotary evaporation and the complex dried under reduced pressure.

Mass spec: HR-ESI Calc for [M^+] 440.1130 found 440.1125, (corresponds to [Cu(**2**)$_2$](OTf)

Preparation of [Cu(13b)](OTf)$_2$

Copper(II) triflate (0.2 g, 0.55 mmol) was placed into a round bottom flask with a sidearm under argon. To this, **13b** (0.17 g, 0.55 mmol) was added in methanol (30 ml), and the resulting mixture stirred at room temperature for 1h. Following

this, the solvent was removed by rotary evaporation and the complex dried under reduced pressure.

Mass spec: HR-ESI Calc for [M^+] 518.0041 found 518.0063. Elemental analysis: calc C, 32.4; H, 3.32; N, 4.19 found C, 32.8; H, 3.33; N, 4.80

Preparation of [Cu(14b)](OTf)$_2$

Copper(II) triflate (0.2 g, 0.55 mmol) was placed into a round bottom flask with a sidearm under argon. To this, **14b** (0.24 g, 0.55 mmol) was added in methanol (30 ml), and the resulting mixture stirred at room temperature for 1h. Following this, the solvent was removed by rotary evaporation and the complex dried under reduced pressure.

Mass spec: HR-ESI Calc for [M^+] 643.8688 found 643.8688. Elemental analysis: calc C, 27.2; H, 2.54; N, 3.53 found C, 24.3; H, 3.47; N, 3.48

Preparation of [Cu(16)](OTf)$_2$

Copper(II) triflate (0.2 g, 0.55 mmol) was placed into a round bottom flask with a sidearm under argon. To this, **16** (0.22 g, 0.56 mmol) was added in methanol (30 ml), and the resulting mixture stirred at room temperature for 1h. Following this, the solvent was removed by rotary evaporation and the complex dried under reduced pressure.

Mass spec: HR-ESI Calc for [M^+] 606.1225 found 395.2606 – (ligand calculated at 395.2487). Elemental analysis: calc C, 48.2; H, 2.96; N, 3.74 found C, 44.1; H, 4.13; N, 3.48

Preparation of [Cu(16)$_2$](OTf)$_2$

Copper(II) triflate (0.2 g, 0.55 mmol) was placed into a round bottom flask with a sidearm under argon. To this, **16** (0.44 g, 1.12 mmol) was added in methanol (30 ml), and the resulting mixture stirred at room temperature for 1h. Following this, the solvent was removed by rotary evaporation and the complex dried under reduced pressure.

Mass spec: HR-ESI Calc for [M^+] 606.1225 found 395.2621 – (ligand calculated at 395.2487). Elemental analysis: calc C, 60.5; H, 5.26; N, 4.87 found C, 59.3; H, 5.27; N, 4.80

Preparation of $[Cu_2(21a)](OTf)_4$

Copper(II) triflate (0.2 g, 0.55 mmol) was placed into a round bottom flask with a sidearm under argon. To this, **21a** (0.14 g, 0.25 mmol) was added in methanol (30 ml), and the resulting mixture stirred at room temperature for 1h. Following this, the solvent was removed by rotary evaporation and the complex dried under reduced pressure.

Mass spec: HR-ESI Calc for $[M^+]$ 1075.0249 found 440.1163 (corresponds to $Cu(\mathbf{2})_2(OTf)$, calc 440.1130). Elemental analysis: calc C, 37.2; H, 3.12; N, 4.57 found C, 16.5; H, 2.38; N, 3.17.

Preparation of $[Cu_2(21b)](OTf)_4$

Copper(II) triflate (0.23 g, 0.64 mmol) was placed into a round bottom flask with a sidearm under argon. To this, **21b** (0.20 g, 0.32 mmol) was added in methanol (30 ml), and the resulting mixture stirred at room temperature for 1h. Following this, the solvent was removed by rotary evaporation and the complex dried under reduced pressure.

Mass spec: HR-ESI Calc for $[M^+]$-$(OTf)_2$ 661.2348 found 661.3442. Elemental analysis: calc C, 37.0; H, 3.76; N, 4.54 found C, 26.7; H, 3.43; N, 3.05

Preparation of $[Cu(8a)](OTf)_2$

Copper(II) triflate (0.10 g, 0.28 mmol) was placed in a round bottomed flask which was repeatedly degassed and backfilled with argon. To this, a solution of **8a** (0.19 g, 0.29 mmol) in methanol (30 ml) was added. The mixture was stirred for 30 mins before the solvent was removed by rotary evaporation. The product was dried under reduced pressure.

Mass spec: HR-ESI Calc for $[M^+]$-OTf 721.1963 found 721.2016. Elemental analysis: Found C, 52.2; H, 3.99; N, 2.71 Expected C, 54.1; H, 3.95; N, 2.75.

Preparation of $[Cu(8b)](OTf)_2$

Copper(II) triflate (0.12 g, 0.33 mmol) was placed in a round bottomed flask which was repeatedly degassed and backfilled with argon. To this, a solution of **8b** (0.22 g, 0.33 mmol) in methanol (30 ml) was added. The mixture was stirred for 30 mins before the solvent was removed by rotary evaporation. The product was dried under reduced pressure.

^{1}H (MeOD) 0.91 (m, 4H), 1.64 (m, 2H), 1.74 (m, 2H), 2.34 (m, 2H), 3.72 (d J = 13 Hz, 2H, C**H$_2$**NH), 3.94 (d J = 13 Hz, 2H, C**H$_2$**NH), 6.95 (m, 6H), 7.13 (m, 4H), 7.35 (m, 16H), 7.47 (m, 2H). ^{13}C{^{1}H} (MeOD) 25.9 (CH_2), 30.7 (CH_2), 51.6 (CH_2NH) 60.6 (CHNH), 130.4 CH), 132.2 (CH), 132.7 (C), 134.0 (CH), 134.3 (CH), 135.9 (CH), 140.3 (CHN). ^{31}P{^{1}H} (MeOD) -7.65 (PPh_2). Mass spec: HR-ESI Calc for [M^{+}]-OTf 727.2258 found 727.2302. Elemental analysis: Found C, 61.6; H, 5.03; N, 3.19 Expected C, 61.7; H, 5.06; N, 3.20

Single Crystal X-Ray Diffraction:

Empirical formula	$C_{46}H_{48}N_2F_3O_4P_2SCu$	
Formula weight	907.40	
Temperature	150(2) K	
Wavelength	0.71073 Å	
Crystal system	Orthorhombic	
Space group	$P2_12_12_1$	
Unit cell dimensions	a = 11.0140(3) Å	α = 90°
	b = 19.0480(6) Å	β = 90°
	c = 20.6980(5) Å	γ = 90°
Volume	4342.3(2) Å^3	
Z	4	
Density (calculated)	1.388 Mg/m^3	
Absorption coefficient	0.683 mm^{-1}	
F(000)	1888	
Crystal Size	0.20 × 0.20 × 0.20 mm	
Theta range for data collection	3.65 to 27.51°	
Limiting indices	-14<=h<=14, -24<=k<=24, -26<=l<=26	
Reflections collected	60243	
Independent reflections	9970 [R(int) = 0.0407]	
Completeness to theta = 27.51°	99.6 %	
Absorption correction	Multi scan	
Max. and Min. transmission	0.8755 and 0.8755	
Refinement method	Full-matrix least-squares on F^2	
Data / restraints / parameters	9970 / 0 / 545	
Goodness-of-fit on F^2	1.028	
Final R indices [I>2sigma(I)]	R1 = 0.0243, wR2 = 0.0581	
R indices (all data)	R1 = 0.0276, wR2 = 0.0598	
Absolute structure parameter	-0.003(5)	
Largest diff. peak and hole	0.262 and -0.296 e.Å^{-3}	

Preparation of [Cu(18a)](OTf)$_2$

Copper(II) triflate (0.20 g, 0.55 mmol) was placed in a round bottomed flask which was repeatedly degassed and backfilled with argon. To this, a solution of 18a (0.22 g, 0.55 mmol) in methanol (30 ml) was added. The mixture was stirred for 30 mins before the solvent was removed by rotary evaporation. The product was dried under reduced pressure.

Mass spec: HR-ESI Calc for [M^{2+}]-OTf 463.1364 found 463.1412. Elemental analysis: Found C, 37.9; H, 4.03; N, 3.69 Expected C, 44.1; H, 3.84; N, 3.68.

Preparation of [Cu(18b)](OTf)$_2$

Copper(II) triflate (0.20 g, 0.55 mmol) was placed in a round bottomed flask which was repeatedly degassed and backfilled with argon. To this, a solution of **18b** (0.23 g, 0.57 mmol) in methanol (30 ml) was added. The mixture was stirred for 30 mins before the solvent was removed by rotary evaporation. The product was dried under reduced pressure.

Mass spec: HR-ESI Calc for [M^{+}] [complex]-(OTf) 465.1521 found 465.1569. Elemental analysis: Found C, 39.8; H, 4.06; N, 3.29 Expected C, 44.0; H, 4.09; N, 3.67.

Single Crystal X-Ray Diffraction:

Empirical formula	$C_{29}H_{36}N_2F_6O_9S_2Cu$	
Formula weight	829.23	
Temperature	150(2) K	
Wavelength	0.71073 Å	
Crystal system	Orthorhombic	
Space group	$P2_12_12_1$	
Unit cell dimensions	a = 8.38600(10) Å	α = 90°
	b = 19.5840(3) Å	β = 90°
	c = 21.8750(4) Å	γ = 90°
Volume	3592.56(10) Å^3	
Z	4	
Density (calculated)	1.533 Mg/m^3	
Absorption coefficient	0.852 mm^{-1}	
F(000)	1704	
Crystal Size	0.20 × 0.20 × 0.15 mm	
Theta range for data collection	3.63 to 25.01°	

Limiting indices	-9<=h<=9, -22<=k<=23, -25<=l<=26
Reflections collected	31246
Independent reflections	6275 [R(int) = 0.0662]
Completeness to theta = 25.01°	99.2 %
Absorption correction	None
Max. and Min. transmission	0.8829 and 0.8481
Refinement method	Full-matrix least-squares on F^2
Data / restraints / parameters	6275 / 3 / 475
Goodness-of-fit on F^2	1.034
Final R indices [I>2sigma(I)]	R1 = 0.0617, wR2 = 0.1588
R indices (all data)	R1 = 0.0700, wR2 = 0.1656
Absolute structure parameter	-0.01(2)
Largest diff. peak and hole	1.177 and -0.825 e.Å^{-3}

Preparation of [Ti(7b)](O^{i}Pr)$_2$

7b (0.55 g, 1.69 mmol) was placed in a schlenk flask which was repeatedly degassed and backfilled with argon. This was dissolved in dry dichloromethane (10 ml) and Ti(O^{i}Pr)$_4$ was added (0.5 ml, 1.69 mmol). The reaction mixture was stirred at room temperature for 1h before the solvent was removed and the product dried under reduced pressure. 75 % yield.

^{1}H ($CDCl_3$) 0.76 (m, 2H), 0.95 (m, 2H), 1.13 (m, 12H, OCH(C**H$_3$**)$_2$), 1.57 (m, 4H), 2.18 (m, 2H), 2.30 (m, 2H), 3.84 (d J = 14 Hz, 2H, C**H$_2$**NH), 4.72 (d J = 14 Hz, 2H, C**H$_2$**NH), 4.77 (m, 2H, OC**H**(CH_3)$_2$), 6.61 (m, 4H), 6.87 (m, 2H), 7.08 (m, 2H). ^{13}C{^{1}H} ($CDCl_3$) 23.4 (CH_2), 24.7 (CH3 O^{i}Pr), 28.9 (CH_2), 48.2 (CH_2NH), 56.8 (CHNH cyclohexane), 76.4 (CH O^{i}Pr), 116.1 (CH), 117.0 (CH), 121.0 (C), 127.5 (CH), 128.0 (CH), 161.4 (COH). Mass spec: HR-ESI Calc for [M$^+$] 493.2546 found 493.2030

Single Crystal X-Ray Diffraction:

Empirical formula	$C_{33}H_{46}N_2O_4Ti$	
Formula weight	582.62	
Temperature	150(2) K	
Wavelength	0.71073 Å	
Crystal system	Orthorhombic	
Space group	$P2_12_12_1$	
Unit cell dimensions	a = 10.1010(2) Å	α = 90°
	b = 16.8840(4) Å	β = 90°

	c = 18.1880(2) Å γ = 90°
Volume	3101.88(10) $Å^3$
Z	4
Density (calculated)	1.248 Mg/m^3
Absorption coefficient	0.314 mm^{-1}
F(000)	1248
Crystal Size	0.20 × 0.20 × 0.20 mm
Theta range for data collection	3.79 to 27.47°
Limiting indices	-13<=h<=13, -20<=k<=21, -23<=l<=22
Reflections collected	66549
Independent reflections	7050 [R(int) = 0.0361]
Completeness to theta = 27.47°	99.1 %
Absorption correction	None
Max. and Min. transmission	0.9398 and 0.9398
Refinement method	Full-matrix least-squares on F^2
Data / restraints / parameters	7050 / 0 / 404
Goodness-of-fit on F^2	1.087
Final R indices [I>2sigma(I)]	R1 = 0.0305, wR2 = 0.0808
R indices (all data)	R1 = 0.0356, wR2 = 0.0869
Absolute structure parameter	-0.023(17)
Largest diff. peak and hole	0.182 and -0.265 $e.Å^{-3}$

Preparation of [Ti(22)](O^iPr)$_2$

22 (0.78 g, 1.68 mmol) was placed in a schlenk flask which was repeatedly degassed and backfilled with argon. This was dissolved in dry dichloromethane (10 ml) and Ti(O^iPr)$_4$ was added (0.5 ml, 1.69 mmol). The reaction mixture was stirred at room temperature for 1h before the solvent was removed and the product dried under reduced pressure. 49 % yield.

^{1}H ($CDCl_3$) 1.13 (m, 12H, OCH(C**H$_3$**)$_2$), 1.64 (m, 4H), 2.19 (m, 6H), 3.79 (d J = 14.5 Hz, 2H, C**H$_2$**NH), 4.72 (d J = 14.5 Hz, 2H, C**H$_2$**NH), 4.89 (sp, 2H, OC**H**(CH_3)$_2$), 6.77 (m, 2H), 7.19 (m, 2H). ^{13}C{^{1}H} ($CDCl_3$) 21.6 (CH_2), 23.5 (CH_3 O^iPr), 28.7 (CH_2), 48.5 (CHNH cyclohexane), 54.6 (CH_2NH), 77.7 (CH O^iPr), 119.58 (C), 122.0 (C), 123.00 (C), 126.4 (CH), 127.5 (CH), 155.7 (COH). Mass spec: HR-ESI Calc for [M^+] 567.0251 found 567.0295

Preparation of [Ti(23)](O^iPr)$_2$

23 (0.93 g, 1.69 mmol) was placed in a schlenk flask which was repeatedly degassed and backfilled with argon. This was dissolved in dry dichloromethane (10 ml) and $Ti(O^iPr)_4$ was added (0.5 ml, 1.69 mmol). The reaction mixture was stirred at room temperature for 1h before the solvent was removed and the product dried under reduced pressure. 67 % yield.

^1H ($CDCl_3$) 0.92 (m, 4H), 1.47 (m, 18H, $_tBu$), 1.52 (m, 12H, OCH($C\mathbf{H_3}$)$_2$), 1.59 (m, 3H), 1.78 (m, 3H), 3.64 (d J = 13 Hz, 1H, $C\mathbf{H}_2NH$), 3.80 (d J = 13 Hz, 1H, $C\mathbf{H}_2NH$), 4.46 (d J = 13 Hz, 1H, $C\mathbf{H}_2NH$), 4.62 (d J = 13 Hz, 1H, $C\mathbf{H}_2NH$), 4.93 (sp, 2H, $OC\mathbf{H}(CH_3)_2$), 6.78 (m, 2H), 7.07 (m, 2H). $^{13}C\{^1H\}$ ($CDCl_3$) 23.7 (CH_2), 25.6 (CH_3), 28.5 (CH_3), 29.2 (CH_2), 30.6 (CH_3), 34.1 (C *t*Bu), 48.9 (CH_2NH), 57.2 (CHNH cyclohexane), 75.2 (CH O^iPr), 120.5 (C), 121.2 (CH), 122.5 (CH), 134.6 (C), 137.0 (C), 158.1 (COH). Mass spec: HR-ESI Calc for [M^+] 714.4803 found 714.4367

Single Crystal X-Ray Diffraction:

Empirical formula	$C_{42}H_{70}N_2O_4Ti$	
Formula weight	714.90	
Temperature	150(2) K	
Wavelength	0.71073 Å	
Crystal system	Orthorhombic	
Space group	$P2_12_12_1$	
Unit cell dimensions	a = 9.80600(10) Å	α = 90°
	b = 14.89800(10) Å	β = 90°
	c = 29.0190(3) Å	γ = 90°
Volume	4239.38(7) $Å^3$	
Z	4	
Density (calculated)	1.120 Mg/m^3	
Absorption coefficient	0.241 mm^{-1}	
F(000)	1560	
Crystal Size	0.20 × 0.15 × 0.10 mm	
Theta range for data collection	3.71 to 27.48°	
Limiting indices	-12<=h<=12, -19<=k<=19, -37<=l<=37	
Reflections collected	74300	
Independent reflections	9699 [R(int) = 0.0967]	
Completeness to theta = 27.48°	99.6 %	
Absorption correction	None	
Max. and Min. transmission	0.9763 and 0.9534	

Refinement method	Full-matrix least-squares on F^2
Data / restraints / parameters	9699 / 0 / 466
Goodness-of-fit on F^2	1.014
Final R indices [I>2sigma(I)]	R1 = 0.0485, wR2 = 0.0991
R indices (all data)	R1 = 0.0832, wR2 = 0.1125
Absolute structure parameter	-0.03(2)
Largest diff. peak and hole	0.385 and -0.271 e.Å^{-3}

Preparation of [Zr(7b)](O^{i}Pr)$_2$

$Zr(O^iPr)_4.{}^iPrOH$ (0.3 g, 0.77 mmol) was placed in a schlenk flask which was repeatedly degassed and backfilled with argon. This was dissolved in dry dichloromethane (10 ml), and **7b** added (0.25 g, 0.76 mmol). The reaction mixture was stirred for 1h at room temperature, before the solvent was removed and the product dried under reduced pressure. 75 % yield.

^{1}H ($CDCl_3$) 0.82 (m, 1H), 1.22 (m, 6H), 1.77 (m, 2H), 2.38 (m, 1H), 3.53 (m, 2H, CH2NH), 3.87 (m, 2H, OCH(CH3)2), 4.40 (m, 2H, CH2NH), 6.02 (m, 2H), 6.42 (m, 2H), 6.59 (m, 2H), 6.75 (m, 2H), 6.90 (m, 2H). $^{13}C\{^1H\}$ ($CDCl_3$) 24.2 (CH_2), 26.6 (CH_3 O^{i}Pr), 29.5 (CH_2), 46.5 (CH_2NH), 60.0 (CHNH cyclohexane), 68.6 (CH O^{i}Pr), 118.0 (C), 121.0 (C), 125.8 (CH), 127.1 (CH), 127.9 (C), 158.1 (COH). Mass spec: HR-ESI Calc for [M^+] 472.1304 found 327.2153 – corresponds to ligand.

Single Crystal X-Ray Diffraction:

Empirical formula	$C_{41.75}H_{51.50}N_4Cl_{3.50}O_4Zr$	
Formula weight	888.66	
Temperature	150(2) K	
Wavelength	0.71073 Å	
Crystal system	Tetragonal	
Space group	$P3_12_1$	
Unit cell dimensions	a = 14.095 Å	α = 90°
	b = 14.095 Å	β = 90°
	c = 38.173 Å	γ = 120°
Volume	6567.8 Å^3	
Z	6	
Density (calculated)	1.348 Mg/m^3	
Absorption coefficient	0.508 mm^{-1}	
F(000)	2769	

Crystal Size	0.10 × 0.05 × 0.05 mm
Theta range for data collection	3.59 to 24.41°
Limiting indices	-16<=h<=16, -16<=k<=16, -44<=l<=44
Reflections collected	47915
Independent reflections	7129 [R(int) = 0.1337]
Completeness to theta = 24.41°	98.9 %
Absorption correction	None
Max. and Min. transmission	0.9750 and 0.9509
Refinement method	Full-matrix least-squares on F^2
Data / restraints / parameters	7129 / 4 / 521
Goodness-of-fit on F^2	1.017
Final R indices [I>2sigma(I)]	R1 = 0.0704, wR2 = 0.1492
R indices (all data)	R1 = 0.1377, wR2 = 0.1768
Absolute structure parameter	-0.02(7)
Largest diff. peak and hole	0.504 and -0.674 e.$Å^{-3}$

Preparation of Zr(7b)$_2$

$Zr(O^iPr)_4.{}^iPrOH$ (0.3 g, 0.77 mmol) was placed in a schlenk flask which was repeatedly degassed and backfilled with argon. This was dissolved in dry dichloromethane (10 ml), and **7b** added (0.51 g, 1.56 mmol). The reaction mixture was stirred for 1h at room temperature, before the solvent was removed and the product dried under reduced pressure. 61 % yield.

^1H ($CDCl_3$) 1.11 (m, 6H), 1.32 (m, 6H), 1.70 (m, 4H), 2.33 (m, 4H), 3.43 (m, 4H), 3.61 (m, 2H), 3.81 (m, 2H), 6.00 (d, 2H), 6.19 (m, 1H), 6.41 (m, 3H), 6.58 (m, 5H), 6.73 (m, 2H), 6.89 (m, 5H), 7.22 (m, 2H). $^{13}C\{^1H\}$ ($CDCl_3$) 25.7 (CH_2), 30.4 (CH_2), 48.8 (CH_2NH), 60.1 (CHN cyclohexane), 116.4 (CH), 118.7 (CH), 125.8 (C), 130.1 (CH), 162.6 (COH). Mass spec: HR-ESI Calc for [M^+] 738.2707 found 327.2158 – corresponds to ligand. Elemental analysis: expected C, 64.9; H, 6.54; N, 7.57, found C, 60.7; H, 6.40; N, 6.86.

Preparation of [Zr(22)](O^{i}Pr)$_2$

$Zr(O^iPr)_4.{}^iPrOH$ (0.3 g, 0.77 mmol) was placed in a schlenk flask which was repeatedly degassed and backfilled with argon. This was dissolved in dry dichloromethane (10 ml), and **22** added (0.36 g, 0.78 mmol). The reaction mixture was stirred for 1h at room temperature, before the solvent was removed and the product dried under reduced pressure. 63 % yield.

^{1}H ($CDCl_3$) 0.81 (m, 6H), 1.15 (br m, 12H), 1.85 (m, 4H), 3.46 (m, 2H), 3.84 (m, 2H), 4.06 (m, 2H, C**H**$(CH_3)_2$ O^{i}Pr), 6.75 (m, 2H), 6.81 (m, 2H). ^{13}C{^{1}H} ($CDCl_3$) 24.3 (CH_2), 26.9 (**C**H_3 O^{i}Pr), 29.6 (CH_2), 46.2 (CHNH), 54.1 (CH O^{i}Pr), 60.0 (CHN cyclohexane), 118.2 (C), 120.8 (C), 124.9 (CH), 127.5 (CH), 128.0 (C), 156.1 (COH). Mass spec: HR-ESI Calc for [M^+]-O^{i}Pr 553.9267 found 553.4618

Preparation of Zr(22)$_2$

Zr(O^{i}Pr)$_4$.^{i}PrOH (0.3 g, 0.77 mmol) was placed in a schlenk flask which was repeatedly degassed and backfilled with argon. This was dissolved in dry dichloromethane (10 ml), and **22** (0.72 g, 1.55 mmol). The reaction mixture was stirred for 1h at room temperature, before the solvent was removed and the product dried under reduced pressure. 53 % yield.

^{1}H ($CDCl_3$) 1.10 (m, 6H), 1.26 (m, 4H), 1.80 (m, 6H), 2.21 (m, 1H), 2.54 (m, 3H), 2.96-3.57 (m, 8H, C**H$_2$**NH), 6.65 (m, 1H), 6.81 (m, 1H), 6.99 (m, 1H), 7.04 (m, 1H), 7.18 (m, 2H). ^{13}C{^{1}H} ($CDCl_3$) 25.3 (CH_2), 30.5 (CH_2), 47.5 (CH_2NH), 60.1 (CHN cyclohexane), 120.8 (C), 123.9 (C), 126.9 (CH), 127.9 (CH), 128.7 (C), 157.1 (COH). Mass spec: HR-ESI Calc for [M^+] 1014.9624 found 841.0061 (corresponds to [M^+] - $C_7H_4OCl_2$, fragmentation. Calc 840.9985). Corresponding fragment seen at 174.9717, calc 174.9718). Elemental analysis: found C, 46.8; H, 4.58; N, 5.82, expected C, 47.3; H, 3.97; N, 5.52.

Preparation of [Zr(23)](O^{i}Pr)$_2$

Zr(O^{i}Pr)$_4$.^{i}PrOH (0.3 g, 0.77 mmol) was placed in a schlenk flask which was repeatedly degassed and backfilled with argon. This was dissolved in dry dichloromethane (10 ml), and **23** (0.43 g, 0.78 mmol). The reaction mixture was stirred for 1h at room temperature, before the solvent was removed and the product dried under reduced pressure. 78 % yield.

^{1}H ($CDCl_3$) 1.15 (m, 12H, OCH(C**H$_3$**)$_2$), 1.19 (m, 18H, $_{t}$Bu), 1.23 (m, 2H), 1.27 (m, 2H), 1.43 (m, 4H), 1.50 (m, 2H), 3.40 (m, 2H, C**H**$_2$NH), 3.84 (m, 2H, C**H**$_2$NH), 4.30 (m, 2H, OC**H**$(CH_3)_2$), 6.71 (m, 1H), 6.82 (m, 1H), 7.06 (m, 1H), 7.13 (m, 1H). ^{13}C{^{1}H} ($CDCl_3$) 23.6 (CH_2), 27.2 (CH_3 O^{i}Pr), 30.6 (CH_3 *t*Bu), 33.0 (CH_2), 48.3 (CH_2NH), 69.7 (CHN), 121.8 (CH), 123.2 (CH), 134.9 (C), 135.3 (C), 138.0 (C), 157.2 (COH).

6.4 Experimental from Chapter Four

6.4.1 Synthesis of Silica-Supported Ligands

Synthesis of S1

This reaction was carried out in accordance with that reported by Macquarrie et. al.[9] Silica (20 g) was dried at 100°C under reduced pressure for 24 h. The silica used was supplied by Fisher Scientific, 60 Å, 35-70 micron. To this, 3-aminopropyltrimethoxysilane (3.5 ml, 20.0 mmol) in ethanol (250 ml) was added under argon, and the mixture stirred at room temperature for 24 h. The silica material was then collected by vacuum filtration and washed with ethanol and diethyl ether, before being dried under reduced pressure at 100 °C for 24 h. 94 % yield.

$^{13}C\{^{1}H\}$ CP/MAS NMR: peaks at 8.68, 26.49, 43.91, 48.51. Elemental analysis: Found C, 4.46; H, 1.36; N, 1.21.

Synthesis of S2

S1 (10 g, 10 mmol) was suspended in dichloromethane (100 ml), and terephthalaldehyde (1.34 g, 10 mmol) added. The mixture was stirred at room temperature for 2 h before the silica material was collected by vacuum filtration. The product was washed with dichloromethane and dried under reduced pressure. 83 % yield.

$^{13}C\{^{1}H\}$ CP/MAS NMR: peaks at 9.53, 15.94, 23.23, 43.10, 48.34, 58.96, 62.97, 128.74 (Ar), 138.09 (Ar), 161.78 (imine), 193.24 (aldehyde). Elemental analysis: Found C, 8.60; H, 1.39; N, 1.27.

Synthesis of S3

S2 (3.9 g, 3.9 mmol) was suspended in dichloromethane (50 ml), and **2** (0.4 g, 3.9 mmol) added. The mixture was stirred at room temperature for 4 h before the

silica material was collected by vacuum filtration. The product was washed with dichloromethane and dried under reduced pressure. 91 % yield.
$^{13}C\{^{1}H\}$ CP/MAS NMR: peaks at 9.78, 24.56, 33.00, 43.10, 56.07, 62.97, 74.57, 128.11 (Ar), 138.38 (Ar), 161.09 (imine). Elemental analysis: Found C, 8.73; H, 1.90; N, 2.33.

Synthesis of S4

S3 (1.0 g, 1.0 mmol) was suspended in dichloromethane (50 ml), and benzaldehyde (0.1 ml, 1.0 mmol) was added. The mixture was stirred at room temperature for 4 h before the silica material was collected by vacuum filtration. The product was washed with dichloromethane and dried under reduced pressure. 95 % yield.
$^{13}C\{^{1}H\}$ CP/MAS NMR: peaks at 9.23, 24.21, 32.57, 42.36, 62.87, 73.88, 128.30, 137.59, 162.01. Elemental analysis: Found C, 8.47; H, 1.73; N, 1.78.

Synthesis of S5

S3 (1.0 g, 1.0 mmol) was suspended in dichloromethane (50 ml), and 2-methoxybenzaldehyde (0.14 g, 1.0 mmol) was added. The mixture was stirred at room temperature for 4 h before the silica material was collected by vacuum filtration. The product was washed with dichloromethane and dried under reduced pressure. 88 % yield.
$^{13}C\{^{1}H\}$ CP/MAS NMR: peaks at 9.18, 24.40, 32.67, 43.09, 53.81, 63.25, 73.14, 110.23 (OMe), 128.00 (Ar), 137.49 (Ar), 159.02 (imine). Elemental analysis: Found C, 8.63; H, 1.55; N, 1.67.

Synthesis of S6

S3 (1.5 g, 1.5 mmol) was suspended in dichloromethane (50 ml), and 2-methylbenzaldehyde (0.2 ml, 1.5 mmol) was added. The mixture was stirred at room temperature for 4 h before the silica material was collected by vacuum filtration. The product was washed with dichloromethane and dried under reduced pressure. 90 % yield.
$^{13}C\{^{1}H\}$ CP/MAS NMR: peaks at 9.42, 16.47 (Me), 24.30, 32.81, 42.41, 58.55, 62.76, 74.56, 128.19 (Ar), 137.54 (Ar), 161.62 (imine). Elemental analysis: Found C, 8.86; H, 1.66; N, 1.79.

Synthesis of S7

S3 (1.0 g, 1.0 mmol) was suspended in dichloromethane (50 ml), and 2-chlorobenzaldehyde (0.1 ml, 1.0 mmol) was added. The mixture was stirred at room temperature for 4 h before the silica material was collected by vacuum filtration. The product was washed with dichloromethane and dried under reduced pressure. 92 % yield.

$^{13}C\{^{1}H\}$ CP/MAS NMR: peaks at 9.72, 24.20, 33.35, 41.72, 63.20, 75.93, 128.39 (Ar), 137.54 (Ar), 161.47 (imine). Elemental analysis: Found C, 8.41; H, 1.52; N, 1.64.

Synthesis of S8

S3 (1.0 g, 1.0 mmol) was suspended in dry dichloromethane (50 ml), and 2-(diphenylphosphino)benzaldehyde (0.3 g, 1.0 mmol) added. The mixture was stirred at room temperature for 4 h before the silica material was collected by vacuum filtration. The product was washed with dichloromethane and dried under reduced pressure. 87 % yield.

$^{13}C\{^{1}H\}$ CP/MAS NMR: peaks at 9.34, 24.31, 32.68, 42.76, 49.42, 62.92, 73.44, 128.45 (Ar), 137.26 (Ar), 161.92 (imine), 207.87. $^{31}P\{^{1}H\}$ CP/MAS NMR: major peak at -12.45, minor peak at 34.83. Elemental analysis: Found C, 10.6; H, 1.63; N, 1.58.

Synthesis of S9

S2 (1.0 g, 1.0 mmol) was suspended in dry dichloromethane (50 ml), and **17** (0.15 ml, 1.0 mmol) added. The mixture was stirred at room temperature for 4 h before the silica material was collected by vacuum filtration. The product was washed with dichloromethane and dried under reduced pressure. 92 % yield.

$^{13}C\{^{1}H\}$ CP/MAS NMR: peaks at 10.35, 24.45, 42.99, 48.87, 52.24, 58.36, 63.89, 128.00 (Ar), 137.74 (Ar), 160.39 (imine). Elemental analysis: Found C, 8.16; H, 1.64; N, 1.98.

Synthesis of S10

S1 (1.0 g, 1.0 mmol) was suspended in dichloromethane (50 ml), and **24** (0.16 g, 1.0 mmol) was added. The mixture was stirred at room temperature for 4 h before the silica material was collected by vacuum filtration. The product was washed with dichloromethane and dried under reduced pressure. 83 % yield.
$^{13}C\{^{1}H\}$ CP/MAS NMR: peaks at 9.40, 17.43, 23.60, 54.93, 118.28, 123.86, 127.18, 136.00, 165.86 (imine), 176.33 (COH), 191.43 (CHO). Elemental analysis: Found C, 8.89; H, 1.45; N, 1.11.

Synthesis of S11

S10 (1.0 g, 1.0 mmol) was suspended in dichloromethane (50 ml), and **2** (0.11 g, 1.0 mmol) was added. The mixture was stirred at room temperature for 4 h before the silica material was collected by vacuum filtration. The product was washed with dichloromethane and dried under reduced pressure. 78 % yield.
$^{13}C\{^{1}H\}$ CP/MAS NMR: peaks at 9.21, 17.92, 24.58, 32.90, 43.08, 58.75, 75.83, 119.16, 123.56, 158.91 (COH), 164.75 (imine). Elemental analysis: Found C, 7.42; H, 1.69; N, 2.06

Synthesis of S12

S11 (1.0 g, 1.0 mmol) was suspended in dichloromethane (50 ml), and salicylaldehyde (0.1 ml, 1.0 mmol) was added. The mixture was stirred at room temperature for 4 h before the silica material was collected by vacuum filtration. The product was washed with dichloromethane and dried under reduced pressure. 81 % yield.
$^{13}C\{^{1}H\}$ CP/MAS NMR: peaks at 9.67, 24.26, 33.53, 42.17, 58.48, 73.01, 118.89, 131.32, 164.66. Elemental analysis: Found C, 9.58; H, 1.49; N, 1.36.

Synthesis of 25

This oxidation was carried out in accordance with that reported by Ise et. al.[4] 4-methylchlorobenzylalcohol (1.00g, 6.47 mmol) was dissolved in chloroform (50 ml), and activated manganese(IV) oxide added (2.78 g, 32.0 mmol). The reaction mixture was refluxed at 65 °C for 24h. Following this, the mixture was gravity filtered twice, and the solvent removed from the filtrate by rotary evaporation. The product was dried under reduced pressure. 83 % yield.

^{1}H ($CDCl_3$) 4.55 (s, 2H, CH_2Cl), 7.46 (d, 2H), 7.78 (d, 2H), 9.93 (s, 1H, CHO). $^{13}C\{^{1}H\}$ ($CDCl_3$) 45.3 (CH_2Cl), 129.2 (CH), 130.1 (CH), 136.2 (C), 143.9 (C), 191.7 (CHO). Mass spec: HR-ESI Calc for [M^+] 154.0185 found 154.0462

Synthesis of 26

This reaction was carried out in accordance with that reported by Nguyen et. al.[3] **20a** (0.50 g, 2.10 mmol) and potassium carbonate (0.60 g, 6.05 mmol) were dissolved in methanol (40 ml), and **25** (0.32 g, 2.10 mmol). The reaction mixture was stirred continuously at room temperature for 24 h. Following this, the solvent was removed by rotary evaporation, and the residue dissolved in 50:50 dichloromethane:water. The organic layer was decanted off, and the remaining aqueous layer washed three times with dichloromethane. The organic layers were combined and dried over magnesium sulphate. This was gravity filtered and the solvent removed by rotary evaporation. The product was dried under reduced pressure. 51 % yield.

^{1}H ($CDCl_3$) 1.39 (m, 2H), 1.78 (m, 6H), 3.35 (m, 2H), 4.46 (s, 2H, CH_2Cl), 7.24 (m, 3H), 7.50 (m, 6H), 8.13 (s, 2H, CHN imine). $^{13}C\{^{1}H\}$ ($CDCl_3$) 23.5 (CH_2), 31.9 (CH_2), 44.8 (CH_2Cl), 72.8 (CHN cyclohexane), 126.5 (CH), 126.9 (CH), 127.4 (CH), 128.7 (CH), 129.8 (CH), 135.4 (C), 138.3 (C), 160.0 (CHN imine). Mass spec: HR-ESI Calc for [M^+] 339.1628 found 339.1722

Synthesis of S13

S1 (1.0 g, 1.0 mmol) was suspended in dry dichloromethane (50 ml), and **26** (0.34 g, 1.0 mmol) added. The mixture was stirred at room temperature for 3 h before the silica material was collected by vacuum filtration. The product was washed with dichloromethane and dried under reduced pressure. 82 % yield.

$^{13}C\{^{1}H\}$ CP/MAS NMR: peaks at 8.98, 16.03, 24.35, 42.86, 57.54, 58.82, 63.62, 128.13 (Ar), 135.18 (Ar), 161.32 (CHN imine). Elemental analysis: Found C, 8.03; H, 1.58; N, 1.41.

6.4.2 Synthesis of Silica-Supported Complexes

Preparation of [Ir(S6)(cod)]BF_4

$[IrCl(cod)]_2$ (100 mg, 0.15 mmol) was placed in a schlenk flask which was repeatedly degassed and backfilled with argon. This was dissolved in dry THF (10 ml), and $AgBF_4$ added (60 mg, 0.31 mmol). The reaction mixture was stirred for 30 mins before being filtered. **S6** (1.00 g, 1.0 mmol) was added to the filtrate and this was stirred for a further 30 mins. Following this the solution was decanted off, and the resulting heterogeneous complex was washed repeatedly with dry THF (3 × 10 ml), before being dried under reduced pressure.

$^{13}C\{^1H\}$ CP/MAS NMR: peaks at 9.57, 24.89, 33.26, 42.51, 62.52, 128.00 (Ar), 137.15 (Ar), 160.98 (imine). Elemental analysis: Found C, 9.70; H, 1.78; N, 1.28.

Preparation of [Ir(S8)(cod)]BF_4

$[IrCl(cod)]_2$ (100 mg, 0.15 mmol) was placed in a schlenk flask which was repeatedly degassed and backfilled with argon. This was dissolved in dry THF (10 ml), and $AgBF_4$ added (60 mg, 0.31 mmol). The reaction mixture was stirred for 30 mins before being filtered. **S8** (1.00 g, 1.0 mmol) was added to the filtrate and this was stirred for a further 30 mins. Following this the solution was decanted off, and the resulting heterogeneous complex was washed repeatedly with dry THF (3 × 10 ml), before being dried under reduced pressure.

$^{13}C\{^1H\}$ CP/MAS NMR: peaks at 9.46, 24.14, 43.22, 64.02, 128.91 (Ar), 137.38 (Ar), 162.97 (imine), 196.94. $^{31}P\{^1H\}$ CP/MAS NMR: major peaks at -13.31, 3.58, 17.23, 32.31, minor peak at 95.19. Elemental analysis: Found C, 10.9; H, 1.78; N, 1.28.

Preparation of [Rh(S4)(cod)]BF_4

$[RhCl(cod)]_2$ (100 mg, 0.20 mmol) was placed in a schlenk flask which was repeatedly degassed and backfilled with argon. This was dissolved in dry THF (10 ml), and $AgBF_4$ added (80 mg, 0.41 mmol). The reaction mixture was stirred for 30 mins before being filtered. **S4** (1.00 g, 1.0 mmol) was added to the filtrate and this was stirred for a further 30 mins. Following this the solution was decanted off, and the resulting heterogeneous complex was washed repeatedly with dry THF (3 × 10 ml), before being dried under reduced pressure. 65 % yield.

$^{13}C\{^{1}H\}$ CP/MAS NMR: peaks at 9.34, 21.19, 24.91, 29.90, 42.83, 67.69, 76.31, 128.40, 171.67. Elemental analysis: Found C, 7.87; H, 1.58; N, 1.11

Preparation of [Rh(S7)(cod)]BF_4

$[RhCl(cod)]_2$ (100 mg, 0.20 mmol) was placed in a schlenk flask which was repeatedly degassed and backfilled with argon. This was dissolved in dry THF (10 ml), and $AgBF_4$ added (80 mg, 0.41 mmol). The reaction mixture was stirred for 30 mins before being filtered. **S7** (1.00 g, 1.0 mmol) was added to the filtrate and this was stirred for a further 30 mins. Following this the solution was decanted off, and the resulting heterogeneous complex was washed repeatedly with dry THF (3 × 10 ml), before being dried under reduced pressure.

$^{13}C\{^{1}H\}$ CP/MAS NMR: peaks at 9.62, 25.18, 30.61, 42.51, 62.86, 67.85, 109.79 (cod), 128.34 (Ar), 135.24 (Ar), 160.79 (imine). Elemental analysis: Found C, 8.77; H, 1.53; N, 1.29.

Preparation of [Rh(S8)(cod)]BF_4

$[RhCl(cod)]_2$ (100 mg, 0.20 mmol) was placed in a schlenk flask which was repeatedly degassed and backfilled with argon. This was dissolved in dry THF (10 ml), and $AgBF_4$ added (80 mg, 0.41 mmol). The reaction mixture was stirred for 30 mins before being filtered. **S8** (1.00 g, 1.0 mmol) was added to the filtrate and this was stirred for a further 30 mins. Following this the solution was decanted off, and the resulting heterogeneous complex was washed repeatedly with dry THF (3 × 10 ml), before being dried under reduced pressure.

$^{13}C\{^{1}H\}$ CP/MAS NMR: peaks at 9.75, 25.02, 33.63, 41.85, 62.70, 128.72 (Ar), 138.31 (Ar), 161.65 (imine), 199.82. $^{31}P\{^{1}H\}$ CP/MAS NMR: minor peaks at -27.94, 49.05 and 96.85, major peak at 34.80. Elemental analysis: Found C, 11.3; H, 1.76; N, 1.21.

Preparation of [Rh(S13)(cod)]BF_4

$[RhCl(cod)]_2$ (40 mg, 0.08 mmol) was placed in a schlenk flask which was repeatedly degassed and backfilled with argon. This was dissolved in dry THF (10 ml), and $AgBF_4$ added (32 mg, 0.16 mmol). The reaction mixture was stirred

for 30 mins before being filtered. **S13** (0.40 g, 0.40 mmol) was added to the filtrate and this was stirred for a further 30 mins. Following this the solution was decanted off, and the resulting heterogeneous complex was washed repeatedly with dry THF (3 × 10 ml), before being dried under reduced pressure.

$^{13}C\{^{1}H\}$ CP/MAS NMR: peaks at 9.08, 16.13, 25.14, 29.84, 43.15, 59.01, 67.92, 82.22 (CH cod), 128.13 (Ar), 135.28 (Ar), 162.30 (CHN imine).

Preparation of [Cu(S4)](OTf)$_2$

$Cu(OTf)_2$ (0.22 g, 0.61 mmol) and **S4** (0.40 g, 0.40 mmol) were placed in a round bottomed flask which was repeatedly degassed and backfilled with argon. Methanol was added (30 ml), and this was stirred at room temperature for 3h. Following this, the product was collected by vacuum filtration, and dried under reduced pressure.

Elemental analysis: Found C, 6.10; H, 1.36; N, 1.23.

Preparation of [Cu(S5)](OTf)$_2$

$Cu(OTf)_2$ (0.22 g, 0.61 mmol) and **S5** (0.40 g, 0.40 mmol) were placed in a round bottomed flask which was repeatedly degassed and backfilled with argon. Methanol was added (30 ml), and this was stirred at room temperature for 3h. Following this, the product was collected by vacuum filtration, and dried under reduced pressure.

Elemental analysis: Found C, 6.43; H, 1.30; N, 1.24.

Preparation of [Cu(S6)](OTf)$_2$

$Cu(OTf)_2$ (0.22 g, 0.61 mmol) and **S6** (0.40 g, 0.40 mmol) were placed in a round bottomed flask which was repeatedly degassed and backfilled with argon. Methanol was added (30 ml), and this was stirred at room temperature for 3h. Following this, the product was collected by vacuum filtration, and dried under reduced pressure.

Elemental analysis: Found C, 6.11; H, 1.33; N, 1.18.

Preparation of [Cu(S7)](OTf)$_2$

$Cu(OTf)_2$ (0.22 g, 0.61 mmol) and **S7** (0.40 g, 0.40 mmol) were placed in a round bottomed flask which was repeatedly degassed and backfilled with argon.

Methanol was added (30 ml), and this was stirred at room temperature for 3h. Following this, the product was collected by vacuum filtration, and dried under reduced pressure.

Elemental analysis: Found C, 6.27; H, 1.32; N, 1.19.

Preparation of [Cu(S8)](OTf)$_2$

$Cu(OTf)_2$ (0.22 g, 0.61 mmol) and **S8** (0.40 g, 0.40 mmol) were placed in a round bottomed flask which was repeatedly degassed and backfilled with argon. Methanol was added (30 ml), and this was stirred at room temperature for 3h. Following this, the product was collected by vacuum filtration, and dried under reduced pressure.

Elemental analysis: Found C, 8.25; H, 1.51; N, 0.93.

Preparation of [Cu(S9)](OTf)$_2$

$Cu(OTf)_2$ (0.22 g, 0.61 mmol) and **S9** (0.40 g, 0.40 mmol) were placed in a round bottomed flask which was repeatedly degassed and backfilled with argon. Methanol was added (30 ml), and this was stirred at room temperature for 3h. Following this, the product was collected by vacuum filtration, and dried under reduced pressure.

Elemental analysis: Found C, 6.57; H, 1.40; N, 1.44

Preparation of [Cu(S13)](OTf)$_2$

$Cu(OTf)_2$ (0.22 g, 0.61 mmol) and **S13** (0.40 g, 0.40 mmol) were placed in a round bottomed flask which was repeatedly degassed and backfilled with argon. Methanol was added (30 ml), and this was stirred at room temperature for 3h. Following this, the product was collected by vacuum filtration, and dried under reduced pressure.

Preparation of [Ti(S12)](O^{i}Pr)$_2$

S12 (0.50 g, 0.50 mmol) was placed in a schlenk flask which was repeatedly degassed and backfilled with argon. To this, dry dichloromethane (10 ml) and $Ti(O^iPr)_4$ (0.15 ml, 0.51 mmol) were added, and the reaction stirred at room temperature for 1.5 h. Following this, the solution was decanted off, and the resulting heterogeneous complex was washed repeatedly with dry dichloromethane (3 × 10 ml), before being dried under reduced pressure.

$^{13}C\{^{1}H\}$ CP/MAS NMR: peaks at 10.93, 25.52, 64.09, 78.19, 118.23, 123.13, 133.02, 163.17. Elemental analysis: Found C, 13.1; H, 2.28; N, 0.95.

Preparation of [Zr(S12)](O^{i}Pr)$_2$

$Zr(O^{i}Pr)_4.{}^{i}PrOH$ (0.19 g, 0.50 mmol) was placed in a schlenk flask which was repeatedly degassed and backfilled with argon. This was dissolved in dry dichloromethane (10 ml), and **S12** was added (0.50 g, 0.50 mmol). The reaction was stirred at room temperature for 1.5 h. Following this, the solution was decanted off, and the resulting heterogeneous complex was washed repeatedly with dry dichloromethane (3 × 10 ml), before being dried under reduced pressure. $^{13}C\{^{1}H\}$ CP/MAS NMR: peaks at 10.44, 24.34, 30.12, 64.48, 70.85, 116.47, 123.32, 132.92, 161.80. Elemental analysis: Found C, 10.5; H, 1.86; N, 1.19.

6.4.3 Synthesis of Silsesquioxane-Supported Ligands

Synthesis of SQ1

The following reaction was carried out in accordance with that reported by Maschmeyer et. al.[10] Silsesquioxane (1,3,5,7,9,11,14-Heptaisobutyl-tricyclo[7.3.3.1(5,11)]hepta-siloxane-endo-3,7,14-triol) (2.0 g, 2.53 mmol) was dissolved in dry THF (50 ml), and 3-aminopropyltrimethoxysilane added (0.5 ml, 2.86 mmol). The reaction mixture was stirred continuously at room temperature for 36 h, before the solvent was removed by rotary evaporation. The residue was washed with acetonitrile, and the product dried under reduced pressure. 82 % yield.

^{1}H ($CDCl_3$) 0.58 (m, 14H, C**H**$_2$CH$(CH_3)_2$), 0.94 (m, 42H, $CH_2CH(CH_3)_2$), 1.15 (m, 2H, C**H**$_2CH_2CH_2NH_2$), 1.53 (quin, 2H, $CH_2CH_2CH_2NH_2$), 1.85 (m, 7H, $CH_2CH(CH_3)_2$), 2.67 (t, 2H, $CH_2CH_2CH_2NH_2$).

Synthesis of 27

Ethanol (250 ml) and THF (350 ml) were cooled to 5 °C for 20 mins, and to this terephthalaldehyde (20 g, 149 mmol) and sodium borohydride (1.7g, 44.9 mmol)

were added. The mixture was stirred for a further 2 h at 5 °C before being filtered, and the solvent removed. Distilled water (100 ml) was added, and the products extracted with ethyl acetate (2 × 200 ml). The organic solution was dried over magnesium sulphate, filtered and the solvent removed. Chloroform (150 ml) was added to the residue and the resulting solution obtained by gravity filtration. This solution was then cooled to -20 °C for 72 h before being filtered again and the solvent removed. The product was dried under reduced pressure.

^{1}H ($CDCl_3$) 3.00 (s, 1H, OH), 4.68 (s, 2H, C**H$_2$**OH), 7.42 (d J = 8 Hz, 2H), 7.72 (d J = 8 Hz, 2H), 9.85 (s, 1H, CHO). ^{13}C{^{1}H} ($CDCl_3$) 64.7 (CH_2OH), 127.3 (CH), 130.3 (CH), 135.8 (C), 148.6 (C), 192.8 (CHO). Mass spec: HR-ESI Calc for [M^+] + MeOH 136.0524 found 168.0635

Synthesis of SQ2

SQ1 (1.0 g, 1.15 mmol) was dissolved in dry THF (40 ml), and a solution of **27** (0.16 g, 1.18 mmol) in dry THF (20 ml) added. The reaction mixture was stirred continuously at room temperature for 4 h, before the solvent was removed by rotary evaporation. The residue was washed with acetonitrile, and the product dried under reduced pressure. 77 % yield.

^{1}H ($CDCl_3$) 0.54 (m, 14H, C**H**$_2$CH(CH_3)$_2$), 0.87 (m, 42H, CH_2CH(C**H**$_3$)$_2$), 1.78 (m, 7H, CH_2C**H**(CH_3)$_2$), 3.53 (m, 2H, (CH_2CH_2C**H**$_2NH_2$), 4.65 (s, 2H, CH_2Cl), 7.32 (d, 2H, Ar), 7.63 (d, 2H, Ar), 8.18 (s, 1H, CHN imine).

Synthesis of SQ3

SQ2 (1.0 g, 1.01 mmol) was dissolved in chloroform (70 ml), and activated manganese(IV) oxide added (0.36 g, 4.14 mmol). The reaction mixture was refluxed at 65 °C for 6h, before being gravity filtered twice. The solvent was removed from the filtrate by rotary evaporation, and the residue washed with acetonitrile. The product dried under reduced pressure. 86 % yield.

^{1}H ($CDCl_3$) 0.52 (m, 14H, C**H**$_2$CH(CH_3)$_2$), 0.87 (m, 42H, CH_2CH(C**H**$_3$)$_2$), 1.80 (m, 7H, CH_2C**H**(CH_3)$_2$), 3.57 (t, 2H, CH_2CH_2C**H**$_2NH_2$), 7.19 (d, 2H, Ar), 7.70 (d, 2H, Ar), 8.21 (s, 1H, CHN imine), 9.97 (s, 1H, CHO aldehyde).

Synthesis of SQ4

SQ3 (1.0 g, 1.01 mmol) was dissolved in dry THF (40 ml), and **2** added (0.11 g, 0.96 mmol). The reaction mixture was stirred at room temperature for 4 h, before the solvent was removed by rotary evaporation. The residue was washed with acetonitrile, and the product dried under reduced pressure. 92 % yield.

^{1}H ($CDCl_3$) 0.55 (d, 14H, C**H**$_2$CH(CH_3)$_2$), 0.87 (d, 42H, $CH_2CH(CH_3)_2$), 1.29 (m, 4H), 1.46 (m, 3H), 1.80 (m, 7H, $CH_2CH(CH_3)_2$), 2.60 (m, 1H), 3.54 (m, 1H), 7.34 (m, 1H), 7.71 (m, 2H), 8.22 (s, 1H, CHN imine).

Synthesis of SQ5a

SQ4 (1.0 g, 0.95 mmol) was dissolved in dry THF (40 ml), and benzaldehyde added (0.1 ml, 0.98 mmol). The reaction mixture was stirred continuously at room temperature for 3 h, before the solvent was removed by rotary evaporation. The residue was washed with acetonitrile, and the product dried under reduced pressure. 81 % yield.

^{1}H ($CDCl_3$) 0.54 (m, 14H, C**H**$_2$CH(CH_3)$_2$), 0.88 (d, 42H, $CH_2CH(CH_3)_2$), 1.78 (m, 7H, $CH_2CH(CH_3)_2$), 3.55 (m, 2H), 7.35 (m, 2H), 7.67 (m, 2H), 8.21 (s, 1H, CHN imine). ^{13}C{^{1}H} ($CDCl_3$) 22.5 (CH_2), 23.9 (CH or CH_3), 24.3 (CH_2), 25.7 (CH or CH_3), 128.3 (CH), 130.5 (CH), 160.9 (CHN imine). Product not observed in mass spectrum.

Synthesis of SQ5b

SQ5a (1.0 g, 0.87 mmol) was dissolved in methanol (40 ml), and sodium borohydride (0.13 g, 3.44 mmol) added. The reaction mixture was stirred continuously for 24h, before the solvent was removed by rotary evaporation. The residue was dissolved in dichloromethane, and this was gravity filtered. The solvent was removed from the filtrate by rotary evaporation, and the product dried under reduced pressure. 27 % yield.

^{1}H ($CDCl_3$) 0.51 (m, 14H, C**H**$_2$CH(CH_3)$_2$), 0.86 (d, 42H, $CH_2CH(CH_3)_2$), 1.79 (m, 7H, $CH_2CH(CH_3)_2$), 3.53 (m, 2H, $CH_2CH_2CH_2NH$), 7.34 (m, 2H), 7.67 (m, 2H), 8.22 (s, CHN imine). ^{13}C{^{1}H} ($CDCl_3$) 22.5 (CH_2), 23.9 (CH or CH_3), 24.3 (CH_2), 25.7 (CH or CH_3), 128.2 (CH), 130.5 (CH), 160.9 (CHN imine). Product not observed in mass spectrum.

Synthesis of SQ6a

SQ4 (1.0 g, 0.95 mmol) was dissolved in dry THF (40 ml), and 2-methoxybenzaldehyde (0.13 g, 0.96 mmol) added. The reaction mixture was stirred continuously at room temperature for 4 h, before the solvent was removed by rotary evaporation. The residue was washed with acetonitrile, and the product dried under reduced pressure. 77 % yield.

^{1}H ($CDCl_3$) 0.54 (m, 14H, C**H**$_2$CH(CH_3)$_2$), 0.87 (d, 42H, $CH_2CH(CH_3)_2$), 1.76 (m, 12H, CH_2C**H**(CH_3)$_2$, also CH_2 underneath), 3.52 (m, 2H), 3.61 (m, 1H), 3.80 (s, 3H, OCH_3), 6.83 (m, 2H), 7.32 (m, 1H), 7.45 (m, 3H), 7.70 (m, 1H), 8.07 (s, 1H, CHN imine), 8.63 (s, 1H, CHN imine). ^{13}C{^{1}H} ($CDCl_3$) 22.5 (CH_2), 23.9 (CH or CH_3), 24.4 (CH_2), 25.7 (CH or CH_3), 55.5 (OCH_3), 64.4 (CH_2N), 74.0 (CHN cyclohexane), 111.0 (CH), 120.8 (CH), 127.3 (CH), 128.2 (CH), 131.6 (CH), 156.9 (CHN imine), 160.4 (CHN imine). Product not observed in mass spectrum.

Synthesis of SQ6b

SQ6a (1.0 g, 0.85 mmol) was dissolved in methanol (40 ml), and sodium borohydride (0.13 g, 3.44 mmol) added. The reaction mixture was stirred continuously for 24h, before the solvent was removed by rotary evaporation. The residue was dissolved in dichloromethane, and this was gravity filtered. The solvent was removed from the filtrate by rotary evaporation, and the product dried under reduced pressure. 28 % yield.

^{1}H ($CDCl_3$) 0.53 (d, 14H, C**H**$_2$CH(CH_3)$_2$), 0.87 (d, 42H, $CH_2CH(CH_3)_2$), 1.79 (m, 7H, CH_2C**H**(CH_3)$_2$), 3.51 (m, 2H), 3.63 (m, 2H), 3.89 (m, 2H), 6.85 (m, 2H), 6.93 (m, 2H), 7.30 (m, 2H), 7.69 (m, 2H). ^{13}C{^{1}H} ($CDCl_3$) 22.5 (CH_2), 23.9 (CH or CH_3), 24.3 (CH_2), 24.4 (CH_2), 25.7 (CH or CH_3), 55.5 (OCH_3), 64.4 (CH_2NH), 111.0 (CH), 120.8 (CH), 127.3 (CH), 128.0 (CH), 128.2 (CH), 131.6 (CH). Product not observed in mass spectrum.

Synthesis of SQ7a

SQ4 (1.0 g, 0.95 mmol) was dissolved in dry THF (40 ml), and 2-methylbenzaldehyde (0.1 ml, 0.86 mmol) added. The reaction mixture was stirred continuously at room temperature for 4 h, before the solvent was removed by rotary evaporation. The residue was washed with acetonitrile, and the product dried under reduced pressure. 88 % yield.

^{1}H ($CDCl_3$) 0.53 (m, 14H, C**H**$_2$CH(CH_3)$_2$), 0.89 (d, 42H, CH_2CH(C**H**$_3$)$_2$), 1.76 (m, 12H, CH_2C**H**(CH_3)$_2$, also CH_2 underneath), 2.20 (m, 2H), 2.42 (s, CH_3), 3.33 (m, 2H), 3.57 (m, 2H), 7.11 (m, 2H), 7.32 (m, 1H), 7.45 (m, 3H), 7.70 (m, 1H), 8.19 (s, 1H, CHN imine), 8.50 (s, 1H, CHN imine). ^{13}C{^{1}H} ($CDCl_3$) 22.5 (CH_2), 23.9 (CH or CH_3), 24.3 (CH_2), 25.7 (CH or CH_3), 126.0 (CH), 127.0 (CH), 127.4 (CH), 128.2 (CH), 130.1 (CH), 130.7 (CH), 156.5 (CHN imine), 160.4 (CHN imine). Product not observed in mass spectrum.

Synthesis of SQ7b

SQ7a (1.0 g, 0.86 mmol) was dissolved in methanol (40 ml), and sodium borohydride (0.13 g, 3.44 mmol) added. The reaction mixture was stirred continuously for 24h, before the solvent was removed by rotary evaporation. The residue was dissolved in dichloromethane, and this was gravity filtered. The solvent was removed from the filtrate by rotary evaporation, and the product dried under reduced pressure. 36 % yield.

^{1}H ($CDCl_3$) 0.52 (d, 14H, C**H**$_2$CH(CH_3)$_2$), 0.89 (d, 42H, CH_2CH(C**H**$_3$)$_2$), 1.36 (m, 1H), 1.78 (m, 7H, CH_2C**H**(CH_3)$_2$), 2.22 (m, 3H), 2.41 (m, 1H), 2.60 (m, 1H), 3.53 (m, 2H), 3.79 (m, 2H), 4.61 (m, 2H), 7.08 (m, 3H), 7.19 (m, 3H), 7.70 (m, 2H). ^{13}C{^{1}H} ($CDCl_3$) 21.5 (CH_2), 22.8 (CH or CH_3), 23.2 (CH_2), 24.1 (CH_2), 24.7 (CH or CH_3), 63.5 (CH_2NH), 124.8 (CH), 125.8 (CH), 126.4 (CH), 127.2 (CH), 129.2 (CH), 129.7 (CH). Product not observed in mass spectrum.

Synthesis of SQ8

This reaction was carried out in accordance with that reported by Zheng et. al.[11] Silsesquioxane (1,3,5,7,9,11,14-Heptaisobutyl-tricyclo[7.3.3.1(5,11)]hepta-siloxane-endo-3,7,14-triol) (1.0 g, 1.26 mmol) was dissolved in dry THF (40 ml), and triethylamine added (0.18 ml, 1.26 mmol). The reaction mixture was cooled to 0 °C, and 3-bromopropyltrichlorosilane added (0.22 ml, 1.38 mmol). The reaction mixture was allowed to come to room temperature and stirred for 24h. Following this, the solvent was removed by rotary evaporation, and the residue washed with acetonitrile. The product was dried under reduced pressure. 82 % yield.

^{1}H ($CDCl_3$) 0.57 (m, 14H, C**H**$_2$CH(CH_3)$_2$), 0.92 (d, 42H, CH_2CH(C**H**$_3$)$_2$), 1.38 (t, 4H, C**H**$_2$$CH_2$C**H**$_2$Br), 1.80 (m, 7H, CH_2C**H**(CH_3)$_2$), 3.06 (quin, CH_2C**H**$_2$$CH_2$Br).

$^{13}C\{^{1}H\}$ ($CDCl_3$) 22.4 (CH_2), 23.8 (CH or CH_3), 24.3 (CH_2), 25.7 (CH or CH_3), 26.7 (CH_2), 45.8 (CH_2Br). Mass spec: HR-ESI Calc for [M^+] + acetonitrile 979.2550 found 979.2107.

Synthesis of SQ9a

This reaction was carried out in accordance with that reported by Nguyen et. al.[3] **SQ8** (1.0 g, 1.07 mmol) was dissolved in THF (20 ml) and methanol (20 ml). To this, **20a** (0.25 g, 1.05 mmol) and potassium carbonate (0.29 g, 2.10 mmol) were added, and the reaction mixture stirred continuously at room temperature. Following this, the solvent was removed by rotary evaporation, and the residue dissolved in dichloromethane. This was gravity filtered, and the solvent removed from the filtrate by rotary evaporation. The product was dried under reduced pressure. 88 % yield.

^{1}H ($CDCl_3$) 0.54 (d, 14H, C**H**$_2$CH(CH_3)$_2$), 0.70 (m, 3H), 0.89 (d, 42H, $CH_2CH(CH_3)_2$), 1.78 (m, 7H, $CH_2CH(CH_3)_2$), 1.89 (m, 3H), 3.35 (t, 4H). $^{13}C\{^{1}H\}$ ($CDCl_3$) 22.4 (CH_2), 23.9 (CH or CH_3), 24.5 (CH_2), 25.7 (CH or CH_3), 26.7 (CH_2), 33.0 (CH_2), 36.4 (CH_2), 73.8 (CHN cyclohexane), 127.9 (CH), 128.4 (CH), 130.2 (CH), 136.4 (C), 161.1 (CHNcyclohexane). Product not observed in mass spectrum.

Synthesis of SQ9b

SQ9a (1.0 g, 0.95 mmol) was dissolved in methanol (40 ml), and sodium borohydride (0.10 g, 2.64 mmol) added. The reaction mixture was stirred continuously for 24h, before the solvent was removed by rotary evaporation. The residue was dissolved in dichloromethane, and this was gravity filtered. The solvent was removed from the filtrate by rotary evaporation, and the product dried under reduced pressure. 34 % yield.

^{1}H ($CDCl_3$) 0.54 (m, 14H, C**H**$_2$CH(CH_3)$_2$), 0.68 (m, 3H), 0.90 (d, 42H, $CH_2CH(CH_3)_2$), 1.79 (m, 7H, $CH_2CH(CH_3)_2$), 1.91 (m, 3H), 2.11 (m, 1H), 2.20 (m, 1H), 3.34 (m, 2H), 3.59 (d J = 13 Hz, 1H, C**H**$_2$NH), 3.83 (d J = 13 Hz, 1H, C**H**$_2$NH), 7.17 (m, 1H), 7.24 (m, 3H). $^{13}C\{^{1}H\}$ ($CDCl_3$) 21.4 (CH_2), 22.8 (CH or CH_3), 24.0 (CH_2), 24.7 (CH or CH_3), 25.7 (CH_2), 30.5 (CH_2), 35.3 (CH_2), 49.8 (C**H**$_2$NH), 59.8 (CHN cyclohexane), 124.5 (CH), 125.7 (CH), 127.0 (CH). Product not observed in mass spectrum.

6.4.5 Synthesis of Silsesquioxane-Supported Complexes

Preparation of [Rh(SQ9b)(cod)]BF_4

$[RhCl(cod)]_2$ (100 mg, 0.20 mmol) was placed in a schlenk flask which was repeatedly degassed and backfilled with argon. This was dissolved in dry THF (10 ml), and $AgBF_4$ added (80 mg, 0.41 mmol). The reaction mixture was stirred for 30 mins before being filtered. **SQ9b** (180 mg, 0.17 mmol) was added to the filtrate and this was stirred for a further 30 mins. Following this, the solvent was removed under reduced pressure, and the product washed three times with dry acetonitrile, with the washings being decanted off. The product was dried under reduced pressure. 55 % yield.

^1H ($CDCl_3$) 0.62 (d, 14H, C**H**$_2$CH$(CH_3)_2$), 0.74 (m, 3H), 0.94 (d, 42H, $CH_2CH(CH_3)_2$), 1.21 (m, 2H), 1.45 (m, 2H), 1.83 (m, 7H, $CH_2CH(CH_3)_2$), 1.96 (m, 3H), 2.57 (m, 8H), 3.46 (m, 2H), 4.30 (m, 4H, CH cod), 7.34 (m, 5H). $^{13}C\{^1H\}$ ($CDCl_3$) 21.4 (CH_2), 22.8 (CH or CH_3), 24.7 (CH or CH_3), 25.7 (CH_2), 29.9 (CH_2), 35.4 (CH_2), 77.8 (CH cod). $^{29}Si\{^1H\}$ ($CDCl_3$) broad peak at -109.1, peak at -67.9, peak at -67.6. Product not observed in mass spectrum.

Preparation of [Cu(SQ9b)]$(OTf)_2$

$Cu(OTf)_2$ (0.22 g, 0.61 mmol) and **SQ9b** (0.54 g, 0.51 mmol) were placed in a round bottomed flask which was repeatedly degassed and backfilled with argon. THF was added (30 ml), and this was stirred at room temperature for 3h. Following this, the product was collected by vacuum filtration, and dried under reduced pressure.

Mass spec: HR-ESI calc for $[M^+]$ – OTf + MeOH 980.2564 found 980.2671.

6.5 Catalytic Screening

6.5.1 Asymmetric Nitroaldol Reaction

In the following descriptions of catalytic conditions:

- "Aldehyde" corresponds to benzaldehyde (0.10 ml, 1.0 mmol) or 4-nitrobenzaldehyde (0.15 g, 1.0 mmol)
- "Nitroalkane" corresponds to nitromethane (0.55 ml, 10 mmol) or nitroethane (0.72 ml, 10 mmol)
- "Base" corresponds to triethylamine (17 µl, 0.12 mmol), diisopropylamine (17 µl, 0.12 mmol) or 1-methylpyrrolidine (14 µl, 0.13 mmol)

Homogeneous Catalysis

The catalyst was placed in a Young's ampoule under argon, and dissolved in ethanol (10 ml). To this, aldehyde (1.0 mmol), nitroalkane (10 mmol) and base (0.12 mmol) were added. After the appropriate length of time had elapsed, the solvent was removed by rotary evaporation and the residue re-dissolved in ethanol. This was filtered through silica, and the solvent removed by rotary evaporation.

Heterogeneous Catalysis

The catalyst (100 or 200 mg) was placed in a Young's ampoule under argon, and suspended in ethanol (10 ml). To this, aldehyde (1.0 mmol), nitroalkane (10 mmol) and base (0.12 mmol) were added. After the appropriate length of time

had elapsed, the mixture was filtered through cotton wool, and the solvent removed by rotary evaporation.

6.5.2 Asymmetric Hydrogenation Reaction

In the following descriptions of catalytic conditions:

- "Ketone" corresponds to methyl benzoyl formate (0.5 ml, 3.52 mmol), acetophenone (0.5 ml, 4.29 mmol), 2'-chloroacetophenone (0.5 ml, 3.85 mmol) or 2'-methylacetophenone (0.5 ml, 3.82 mmol)
- "Imine" corresponds to N-benzylidenemethylamine (0.5 ml, 4.06 mmol) or phenyl-1(1-phenylethylidene) amine (0.84 g, 4.30 mmol)
- "Closed vessel" corresponds to the reaction being under argon and the lid of the Young's ampoule being sealed
- "Open vessel" corresponds to the reaction being kept under argon for the duration of the reaction, but the lid of the Young's ampoule not being sealed

Direct Hydrogenation

The catalyst (0.043 mmol), and ketone or imine were dissolved in methanol (10 ml) in a glass tube, which was placed inside an autoclave. Hydrogen gas (20 bar) was released into the autoclave, which then stirred the reaction mixture at room temperature for the appropriate length of time. Following this, the solvent was removed by rotary evaporation.

Transfer Hydrogenation

The catalyst (0.043 mmol) and ketone or imine were dissolved in a solution of potassium hydroxide in anhydrous isopropanol (10 ml, 4.29×10^{-5} mol dm^{-3}) in a Young's Ampoule under argon. This was stirred at the appropriate temperature for the appropriate length of time. Unless otherwise stated, the reaction was performed in a closed vessel. Following the reaction, the solvent was removed by rotary evaporation.

Transfer Hydrogenation in the presence of Hydrogen Gas

The catalyst (0.043 mmol) and ketone or imine were dissolved in a solution of potassium hydroxide in anhydrous isopropanol (10 ml, 4.29×10^{-5} mol dm^{-3}) in a glass tube. This was placed inside an autoclave, and hydrogen gas (20 bar) added after the system was purged. This was stirred at room temperature for the appropriate length of time. Following the reaction, the solvent was removed by rotary evaporation.

6.5.3 Asymmetric Aldol Reaction

Without Acid

The catalyst (1.0 mmol) and benzaldehyde (0.5 ml, 5.0 mmol) were dissolved in acetone (10 ml) under argon. This was stirred continuously at room temperature for the appropriate length of time, before the solvent was removed by rotary evaporation at 23 °C.

With Acid

The catalyst (1.0 mmol), benzaldehyde (0.5 ml, 5.0 mmol) and glacial acetic acid (60 µl, 1.0 mmol) were dissolved in acetone (10 ml) under argon. This was stirred continuously at room temperature for the appropriate length of time, before the solvent was removed by rotary evaporation at 23 °C.

As an alternative to glacial acetic acid, trifluoroacetic acid was trialled (0.08 ml, 1.0 mmol).

With base

The catalyst (1.0 mmol), benzaldehyde (0.5 ml, 5.0 mmol) and triethylamine (35 µl, 0.25 mmol) were dissolved in acetone (10 ml) under argon. This was stirred continuously at room temperature for the appropriate length of time, before the solvent was removed by rotary evaporation at 23 °C.

6.5.4 Asymmetric Allylic Oxidation Reaction

The catalyst (0.03 mmol), cyclohexene (0.2 ml, 2.0 mmol), t-butylperoxybenzoate (0.1 ml, 0.53 mmol) and acetone (1ml) were stirred continuously in a sample vial, at room temperature for the appropriate length of time. Following this, a drop of the solution was taken for NMR spectroscopy and GC-MS.

6.5.5 Asymmetric Epoxidation Reaction

The catalyst (0.22 mmol), styrene (8 µl, 0.07 mmol), hydrogen peroxide (30 %, 11 µl, 0.10 mmol) and dichloromethane (2 ml) were placed in a Young's ampoule under argon, and stirred continuously at room temperature for the appropriate length of time. Following this, the solvent was removed by rotary evaporation.

6.5.6 Stereoselective Polymerisation of *rac*-lactide

Under Melt Conditions

The catalyst (0.02 mmol) and recrystallised *rac*-lactide (1.0 g, 6.9 mmol) were placed in a Young's ampoule under argon. This was stirred for 2h at 130 °C. Following this, methanol was added (3 ml), and then dichloromethane was added (3 ml), to dissolve the contents of the Young's ampoule. The solvent was removed under reduced pressure.

Under Solution Conditions

The catalyst (0.02 mmol) and recrystallised *rac*-lactide (0.33 g, 2.3 mmol) were placed in a Young's ampoule under argon, and dry toluene added (10 ml). This was stirred for the appropriate length of time at 80 °C. Following this, methanol was added (3 ml), and then dichloromethane was added (3 ml), to dissolve the

contents of the Young's ampoule. The solvent was removed under reduced pressure.

6.6 References

(1) Larrow, J. F.; Jacobsen, E. N.; Gao, Y.; Hong, Y. P.; Nie, X. Y.; Zepp, C. M. *J. Org. Chem.* **1994**, *59*, 1939.

(2) Rafii, E.; Giorgi, M.; Vanthuyne, N.; Roussel, C. *Arkivoc* **2005**, 86.

(3) Campbell, E. J.; Nguyen, S. T. *Tetrahedron Lett.* **2001**, *42*, 1221.

(4) Ise, T.; Shiomi, D.; Sato, K.; Takui, T. *Chem. Mat.* **2005**, *17*, 4486.

(5) Jones, M. D.; Mahon, M. F. *J. Organomet. Chem.* **2008**, *693*, 2377.

(6) Jones, M. D.; Paz, F. A. A.; Davies, J. E.; Raja, R.; Klinowski, J.; Johnson, B. F. G. *Inorg. Chim. Acta* **2004**, *357*, 1247.

(7) van Albada, G. A.; Mutikainen, I.; Turpeinen, U.; Reedijk, J. *J. Chem. Crystallogr.* **2006**, *36*, 259.

(8) Whitelaw, E. L.; Jones, M. D.; Mahon, M. F. *Inorg. Chem.* **2010**, *49*, 7176.

(9) Utting, K. A.; Macquarrie, D. J. *New J. Chem.* **2000**, *24*, 591.

(10) Pescarmona, P. P.; Masters, A. F.; van der Waal, J. C.; Maschmeyer, T. *J. Mol. Catal. A-Chem.* **2004**, *220*, 37.

(11) Zeng, K.; Zheng, S. X. *Macromol. Chem. Phys.* **2009**, *210*, 783.